Determination of Stable Time-delay Regions in Incremental Control Systems

Master of Science Thesis

Isabelle El-Hajj

Delft University of Technology

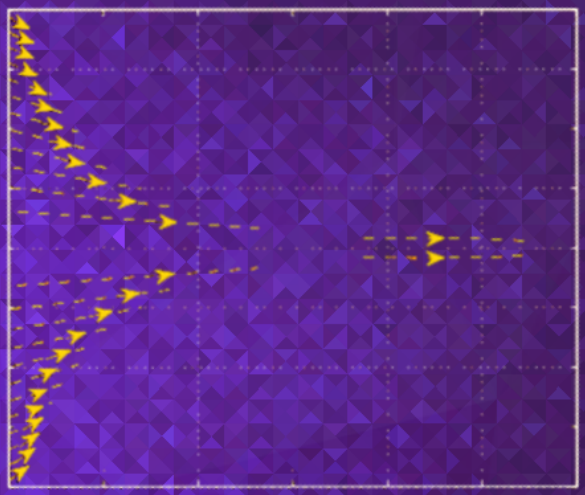

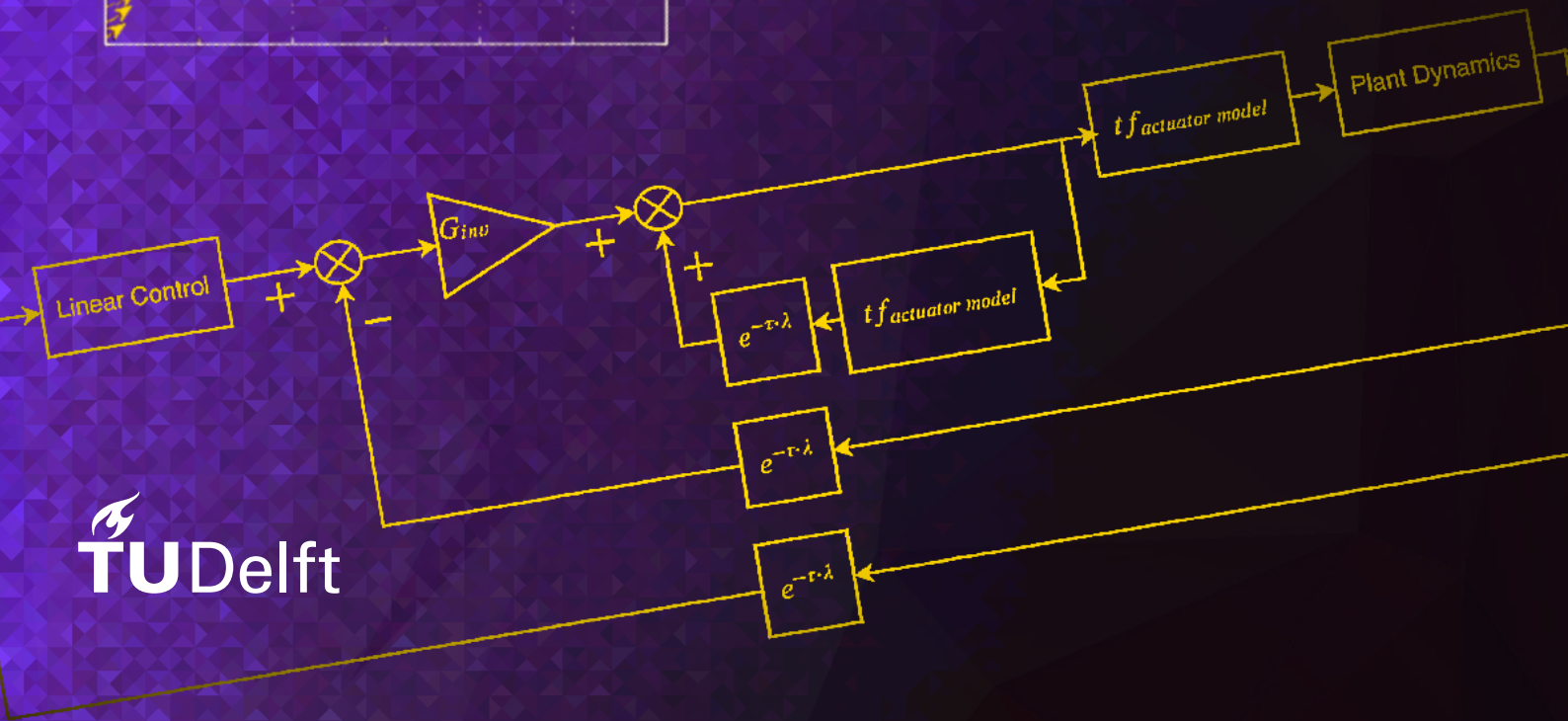

TU Delft

This page was intentionally left blank.

Determination of Stable Time-delay Regions in Incremental Control Systems

Master of Science Thesis

by

Isabelle El-Hajj

to obtain the degree of Master of Science
at the Delft University of Technology

Supervisors: Dr. ir. E. van Kampen
Dr. Q.P. Chu
Dr. X. Wang

TU Delft

This page was intentionally left blank.

Contents

This page was intentionally left blank.

List of Figures

List of Tables

This page was intentionally left blank.

List of Algorithms

This page was intentionally left blank.

Acronyms

BMI Bilinear Matrix Inequality. 112

CDIR Crossing Direction of Imaginary Root. 117–119
CIR Critical Imaginary Root. 117, 118

DDAE Delay-difference Algebraic Equation. 76, 77

FBW Fly-by-Wire. 54
FINDI Finite Time Convergence Incremental Nonlinear Dynamic Inversion. 55
FTC Fault-tolerant Control. 54

GLA Gust Load Alleviation. 54

IBS Incremental Backstepping. 5, 157
INDI Incremental Nonlinear Dynamic Inversion. iii, iv, vii, ix, 3–7, 43, 51–55, 113–116, 155, 157
IO Input-Output. 113
IQC Integral Quadratic Constraint. 94

LFT Linear Fractional Transformation. 94
LK Lyapunov-Krasovskii. 91, 92, 94–96, 102, 104–107
LMI Linear Matrix Inequality. 110, 112
LPV Linear Parameter Varying. 157
LR Lyapunov-Razumikhin. 91, 92, 94, 96, 98, 101, 104

LTI Linear Time-invariant. 71, 73, 77, 81, 94, 126, 155, 157

MIMO Multiple Input Multiple Output. 43, 48–50

NDI Nonlinear Dynamic Inversion. iv, vii, 7, 43, 51, 53, 54, 113, 115, 155, 157

PCH Pseudo-Control Hedging. 55
PID Proportional Integral Derivative. vii, 54

RLV Reusable Launch Vehicle. 53

SAS Stability Augmentation System. 54
SISO Single Input Single Output. 48–50
SIVIA Set Inversion Via Interval Analysis. 156

TDS Time-Delay System. vii, 7, 63–69, 71–78, 81, 83, 85–92, 94–96, 98, 102, 104, 105, 107, 111, 112, 120, 123, 126, 129–132, 141, 143, 148, 155–157

UAV Unmanned Aerial Vehicle. 53

V/STOL Vertical/Short Takeoff and Landing. 53
VTOL Vertical Takeoff and Landing. 53

ZOH Zero-Order-Hold. 60, 157

This page was intentionally left blank.

Nomenclature

Greek symbols

α	Strictly positive constant
β	Strictly positive constant
Δ	Schur-Cohn matrix, Increment in a value, Change in variable value
δ	Perturbation term
λ	Characteristic root
$\nabla(\cdot)$	Gradient
ν	Virtual control
Ω	Domain, Solution set for the critical imaginary frequencies
ω	Critical imaginary frequency
Ω_N	Set of parts of the discretized delay interval
ϕ	Initial condition for the state of time-delay system
Π_N	Part of matrix pencil of the discretized spectrum problem
ρ	Spectral radius
σ	Spectrum
Σ_N	Part of matrix pencil of the discretized spectrum problem
τ	Time-delay
θ	Angle
θ_N	Segment of discretized delay interval
ξ	Part of trajectory of time-delay system
ζ	Initial condition for the input of time-delay system

Roman symbols

$\dot{y}$	Output derivative
$\mathbb{R}$	Set of real numbers
$\mathbf{u}$	Control input vector
$\mathbf{x}$	State vector
$\mathbf{y}$	Output vector
$\mathfrak{I}$	Imaginary part of a complex variable
$\mathfrak{R}$	Real part of a complex variable
$\mathscr{A}$	Infinitesimal generator
$\mathscr{C}$	Banach space
$\mathscr{T}$	Solution operator of a time-delay system
$\tilde{x}_N$	Augmented state
A	State or system matrix
A_k	Matrix of coefficients of the state delays
C	Matrix of coefficients of the neutral delays, Free parameter used in model transformation
H	Matrix of coefficients of neutral delays and their derivatives, Schur-Cohn-Fujiwara matrix
I	Identity matrix
K_p	Proportional gain
k_i	Gain
$L_f h$	Lie derivative
NU	Number of unstable roots
P	Positive-definite matrix
p_N	Discretized polynomial
Q	Positive-definite matrix
q	Conjugate polynomial
R	Positive-definite matrix
u	Continuous non-decreasing function
v	Continuous non-decreasing function
w	Continuous non-decreasing function
x_t	Shimanov Notation
Y_p	Pilot transfer function
Y_{OL}	Open-loop transfer function
e	Tracking error
F	Linearized state dynamics with respect to the state variable(s)
f	State dynamics
G	Control effectiveness matrix, Input dynamics
h	Output dynamics
p	Characteristic quasipolynomial
S	Shift matrix, Positive-definite matrix
s	Laplace variable
T	Pseudo-delay, Local state transformation, Positive-definite matrix
t	time
u	Control input
V	Lypapunov-Razumikhin function, Lyapunov-Krasovskii functional
x	State
y	Scalar output
z	Transformed state

This page was intentionally left blank.

Preface

This thesis marks a five and a half year sprint as a student at the faculty of Aerospace Engineering at TU Delft. Looking back, the development on both a personal and technical level has been immense, and for that, I am proud and grateful. However, this would not have been possible without the help of many to whom I owe my deep appreciation.

First of all, I would like to express my gratitude to my supervisors Dr. Q.P. Chu and Dr. ir. E. van Kampen, for their guidance, support, and encouragement during the period of this thesis. I would also like to thank Dr. X. Wang for both helping me on a technical level as well as giving me useful advice whenever I needed it.

I would also like to thank many of my peers at C& S for many interesting and enriching discussions. I am deeply grateful for my friends who have kept my spirits high during the trying times and have made the time living in Delft memorable and endearing. I am also very thankful for Thomas, Mieke, Edwin, Tessa, Ed, and Ria whom I consider to be my closest to family in the Netherlands. Finally, I owe my deepest gratitude to my family for their unconditional love and support in all that I do.

Isabelle El-Hajj
Delft, February 2020

This page was intentionally left blank.

1

Introduction

1.1 Project Context and Motivation

In the past years, there has been a rapid growth in air traffic volume [12]. With this increase in total air transport, it is important that flight safety is continuously enhanced. As flight-control-related issues are a major deterrent to flight safety and often a source of catastrophe, significant responsibility befalls flight control engineers in addressing the impending need for enhancing flight safety.

Due to this responsibility, flight control engineers have sought more advanced control techniques than the often-used linear control techniques. Historically, in the automatic flight control of both commercial and military aircraft, a broadly applied strategy is to rely on local linear controllers and use gain-scheduling to synthesize a global controller. This entails partitioning the flight envelope, linearizing the plant's dynamics about a steady-state condition in every partition, and therein designing local linear controllers. During flight, the correct gains are used. However, gain-scheduling requires that parameters change slowly, which may not be fulfilled in aggressive maneuvers. Additionally, whenever the state departs significantly from the points of linearization, gain-scheduling is not always able to ensure closed-loop stability [13]. This is because linear controllers are by construction only valid for a small range of operation, and when a larger range of operation is required, the linear controller behaves poorly. Model uncertainty also presents a major setback to linear control methods.

These limitations of linear control and the ability of nonlinear control to address these problems, as discussed in [14], have propelled an interest in nonlinear flight control. Nonlinear control methods can be tailored to handle uncertainties in model designs, as is the case in robust controllers and adaptive controllers. Nonlinear controllers are designed to handle nonlinearities which can make them suitable for large ranges of operation. Sometimes, nonlinear controllers can have a simpler design than ones based on linear control. Moreover, nonlinear controllers can, sometimes, be more cost effective while providing better performance than linear controllers [14].

Important nonlinear control techniques that emerged are nonlinear dynamic inversion, sliding mode control, and backstepping control [13, 15]. While these techniques do not suffer from a limited operation range as in the case of gain-scheduling, they do demonstrate significant dependence on the plant model. Thus, these nonlinear control techniques are not robust to cases of model mismatch.

In order to alleviate the dependence on plant model, incremental variants of these control methods were developed, as well as hybridizations of these methods [16–18]. The incremental forms of these controllers permit the usage of sensor information which makes the performance more resilient in the case of model mismatches. Indeed, incremental control techniques have demonstrated many recent successes and have been the subject of increasing attention, due to their robustness to uncertainties and their looser dependence on the model of the controlled plant [19]. Despite their demonstrated effectiveness, several theoretical gaps remain regarding their robustness. Specifically, the analyses of robustness of those methods regarding uncertainties, pure time-delays, as well as regarding the controller sampling frequency, need to be investigated [20].

First, the theoretical gap regarding the controller sampling frequency shall be elaborated on. Due to the assumptions that are made in the construction of incremental controllers, these control techniques require that the controller sampling frequency is "high enough". Indeed, the detrimental effect of smaller controller sampling frequencies on performance of an INDI-controlled motion control system can be seen from fig. 1.1, where a decreased sampling frequency had led to an increase in the normalized force error.

This theoretical gap regarding the controller sampling frequency means that what comprises a "high-enough controller sampling frequency" has not been quantified in the literature. In principle, the controller sampling frequency could simply be made exceedingly high, had it not been for hardware limitations. A dramatic example of limitations on the controller sam-

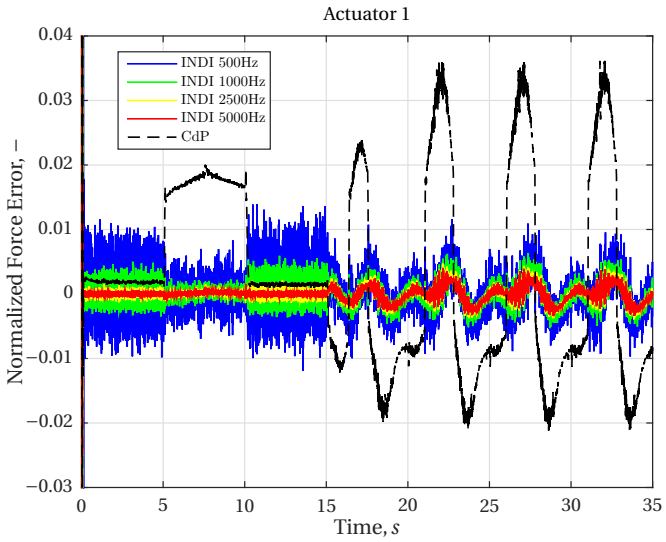

Figure 1.1: Influence of the sampling rate on the performance of the INDI control of a motion control system [1]

pling frequency occur in the case of spacecraft control systems where a controller sampling frequency of only a few Hz can be attained [21].

In principle, the problem of selecting a sampling-rate is a multi-dimensional one. That is, several factors need to be accounted for in this selection. This includes abiding by the sampling theorem as well as ensuring stability. In addition, there are a number of performance-related aspects that need to be considered. These include the effect of the sampling rate on the time response, smoothness, and arising time-delays, its influence on the effectiveness of the system in handling disturbances and parameter variations, as well as its effect on the error that arises due to measurement noise [4]. However, in this case, only the stability problem will be considered. In order to analyze the stability, the control system has to be represented appropriately. In principle, a computer-controlled system is a sampled-data system, a subset class of the more general class of hybrid dynamical systems. In general, there are three main ways that have been used to analyze sampled-data systems: as discrete-time systems, as time-delay systems, or as hybrid systems [22]. With regards to the analysis in discrete-time, the information between two sampling instances is lost. That is why, this approach is not favoured. As for the latter two, they are both considered in the analysis of sampled-data systems [22]. While the analysis as a hybrid dynamical system is expected to be a more accurate representation as it accommodates for the discrete nature of the controller and the continuous nature of the plant, the time-delay representation serves as a good starting point, that tackles the problem of determining the stable regions in the delay space of the control system.

As mentioned earlier, another of the theoretical gaps regarding the robustness of incremental controllers are time-delays. Delays are an inevitable part of control systems [23]. In aerospace computer-controlled systems, there are many sources of delay. Besides the pure time-delays occurring due to controller sampling and hold processes, time-delays may occur due to signal transmission delays, computation delays, sensor measurement delays, and physical transport delays [3, 4, 23–27]. Another source of delay that needs to mentioned is the data bus [28].

It is well known that the human operator is also a source of delay in the closed-loop control system. This is due to the physical limitations in the performance of humans; they require some time in order to perceive stimuli, process the sensory information, and react accordingly. Delays occurring from visual perception are usually ±350 ms; whereas, the vestibular system introduces slightly smaller delays which are usually less than 150 ms [26].

However, a well-known empirical result from cybernetics is the crossover model [29]. According to this model, humans, in general, adapt their control strategy so that the open-loop transfer function in the crossover region is of the form shown in

$$Y_{OL}(j\omega) = Y_p(j\omega)\,Y_c(j\omega) = \frac{\omega_c}{j\omega}\,e^{-j\omega\tau_e} \tag{1.1}$$

where ω_c denotes the crossover frequency $\left|Y_{OL}(j\omega)\right|_{\omega=\omega_c} = 1.0$ and τ_e represents an effective time-delay that accounts for information-processing delays of the pilot.

The presence of delays has an impact on stability and performance [30], and this makes the analysis of stability regions in

the delay space of control systems a subject of increasing interest [31]. For aerospace control systems, the effect of time-delays on stability and performance translates to an impact on flight safety. This is supported by the fact that it has been seen that time-delays could lead to pilot induced oscillations as well as persistent errors [32].

In alignment with this relation to flight safety, the stability regions in the delay space of a control system are important for the certification of aerospace control systems [33]. This is especially relevant for more advanced control techniques. The certification gap for adaptive control, for example, has been discussed in [33]. The authors mention that while there are intuitive metrics for robustness and performance for classical linear control methods, these metrics cannot be used for nonlinear systems. However, the time-delay margin has been proposed as one of the possible metrics that may be used to close the certification gap [33, 34].

Additionally, time-delays are particularly interesting for the stability analysis of the incremental control approaches. Besides that these approaches make use of state measurements and/or state estimates from previous timesteps, the effect of control input increments on the output need to be seen by the controller before further control increments can be determined and applied [35]. Furthermore, the need to account for delay in the analysis of incremental nonlinear dynamic inversion has been previously expressed in the literature involving the use of INDI control, as is the case in the work of Sieberling et al., Smeur et al, as well as Huang et al. [1, 3, 27]. Similarly, the performance degradation in the presence of time-delays of another incremental control technique, Incremental Backstepping (IBS), has been expressed by Koschorke [36].

To the knowledge of the author, so far, the attempts to determine the stability regions in the delay space of aerospace control systems utilizing incremental nonlinear controllers, have been limited. Towards this end, an attempt has been made based on a discretization approach of the sampled-data system for the case of a control system employing incremental nonlinear dynamic inversion (INDI) [19]. Another attempt was made for estimating the time-delay margin for the case of a system utilizing IBS controller which was an analysis in continuous time [36]. For the former, this means that the inter-sample information is lost. As for the latter, the closed-loop formulation used in this method is based on neglecting the higher-order terms as well as the assumption of time-scale separation (thus the assumptions made in the construction of the controller were also applied to the controlled plant as well). Additionally, the analysis did not consider the effect of uncertainties [36].

The preceding discussion indicates a clear knowledge gap and a design research problem to be addressed. It can, thus, be seen that there is a pressing need to investigate the effects of time-delays on the stability of incremental nonlinear dynamic inversion and to establish a reliable and versatile method to estimate the time-delay intervals for which the control system is robustly stable.

1.2 Research Objective and Research Framework

Based on the project context discussed, the following research objective has been formulated for the research problem at hand.

> The research objective is to ensure the robust stability of a flight system, controlled by an incremental nonlinear controller, in the presence of time-delays by designing a tool that can determine the stable regions in the delay space of the closed-loop control system while considering uncertainties and actuator dynamics.

Based on this research objective, the research framework depicted in fig. 1.2 was constructed. The formulation of the research framework is as follows: (a) A study of general theory on time-delay systems, as well as time domain techniques and frequency domain techniques for stability analysis leads to a collection of suitable techniques to determine the stability regions in the delay space, (b) by means of which the closed-loop linear time-delay system will be analyzed and the stability regions in the delay space of the aerospace controlled system will be determined. (c) Finally, the means to make the analysis robust are determined and implemented.

1.3 Research Questions

Subdividing the research framework shown in fig. 1.2 leads to the resulting central research questions. The first central research question reads as follows:

Q1 - What are the ways to represent the nonlinear system and the incremental controller, which is implemented on a digital computer, in order to obtain the closed-loop formulation in the form of a linear time-delay system?

The second central question is related to the confrontation occurring at the bottom left part of the research framework.

Q2 - What methods are suitable to analyze the stability of linear time-delay systems?

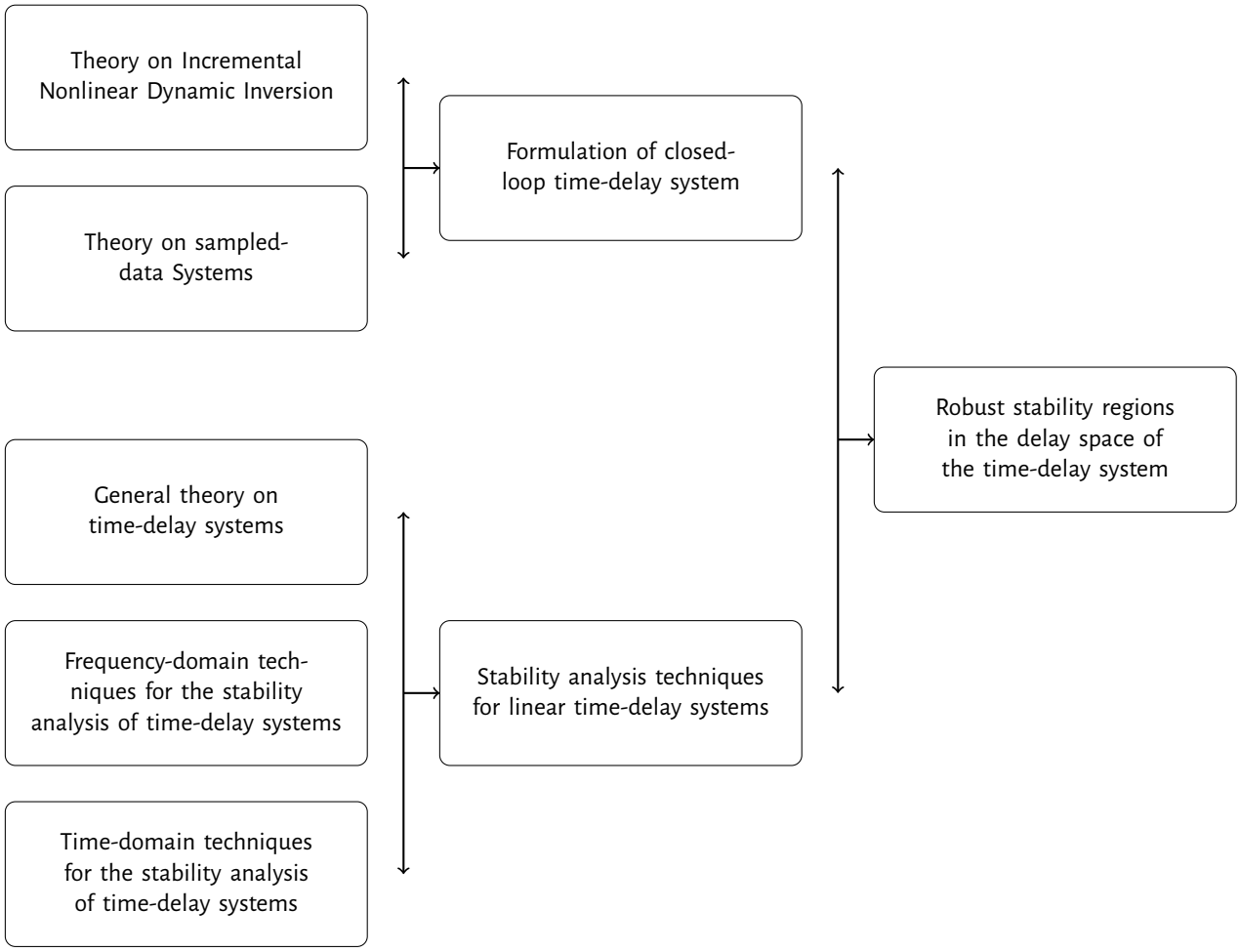

Figure 1.2: Research Framework

The final central question would be related to the rightmost part of the research framework, the confrontation occurring at the right part of the research framework.

Q3 - What are the additional steps that need to be taken to make the stability analysis robust to uncertainties in the control system?

In order to fill the knowledge gap and provide the answer to the central questions, it helps to address the following sub-questions first:

Q1.1 - What are the steps involved in constructing an INDI controller?

Q1.2 - What are the possibilities for modeling a sampled-data system as a fully continuous control system?

As for the second central questions, the sub-questions are:

Q2.1 - What are time-delay systems?

Q2.2 - What techniques can be used for the stability analysis of linear time-delay systems in the frequency domain?

Q2.3 - What techniques can be used for the stability analysis of linear time-delay systems in the time domain?

And finally, for the third central question, the following sub-questions emerge:

Q3.1 - What are suitable ways to characterize the uncertainties in the TDS system?

Q3.2 - Which existing robust stability analysis techniques for TDSs are applicable for the linear TDS obtained?

Q3.3 - Can a new technique for the robust stability analysis of time-delay systems be developed?

Moreover, subquestion *Q3.3* can be further subdivided into parts:

Q3.3.1 - What are techniques, that have been used for the robust stability analysis of systems without time-delays, which can be used to inspire a new robust stability analysis technique for the linear time-delay systems considered?

Q3.3.2 - What are the steps that can be taken in order to augment the delay-dependent stability analysis techniques implemented with those newly considered techniques, in order to make the resultant method applicable to the robust stability analysis of time-delay systems?

1.4 Report Structure

The articulated research objective and the formulated research questions define a clear scope for the research work intended for this thesis. The remainder of this report presents the thesis work that emerged from the research that has been done in the pursuit of addressing these questions.

The structure of the rest of the report is as follows. The next part of the report is an article summarizing the main scientific contribution of this thesis work. The part after that presents a literature review of the relevant building blocks in the research framework. This includes a review of the nonlinear control technique Nonlinear Dynamic Inversion (NDI) and its incremental counterpart, Incremental Nonlinear Dynamic Inversion (INDI). These are discussed in chapter 2. Thereafter, in chapter 3, a brief introduction to sampled-data systems is made, and several ways to model sampled-data systems are presented.

The three chapters after that include literature on time-delay systems. The first of these chapters, chapter 4, gives an introduction to time-delay systems which includes a discussion on the dual nature of the effects of delays on stability, the ways to represent time-delays, a classification of time-delay systems, and finally, some of the spectral properties of time-delay systems. Next, chapter 5 offers a discussion on frequency domain techniques to analyze the stability of time-delay systems, and in chapter 6 the time-domain techniques are discussed, which all mainly fall under the category of Lyapunov-based methods.

After the literature review, a part on preliminary thesis results is presented. This single-chaptered part, chapter 7, demonstrates the INDI control of a damped pendulum. It also applies a selection of techniques that were presented in the earlier chapters. Methods from both chapter 5 and chapter 6 are implemented. The determined stability regions from the implemented methods are in accord with one another. Moreover, partial verification of the results was done through simulation.[1]

Thereafter, the part that follows is dedicated to presenting relevant additional literature that has been instrumental to the final results presented in the article, which is mainly on the robust stability analysis of TDS. In particular, chapter 8 discusses the topic of uncertainty characterization, and chapter 9 presents a number of concepts, tools, and principles that can be used for the robust stability analysis of TDSs.

The part that follows, which is the one that is before the last, presents some additional results. Specifically, chapter 10 presents a derivation of new stability results in the time domain for neutral TDSs. The matrix inequalities were tested on an example from the literature. The results have proven to be efficient in comparison to existing matrix inequalities for neutral TDSs. However, it is suspected that the stability results as well as their implementation might need further verification and testing.

The last part of this report is a wrap up of this thesis work. Chapter 11 summarizes the results obtained in this thesis. It also reflects back on the research questions formulated at the beginning of the report and checks the progress on addressing these questions. After this assessment, recommendations for future research are made.

[1] Note that, chapter 2, chapter 3, chapter 4, chapter 5, chapter 6, and chapter 7 are previously graded chapters.

This page was intentionally left blank.

I

Article

This page was intentionally left blank.

Determination of Stable Time-delay Regions in Incremental Control Systems

Isabelle El-Hajj

Abstract

Incremental control techniques such as Incremental Nonlinear Dynamic Inversion (INDI) and Incremental Backstepping (IBS) have gained recent popularity, especially in the aerospace community, due to their versatility and effectiveness which entails robustness to imprecise knowledge about the controlled system as well as robustness to external disturbances. Despite a control authority that has been proven, in several applications, to exceed that of classical control techniques, there is yet much to be studied about these control techniques. Theoretical gaps include the effectiveness of these techniques in handling time-delays as well as their robustness to sampling rates. Addressing this theoretical gap has been the focus of the research that is presented in this note. To meet this research aim, the control system has been analyzed through the lens of the Time-Delay System (TDS) framework. In particular, the analytic curve frequency sweeping approach as well as a set of suitable matrix inequalities that are based on the discretized Lyapunov functional method have been applied to perform this analysis in the frequency domain and the time domain, respectively. Moreover, a new robust stability analysis technique is presented which is based on combining the analytic curve frequency sweeping approach with the edge theorem. The effectiveness of these methods has been shown through their application to an INDI-controlled damped pendulum and to the INDI-controlled short period dynamics of a fixed-wing aircraft. Finally, a number of recommendations for future research are made.

Index Terms

Time-delay systems, incremental control, robust stability analysis, analytic curve frequency sweeping approach, edge theorem, linear matrix inequality, Bessel-Legendre inequality, Legendre polynomials, discretized Lyapunov functional method, commensurate delays, parametric uncertainty.

NOMENCLATURE

A_0	Matrix associated with the delay-free state vector.	$L_k(s)$	Legendre polynomial.
A_1	Matrix associated with the delayed state vector.	N	Discretization variable.
$\mathbf{a}$	Coefficient vector of a quasipolynomial.	P	Symmetric matrix.
b	Dampling coefficient of the pendulum ($\frac{kg \cdot m^2}{s}$).	P_N	Positive-definite matrix.
C	Matrix associated with the derivative of the delayed state vector.	Q	Uncertainty bounding set, Matrix that is part of stability result.
E_k	Edge of a polytope.	q	Pitch rate (rad/s).
F	Family of uncertain quasipolynomials.	$\mathbf{r}$	Exponent coefficient vector of a quasipolynomial.
f	System dynamics.	R	Symmetric positive-definite matrix.
f_λ	Derivative of f with respect to λ.	$\mathfrak{R}$	Real part of complex variable.
f_τ	Derivative of f with respect to τ.	R_N	Symmetric positive-definite matrix.
g	Gravitational acceleration of an object in a vacuum near the surface of the Earth ($\frac{m}{s^2}$).	S	Symmetric positive-definite matrix.
G	Control effectiveness matrix.	$\mathcal{S}_n^+$	Set of symmetric positive-definite matrices.
G_N	Matrix to transform from $\xi_N(t)$ to $\tilde{x}_N(t)$.	$\mathscr{T}_D(t)$	Solution operator of a time-delay system.
H_N	Matrix to transform from $\xi_N(t)$ to $\dot{\tilde{x}}_N(t)$.	$\mathscr{T}_N(t)$	Solution operator of a time-delay system.
I	Moment of inertia of the pendulum ($kg \cdot m^2$).	t	Time (s).
I_n	Identity matrix of dimensions n by n.	$\mathbf{u}$	Control input vector.
$\mathfrak{I}$	Imaginary part of a complex variable.	V_F	Value set of family of quasipolynomials.
J_N	Matrix to transform from $\psi_N(t)$ to $\xi_N(t)$.	X	Symmetric matrix.
k_d	Derivative gain.	$\mathbf{x}$	State vector.
k_p	Proportional gain.	$\tilde{x}_N$(t)	Augmented state vector.
l	Length of the pendulum (m).	Y	Symmetric positive-definite matrix.
		$\mathbf{y}$	Output vector.

I. El-Hajj is a graduate student at the Control and Simulation Group at the Faculty of Aerospace Engineering at Delft University of Technology Kluyverweg 1, 2629HS Delft, the Netherlands.

z	Variable to denote $e^{-j\omega\tau}$.	$\boldsymbol{\nu}$	Virtual control input vector.
$\tilde{z}$	Augmented state vector.	ξ_N(t)	Augmented state vector.
α	Angle of attack (rad).	σ	Spectrum of the delay-difference equation.
γ	Part of the matrix Γ_N.	σ_e	Essential spectrum of the delay-difference equation.
Γ_N	Matrix that is part of the matrix H_N.		
Δ	Increment in one time-step.	τ	Time-delay (s).
ζ	Initial condition for the input of the time-delay system.	ϕ	Initial condition for the state of the time-delay system.
θ	Time-delay (s), Angular deflection of the pendulum (rad).	ψ_N(t)	Augmented state vector.
		ω	Imaginary part of the characteristic root (rad/s).
λ	Characteristic root (rad/s).	∇	Gradient operator.
μ	Portion of an edge of a polytope.		

I. Introduction

Processes in real systems do not occur instantaneously. This makes delays an inevitable part of control systems [1]. The presence of delays has an impact on stability and performance [2], and this makes the analysis of stability regions in the delay space of control systems an important aspect [3]. This issue, alongside other reasons, has led to an increased interest in Time-delay Systems (TDS)s (which are also known as hereditary systems or systems with aftereffects [4]), and this is reflected in the tremendous amount of research that has been performed on the subject.

In the field of aerospace, notwithstandingly, the importance of taking the presence of delays into account in the stability analyses is great. In aerospace computer-controlled systems, there are many sources of delay. Besides the pure time-delays occurring due to controller sampling and hold processes, time-delays may occur due to signal transmission delays, computation delays, sensor measurement delays, and physical transport delays [1], [4]–[9]. Another source of delay that needs to be mentioned is the data bus [10]. Furthermore, if the vehicle is piloted, the human operator introduces another source of delay in the closed-loop control system. This is due to the physical limitations in the performance of humans; they require some time in order to perceive stimuli, process the sensory information, and react accordingly [8].

Furthermore, for aerospace control systems, the effect of time-delays on stability and performance translates to an impact on flight safety. This is supported by the fact that it has been seen that time-delays could lead to pilot induced oscillations as well as persistent errors [11]. In alignment with this relation to flight safety, the stability regions in the delay space of a control system are important for the certification of aerospace control systems [12]. This is especially relevant for more advanced control techniques. The certification gap for adaptive control, for example, has been discussed in [12]. The authors mention that while there are intuitive metrics for robustness and performance for classical linear control methods, these metrics cannot be used for other classes of control systems, such as nonlinear systems. However, the time-delay margin has been proposed as one of the possible metrics that may be used to close the certification gap [12], [13].

Additionally, time-delays are particularly interesting for the stability analysis of the incremental control approaches, a group of techniques that has demonstrated many recent successes and has been the subject of increasing attention, due to its robustness to uncertainties and its looser dependence on the model of the controlled plant [14]. Besides that these approaches make use of state measurements and/or state estimates from previous time-steps, the effect of the control input increments on the output needs to be seen by the controller before further control increments can be determined and applied [15]. The need to account for time-delays in the analysis of INDI has been expressed by Sieberling et al., Smeur et al, as well as Huang et al. [6], [9], [16]. Similarly, another incremental control technique, Incremental Backstepping (IBS), has shown performance degradation in the presence of time-delays [17]. An analysis of the robustness regarding time-delays presents one of the theoretical knowledge gaps regarding incremental control techniques.

Another related theoretical gap is the robustness of an incremental control system to the sampling rate. Due to the assumptions that are made in the construction of incremental controllers, these control techniques require that the controller sampling frequency is "high". Indeed, the detrimental effect of smaller controller sampling frequencies on the performance of an INDI-controlled motion control system can be seen in the work of Huang et al. [16]. The theoretical gap regarding the controller sampling frequency means that what comprises a "high-enough" controller sampling frequency has not been quantified in the literature. Despite being a complex and multifaceted problem, the selection of a suitable sampling rate, in relation to its effect on stability, is connected to the problem of determination of the stable time-delay regions in the delay space of the control system. Therefore, the two aforementioned knowledge gaps can be tackled though determining the stability regions in the time-delay space of incremental control systems.

To the knowledge of the author, so far, there have been two main attempts to determine the stability regions in the delay space of aerospace control systems utilizing incremental nonlinear controllers. One has been based on a discretization approach of the sampled-data system for the case of a control system employing incremental non-linear dynamic inversion (INDI) [14]. The other attempt was made for estimating the time-delay margin for the case of a system utilizing Incremental Backstepping (IBS) controller which was an analysis in continuous time [17]. In the case of the discretization approach, this means that the

inter-sample information is lost. As for the latter attempt, the closed-loop formulation used in this method is based on neglecting the higher-order terms as well as the assumption of time-scale separation (thus the assumptions made in the construction of the controller were also applied to the controlled plant). Additionally, the analysis did not consider the effect of uncertainties [17].

In this article, this knowledge gap is addressed through the implementations of techniques in both the frequency domain and the time domain that can determine the time-delay intervals for which the control system is robustly stable. Specifically, this article implements the analytic curve frequency sweeping approach. It also applies a set of matrix inequalities that are based on the discretized Lyapunov functional method. The analysis in the frequency domain is made robust through the edge theorem. As for the time domain analysis, vertex results can be leveraged in the case of subpolytopic uncertainty, and the results obtained corroborate those from the frequency domain analysis.

The organization of the article is as follows. First, a brief review of INDI is presented in section II. Thereafter, a primer on TDSs is discussed in section III. This is followed by section IV, which represents a select number of stability methods that will be applied to the stability analysis of the system. After that, a discussion on a number of concepts and theorems that are relevant for the robust stability analysis of TDSs is presented in section V. The proposed methods are applied on an INDI-controlled pendulum in section VI and on the INDI control of short period dynamics in section VII. The final section, section VIII, summarizes the contribution of this article and presents a number of recommendations for future research.

II. Incremental Nonlinear Dynamic Inversion (INDI)

The INDI control approach emerged as a more robust variant of NDI by alleviating the dependency control approach on the plant model. This is realized by linearizing the system about the current state and control input. The incremental form that arises allows to feed back sensor measurements. As will be seen in the following, for INDI, only the knowledge of the value of the control effectiveness matrix is needed.

In the following, the continuous-time formulation for INDI will be presented. It should be noted that for INDI, a system which is affine in the control should be considered. A general example of such a system is shown in eq. (1). This equation is the starting point for the discussion on the continuous-time formulation of INDI.

$$\begin{aligned} \dot{\mathbf{x}} &= f(\mathbf{x}) + G(\mathbf{x})\mathbf{u} \\ y &= h(\mathbf{x}) \end{aligned} \tag{1}$$

Linearizing the dynamics in this equation leads to eq. (2).

$$\dot{\mathbf{x}} \approx \dot{\mathbf{x}}_0 + \mathbf{G}\left(\mathbf{x}_0\right)\left(\mathbf{u}-\mathbf{u}_0\right) + \left.\frac{\partial[f(\mathbf{x})+\mathbf{G}(\mathbf{x})\mathbf{u}]}{\partial \mathbf{x}}\right|_0 \left(\mathbf{x}-\mathbf{x}_0\right) + \mathbf{O}\left[\left(\mathbf{x}-\mathbf{x}_0\right)^2\right] \tag{2}$$

Neglecting the higher order terms in the linearized system dynamics shown in eq. (2) leads to the following:

$$\dot{\mathbf{x}} \approx \dot{\mathbf{x}}_0 + \mathbf{G}\left(\mathbf{x}_0\right)\left(\mathbf{u}-\mathbf{u}_0\right) + \left.\frac{\partial[f(\mathbf{x})+\mathbf{G}(\mathbf{x})\mathbf{u}]}{\partial \mathbf{x}}\right|_0 \left(\mathbf{x}-\mathbf{x}_0\right) \tag{3}$$

As mentioned in the introduction, this simplification holds for cases where the control sampling frequency is "high", but for which a specific requirement has not been previously quantified in the literature [16], [18].

Furthermore, following the usual derivation pipeline of INDI, time-scale separation is assumed. This means that the actuator dynamics are assumed to be fast and that the evolution of the state variables is quite slow in comparison. This assumption allows to neglect the term involving the change in state, which leaves eq. (4).

$$\dot{\mathbf{x}} \approx \dot{\mathbf{x}}_0 + \mathbf{G}\left(\mathbf{x}_0\right)\left(\mathbf{u}-\mathbf{u}_0\right) = \dot{\mathbf{x}} \approx \dot{\mathbf{x}}_0 + \mathbf{G}\left(\mathbf{x}_0\right)\Delta\mathbf{u} \tag{4}$$

After the linearization, the virtual control $\boldsymbol{\nu}$ can replace $\dot{\mathbf{x}}$ and the inversion of the dynamics is performed. Thereafter, the incremental control is obtained.

$$\Delta\mathbf{u} = \hat{\mathbf{G}}^{-1}\left(\boldsymbol{\nu}-\dot{\mathbf{x}}_0\right) \tag{5}$$

Thus, the control law is of the form shown in eq. (6).

$$\mathbf{u} = \mathbf{u}_0 + \hat{\mathbf{G}^{-1}}\left(\boldsymbol{\nu}-\dot{\mathbf{x}}_0\right) \tag{6}$$

III. TIME-DELAY SYSTEMS

A. Representation of Time-delay Systems

Time delay systems are usually described by functional differential equations. Equation (7) shows a functional differential equation that represents a generic TDS [19].

$$\begin{cases} \dot{x}(t) = f\left(t, x(t), x_t, u_t\right) & \\ x_{t_0} = \phi(\theta), & \forall\theta \in [t_0 - \tau, t_0] \\ u_{t_0} = \zeta(\theta), & \forall\theta \in [t_0 - \tau, t_0] \end{cases} \tag{7}$$

In this equation, ϕ and ξ denote the initial conditions for the state and the input, respectively. Moreover, τ denotes a time-delay, and as such $\tau > 0$. As for x_t, it is defined according to eq. (8):

$$x_t : \begin{cases} [-\tau, 0] \to \mathbb{R}^n \\ \theta \mapsto x_t(\theta) = x(t+\theta) \end{cases} \tag{8}$$

and u_t is defined according to eq. (9):

$$u_t : \begin{cases} [-\tau, 0] \to \mathbb{R}^n \\ \theta \mapsto u_t(\theta) = u(t+\theta) \end{cases} \tag{9}$$

The notation x_t and u_t corresponding to the definitions in eq. (8) and eq. (9) is referred to as the Shimanov notation. Moreover, it is clear that eq. (7) shows the dependence of the functional differential equation on current as well as past states and inputs.

B. Classification of Time-delay Systems

TDSs are described and categorized based on a number of aspects including the model of the delay, the number of delays in the systems, and the type of delays in the system. Each of these categories will be discussed in the following.

1) Model of Delay: Discrete or Distributed

There are two main ways to model delays: either as discrete (also referred to as point-wise delays) or as distributed delays. States with discrete delays in their arguments such as $x(t-\tau)$ can be understood as values from a specific moment in the past which is in this case $t-\tau$. Furthermore, a discrete delay may either be constant or may vary with time. This again means that the dynamics depend on a precise moment in the past, but this pointwise moment varies with time.

The choice of whether to model a time-delay as fixed or as time-varying is important for the validity of the results. Furthermore, when the systems with discrete delays are compared with the systems with time-varying delays, the phenomenon of quenching is witnessed. That is, quenching happens at certain time-delays at which the system with discrete time-delays is stable but for which when the time-delays are assumed to be time-varying, stability is lost (or vice versa, i.e. having stable delay intervals for the case of time-varying delays for which the TDS with discrete delays is no longer stable) [20].

As for distributed delays, the states from an interval of time occurring in the past $[-\tau_1, -\tau_2]$, where $\tau_1 > \tau_2 \geq 0$, are used. This interval is then weighed with a kernel. It is this information that is incorporated into the dynamics [21]. An example of a system with distributed delay is shown in eq. (10) [22].

$$\dot{x}(t) = \int_{-r}^{0} c(\theta) x(t+\theta) d\theta \tag{10}$$

It should be remarked that the information captured by modeling the dependence on past information through distributed delays is a more complex but richer representation. Distributed delays are able to incorporate "memory" of a sequence occurring in the past which is more insightful than just looking at discrete points in the past. An example of using distributed delays in the representation of a system is in the case of describing the delay response of human drivers. Physically, the interpretation for the use of distributed delays rather than discrete delays is that drivers make use of a cumulative continuous stream of past information they have perceived to take a control action [23].

Besides their use in the system representation, distributed time-delays are also important in the derivation of delay-dependent stability criteria in the time-domain, for TDSs with point-wise delays.

2) Type of Delay: Retarded or Neutral

Another important classifying aspect for TDSs is how the delay influences the states or the derivatives of the states in the system [21]. There are three main ways in which delays influence the states or the derivatives of the states in the system. Those are the retarded type TDSs, the neutral type TDSs, and the advanced type TDSs. It is important to make this distinction between the types because the type has important implications on the properties of the system, on the necessary conditions for their stability, and consequently, on the approaches for stability analysis. In the following, it is explained how to differentiate between those three types.

In the case of retarded TDSs, the highest order derivative in the system is not affected by time-delays. The general form of the retarded type TDS is given by the functional differential equation given in eq. (11) [24].

$$\dot{x}(t) = f\left(t, x_t\right) \tag{11}$$

A generic example of a retarded TDS is eq. (12).

$$\dot{x}(t) = A_0 x(t) + \sum_{i=1}^{m} A_i x\left(t - \tau_i\right) \tag{12}$$

However, for neutral TDSs, there are two terms with the highest-order derivative, one that does depend on the time-delay and another that does not. The general form of the neutral type TDS is given by the functional differential equation in eq. (13) [24].

$$\dot{x}(t) = f\left(t, x_t, \dot{x}_t\right) \tag{13}$$

A generic example of neutral TDS is eq. (14), where the term indicated with the underbrace is commonly referred to as the delay-difference operator.

$$\frac{d}{dt}\left(\underbrace{x(t) + \sum_{k=1}^{m} Cx\left(t - \tau_k\right)}_{\text{Delay-difference operator}}\right) = A_0 x(t) + \sum_{i=1}^{m} A_i x\left(t - \tau_i\right) \tag{14}$$

Moreover, the equation based on the delay-difference operator (also known as the discrete kernel operator [24]), shown in eq. (15), is that of associated delay-difference equation. The stability of this equation is tied to that of the neutral TDS as will be discussed later.

$$x(t) + \sum_{k=1}^{m} Cx\left(t - \tau_k\right) = 0 \tag{15}$$

As for the case where there is only one term for the highest-order derivative and this term depends on the time-delay, this case characterizes an advanced type TDS [21], [24], [25].

The distinction between the three types is further clarified with the examples of the scalar systems shown in eq. (16), eq. (17) (as taken from [26]), and eq. (18). From eq. (16), it can be seen that the highest order derivative which is a second order derivative does not depend on the state, but the first order derivative does. Thus, although there are state derivatives that depend on the delays in the system, this is a retarded type TDS.

$$\ddot{x}(t) = a\dot{x}(t - \tau) + bx(t), \quad x(t) \in \mathbb{R} \tag{16}$$

As for eq. (17), it can be seen that the highest-order derivative does also depend on the time-delay: $\ddot{x}(t - \tau)$. Therefore, this system is of neutral type.

$$\ddot{x}(t) = a\ddot{x}(t - \tau) + bx(t), \quad x(t) \in \mathbb{R} \tag{17}$$

Moreover, if the case where the $\ddot{x}(t)$ of eq. (17) is no longer part of the equation is encountered, as in the case shown in eq. (18), this becomes an advanced type TDS since the term with the highest order derivative, $a\ddot{x}(t - \tau)$, depends on the time-delay.

$$a\ddot{x}(t - \tau) + bx(t) + \dot{x}(t) = 0, \quad x(t) \in \mathbb{R} \tag{18}$$

It should be noted however that, for the sake of engineering applications, the advanced type is not as relevant [24]. The reason for this is that, in an advanced type TDS, the quantity described by the dynamics depends on its future values [27]. Since the dependence of a state on future values is not physically possible, only the retarded and the neutral types will be discussed in the parts to follow.

One main difference between retarded TDSs and neutral TDSs is the smoothness of solutions of the system. While for the case retarded TDSs, the solutions become smoother with the passing of time, such a smoothing effect does not always occur in the case of neutral TDS.

Another difference occurs in the spectral properties of the TDSs. In the case of retarded TDSs, it is guaranteed that there will be a finite number of roots to the right side of any vertical line drawn in the complex plane. However, in the case of neutral TDSs, there may be an infinite number of unstable roots. The stability of the delay-difference operator however induces

the number of unstable roots for the neutral TDS to become finite. The discussion on the spectral properties will be further developed in section III-C.

3) Number of Delays: Single or Multiple Delays

The final aspect to consider in the classification of TDSs relates to the number of delays in the system. The two categories here are the case of single delay in the system or multiple delays. If there are multiple delays in the system, it may either be the case of commensurate delays (when the delays are multiple of a certain baseline delay) or incommensurate delays [21].

It should be noted that a slightly confusing terminology has been adopted in the literature to describe systems with commensurate delays. Despite there being multiple delays in such a system, the system is referred to as a single delay system. In order to determine what multiple of the baseline delay occur in the system, the commensurate degree (denoted by L) is introduced. Therefore, when the terms $x_1(t-\tau), x_2(t-2\tau)$ and $x_3(t-3\tau)$ are present in the system, the commensurate degree is 3, i.e. $L = 3$. As for the case of a system with a single delay, the commensurate degree is 1, i.e. $L = 1$.

Dealing with TDSs with incomensurate delays is often much more complicated than dealing with TDSs with commensurate delays. One key challenge is the computational complexity which in the case of the stability analysis of multiple-delay systems is $\mathcal{NP}$-hard. Here, $\mathcal{NP}$ stands for non-deterministic polynomial time. However, it should be noted that $\mathcal{NP}$-hard problems constitute a completely different set of problems than that of $\mathcal{NP}$ problems. For both classes of problems, it is not possible to obtain a solution that is tractable and scalable with the size of the problem. Here, tractable means that the problem can be solved in polynomial time even in worst-case scenarios. The key difference between $\mathcal{NP}$ and $\mathcal{NP}$-hard problems is that for $\mathcal{NP}$ problems verifying a postulated solution is possible using a polynomial-time algorithm while for $\mathcal{NP}$-hard problems, it isn't. This makes $\mathcal{NP}$-hard problems the toughest class of problems to deal with.

To give an intuition of why the problem of analyzing the stability of TDSs with incommensurate delays is $\mathcal{NP}$-hard, consider the stability analysis of a system with two distinct delays. This problem may be considered as the stability analysis of a system with commensurate delays but whereby all possible ratios between the two delays are attempted. Clearly, this makes it an intractable problem [21]. A formal proof of the $\mathcal{NP}$-hardness of the stability analysis in the case of incommensurate delays is provided by Gu et al. in [22].

C. Spectral Properties of Time-delay Systems

It is important to discuss the spectral properties of TDSs, as the spectral properties provide useful insights for the stability analysis techniques that will be explained later. Some of the spectral properties of retarded TDSs and of neutral TDSs will be individually discussed. However, before this discussion ensues, there are main properties that are applicable to the spectra of both retarded and neutral TDSs that need to be mentioned.

First and foremost, TDSs have infinitely many roots, and this is one of the aspects that reflect the infinite dimensional nature of TDSs. This property is easily seen from examining the characteristic quasipolynomial of any TDS. The Laplace transform of delayed terms such as $x(t-\tau)$ leads to exponential terms in the characteristic equation. Since the exponential function is a transcendental function, its presence in the characteristic equation leads to an infinite number of zeros [28], [29].

Another important property of the spectrum of both retarded and neutral type TDSs is that when the coefficients of the quasipolynomial are real, the spectrum is symmetric with respect to the x-axis. This is applicable in the case of both retarded and neutral TDSs.

1) Spectral Properties of Retarded Time-delay Systems

Despite there being infinitely many characteristic roots, usually there is a finite number of unstable roots. For retarded systems, this is always applicable. As for neutral systems, this is guaranteed when the delay-difference operator is stable [29]. Conversely, when the delay-difference operator is unstable, there can appear infinitely many unstable roots for the neutral TDS [3].

For retarded TDSs, if there is a sequence of roots whose magnitude tends to $+\infty$, then the real part of those roots tends to $-\infty$. [29]. This is in alignment with the property that retarded systems have a finite number of unstable roots. That is, if the magnitude is getting increasingly large and it is known that the number of unstable roots has to be finite, then it must be that those roots are tending towards the extremes of the other half-plane. If there exists a sequence $\{\lambda_k\}$ of characteristic roots of the retarded system such that $\lim_{k\to\infty} \Re(\lambda_k) \to -\infty$ [29].

Additionally, there is a finite number of roots within any vertical strip in the complex plane. The vertical strip is formally expressed in eq. (19) where $\alpha, \beta \in \mathbb{R}$ and $\alpha < \beta$.

$$\{\lambda \in \mathbb{C} : \alpha < \Re(\lambda) < \beta\} \tag{19}$$

A special case of this property occurs when this vertical strip is narrowed down to an infinitesimally thin strip about the imaginary axis. Thus, it can be said that the number of eigenvalues on the imaginary axis is always finite.

Another property is that there is a vertical line to the left-side of which will be all the roots of the retarded TDS. Let this vertical line be represented with $x = \gamma$. Formally, this is described with eq. (20).

$$\{\lambda \in \mathbb{C} : \Re(\lambda) < \gamma\} \tag{20}$$

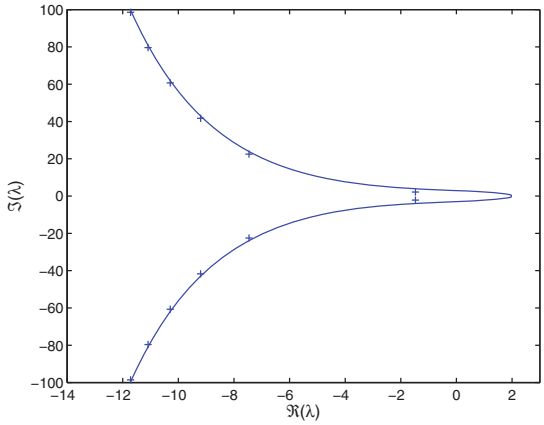

Fig. 1: Example curve envelope of the spectrum of a TDS [29].

An even stronger case of the latter is the proposition that yields the envelope curve of the spectrum. For the retarded TDS described by eq. (12), the envelope is described by eq. (21). The proof for this proposition is provided by Michiels et al. in [29]. An example of such an envelope is shown in fig. 1.

$$|\lambda| \leq \|A_0\|_2 + \sum_{i=1}^{m} \|A_i\|_2 \, e^{-\Re(\lambda)\tau_i} \tag{21}$$

The envelope curve provides very nice information regarding the location of the Critical Imaginary Root (CIR)s which are the roots of the characteristic equation that occur on the imaginary axis of the complex plane. Knowing about the presence and location of the CIRs is important because, for retarded systems, the gain or loss of stability is related to the crossing of the imaginary axis. Being imaginary roots, λ in eq. (21) can be replaced with $j\omega$. Moreover, the real part of the characteristic root is zero i.e. $\Re(j\omega) = 0$. This leads to eq. (22) [29].

$$\begin{aligned} |j\omega| &\leq \|A_0\|_2 + \sum_{i=1}^{m} \|A_i\|_2 \, e^0 \\ \implies |\omega| &\leq \|A_0\|_2 + \sum_{i=1}^{m} \|A_i\|_2 \\ \implies |\omega| &\leq \sum_{i=0}^{m} \|A_i\|_2 \end{aligned} \tag{22}$$

From eq. (22), it is known that there is an interval over the imaginary axis of finite width that is guaranteed to contain the CIRs. It can also be noted, based on this inequality, that this interval is independent of the delay values [29].

The spectra of retarded TDSs also possess nice continuity properties. That is, the characteristic roots behave continuously with respect to the variations of system matrices and delays. Additionally, the spectral abscissa, which is the largest real part available from the roots in the spectrum i.e. $\max_i \{\mathrm{Re}\,(\lambda_i)\}$, is also continuous with respect to these variations.

2) Spectral Properties of Neutral Time-delay Systems

The properties of the spectrum of the associated delay-difference equation, shown in eq. (15), heavily dictate those of the spectrum of the neutral type TDS. It is also this aspect that leads to the additionaly necessary stability condition for the exponential stability of the null solution of the neutral type TDS, which is the exponential stability of the null solution of the delay-difference equation [29].

An important aspect of the relation between the spectrum of the neutral type TDS and that of the associated delay difference equation is that the real part of the sequence of characteristic roots $\{\lambda_n\}_{n\geq 1}$ of the neutral type TDS (eq. (14)) tends to the limit of that of the delay-difference equation, denoted by ζ. Moreover, the imaginary part of the sequence of characteristic roots tends to infinity; thus, the neutral TDS is said to have vertical asymptotic chains [30]. Both of these characteristics are expressed in eq. (23).

$$\lim_{n\to\infty} \Re\,(\lambda_n) = \zeta, \quad \lim_{n\to\infty} = \Im\,(\lambda_n) = \infty \tag{23}$$

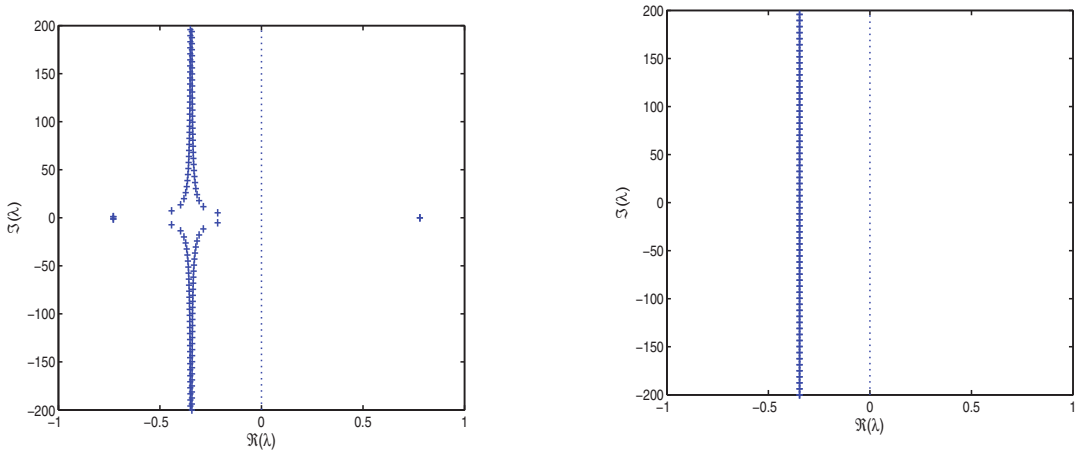

(a) Spectrum of the neutral type TDS [29].

(b) Spectrum of the corresponding delay-difference equation [29].

Fig. 2: Spectrum of a neutral type TDS and that of the corresponding delay-difference equation.

An example spectrum demonstrating these properties is shown in fig. 2. Examining the spectrum of the neutral TDS shown in fig. 2a, it can be seen that the sequence of eigenvalues tends to the vertical line at around -0.35, which happens to be the location of where all the roots of the delay-difference equation are located, as seen in fig. 2b.

Another property is that neutral type time-delay equation has a finite number of roots that are in the right-half plane and that are to the right of the spectral abscissa of the delay-difference equation, which is denoted by c_D. This again can be seen from fig. 2a where it can be seen that there is only one root in the right half-plane, which also happens to be on the right-hand side of the spectral abscissa of the characteristic roots of the delay-difference operator which occurs at about -0.35.

Small perturbations can remove the stability of the delay-difference equation, which is known as the delay sensitivity problem of the delay-difference equation. This susceptibility to small perturbations is eliminated when the delay-difference equation is strongly stable, which is ensured when condition eq. (24) is satisfied. In this case, it can also be said that the delay-difference operator is strongly stable.

$$\sum_{k=1}^{m} \|C\| < 1 \tag{24}$$

When the strong stability of the delay-difference operator is ensured, the loss or gain of stability, as in the case of retarded TDSs, is related to crossing the imaginary axis in the complex plane. This ties to the fact that, as mentioned earlier, the strong stability of the delay-difference operator induces a finite number of unstable roots.

IV. Methodology for Stability Analysis

In the following, two approaches for the stability analysis of TDSs, which will be applied later on, are discussed: the analytic curve frequency sweeping approach and the stability results in the form of matrix inequalities based on the discretized Lyapunov functional method. The former method involves an analysis in the frequency-domain, while the latter results are constructed for an analysis in the time domain. The reason to consider methods that pertain to each of the frequency domain and the time domain is that each presents its own set of advantages. Particularly, the main advantage of the frequency domain methods is their relative simplicity in comparison to the time-domain-based methods. Their main drawback, however, is their exclusive applicability to LTI systems. In relation to this aspect, the stability results that are derived in the time-domain have the advantage that they can more readily deal with nonlinearities and time-varying systems [22]. Their major drawback is that the stability results are applicable to the systems for which they were derived, which have a specific structure.

A. Analytic Curve Frequency Sweeping Approach

The stability analysis of LTI systems can usually be performed by examining the real parts of the eigenvalues of a control system. However, in the case of LTI TDSs, due to their infinite-dimensional nature, it is preferable to circumvent determining the eigenvalues of the closed-loop system, and some of the properties mentioned earlier allow that.

One of the properties of TDSs that have been previously discussed is that there is a finite number of characteristic roots in the right half-plane for retarded TDSs and for neutral TDSs with strongly stable delay-difference operators. Moreover, this property bore a stability property: that the gain or loss of stability of these systems is determined by the crossing of the imaginary axis.

Therefore, the stability problem gets transformed into one of counting the number of unstable roots as the time-delay(s) is/are varied. This is done based on determining the crossings with the imaginary axis and determining the time-delays at which these crossings occur. The combinations of the CIRs with their associated time-delays are known as critical pairs. With the delay intervals or regions (for the case of multiple delays) established, the final step is to determine whether the intervals/regions are stable or not. It should be noted that there have been many different methods discussed in the literature for the implementation of the first two od the three previously mentioned steps.

The analytic curve frequency sweeping approach, described in [28], is a stability analysis method that follows these three main steps. It makes use of frequency sweeping in order to determine the critical pairs. The frequency sweeping is combined with an eigenvalue perturbation-based approach to study the asymptotic behaviour of the critical pairs. Finally, the stable time-delay regions are determined through thorough book-keeping of the number of unstable roots. In the following, the details of these three main steps for this outlined approach are discussed.

1) Critical Pairs

One of the ways to detect CIRs is through the frequency sweeping curves. The construction of frequency sweeping curve(s) is as follows. The frequencies in a certain range with a certain step size are iterated over. For each frequency, the value(s) for z are determined, where z is defined as $z = e^{-j\omega\tau}$. Thereafter, the magnitude(s) of the z value(s) are obtained. These values are plotted against the values of ω at which they were obtained. Note that each z expression corresponds to one frequency sweeping plot. The CIRs are the intersections with the horizontal line $\Gamma = 1$.

It can be seen that frequency sweeping can be done programmatically as well. The risk of this, however, is that an automated procedure eliminates the human's role in determining the CIRs. This means that if the steps used in the frequency sweeps are too large, that some roots may be missed.

In order to make use of the automated determination of the CIRs through programmatic frequency sweeping and avoid problems of undetected roots, the frequency sweeping curves can be generated as well, which can be later checked to verify whether all the CIRs have been determined. If the possibility of missed roots is noticed, the analysis is repeated using smaller frequency steps.

2) Asymptotic Behaviour of Critical Pairs

The crossing direction of an imaginary root is defined as the sign of the change in the value of eigenvalues around the imaginary axis with respect to an increase in the time-delay. This is shown in eq. (25).

$$CDIR = \text{sign}\left[\frac{d\lambda}{d\tau}\right]_{\lambda=\omega_{C,i}} \tag{25}$$

If a CIR is simple, then the asymptotic behaviour can be studied based on the implicit function theorem from which it holds that expression for $\frac{d\lambda}{d\tau}$ can be determined with eq. (26).

$$\frac{d\lambda}{d\tau} = -\frac{f_\tau}{f_\lambda} \tag{26}$$

However, when the multiplicity of the root is larger than 1, then the implicit function theorem no longer applies. In this case, an alternative is to study the asymptotic behaviour through a series expansion of the relation between a time-delay τ and the characteristic root λ. Since the Puiseux series allows to describe the local behaviour of a power series, the asymptotic behaviour can be studied through n Puiseux series, where n is an important index that will be explained in the following paragraphs [28]. To the knowledge of the author, Chen et al. were the first to use an eigenvalue perturbation-based approach to determine the asymptotic behaviour of the CIRs and to consequently determine the regions of stability [31].

The procedure for obtaining the Puiseux series is summarized with algorithm 1, obtained from [28]. However, before proceeding with presenting the algorithm, there are two important non-negative indices that need to be discussed, the indices n and g, that are associated with a critical pair $(\lambda_a, \tau_{a,k})$. The index n is defined according to eq. (27).

$$f_{\lambda^0} = \cdots = f_{\lambda^{n-1}} = 0, f_{\lambda^n} \neq 0 \tag{27}$$

From this definition, it can be seen that the index n corresponds to the multiplicity of a critical pair. As for the index g, it is defined according to eq. (28).

$$f_{\tau^0} = \cdots = f_{\tau^{g-1}} = 0, f_{\tau^g} \neq 0 \tag{28}$$

It should be noted that both of the indices are guaranteed to be bounded if the CIR to which they are associated is not zero [28]. Moreover, one of the properties is that the index g is constant for all $\tau_{\alpha,k}$. However, the index n can possibly vary with $\tau_{\alpha,k}$.

Now that the definitions of those two important indices have been established, the algorithm for obtaining the Puiseux series of a quasipolynomial at a critical pair can be presented, and it reads as shown in algorithm 1.

Algorithm 1 Algorithm to determine the Puiseux series [28]

procedure GETPUISEUXSERIES($f(\lambda,\tau), n, g$)
  $\alpha_0 \leftarrow 0$
  $\beta_0 \leftarrow g$
  while True **do**
    $\mu \leftarrow \max\left\{\frac{\beta_0-\beta}{\alpha-\alpha_0} > 0 : L_{\alpha\beta} \neq 0, \alpha > \alpha_0, \beta < \beta_0\right\}$ ▷ Note that $L_{il} = \frac{f_{\lambda i}\tau^l}{(i+l)!}\begin{pmatrix} i+l \\ i \end{pmatrix}\begin{pmatrix} i+l \\ i \end{pmatrix}$
    if μ exists **then**
      Determine all nonzero $L_{\alpha\beta}$ such that $\frac{\beta_0-\beta}{\alpha-\alpha_0} = \mu$
      Form the set $\left\{L_{\alpha_1\beta_1}(\Delta\lambda)^{\alpha_1}(\Delta\tau)^{\beta_1}, L_{\alpha_2\beta_2}(\Delta\lambda)^{\alpha_2}(\Delta\tau)^{\beta_2}, \ldots\right\}$ such that $\alpha_1 > \alpha_2 > \ldots$
      Determine coefficients satisfying the equation $L_{\alpha_1\beta_1}C^{\alpha_1-\alpha_0} + L_{\alpha_2\beta_2}C^{\alpha_2-\alpha_0} + \cdots + L_{\alpha_0\beta_0} = 0$ ▷ denoted $\widetilde{C}_{\mu,l}$
      $\Delta\lambda \leftarrow \widetilde{C}_{\mu,l}(\Delta\tau)^{\mu} + o\left((\Delta\tau)^{\mu}\right), l = 1, \ldots, \alpha_1 - \alpha_0$
      $\alpha_0 \leftarrow \alpha_1$
      $\beta_0 \leftarrow \beta_1$
    else
      return $\Delta\lambda(\Delta\tau)$
    end if
  end while
end procedure

Once the Puiseux series $\Delta\lambda(\Delta\tau)$ are obtained, the effect of $\Delta\tau = +\epsilon$ and $\Delta\tau = -\epsilon$ on the real part of $\Delta\lambda$ can be determined. Based on this, it is possible to tell what the asymptotic behaviour is when the time-delay changes from $\tau_\alpha - \epsilon$ to $\tau_\alpha + \epsilon$.

However, in some cases which are referred to as degenerate cases, the resultant Puiseux series involves only an imaginary term. This means that the first order Puiseux series is insufficient. In order to address this issue, higher order Puiseux series need to be determined, which is done by applying algorithm 1, iteratively [28].

3) Stability Regions in the Delay Space

After having determined the critical pairs and the asymptotic behaviour associated with them, it finally remains to determine the stability regions in the delay space of the TDS. This entails monitoring the change in the number of unstable roots and keeping track of the number of unstable roots pertaining to the time-delay intervals. The change in the number of unstable roots is mathematically described in eq. (29) [28].

$$\Delta NU_\alpha(\beta) \triangleq NU_\alpha\left(\beta^+\right) - NU_\alpha\left(\beta^-\right) \tag{29}$$

The notation $\Delta NU_\alpha(\beta)$ signifies the change in the number of unstable roots that is associated with the critical pair (α, β), with α being the CIR and β being the associated critical time-delay. As shown from eq. (29), $\Delta NU_\alpha(\beta)$ corresponds to the change that occurs when the time-delay is increased from β^- to β^+.

B. Matrix Inequalities

There are many stability results that have been proposed in the literature for the stability analysis of TDSs in the time-domain. However, since the interest is in time-domain stability results that would corroborate the results obtained from the frequency domain analysis (which are exact results), the set of candidate stability results is narrowed down to the results that are based on the discretized Lyapunov functional method because, for increasing N, the solutions of these matrix inequalities tend to those exact results. Several matrix inequalities based on the discretized Lyapunov functional method have been derived in the literature [32]–[35]. However, more recently, stability results, that are based on the use of the Bessel-Legendre inequality (see Lemma 1) as well as the use of Legendre polynomials (see Definition 1) as a basis for the discretization, have proven to be particularly efficient in comparison to other stability results in this category.

Lemma 1 (Bessel-Legendre Inequality [36]): *Let $x \in \mathcal{L}_2(\mathcal{I} \to \mathbb{R}^n)$ and $R \in \mathcal{S}_n^+$. The integral inequality*

$$\int_{-\tau}^{0} x(u)Rx(u)\mathrm{d}u \geq \frac{1}{\tau}\begin{bmatrix} \Omega_0 \\ \vdots \\ \Omega_N \end{bmatrix}^T R_N \begin{bmatrix} \Omega_0 \\ \vdots \\ \Omega_N \end{bmatrix} \tag{30}$$

holds, for all $N \in \mathbb{N}$, where

$$\begin{aligned} R_N &= \operatorname{diag}(R, 3R, \ldots, (2N+1)R) \\ \Omega_k &= \int_{-\tau}^{0} L_k(u)x(u)\mathrm{d}u, \text{ for all } k \in \mathbb{N} \end{aligned} \tag{31}$$

Definition 1 (Legendre Polynomial [36]): *The Legendre polynomials considered over the interval $[-\tau, 0]$ are defined by:*

$$\forall k \in \mathbb{N}, \quad L_k(u) = (-1)^k \sum_{l=0}^{k} p_l^k \left(\frac{u+\tau}{\tau}\right)^l \tag{32}$$

with $p_l^k = (-1)^l \begin{pmatrix} k \\ l \end{pmatrix} \begin{pmatrix} k+l \\ l \end{pmatrix}$.

Two such stability results have been been derived for retarded TDSs with single delays [36], [37]. Because they are comparable results, only one of them will be presented in the following.

Consider the retarded TDS with a single delay shown in eq. (33).

$$\dot{x}(t) = A_0 x(t) + A_1 x(t-\tau), \quad \tau \geq 0 \tag{33}$$

As mentioned in the earlier paragraphs, two similar stability results that are based on the discretized Lyapunov functional method, and the use of Bessel-Legendre inequality as well as the use of Legendre polynomials as basis for the discretization, have been developed in the literature [36], [37]. In the following, only one of the results will be presented. In particular, Theorem 1 presents the stability result that has been derived in [37].

Theorem 1 ([37]): *For a given N and a constant delay τ, assume that there exist a matrix $P_N \in \mathbb{S}_{(N+1)n}$ and two matrices $S, R \in \mathbb{S}_n^+$ such that*

$$\begin{aligned} \Theta_N(\tau) &= \begin{cases} P_N \succ 0, & \text{if } N = 0 \\ P_N + \frac{1}{\tau} \begin{bmatrix} 0 & & & \\ & S & & \\ & & \ddots & \\ & & & (2N-1)S \end{bmatrix} \succ 0, & \text{if } N > 0 \end{cases} \\ \Phi_N(\tau) &= \Phi_{N0}(\tau) - \begin{bmatrix} \Gamma_N(0) \\ \vdots \\ \Gamma_N(N) \end{bmatrix}^\top \begin{bmatrix} R & & & \\ & 3R & & \\ & & \ddots & \\ & & & (2N+1)R \end{bmatrix} \begin{bmatrix} \Gamma_N(0) \\ \vdots \\ \Gamma_N(N) \end{bmatrix} \prec 0 \\ \Phi_{N0}(\tau) &= \operatorname{He}\left(G_N^\top(\tau) P_N H_N\right) + \tilde{S}_N + (\tau)^2 F_N^\top R F_N \\ \tilde{S}_N &= \operatorname{diag}\{S, -S, 0_{Nn}\} \\ S_N &= \operatorname{diag}\{S, 3S, \ldots, (2N+1)S\} \\ F_N &= \begin{bmatrix} A_0 & A_1 & 0_{n,nN} \end{bmatrix} \\ G_N(\tau) &= \begin{bmatrix} I_n & 0_n & 0_{n,nN} \\ 0_{nN,n} & 0_{nN,n} & \tau I_{nN} \end{bmatrix} \\ H_N &= \left[F_N^\top \ \Gamma_N^\top(0) \ \Gamma_N^\top(1) \ldots \Gamma_N^\top(N-1)\right]^\top \end{aligned} \tag{34}$$

where $\Gamma_N(k)$ for all $k = 0, \ldots, N$ are defined as follows:

$$\begin{aligned} \Gamma_N(k) &= \begin{cases} [I \ -I], & \text{if } N = 0 \\ I \ (-1)^{k+1} I \ \gamma_{Nk}^0 I \ldots \gamma_{Nk}^{N-1} I], & \text{if } N > 0 \end{cases} \\ \gamma_{Nk}^i &= \begin{cases} -(2i+1)\left(1-(-1)^{k+i}\right), & \text{if } i \leq k \\ 0, & \text{if } i > k \end{cases} \end{aligned} \tag{35}$$

The stability intervals of the retarded TDS with a single delay (eq. (33)) are the values of time-delay for which eq. (34) is satisfied.

V. Robust Stability Analysis

For real-world applications, it is practically impossible to describe a system precisely. Uncertainties in the linear system representation occur due to many reasons. These include approximate or incorrect knowledge about certain parameters in the system. Another source of uncertainty is the linearization of system dynamics; some parameters may be time-varying because of nonlinearities in the actual system dynamics or because of different operating conditions. Furthermore, the limited measurement accuracy of sensors introduces uncertainties in the signals in the system. In some situations, despite having accurate insight about the plant model, it may be preferred to deal with a deliberately simplified version of the model and to represent the parts that were neglected with uncertainties [38].

Considering the inevitable presence of uncertainties in practice, it is important to make the analysis robust to such uncertainties. It should be noted that, in the case of TDSs, uncertainties may arise in two main ways: either as uncertainties in the coefficients or as uncertainties in the time-delay parameters themselves. For the case of the problem analyzed in this thesis, the research aim is to determine the time-delays for which the stability of the control system is ensured while considering uncertainties in the knowledge about the modelled parts of the system, rather than assessing the stability for time-delay intervals that are known a priori. Therefore, in this article, the concern is with uncertainties in the coefficient matrices (in the case of the time domain) or the coefficient vectors of the quasipolynomials (in the case of the frequency domain).

A. Preliminaries

Because of their relevance to the methods that will be discussed in section V-B, two preliminary concepts will be explained. Those are the concept of uncertain quasipolynomials and that of the value set.

1) Uncertain Quasipolynomial

Consider the quasipolynomial defined in eq. (36).

$$f(\lambda) = \sum_{j=0}^{n} \sum_{i=0}^{m} a_{ji} \lambda^{n-j} e^{-\tau_i \lambda} = \sum_{i=0}^{m} p_i(\lambda) e^{-\tau_i \lambda} \quad \text{where} \quad 0 = \tau_0 < \tau_1 < \ldots < \tau_m \tag{36}$$

There are two vectors defined in association with the equation of the quasipolynomial in eq. (36): the coefficient vector shown in eq. (37) and the exponent coefficient vector seen in eq. (38) [22].

$$\mathbf{a} = (a_{00}, \ldots, a_{0n}, a_{10}, \ldots, a_{1n}, \ldots, a_{mn}) \tag{37}$$

$$\mathbf{r} = (r_1, r_2, \ldots, r_m) \tag{38}$$

In the case of uncertainties, where the uncertain parameters belong to some uncertainty bounding set Q_F, the result is a family of uncertain quasipolynomials, denoted by F:

$$F = \{f(s, \mathbf{a}, \mathbf{r}) | (\mathbf{a}, \mathbf{r}) \in Q\} \tag{39}$$

However, as previously mentioned, uncertainties in the time-delays will not be considered. Only the cases where there are uncertainties in the coefficient vector $\mathbf{a}$ will be of concern in this thesis. Thus, the elements of the coefficient vector may be in terms of a number of uncertain elements, where such uncertain elements shall be denoted by q_i.

2) Value Set

The value set is an important tool for the robust stability analysis of uncertain functions. However, before explaining why it is such an important concept, a definition of the value set will be presented, in the context of uncertain quasipolynomials. Informally stated, the value set is the range of an uncertain function at a particular imaginary frequency.

Definition 2 (Value Set [22]): *The value set of a family of quasipolynomials F is defined according to:*

$$V_F(\lambda_0) = \{f(\lambda_0) | f \in F\} \tag{40}$$

where λ_0 is a complex number and specifically a pure imaginary complex number at which the value set is evaluated.

One particular reason why the value set is considered to be important is that it is needed to check for the zero-exclusion principle which is one of the more general principles that are applicable across the different uncertainty structures in the hierarchy, and which will be explained in the following subsection. Moreover, since the zero-exclusion principle has been instrumental to the derivation of several other theorems, the value set, by extension, can be needed to check the conditions of other theorems as well, as is the case, for example, for the Finite Inclusions Theorem. Another important, and often convenient, property of the value set is that it is always two-dimensional, irrespective of the nature of the uncertain function or of the type of uncertainty structure involved.

B. Robust Analytic Curve Frequency Sweeping Approach

1) Affine Uncertainty Structure

The edge theorem was originally developed for the stability of uncertain polynomials that have an affine uncertainty structure. This theorem was later extended to the case of retarded uncertain quasipolynomials by Fu et al. [39]. These results were further extended to the case of neutral TDS by the same researchers [40].

The theorem states that when the system can be described as a polytopic family of quasipolynomials, the stability of that family can be deduced from the stability of the edges of its polytope. Specifically, the family is stable if and only if all the edges of the family are stable.

Given the affine uncertainty structure, the quasipolynomial describing an edge can be determined from the linear combination of two vertex quasipolynomials pertaining to a particular edge, denoted by $f_0(s)$ and $f_1(s)$. This is shown in eq. (41).

$$f_\mu(\lambda) = (1-\mu)f_0(\lambda) + \mu f_1(\lambda), \text{ where } \mu \in [0,1] \tag{41}$$

In the literature, Tuzcu et al. have used the edge theorem to extend the stability analysis approach based on the direct method to the case of TDS with polytopic uncertainty [41]. Along this line of research, it was interesting to attempt to extended the analytic curve frequency sweeping approach with the edge theorem. As the analytic curve frequency sweeping approach is more general than the direct method, this extension will lead to a robust stability analysis technique in the frequency domain that is applicable to the wider group of TDSs, consisting of TDS with commensurate delays. To the knowledge of the author, this had not been previously presented in the literature. This extension has been made and its results will be presented in this article.

There exist graphical methods for checking the stability of a TDS with affine uncertainty. One such test has been proposed by Fu et al., which allows to verify the results that are obtained based on a robust stability analysis method applied to a system with polytopic uncertainty. The theorem reads as follows:

Theorem 2 ([39]): *Consider a polytope of n-th order (real or complex) quasipolynomials P. E_1, E_2, ... E_t are used to denote the edges of P and $p_{k0}(\lambda)$ and $p_{k1}(\lambda)$ to denote the vertix quasipolynomials of E_k. Then, P is stable if and only if the following two conditions apply for every E_k, $1 \leq k \leq t$:*

- *the frequency response plot of $p_{k0}(j\omega)/(j\omega+1)^n$ does not enclose the origin.*
- *the plot of $\frac{p_{k1}(j\omega)}{p_{k0}(j\omega)}$ does not cross $(-\infty, 0]$ (the non-positive part of the real axis).*

where n is is the order of the principal term.

2) Multilinear Uncertainty Structure

In the case of multilinear uncertainty structure, vertex and edge results cannot be used for studying the robust stability of uncertain functions with multilinear uncertainty. For example, it may be the case that the system is stable for the parameters on the edges of the uncertainty bounding set. However, there may still be a point in the interior of the uncertainty bounding set such that the system is unstable.

This problem can be dealt with using the mapping theorem, which states that for a set of uncertain parameters q_i (the set of which is denoted by Q) and a multilinear function f, such that $f(Q) = \{f(q) : q \in Q\}$, the convex hull of $f(Q)$ is equal to the convex hull of the set $\{f(q_i)\}$ [42]. Such overbounding of the value set with a convex polytope means that the edge theorem can now be applied to the overbounded value set.

It should be noted that this solution comes at the cost of conservativeness. This means that the stability of the overbounded region is only sufficient for the stability of the actual range of the uncertain quasipolynomial. Hence, if the case where the overbounded system is unstable is encountered, then a conclusion cannot be made about the stability of the system.

3) Polynomic Uncertainty Structure

As in the case of dealing with a multilinear uncertainty structure, here too, the problem has to be transformed into that of analyzing the stability of an uncertain system with an affine uncertainty structure, in order to be able to apply the edge theorem.

It has already been established that a system with multilinear uncertainty can be overbounded with a system of an affine uncertainty structure. Thus, for the case of a system with polynomic uncertainty, only the means to transform a system with a polynomic uncertainty structure to that of a system with a multilinear uncertainty structure needs to be found. The solution to this problem, in the case of uncertain polynomials, is the following theorem which was proposed by Sideris and Sanchez Pena [43].

Theorem 3 ([43] as seen in [42]): *Consider the family of polynomials $\mathcal{P} = \{p(\cdot, q) : q \in Q\}$ with $p(s, q)$ having polynomic uncertainty structure and uncertainty bounding set Q which is a polytope. Then there exists a second family of polynomials $\tilde{\mathcal{P}} = \{\tilde{p}(\cdot, \tilde{q}) : \tilde{q} \in \tilde{Q}\}$ such that $\tilde{p}(s, \tilde{q})$ has multilinear uncertainty structure $\tilde{Q}$ is a polytope and*

$$\tilde{\mathcal{P}} = \mathcal{P} \tag{42}$$

Although this theorem has been developed for families of polynomials, this theorem may also be used to obtain an overbounding set of the polynomic family of quasipolynomials. The reason for this is that a quasipolynomial is the sum of the product of polynomial and exponential terms. Thus, if the polynomic polynomials are transformed into equivalent polynomials with a multilinear structure, then a quasipolynomial with multilinear uncertainty is obtained.

Remark 1 (Refinement for Tighter Bound on the Value Set): *Note, how in the construction of the convex hull, the relations that occur between the variables that are introduced because of Theorem 3 are not accounted for. In order to heed this dependence, a concept from interval analysis which is refinement can be used.*

VI. Example: INDI Control of a Damped Pendulum

The forced pendulum with friction is modeled by eq. (43).

$$\ddot{\theta} + \frac{b}{I}\dot{\theta} + \frac{mgl}{I}\sin\theta = u \tag{43}$$

where θ denotes the angular deflection of the pendulum (reference chosen to be the bottom position), u is the input to the system, I is the moment of inertia of the pendulum, b is the damping coefficient of the pendulum, l is the length of the pendulum, and m is the mass of the pendulum. This second order equation, eq. (43), can be transformed into a system of two first-order equations. By setting $x_1 = \theta$ and $x_2 = \dot{\theta}$, eq. (44) is obtained.

$$\begin{aligned} \dot{x_1} &= x_2 \\ \dot{x_2} &= u - \frac{b}{I}x_2 - \frac{mgl}{I}\sin(x_1) \end{aligned} \tag{44}$$

Linearizing this system of equations about $(x_{1,0}, x_{2,0})$ leads to the following system of equations:

$$\begin{aligned} \dot{x_1} &= x_2 \\ \dot{x_2} &= u - \frac{b}{I}x_2 - \frac{mgl}{I}\sin(x_1) - \frac{mgl}{I}\cdot cos(x_{1,0})(x_1 - x_{1,0}) \end{aligned} \tag{45}$$

It can be seen from eq. (45) that $x_{2,0}$ gets canceled in the linearization process and that only the remnant $x_{1,0}$ is relevant for the linearized dynamics. In order to perform IO linearization, a suitable choice of the output variable needs to be made. An important concern related to making this choice are the internal dynamics. Specifically, the choice of output should ensure that the control system either does not have any internal dynamics or if it does, that the internal dynamics are stable. To elaborate on the importance of ensuring the latter, the presence of internal dynamics means that full controllability is not guaranteed, in exception of the cases where it is known that the internal dynamics are stable.

First, the consequences of taking the output to be x_2 are examined. From this choice, it can be seen that there are internal dynamics since a single differentiation of the output equation leads to the appearance of the control input, meaning that the relative degree of the system is equal to 1 which is less than the order of the system, which is 2.

If the output is taken to be $y = x_1$ instead, then the output needs to be differentiated twice in order for the control input to appear, as shown below.

$$\ddot{y} = \ddot{x_1} = \dot{x_2} = u - \frac{b}{I}x_2 - \frac{mgl}{I}\sin(x_1) \tag{46}$$

In this case, the relative degree is zero and the closed-loop system does not have any internal dynamics, which further means that the system is fully controllable. As a result, the output is selected to be x_1.

In INDI, linearization is performed about the current state and control input. In the case of the system shown in eq. (43), linearizing eq. (46) followed by applying the time-scale separation principle leads to:

$$\ddot{y} = \ddot{y_0} + \beta(x_0)\Delta u + \delta(z, \Delta t) \tag{47}$$

where $\delta(z, \Delta t)$ denotes the higher order terms. These terms can usually be neglected which reduces eq. (47) to:

$$\ddot{y} = \ddot{y_0} + \Delta u \tag{48}$$

Setting the virtual control equal to $\ddot{y}$, eq. (48) is re-written as:

$$\Delta u = \nu - \ddot{y_0} \tag{49}$$

TABLE I: Parameters used in the implementation of the INDI control of the pendulum control system.

m (kg)	b (kg/s)	l (m)	I (kgm^2)	$x_{1,0}$ (rad)	$x_{2,0}$ (rad/s)	u_0 (rad/s^2)	k_p	k_d	Actuator model	Sensor model 1	Sensor model 2
0.3	0.1	1	1	0.1	0	1	25	7	$\frac{1}{s+20}$	1	1

For a tracking problem, the outer-loop linear control is again set such that stable error dynamics are obtained i.e. $\nu = \ddot{y}_{ref} + k_p(y_{ref} - y) + k_d(\dot{y}_{ref} - \dot{y})$, which leads to the following incremental control Δu.

$$\Delta u = \ddot{y}_{ref} + k_p(y_{ref} - y) + k_d(\dot{y}_{ref} - \dot{y}) - \ddot{y}_0 \tag{50}$$

Finally, the expression for the control law becomes:

$$u = \Delta u + u_0 = \ddot{y}_{ref} + k_p(y_{ref} - y) + k_d(\dot{y}_{ref} - \dot{y}) - \ddot{y}_0 + u_0 \tag{51}$$

The block diagram of a control system that applies INDI control is shown in fig. 20. Based on this structure and the manipulation of transfer functions, it is possible to obtain the closed-loop formulation for the system dynamics in the frequency domain, for which later a time-domain realization is set up.

In the following, the stability analysis of the INDI-controlled damped pendulum will be discussed, specifically, a pendulum control system whose parameters are shown in table I. First, the analyses in the frequency domain will be discussed. This is followed by a discussion on the analysis in the time-domain. A number of simulation tests verify the results. Thereafter, the robust stability analysis is discussed, both in the frequency and in the time-domain.

1) Direct Method and Analytic Curve Frequency Sweeping Approach

In the following, two frequency domain techniques will be used to analyze the stability of the control system at hand. Besides the analytic curve frequency sweeping approach, which was the chosen method for stability analysis in the frequency domain and which was discussed in section IV-A, another method in the frequency domain will be applied which is called the direct method. This method is specific to systems with a single delay; therefore, it is less general than the analytic curve frequency sweeping approach [44]. However, as the example considered is a TDS with a single time-delay, the application of the direct method can serve as additional verification of the results obtained. In the following, the discussion commences with the application of the direct method. After that, the application of the analytic curve frequency sweeping approach to the pendulum control system is discussed.

The core of the direct method is to eliminate the exponential term that appears in the characteristic equation of the TDS with a single delay whose form is as that of the characteristic equation shown in eq. (52).

$$P(\lambda) + Q(\lambda) \cdot e^{-\tau \cdot \lambda} = 0 \tag{52}$$

If eq. (52) is rearranged, this leads to eq. (53).

$$e^{-\tau \cdot \lambda} = \frac{-P(\lambda)}{Q(\lambda)} \tag{53}$$

Since the interest is in the intersection with the y-axis in the pole-zero map, then λ can be replaced by $j\omega$, and $\|e^{-\tau \cdot j\omega}\|$ is equal to 1. This leads to the magnitude equation shown in eq. (54).

$$\|P(j\omega)\| - \|Q(j\omega)\| = 0 \tag{54}$$

Since the solution of the magnitude equation will be the , then those solutions are the critical angular frequency values, each denoted by $\omega_{C,i}$. For the case of the pendulum control system considered, this leads to two CIRs which are 1.3207 rad/s and 2.0534 rad/s. Actually, it should be noted that there will be crossings at -1.3207 rad/s and -2.0534 rad/s as well, due to symmetry property of the spectrum. However, for a simpler discussion, only the positive frequencies will be considered, and this simplification will be accounted for in the part concerning the determination of the number of unstable roots for different time-delay values [28].

After having determined the CIRs, it is possible to proceed to solving for the critical time-delays. For that, the argument of $e^{-\tau \cdot j\omega}$ is used, since that yields the product of the CIR and the critical time-delay as shown in eq. (55).

$$\arg(e^{-\tau \cdot j\omega_{C,i}}) = -\tau \cdot \omega_{C,i} \tag{55}$$

In order to obtain an expression for the critical time-delay, another expression for the argument of $e^{-\tau \cdot j\omega}$ is needed. It can be obtained by applying the argument operator on either side of eq. (53). Thus,

$$\arg(e^{-\tau \cdot j\omega_{C,i}}) = \arg\left(\frac{-P(j\omega_{C,i})}{Q(j\omega_{C,i})}\right) + 2\pi k \tag{56}$$

By combining eq. (55) and eq. (56), eq. (57) is obtained.

$$\tau = \frac{1}{-\omega_{C,i}} \cdot \left(\arg\left(\frac{-P(j\omega_{C,i})}{Q(j\omega_{C,i})}\right) + 2\pi k\right) \tag{57}$$

Evaluatingeq. (57) at $\omega_{C,1} = 1.3207$ rad/s and $\omega_{C,2} = 2.0534$ rad/s leads to the following expressions for the critical time-delays:

$$\tau_{\omega_{C,1}=1.3207 \text{ rad/s}} = -2.216270 + 4.757412 \cdot k \tag{58}$$

$$\tau_{\omega_{C,2}=2.0534 \text{ rad/s}} = 0.305067 + 3.059841 \cdot k \tag{59}$$

It is known that for TDSs, for every critical frequency $\omega_{C,i}$, there correspond infinitely many critical time-delays, and this is clear here because of the presence of the variable k.

With the expressions for the critical time-delays obtained, it remains to determine the stability intervals. This consists of three main steps, the first of which is determine the number of unstable roots when the time-delay is zero. The step that follows is to determine the Crossing Direction of Imaginary Root (CDIR) associated with the critical roots. Finally, the critical time-delays are sorted in increasing order, and the book-keeping of the number of unstable roots is performed for the intervals between the critical time-delays. This is done based on the determined CDIRs.

Thus, first, the stability of the control system without any time-delays is studied. For the case of the pendulum control system, based on the input values mentioned above, the 3 roots obtained at $\tau = 0$ are: -19.71 rad/s, - 0.1963 - 2.013i rad/s, and - 0.1963 + 2.013i rad/s. These three roots are all stable, therefore the starting count for the number of unstable roots is zero.

The CDIR can be obtained based on eq. (25) and eq. (26) which for convenience is repeated in eq. (60). As mentioned in section IV-A2, this is only applicable when the CIRs are simple [45], [46].

$$CDIR = \text{sign}\left[\frac{d\lambda}{d\tau}\right]_{\lambda=\omega_{C,i}} = \text{sign}\left[-\frac{f_\tau}{f_\lambda}\right]_{\lambda=\omega_{C,i}} \tag{60}$$

Moreover, as discussed in section III, according to the invariance property, for all critical time-delay pertaining to a certain crossing-frequency, the crossing direction will be the same [28]. For the case of the pendulum control system, based on eq. (60), the CDIR corresponding to 1.3207 rad/s is -1. That is, whenever there is a crossing at 1.3207 rad/s, if the time-delay is increased further this particular pole will move to the left-half plane. As for the critical angular frequency 2.0534, the CDIR is +1.

With the CDIRs established, it remains to perform thorough book-keeping of the number of unstable roots. The time-delay intervals based on the sorted sequence of critical time-delays are shown in the first column of table II. The starting score is equal to the number of unstable roots when there are no delays in the systems, which was determined to be zero. For the result of the scores, every time a critical time-delay with a CDIR of +1 is encountered, the score is increased by 2 (this corresponds to a +1 for the positive frequency crossing and another +1 for the conjugate CIR). Conversely, when a critical time-delay with a CDIR of -1 is encountered, the score is decreased by 2. This leads to the scores shown in the second column of table II.

For the pendulum control system, the results of this final step are shown in the right column of table II. From this table as well as fig. 3, it can be seen that the number of unstable roots, denoted by NU, is zero for the time-delay intervals [0,0.305069] and [2.541144, 3.364915] seconds which are the stability intervals. This concludes the discussion on the application of the direct method to the pendulum control system, and in the following, the use of the analytic curve frequency sweeping approach to the pendulum control system will be discussed.

As mentioned in section IV-A, frequency sweeping can be used to determine the critical angular frequencies either *graphically* or *programmatically*. In order to perform frequency sweeping, it is required that the variable z replaces the expression $e^{-\tau \cdot \lambda}$ in the characteristic quasipolynomial, and that the variable λ is replaced by $j\omega$. For the pendulum control system, this leads to the bivariate equation of the form shown in eq. (61).

$$c_0 + c_1 \cdot j\omega + c_2 \cdot z + c_3 \cdot j\omega \cdot z + c_4 \cdot (j\omega)^2 + c_5 \cdot (j\omega)^3 = 0 \tag{61}$$

The frequency sweeping curves are constructed by "sweeping" the frequency, and at each frequency, substituting in eq. (61) computing the values of z, and plotting the magnitude of that. In the case of the pendulum, there is only one frequency sweeping curve which has two intersections with $\Gamma = 1$. The curve is shown in fig. 4, and it is clear from this curve that the two intersection points are at 1.3207 rad/s and 2.0534 rad/s. This is in alignment with the CIRs obtained in the analysis based

TABLE II: Stability Sequence for Pendulum Control System

Critical Time-delay Intervals (s)	Number of Unstable Roots
[0 , 0.305069]	0
[0.305069 , 2.541144]	2
[2.541144 , 3.364915]	0
[3.364915 , 6.424762]	2
[6.424762 , 7.298558]	4
[7.298558 , 9.484609]	2
[9.484609 , 12.055972]	4
[12.055972 , 12.544459]	2
[12.544459 , 15.604303]	4
[15.604303 , 16.813387]	6
[16.813387 , 18.664149]	4
[18.664149 , 21.570801]	6
[21.570801 , 21.723996]	4
[21.723996 , 24.783843]	6
[24.783843 , 26.328215]	8
[26.328215 , 27.843690]	6

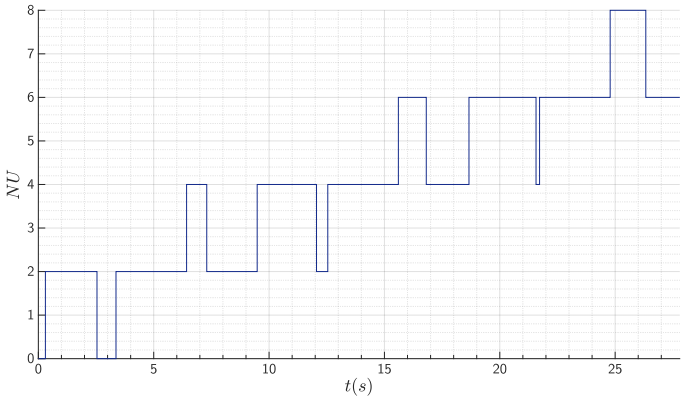

Fig. 3: Plot of the number of unstable roots versus time for the considered pendulum control system.

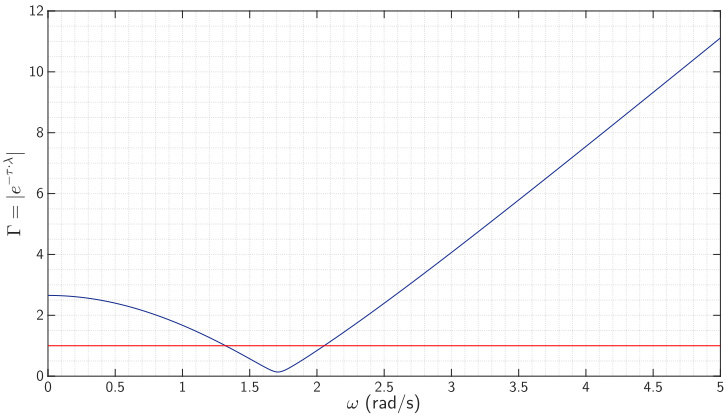

Fig. 4: Frequency sweeping curve for the pendulum control system

on the direct method. Moreover, the associated critical time-delays are obtained in a similar fashion to the way in which they were determined for the case of the direct method.

As for the asymptotic behaviour, it can be determined based upon constructing and analyzing the Puiseux series at a each critical imaginary pair. The procedure to obtain the Puiseux series is an implementation of the pseudocode shown in algorithm 1.

For the critical imaginary pair (1.3207j,- 2.216270 + 4.757412 · k), the following series is obtained:

$$\Delta\lambda = (-0.246395 - 0.284083 \cdot j) \cdot \Delta\tau + o(\Delta\tau) \tag{62}$$

Since $\Delta\tau$ in eq. (62) does not have a fractional power, the series is in fact a special form of the Puiseux series and is in fact a Taylor series. This is expected because the critical roots are simple. Moreover, based on this Taylor series, it can be seen that a small positive increase in τ, i.e. $\Delta\tau = +\epsilon$ leads to a decrease in the real part of λ which means that the CDIR is -1.

As for the critical pair (2.0534j,0.305067 + 3.059841 · k), the following series is obtained:

$$\Delta\lambda = (0.665318 - 0.123293 \cdot j) \cdot \Delta\tau + o(\Delta\tau) \tag{63}$$

Here, again, since the CIR is a simple root, the series in eq. (63) is a Taylor series. Moreover, based on this obtained series, it can be seen that, for $\Delta\tau = +\epsilon$, the real part of $\Delta\lambda$ will be positive, which means that the CDIR is +1.

This can also be verified by examining the frequency sweeping curves. From the curve in fig. 4, it can be confirmed that the CDIR is -1 for $\omega_{C,1} = 1.3207$ rad/s and the CDIR is +1 for $\omega_{C,2} = 2.0534$ rad/s. This is deduced based on the slope of the curve at their intersection with the horizontal line $\Gamma = 1$, whereby a positive slope corresponds to a CDIR equal to +1, and a negative slope corresponds to a CDIR equal to -1.

Since the obtained CIRs and the critical time-delays are the same, the stability sequence will also be the same, and the same stable time-delay regions are obtained: [0,0.305069] and [2.541144, 3.364915] seconds.

2) Time-domain Analysis

Now, the time-domain approach will be used to further verify the results that were obtained from the frequency domain analyses. Specifically, the matrix inequalities described in eq. (34) and eq. (35) will be used. They are used to study the stability of systems of the form:

$$\begin{cases} \dot{x}(t) = A_0 x(t) + A_1 x(t-\tau), & \forall t \geq 0 \\ x(t) = \phi(t), & \forall t \in [-\tau, 0] \end{cases} \tag{64}$$

Thus, the matrices A_0 and A_1 have to be determined for the pendulum control system. As it is easier to determine the overall system representation for an LTI system in the frequency domain, the characteristic equation of the pendulum control system (that had been already determined for the above analyses) is used to obtain an equivalent description in the time domain, which entails applying the inverse Laplace transform to the control system's characteristic equation. The obtained delay-differential equation is of the form shown in eq. (65), with $a_1 \dots a_2$ and b_0, b_1 being the appropriate coefficients.

$$\dddot{x} + a_0 \cdot x + a_1 \cdot \dot{x} + a_2 \cdot \ddot{x} + b_0 \cdot x(t-\tau) + b_1 \cdot \dot{x}(t-\tau) = 0 \tag{65}$$

It is clear from the structure of eq. (65) that the pendulum is a retarded type TDS. The highest order of the derivative of x without time-delay is 3; whereas, the order of derivative including a time-delay is 1. Since the former is strictly greater than the latter, the system is a retarded system.

In order to obtain a state space representation from the differential equation eq. (65), a state vector denoted by $\tilde{z} = \begin{bmatrix} x, & \dot{x}, & \ddot{x} \end{bmatrix}^\top$ is proposed. Re-writing eq. (65) in terms of $\tilde{z}$ leads to eq. (66).

$$\begin{cases} \dot{\tilde{z}} & = A_0 \tilde{z} + A_1 \tilde{z}(t-\tau) \\ A_0 & = \begin{bmatrix} 0 & 1 & 0 \\ 0 & 0 & 1 \\ -a_0 & -a_1 & -a_2 \end{bmatrix} \\ A_1 & = \begin{bmatrix} 0 & 0 & 0 \\ 0 & 0 & 0 \\ -b_0 & -b_1 & 0 \end{bmatrix} \end{cases} \tag{66}$$

Since eq. (66) has the form that is suitable for the stability results in eq. (34) and eq. (35), it is possible to proceed to the step of solving for the matrix inequalities for the determined A_0 and A_1 matrices of the pendulum control system. Although, an efficient way to solve those matrix inequalities (which happen to be bilinear matrix inequalities) has not been found, it is still possible to check the feasibility of the solution of the matrix inequalities for different values of time-delay.

a) Checking for the first interval [0,0.305069]s

The correctness of the first stability interval, [0,0.305069]s, can be verified by checking the feasibility of the solution of the matrix inequalities in eq. (34) and eq. (35) for the entirety of this interval. Moreover, once the limit of the first interval is reached, the set of matrix inequalities no longer has a feasible solution, not until the second stability interval. This is clear from fig. 5, where the residuals of V and $\dot{V}$ constraints both reach zero at what is visibly around 0.305 s.

For finer results on the upper bound of this stability interval, starting with τ = 0.3s and taking increments of 0.0001s, the matrix inequalities are feasible up to 0.3050s. N $\geq$ 1 is sufficient to obtain this result. If the steps are taken to be 0.000001, N$\geq$ 3 is sufficient to obtain 0.305068 as the largest number that makes the matrix inequalities feasible (for the first stability interval). The value of N that is sufficient to obtain a certain precision is also dependent on the constraints set for the matrix inequalities.

b) Checking for the second interval [2.541144,3.364915]s

A similar procedure is applied to check the second stability interval. To do so, checking the feasibility of the matrix inequalities is broken down into two tests. Both tests start by checking the feasibility of some interior point for the interval, say 3s. One test would apply delay decrements to this initial starting delay, and the other would apply delay increments. The results of those tests in terms of constraint residuals, for the Lyapunov functional constraint and the Lyapunov functional derivative constraint, are shown in fig. 6 and fig. 7, respectively. It is seen from fig. 6 that the solution of the set of matrix inequalities does not have a feasible solution for values that are smaller than around 2.54s (and which are larger than 0.305069s) because the $\dot{V}$ constraint residual had already reached zero at this limit. In fig. 7, it is seen how the plots of the constraint residuals terminate at around 3.365s.

To attain the bound 2.541144s with a precision of 6 decimal points (2.541144s as 2.541143s is already in the infeasible region), if one starts with a value larger than 2.541144s and takes decrements with step size 0.000001s, the value of 2.541144s is attained with N$\geq$ 8.

The bound 3.364915s can be checked in the same manner that was used for the upper bound of the first stability interval, through delay increments. To attain a value of 3.364915s, N$\geq$ 8 is needed.

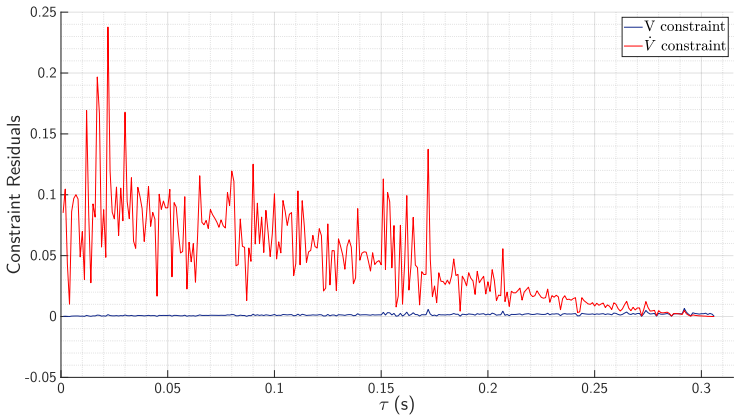

Fig. 5: Plot showing the evolution of the constraint residuals for the Lyapunov functional condition and the Lyapunov functional derivative condition.

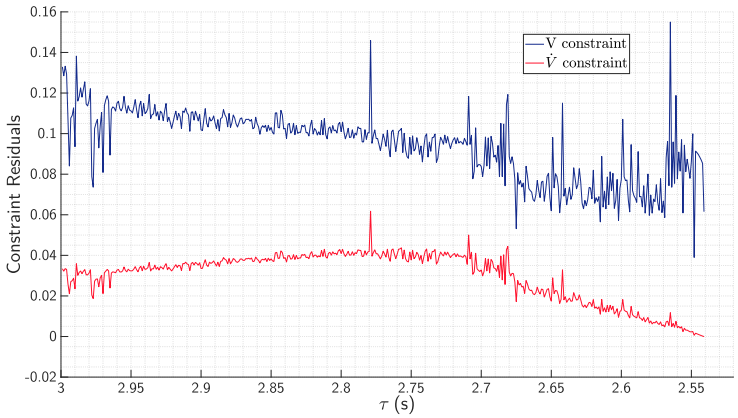

Fig. 6: Plot showing the evolution of the constraint residuals for the Lyapunov functional condition and the Lyapunov functional derivative condition.

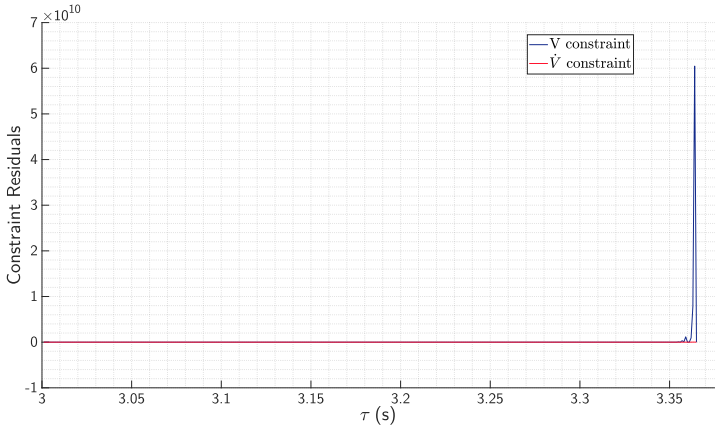

Fig. 7: Plot showing the evolution of the constraint residuals for the Lyapunov functional condition and the Lyapunov functional derivative condition.

3) Verification with the Simulink Model

Based on simulations of the control system considered (at a rate of 10,000Hz), to a 0 reference signal (stabilization), leads to the system responses which are shown in fig. 8a, fig. 8b, fig. 8c, fig. 8d, fig. 8e, fig. 8f, fig. 8g, and fig. 8h. From those

results, the system appears to be stable for the cases of $\tau = 0.1$s (see fig. 8a) and $\tau = 3$s (see fig. 8e), and it appears to be stable for $\tau = 0.32$s, $\tau = 2$s, $\tau = 4$s, and $\tau = 6$s. Based on fig. 8d and fig. 8f, it appears that the system is on the verge stability/instability for the cases of $\tau = 2.55$s and $\tau = 3.365$s.

These results concur with the stability intervals obtained. It should be noted that the reddish hue in those plots indicates that there has been an onset of increase in amplitude that continues till the end of the plot (although it has only been indicated for the top part of the plots).

Remark 2 (Case of Neutral Time-delays for the Pendulum Control System):
It has been discussed that in order to obtain a neutral TDS, the polynomials pertaining to each of the delayed parts and the non-delayed parts have to have the same order. In order to investigate the possibility of such occurrence for the pendulum control system, the symbolic expression of the characteristic equation of the pendulum control system is investigated:

$$\begin{aligned}&\big(10 \cdot tf_{actuator} \cdot \lambda + 100 \cdot I \cdot tf_{actuator} \cdot \lambda^2 - 100 \cdot I \cdot tf_{actuator} \cdot \lambda^2 \cdot tf_{sensor1} + 981 \cdot tf_{actuator} \cdot l \cdot m \cdot cos(x_{1,0}) \\ &-100 \cdot I \cdot Kp \cdot tf_{actuator} \cdot tf_{sensor2} - 100 \cdot I \cdot k_d \cdot tf_{actuator} \cdot \lambda \cdot tf_{sensor2}\big) \cdot e^{(-\lambda \cdot \tau} \\ &- 100 \cdot I \cdot \lambda^2 - 10 \cdot \lambda - 981 \cdot l \cdot m \cdot cos(x_{1,0}) = 0\end{aligned} \tag{67}$$

Based on the expression on the left-hand side, the order of the non-delayed part which is the expression $-100 \cdot I \cdot \lambda^2 - 10 \cdot \lambda - 981 \cdot l \cdot m \cdot cos(x_{1,0})$ is 2 and cannot be affected by the symbolic parameters, because the parameters involved in this expression take scalar values. Thus, in order to obtain a neutral TDS, the "delayed" expression has to have the same order which is 2. It can be seen that in order to obtain this order, at least one of the λ^2 terms appearing in the expression has to remain. Since the transfer function of the actuator appears in both these terms, then it becomes clear that the actuator dynamics cannot be represented by a strictly proper transfer function. The only means for this system to be neutral is for the actuator to have a biproper transfer function, where the number of zeros is equal to the number of poles. This is usually not the case encountered, as actuator are often modeled with strictly proper transfer functions, usually as first or second order transfer functions. One may assume however that for an overall system with a different structure, having neutral delays may be possible for the pendulum control system. In any case, it should be noted that if sensor 1 is ideal, then the terms involving λ^2 will cancel out. Thus, some dynamics need to be taken for this sensor. As for the dynamics of the second sensor, they have no influence on the resulting type of TDS. For now, the discussion on the neutral time-delays is reserved for the second of the presented examples, which is that of the INDI-controlled short period dynamics, where this type of delay has "naturally" occurred. The reason for that is the difference in the transfer functions of the pendulum model and that of the short period dynamics. In the case of the pendulum control system, its transfer function has a relative degree 2, with the denominator being a second order polynomial and the numerator being 1. As for the short period dynamics, they have a relative degree of one because the numerator is a first order polynomial and the denominator is a second order polynomial.

A. Robust Stability Regions in the Delay Space of the Pendulum Control System

In order to discuss robust stability, first, the type of uncertainty structure that the control system possesses needs to be determined. To establish the type of uncertainty structure, where and how the uncertain parameters appear in the characteristic equation need to be determined. That is why, the symbolic expression for the pendulum control system, which is shown in eq. (67), should be examined.

1) Uncertainty in the Length

If uncertainties in the length of the pendulum are considered, it can be seen from the symbolic expression for the characteristic quasipolynomial of the pendulum control system shown in eq. (67) that the uncertainties appear in two terms in the quasipolynomial: $(981 \cdot tf_{actuator} \cdot l \cdot m \cdot cos(x_{1,0})) \cdot e^{\lambda \cdot \tau}$ and $-981 \cdot l \cdot m \cdot cos(x_{1,0})$. This means that there is a dependence between the expressions, and in this case, there is an affine uncertainty structure. Thus, it is possible to make use of the edge theorem in the robust stability analysis of this uncertain system.

As an example, if l is no longer equal to 1m and can take any value between 0.8m and 1.2m, then, based on the analysis based on the analytic curve frequency sweeping approach combined with the edge theorem, the stability regions become: [0,0.3030]s and [3.0807,3.1745]s. This a region that is within the original one: [0,0.3051]s and [2.5411, 3.3649]s.

The robust stability analysis can be done in the time-domain as well. In this particular case, the system matrices have the following structure:

$$\begin{bmatrix} 0 & 1.0 & 0 \\ 0 & 0 & 1 \\ -58.5660 \cdot l & -2.9283 \cdot l - 2.0 & -20.1 \end{bmatrix} \tag{68}$$

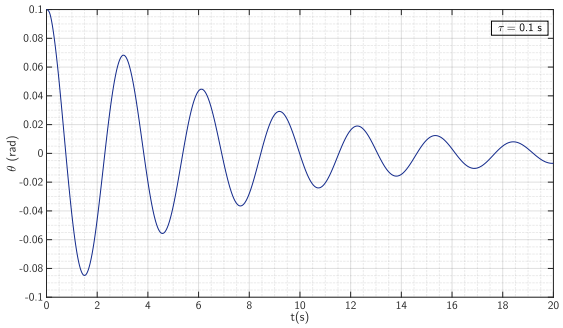

(a) Response corresponding to a delay of 0.10s for the first 20s.

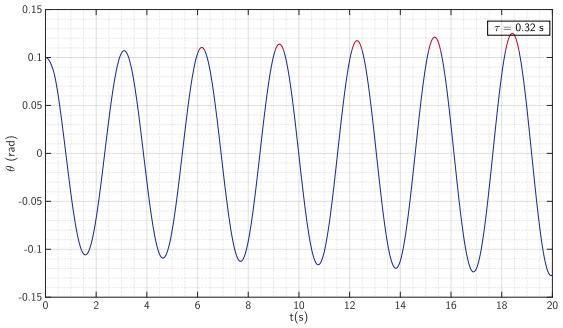

(b) Response corresponding to a delay of 0.32s for the first 20s.

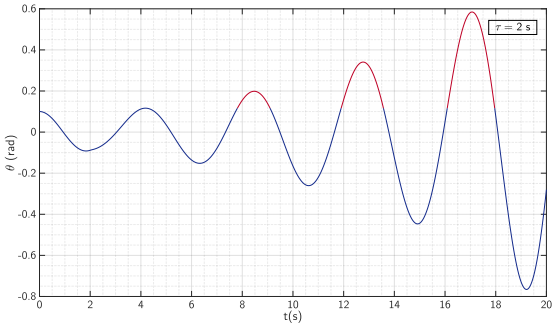

(c) Response corresponding to a delay of 2s for the first 20s.

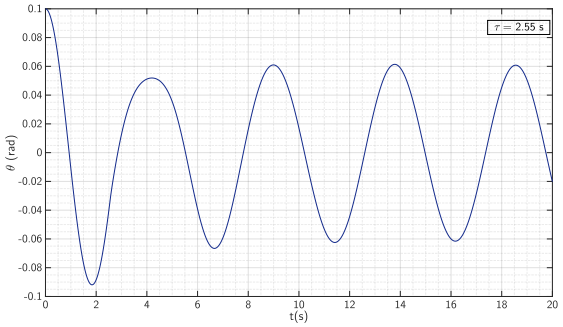

(d) Response corresponding to a delay of 2.55s for the first 20s.

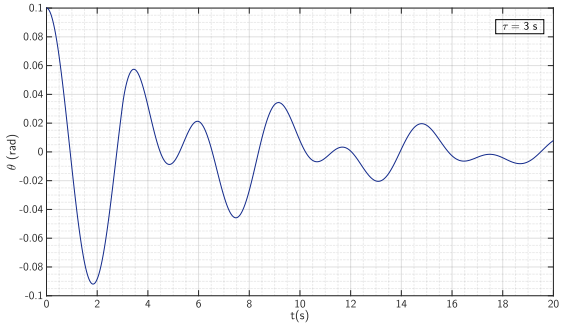

(e) Response corresponding to a delay of 3s for the first 20s.

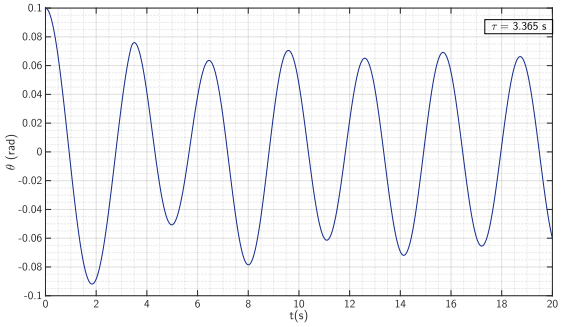

(f) Response corresponding to a delay of 3.365s for the first 40s.

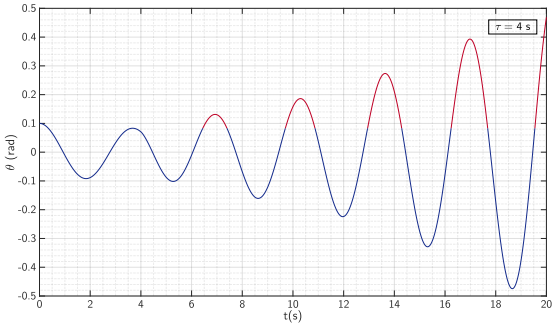

(g) Response corresponding to a delay of 4s for the first 20s.

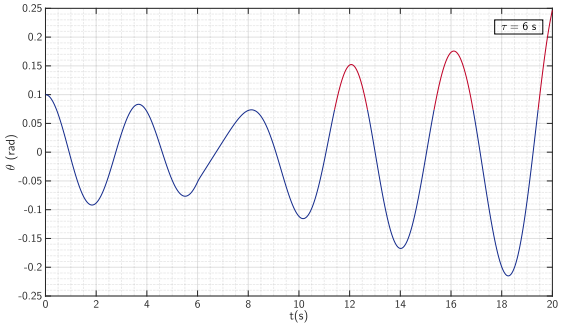

(h) Response corresponding to a delay of 6s for the first 20s.

Fig. 8: Plots of the response of the pendulum control system, shown for the first 20 s, for different time-delays.

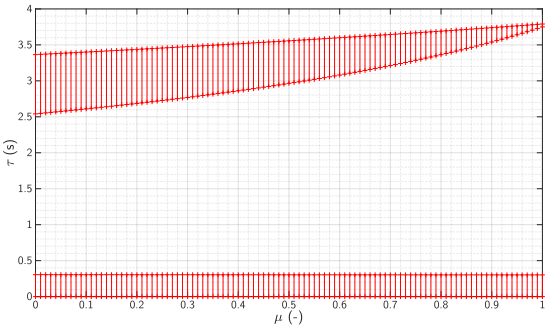

(a) Stability regions pertaining to different points along edge 1.

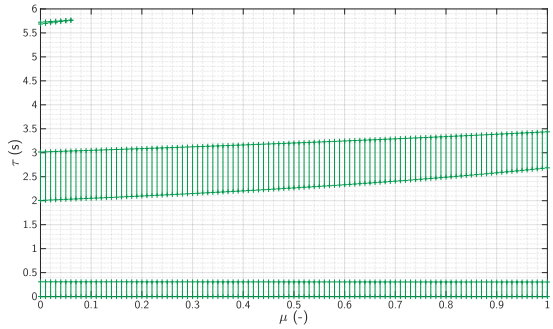

(b) Stability regions pertaining to different points along edge 2.

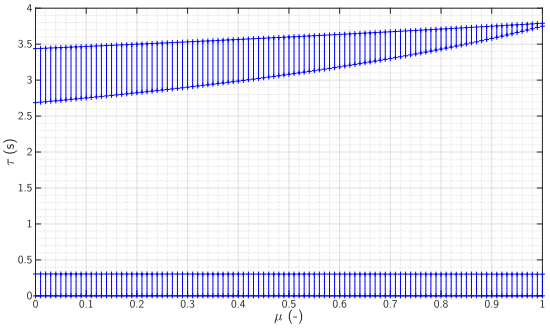

(c) Stability regions pertaining to different points along edge 3.

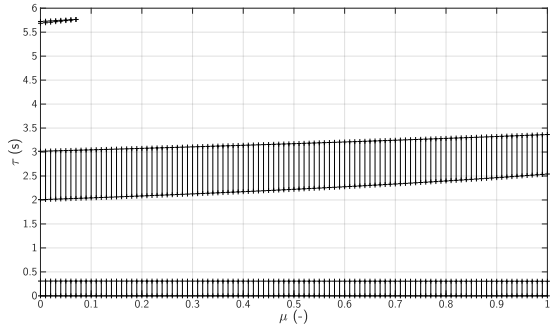

(d) Stability regions pertaining to different points along edge 4.

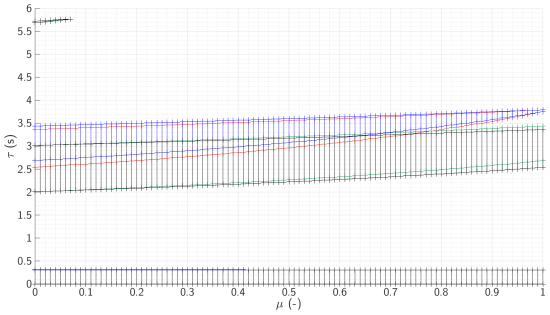

(e) Overlay of the stability regions along the different points on the edges of the polytope.

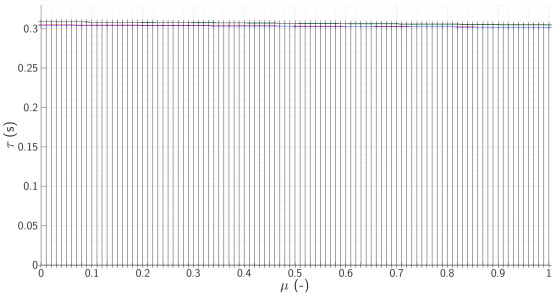

(f) Zoomed-in view of the stability regions along the different points on the edges of the polytope.

Fig. 9: Stability intervals obtained along the four edges of the polytopic family of quasipolynomials.

Clearly, the matrices are polytopic in the length parameter. Thus, it is possible to analyze the vertices of the polytope for the stability of the uncertain system. Specifically, there are two vertices here. In the case of the first vertex, the following stability intervals are obtained: [0,0.30304]s and [3.08075,3.59968]s. In the case of the second vertex, the stability intervals are [0,0.30698]s and [2.2225,3.17448]s. Clearly, the intersection of these two stability intervals are the intervals which had been determined from the analysis in the frequency domain as well.

2) Uncertainty in the Mass and Length

As for the case of uncertainties in both the mass and the length, it can be seen from eq. (67) that the mass and length variables both appear in the same two expressions mentioned before. This means that despite there being two uncertain variables, since they are always multiplied together, it is possible to think of $m \cdot l$ as a single uncertain variable, which means that the ucnertainty structure is effectively affine or polytopic, in this case as well.

For the case when the mass take any values between 0.25 and 0.35 kg (thus l belongs to the range [0.8,1.2]m and m belongs to the range [0.25,0.35]kg), the resultant stability region based on the analysis that assumes polytopic uncertainty is the region [0,0.3016]s. In this case, the enlargement of the uncertainty set has completely eliminated the second stability interval.

The plots of the evolution of the stability regions over the edges are shown in fig. 9a fig. 9b fig. 9c, and fig. 9d. Combining these plots leads to fig. 9e.

The stability interval obtained based on the grid approach is [0,0.3016]s. It is clear that increasing the mass has a more

dramatic effect on the size of the robust stability intervals.

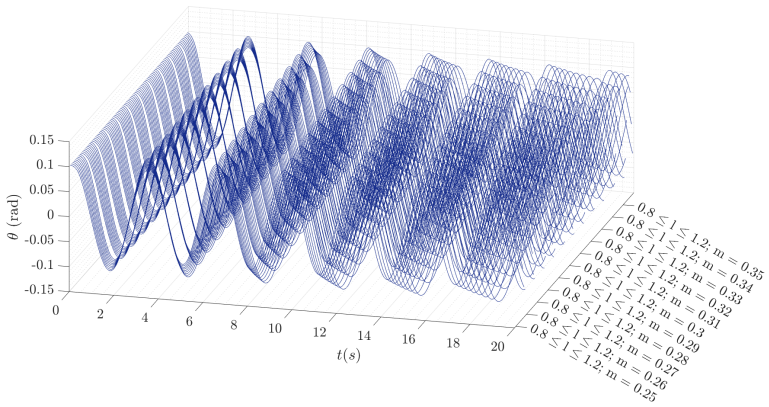

Fig. 10: Pendulum control system response curves for different values of l and m such that $l \in [0.8, 1.2]$m and $m \in [0.25, 0.35]$kg, showing that the system is still robustly stable at $\tau = 0.3$s.

B. Stability Regions in the Delay Space of the Pendulum Control System including Zero-order Hold

In this case, the control system is assumed to have the block diagram shown in fig. 21. From the analytic curve frequency sweeping analysis, the result for the system based on the parameters in table I and a sampling period if 0.1s is that the system is hyperbollically stable. That is, the system is always stable irrespective of what the feedback delay is. There are no resultant CIRs, and there are no unstable roots when there are no delays in the system. This is verified by the frequency sweeping curve shown in fig. 15a, from which it is clearly seen that the curve approaches the horizontal line at 1 but there are no intersections with it.

However, when the sample period is increased to 0.2s, the hyperbolic stability is lost, and instead, there is now a finite number of stability regions. The frequency sweeping curve for this control system is shown in fig. 15b, and it shows that there are two CIRs. Applying the analytic frequency sweeping approach leads ultimately to the following stability regions: [0, 0.5804]s, [1.5898, 4.1460]s [5.3817, 7.7116]s, [9.1736, 11.2772]s, [12.9655, 14.8428]s, [16.7574, 18.4084]s, [20.5493, 21.9740]s, [24.3412, 25.5396]s, [28.1330, 29.1052]s [31.9249, 32.6708]s, [35.7168, 36.2365]s, [39.5087, 39.8021]s, and [43.3006, 43.3677]s.

As for the case when the sampling period is 0.5s, the resultant frequency sweeping curve is the one shown in fig. 15c, and the stability regions are [0, 0.1485]s, [1.8697, 3.5010]s, [5.9657, 6.8534]s, and [10.0617, 10.2058]s.

It is clear that as the sample period is increased, the number and size of the stability regions decrease. These obtained results have also been verified with simulations based on the Simulink®model of the control system which is based off the structure of the block diagram shown in fig. 21.

VII. Example: INDI Control of Short Period Dynamics

The dynamics of the short period eigenmotion are shown in eq. (69).

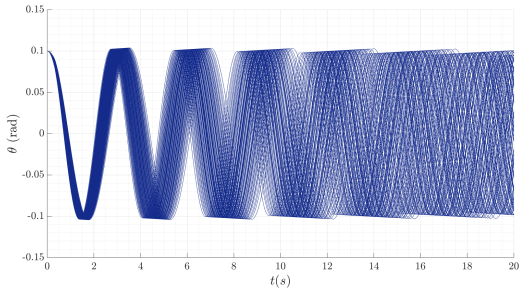

Fig. 11: Pendulum control system response curves for different values of l and m such that $l \in [0.8, 1.2]$m and $m \in [0.25, 0.35]$kg, showing that the system is still robustly stable at $\tau = 0.3$s (Profile view).

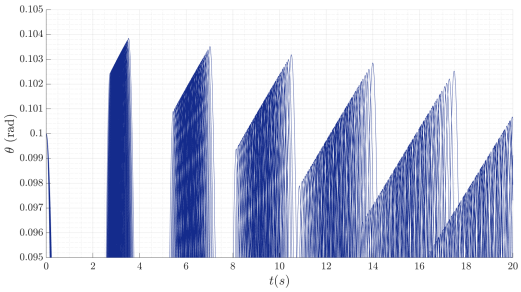

Fig. 12: Pendulum control system response curves for different values of l and m such that $l \in [0.8, 1.2]$m and $m \in [0.25, 0.35]$kg, showing that the system is still robustly stable at $\tau = 0.3$s (Zoomed profile view).

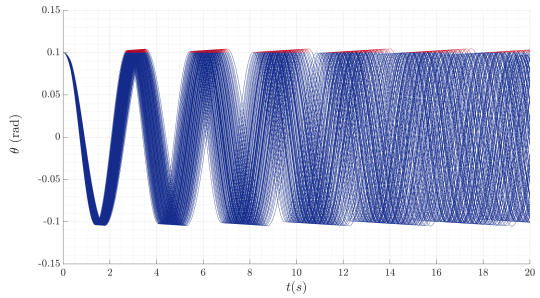

Fig. 13: Pendulum control system response curves for different values of l and m such that $l \in [0.8, 1.2]$m and $m \in [0.25, 0.35]$kg, showing the onset of instability for $\tau = 0.302$s (Profile view).

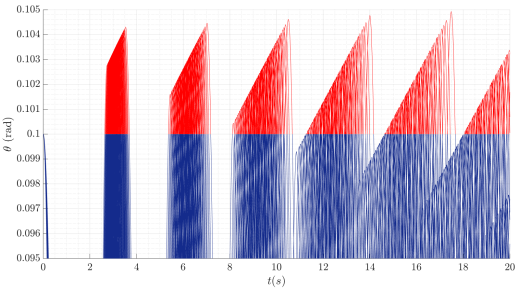

Fig. 14: Pendulum control system response curves for different values of l and m such that $l \in [0.8, 1.2]$m and $m \in [0.25, 0.35]$kg, showing the onset of instability for $\tau = 0.302$s (Zoomed profile view).

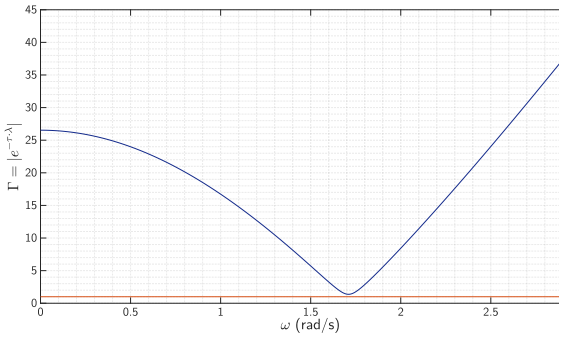

(a) Frequency Sweeping Curve for the pendulum control system with the zero-order hold filter at a sampling period of 0.1s

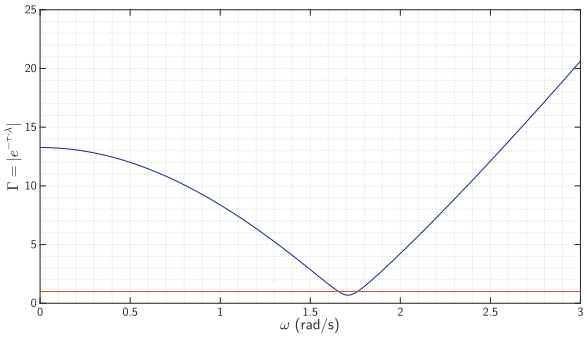

(b) Frequency Sweeping Curve for the pendulum control system with the zero-order hold filter at a sampling period of 0.2s

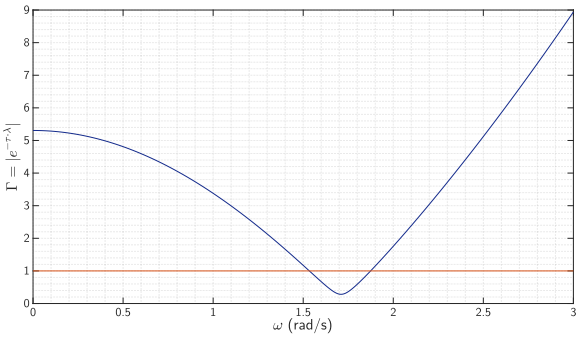

(c) Frequency Sweeping Curve for the pendulum control system with the zero-order hold filter at a sampling period of 0.5s

Fig. 15: Frequency Sweeping Curve for the pendulum control system with the zero-order hold filter at different sampling periods.

$$\begin{aligned} &\begin{bmatrix} C_{Z_\alpha} + (C_{Z_{\dot\alpha}} - 2\mu_c) D_c & C_{Z_q} + 2\mu_c \\ C_{m_\alpha} + C_{m_{\dot\alpha}} D_c & C_{m_q} - 2\mu_c K_Y^2 D_c \end{bmatrix} \begin{bmatrix} \alpha \\ \frac{q\bar{c}}{V} \end{bmatrix} = \begin{bmatrix} -C_{Z_{\delta_e}} \\ -C_{m_{\delta_e}} \end{bmatrix} \begin{bmatrix} \delta_e \end{bmatrix} \\ &\iff \begin{bmatrix} (C_{Z_{\dot\alpha}} - 2\mu_c) & 0 \\ C_{m_{\dot\alpha}} & -2\mu_c K_Y^2 \end{bmatrix} \begin{bmatrix} D_c\alpha \\ D_c\frac{q\bar{c}}{V} \end{bmatrix} = -1 \cdot \begin{bmatrix} C_{Z_\alpha} & C_{Z_q} + 2\mu_c \\ C_{m_\alpha} & C_{m_q} \end{bmatrix} \begin{bmatrix} \alpha \\ \frac{q\bar{c}}{V} \end{bmatrix} + \begin{bmatrix} -C_{Z_{\delta_e}} \\ -C_{m_{\delta_e}} \end{bmatrix} \begin{bmatrix} \delta_e \end{bmatrix} \end{aligned} \tag{69}$$

Given that $D_c = \frac{\bar{c}}{V}\frac{d}{dt}$, eq. (69) becomes:

$$\underbrace{\begin{bmatrix} (C_{Z_{\dot\alpha}} - 2\mu_c) \cdot \frac{\bar{c}}{V} & 0 \\ C_{m_{\dot\alpha}} \cdot \frac{\bar{c}}{V} & -2\mu_c K_Y^2 \cdot \frac{\bar{c}}{V} \end{bmatrix}}_{M_0} \begin{bmatrix} \dot\alpha \\ \frac{\dot q\bar{c}}{V} \end{bmatrix} = \underbrace{-1 \cdot \begin{bmatrix} C_{Z_\alpha} & C_{Z_q} + 2\mu_c \\ C_{m_\alpha} & C_{m_q} \end{bmatrix}}_{A_0} \begin{bmatrix} \alpha \\ \frac{q\bar{c}}{V} \end{bmatrix} + \underbrace{\begin{bmatrix} -C_{Z_{\delta_e}} \\ -C_{m_{\delta_e}} \end{bmatrix}}_{B_0} \begin{bmatrix} \delta_e \end{bmatrix} \tag{70}$$

TABLE III: Parameters used in the implementation of the INDI control of the short period dynamics.

C_{m_α}	$C_{m_{\dot\alpha}}$	C_{m_q}	$C_{m_{\delta_e}}$	C_{z_α}	$C_{z_{\dot\alpha}}$	C_{z_q}	$C_{z_{\delta e}}$	$\bar{c}(m)$	$V(m/s)$	μ_c	K_Y^2	k_p	k_d	$\alpha_0(rad)$
-0.43	-3.7	-7.04	-1.553	-5.16	-1.43	-3.86	-0.6238	2.022	59.9	102.7	0.98	25	7	0.1

It is desired to write the system dynamics in state-space form, i.e. in the form shown in eq. (71).

$$\begin{bmatrix} \dot\alpha \\ \frac{q\bar c}{V} \end{bmatrix} = A \begin{bmatrix} \alpha \\ \frac{q\bar c}{V} \end{bmatrix} + B \begin{bmatrix} \delta_e \end{bmatrix} \tag{71}$$

This means that the matrices A and B must have the following entries:

$$\begin{cases} A &= M_0^{-1} \cdot A_0 = \begin{bmatrix} \frac{-Cz_\alpha}{(\frac{\bar c}{V}\cdot(Cz_{\dot\alpha}-2\cdot\mu_c))} & \frac{(-Cz_q-2\cdot\mu_c)}{(\frac{\bar c}{V}\cdot(Cz_{\dot\alpha}-2\cdot\mu_c))} \\ \frac{((-Cz_{\dot\alpha}+2\cdot\mu_c)\cdot Cm_\alpha+Cm_{\dot\alpha}\cdot Cz_a)}{(2\cdot\frac{\bar c}{V}\cdot(-Cz_{\dot\alpha}+2\cdot\mu_c)\cdot\mu_c\cdot K_Y^2)} & \frac{((2\cdot C_{m_q}+2\cdot Cm_{\dot\alpha})\cdot\mu_c-C_{m_q}\cdot Cz_{\dot\alpha}+Cm_{\dot\alpha}\cdot Cz_q)}{(2\cdot\frac{\bar c}{V}\cdot(-Cz_{\dot\alpha}+2\cdot\mu_c)\cdot\mu_c\cdot K_Y^2)} \end{bmatrix} \\ B &= M_0^{-1} \cdot B_0 = \begin{bmatrix} \frac{Cz_{\delta_e}}{((-Cz_{\dot\alpha}+2\cdot\mu_c)\cdot\frac{\bar c}{V})} \\ \frac{((-Cz_{\dot\alpha}+2\cdot\mu_c)\cdot Cm_{\delta_e}+C_{m_{\dot\alpha}}\cdot Cz_{\delta_e})}{(2\cdot\frac{\bar c}{V}\cdot(-Cz_{\dot\alpha}+2\cdot\mu_c)\cdot\mu_c\cdot K_Y^2)} \end{bmatrix} \end{cases} \tag{72}$$

Since for INDI, the lower triangular form is required, some assumptions need to be made regarding the system dynamics. In particular, in the short period oscillation, it can be assumed that the flight path angle γ is constant. As a result, the relation in eq. (73) can be assumed for $\dot\alpha$.

$$\dot\alpha = \frac{q\bar c}{V} \tag{73}$$

Thus, the system matrices become:

$$\begin{cases} A &= \begin{bmatrix} 0 & 1 \\ \frac{((-Cz_{\dot\alpha}+2\cdot\mu_c)\cdot Cm_\alpha+Cm_{\dot\alpha}\cdot Cz_a)}{(2\cdot\frac{\bar c}{V}\cdot(-Cz_{\dot\alpha}+2\cdot\mu_c)\cdot\mu_c\cdot K_Y^2)} & \frac{((2\cdot C_{m_q}+2\cdot Cm_{\dot\alpha})\cdot\mu_c-C_{m_q}\cdot Cz_{\dot\alpha}+Cm_{\dot\alpha}\cdot Cz_q)}{(2\cdot\frac{\bar c}{V}\cdot(-Cz_{\dot\alpha}+2\cdot\mu_c)\cdot\mu_c\cdot K_Y^2)} \end{bmatrix} \\ B &= \begin{bmatrix} 0 \\ \frac{((-Cz_{\dot\alpha}+2\cdot\mu_c)\cdot Cm_{\delta_e}+C_{m_{\dot\alpha}}\cdot Cz_{\delta_e})}{(2\cdot\frac{\bar c}{V}\cdot(-Cz_{\dot\alpha}+2\cdot\mu_c)\cdot\mu_c\cdot K_Y^2)} \end{bmatrix} \end{cases} \tag{74}$$

This means that the control effectiveness is equal to $\frac{((-Cz_{\dot\alpha}+2\cdot\mu_c)\cdot Cm_{\delta_e}+C_{m_{\dot\alpha}}\cdot Cz_{\delta_e})}{(2\cdot\frac{\bar c}{V}\cdot(-Cz_{\dot\alpha}+2\cdot\mu_c)\cdot\mu_c\cdot K_Y^2)}$. Thus,

$$\hat G^{-1} = \frac{(2\cdot\frac{\bar c}{V}\cdot(-Cz_{\dot\alpha}+2\cdot\mu_c)\cdot\mu_c\cdot K_Y^2)}{((-Cz_{\dot\alpha}+2\cdot\mu_c)\cdot Cm_{\delta_e}+C_{m_{\dot\alpha}}\cdot Cz_{\delta_e})} \tag{75}$$

Moreover, the output is chosen to be the angle of attack α, which means that the matrices C and D are given by eq. (76).

$$\begin{cases} C &= \begin{bmatrix} 1 & 0 \end{bmatrix} \\ D &= \begin{bmatrix} 0 \end{bmatrix} \end{cases} \tag{76}$$

For the construction of the close-loop transfer function of the system, the reader is again referred to the block diagram of the generic INDI-controlled system shown in fig. 20, and the values of the parameters used for the case of this control system are shown in table III.

As commented before, for the case considered of the INDI-control of short period dynamics, a closed-loop system which is a TDS of the neutral type is obtained. This means that for the analysis in the frequency domain, the behaviour of the frequency sweeping curves as $\omega \to \infty$ has to be examined. Specifically, it is required that the frequency sweeping curve remains above the horizontal line $\Gamma = 1$ for when $\omega \to \infty$, because this condition ensures the strong stability of the delay-difference operator in the dynamics of the neutral TDS [28].

A. Stability Regions in the Delay Space of INDI-controlled Short Period Dynamics

The obtained stable time-delay interval is [0, 0.1080529]s, for the case of replacing α equation for the kinematics only for the controller design. The obtained frequency sweeping curve for the control system is shown for different ranges of ω in fig. 16a and in fig. 16b. While fig. 16a more clearly shows the CIR, fig. 16b shows that the Schur-Cohn stability of the delay-difference operator is guaranteed because the frequency sweeping curve remains above $\Gamma = 1$.

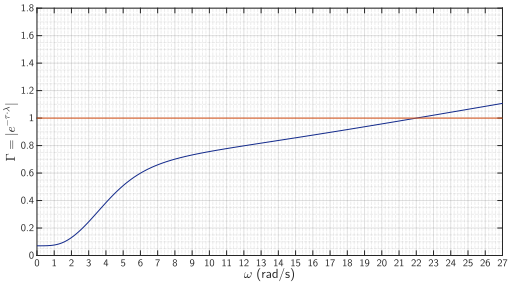

(a) Frequency sweeping curve for the INDI-controlled short period dynamics.

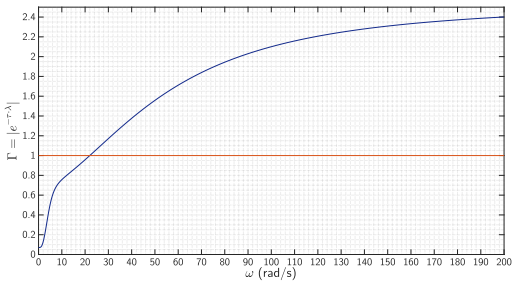

(b) Frequency sweeping curve for the INDI-controlled short period dynamics for $\omega \in [0, 200]$ rad/s.

B. Robust Stability Regions in the Delay Space of INDI-controlled Short Period Dynamics

For the robust stability analysis of this control system, the concern will be with the stability derivatives C_{m_α} and C_{m_q}, and the control derivative $C_{m_{\delta_e}}$. Moreover, it is desired to investigate cases of different uncertainty structures. Those derivatives allow for discussions on polytopic and multilinear uncertainty. However, since, for polynomic uncertainty, the uncertain parameter needs to have a power that is larger than 1, another parameter needs to be considered. Specifically, the stability derivative $C_{m_{\dot\alpha}}$ will be considered as an uncertain parameter in one of the following illustrative examples.

Before proceeding further, the characteristic equation in terms of the parameters C_{m_α}, C_{m_q}, $C_{m_{\delta_e}}$, and $C_{m_{\dot\alpha}}$ needs to be presented, and it is of the form shown in eq. (77).

$$
\begin{aligned}
&((a_1 \cdot C_{m_{\dot\alpha}} + a_2 \cdot C_{m_{\delta_e}} + a_3 \cdot C_{m_q} + a_4 \cdot C_{m_{\dot\alpha}}^2 + a_5 \cdot C_{m_\alpha} \cdot C_{m_{\dot\alpha}} \\
&+ a_6 \cdot C_{m_\alpha} \cdot C_{m_{\delta_e}} + a_7 \cdot C_{m_{\dot\alpha}} \cdot C_{m_{\delta_e}} + a_8 \cdot C_{m_{\dot\alpha}} \cdot C_{m_q} + a_9 \cdot C_{m_{\delta_e}} \cdot C_{m_q}) \\
&+ (a_{10} + a_{11} \cdot C_{m_{\dot\alpha}} + a_{12} \cdot C_{m_{\delta_e}} + a_{13} \cdot C_{m_q} + a_{14} \cdot C_{m_{\dot\alpha}}^2 + a_{15} \cdot C_{m_{\dot\alpha}} \cdot C_{m_{\delta_e}} + a_{16} \cdot C_{m_{\dot\alpha}} \cdot C_{m_q} + a_{17} \cdot C_{m_{\delta_e}} \cdot C_{m_q}) \cdot \lambda \\
&+ (+a_{18} \cdot C_{m_{\dot\alpha}} + a_{19} \cdot C_{m_{\delta_e}} + a_{20} \cdot C_{m_q} + a_{21}) \cdot \lambda^2 \\
&+ a_{22} \cdot \lambda^3) \cdot e^{-\lambda \cdot \tau} + \\
&(b_1 \cdot C_{m_{\dot\alpha}}^2 + b_2 \cdot C_{m_\alpha} \cdot C_{m_{\dot\alpha}} + b_3 \cdot C_{m_\alpha} \cdot C_{m_{\delta_e}} + b_4 \cdot C_{m_{\dot\alpha}} \cdot C_{m_{\delta_e}} + b_5 \cdot C_{m_{\dot\alpha}} \cdot C_{m_q} + b_6 \cdot C_{m_{\delta_e}} \cdot C_{m_q}) \\
&+ (b_7 \cdot C_{m_{\delta_e}} + b_8 \cdot C_{m_{\dot\alpha}} + b_9 \cdot C_{m_{\dot\alpha}}^2 + b_{10} \cdot C_{m_\alpha} \cdot C_{m_{\dot\alpha}} \\
&+ b_{11} \cdot C_{m_\alpha} \cdot C_{m_{\delta_e}} + b_{12} \cdot C_{m_{\dot\alpha}} \cdot C_{m_{\delta_e}} + b_{13} \cdot C_{m_{\dot\alpha}} \cdot C_{m_q} + b_{14} \cdot C_{m_{\delta_e}} \cdot C_{m_q}) \cdot \lambda \\
&+ (+b_{15} \cdot C_{m_{\dot\alpha}} + b_{16} \cdot C_{m_{\delta_e}} + b_{17} \cdot C_{m_{\dot\alpha}}^2 + b_{18} \cdot C_{m_{\dot\alpha}} \cdot C_{m_{\delta_e}} + b_{19} \cdot C_{m_{\dot\alpha}} \cdot C_{m_q} + b_{20} \cdot C_{m_{\delta_e}} \cdot C_{m_q}) \cdot \lambda^2 \\
&+ b_{21} \cdot C_{m_{\dot\alpha}} \cdot \lambda^3 + b_{22} \cdot C_{m_{\delta_e}} \cdot \lambda^3
\end{aligned}
\tag{77}
$$

It should be noted that, for this example a larger number of decimal points is taken in order to be able to notice the influence of some of the uncertain parameters on the obtained stability intervals.

1) Uncertainty in C_{m_α}

For the case when there is uncertainty in the parameter C_{m_α}, specifically that it belongs to $[-0.6, -0.35]$, the resultant stability region is reduced from [0, 0.1080529]s to [0,0.1077114]s. This example showcases the polytopic uncertainty structure because the parameter C_{m_α} appears in several places in the quasipolynomial, but it does not appear with powers higher than one in the characteristic equation. For this analysis, the edge theorem could be readily used, and as there was one uncertain parameter, there was one edge. Since this is an example with polytopic structure, the stability interval obtained is the actual stability interval, and that has been verified through applying the grid approach.

2) Uncertainty in C_{m_α} and C_{m_q}

For the case when there are uncertainties in the parameters C_{m_α} and C_{m_q}, specifically that they belong to $[-0.473, -0.387]$ and $[-7.744, -6.336]$ respectively (which corresponds to a 10 % variation from the nominal values), the resultant stability region is reduced from [0, 0.1080529]s to [0,0.1079465]s. A verification of these results is seen in fig. 17 and fig. 18. This is another example of a system exhibiting a polytopic uncertainty structure because the coefficients C_{m_α} and C_{m_q} do not appear in the same coefficients together. This means that the results obtained from the analysis based on the edge theorem are expected to be exact, and indeed they are. The grid approach applied with steps 0.0086 and 0.1408 has also yielded the same stability interval for first seven decimal places [0,0.1079465]s.

3) Uncertainty in C_{m_α} and $C_{m_{\delta_e}}$

In this example, uncertainties in C_{m_α} and $C_{m_{\delta_e}}$ are considered, whereby $C_{m_\alpha} \in [-0.473, -0.387]$ and $C_{m_{\delta_e}} \in [-1.7083, -1.3977]$. This example showcases a multilinear uncertainty structure because C_{m_α} and $C_{m_{\delta_e}}$ are seen multiplied

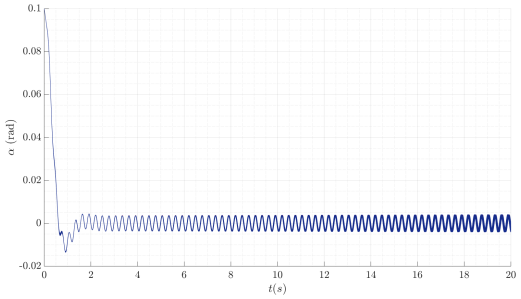

Fig. 17: Profile view for $\tau = 0.1079$s for case of uncertainties in C_{m_α} and C_{m_q}

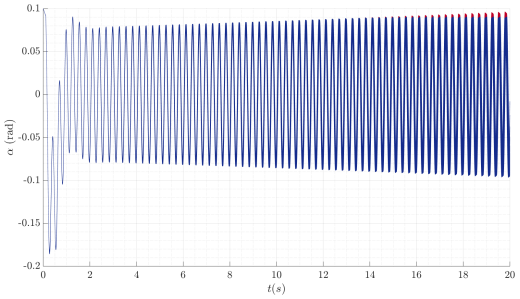

Fig. 18: Profile view for $\tau = 0.1080$s for case of uncertainties in C_{m_α} and C_{m_q}

together in some of the coefficients of the quasipolynomials. This means that the results obtained from the analysis based on the edge theorem are expected to be conservative.

The analysis based on applying the robust analytic curve frequency sweeping approach with increments in μ equal to 0.01, the stability interval obtained is [0,0.10656334]s. The result obtained from a grid approach, using a step of 0.0086 for C_{m_α} and 0.03106 for $C_{m_{\delta_e}}$, leads to the stability interval [0,0.1065634]s, which happens to be equal to value determined from the robust analytic frequency sweeping approach. This is because the range for the coefficients leads to value sets that are almost polytopic. Indeed, the coefficients a_6 and b_{11} in eq. (67) have the same value but opposite signs, which hints at the possibility that the contributions of the multilinear components may be canceling each other.

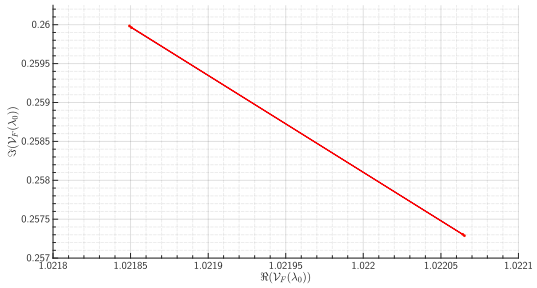

(a) Value set of the quasipolynomial pertaining to the short period dynamics at $\lambda = 1j$ rad/s and $\tau = 0.1$s (blue scatter plot) and the overbounding contour (red plot) based on applying Theorem 3.

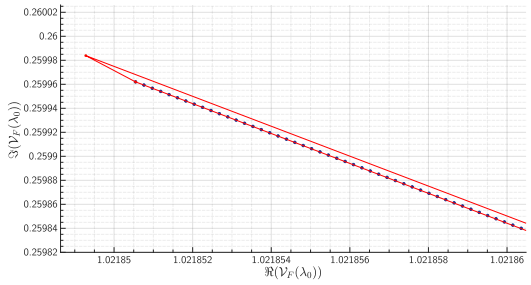

(b) Zoomed view of the top left part of the value set of the quasipolynomial pertaining to the short period dynamics at $\lambda = 1j$ rad/s and $\tau = 0.1$s (blue scatter plot) and the overbounding contour (red plot) based on applying Theorem 3.

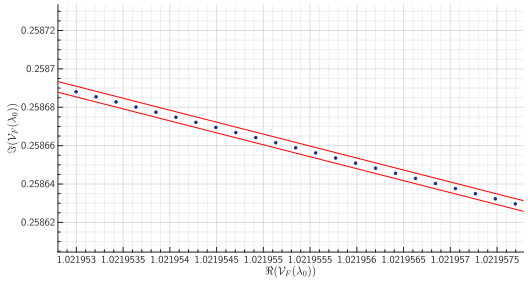

(c) Zoomed view of the middle part of the value set of the quasipolynomial pertaining to the short period dynamics at $\lambda = 1j$ rad/s and $\tau = 0.1$s (blue scatter plot) and the overbounding contour (red plot) based on applying Theorem 3.

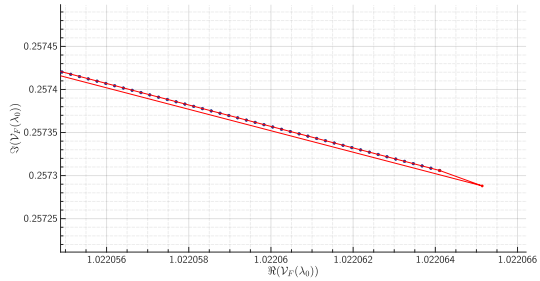

(d) Zoomed view of the bottom right part of the value set of the quasipolynomial pertaining to the short period dynamics at $\lambda = 1j$ rad/s and $\tau = 0.1$s (blue scatter plot) and the overbounding contour (red plot) based on applying Theorem 3.

4) Uncertainty in $C_{m_{\dot\alpha}}$

In this case, uncertainty in the value of $C_{m_{\dot\alpha}}$ is assumed. Specifically, it is assumed that $C_{m_{\dot\alpha}} \in [-4.07, -3.33]$. As can be seen from eq. (77), $C_{m_{\dot\alpha}}$ appears with a power of two in some locations in the characteristic equation. This means that, in this example, a polynomic uncertainty structure is being dealt with.

The result of performing the analysis based on applying Theorem 3, the multilinear theorem, and the edge theorem is [0,0.1080514]s. This is clearly a small decrease in the stability interval from the nominal one which is [0, 0.1080529]s. The

effect of uncertainties in $C_{m_{\dot{\alpha}}}$ is small because it appears in terms where the coefficient is orders of magnitude smaller than some of the other coefficients. Since the value sets are overbounded, it is expected that the stability interval [0,0.1080514]s is an underapproximation of the actual robust stability region. This is clear from the example value sets of the characteristic quasipolynomial of the short period dynamics, which shown over four figures: fig. 19a, fig. 19b, fig. 19c, and fig. 19d. Note that, the value set is an arc in this case. Moreover, the application of Theorem 3 led to a quadrilateral enclosure around this arc, and it is the edges of this quadrilateral that were used in the robust analytic curve frequency sweeping approach.

In order to check the actual robust stability regions, the grid approach is applied, with the stability analysis performed for different values of $C_{m_{\dot{\alpha}}}$ varying between -4.07 and -3.33 with a step size of 0.00074. The result is the stability interval [0,0.1080527]s.

VIII. Conclusions and Recommendations

In conclusion, this article set out to determine the robustly stable time-delay regions of the incremental controller, INDI. Through the use of the analytic curve frequency sweeping approach combined with the edge theorem, a suitable robust stability analysis technique in the frequency domain has been obtained. As for the stability analysis in the time-domain, for the case of retarded TDSs, the stability analysis has been done based on the application of the stability results presented in [37]. The analysis of robust stability in the time-domain for the case of the sub-polytopic uncertainty is relatively easy as only vertex results need to be checked. Moreover, the determined robust stability regions are verified through simulation. Finally, a number of stability results for the control system incorporating the zero-order hold filter are also presented based on the frequency approach. The effectiveness of these stability analysis methods is demonstrated through their application to a pendulum control system and to the INDI-controlled short period dynamics.

Many recommendations can made for future research as this research is merely the beginning for such an analysis on incremental controllers. However, a select few are promoted in the following. First, it is recommended to apply the methods proposed in this thesis to the stability analysis of IBS-controlled systems. IBS is a sibling and competing incremental control technique to INDI, and part of unraveling the theoretical gaps regarding incremental control is to compare those two methods. It is particularly interesting to show how the time-delay stability regions for these control techniques compare. In reality, incommensurate delays occur in a system. That is why, the stability results need to be extended to the case of multiple incommensurate delays. In the frequency domain, such an extension of the analytic curve frequency sweeping approach has already been proposed in the literature, and it is called the "Iterative Frequency Sweeping Approach" [47]. As for the analysis in the time-domain, the stability results for both the retarded and neutral cases need to be extended to the case of multiple delays, possibly following the steps outlined in [22]. Moreover, it is recommended to derive matrix inequalities that account for norm-bounded uncertainty because the analyses in this case can be more tractable (although more conservative) than the robust analyses presented in this article. Finally, it is recommended to develop the time-domain stability results for the case of distributed delays. The reason for this is that, for some control applications, distributed delays are more representative of reality for that system. The results of the analyses based on the systems with different time-delay models are not equivalent, and this discrepancy manifests itself in the phenomenon of quenching.

Appendix A
Block diagrams

A generic block diagram of an INDI-controlled system with time-delays in the feedback signals fig. 20, and a block diagram of an INDI-controlled system with time-delays in the feedback signals but that also incorporates the ZOH filter is shown in fig. 21.

References

[1] G. Perdikaris, *Computer Controlled Systems: Theory and Applications*. Intelligent Systems, Control and Automation: Science and Engineering, Springer Netherlands, 2013.

[2] C. Fielding and P. K. Flux, "Non-linearities in flight control systems," *The Aeronautical Journal (1968)*, vol. 107, no. 1077, p. 673–686, 2003.

[3] J.-P. Richard, "Time-delay systems: an overview of some recent advances and open problems," *Automatica*, vol. 39, no. 10, pp. 1667–1694, 2003.

[4] S.-I. Niculescu, *Delay effects on stability: a robust control approach*, vol. 269. Springer Science & Business Media, 2001.

[5] R. H. Middleton and D. E. Miller, "On the achievable delay margin using lti control for unstable plants," *IEEE Transactions on Automatic Control*, vol. 52, no. 7, pp. 1194–1207, 2007.

[6] E. J. Smeur, G. C. De Croon, and Q. Chu, "Gust disturbance alleviation with incremental nonlinear dynamic inversion," in *IEEE International Conference on Intelligent Robots and Systems*, 2016.

[7] G. F. Franklin, J. D. Powell, M. L. Workman, *et al.*, *Digital control of dynamic systems*, vol. 3. Addison-wesley Menlo Park, CA, 1998.

[8] B. L. Stevens, F. L. Lewis, and E. N. Johnson, *Aircraft control and simulation: dynamics, controls design, and autonomous systems*. John Wiley & Sons, 2015.

[9] S. Sieberling, Q. P. Chu, and J. A. Mulder, "Robust Flight Control Using Incremental Nonlinear Dynamic Inversion and Angular Acceleration Prediction," *Journal of Guidance, Control, and Dynamics*, 2010.

[10] R. van't Veld, "Incremental nonlinear dynamic inversion flight control: Stability and robustness analysis and improvements," Master's thesis, Delft University of Technology, sep 2016.

[11] R. van 't Veld, E.-J. Van Kampen, and Q. P. Chu, "Stability and Robustness Analysis and Improvements for Incremental Nonlinear Dynamic Inversion Control," 2018.

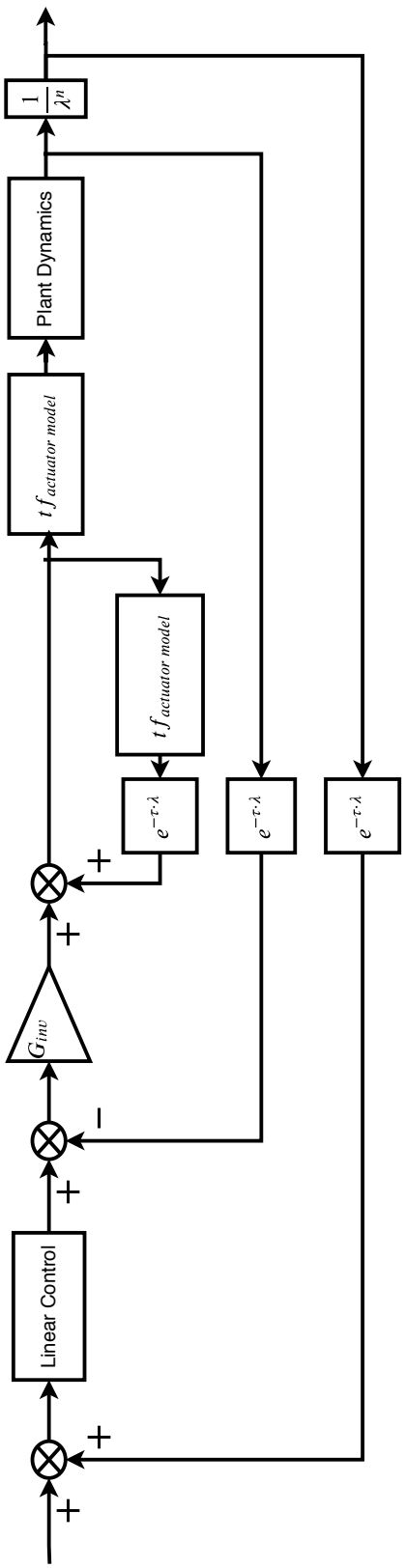

Fig. 20: Block diagram of INDI-controlled system

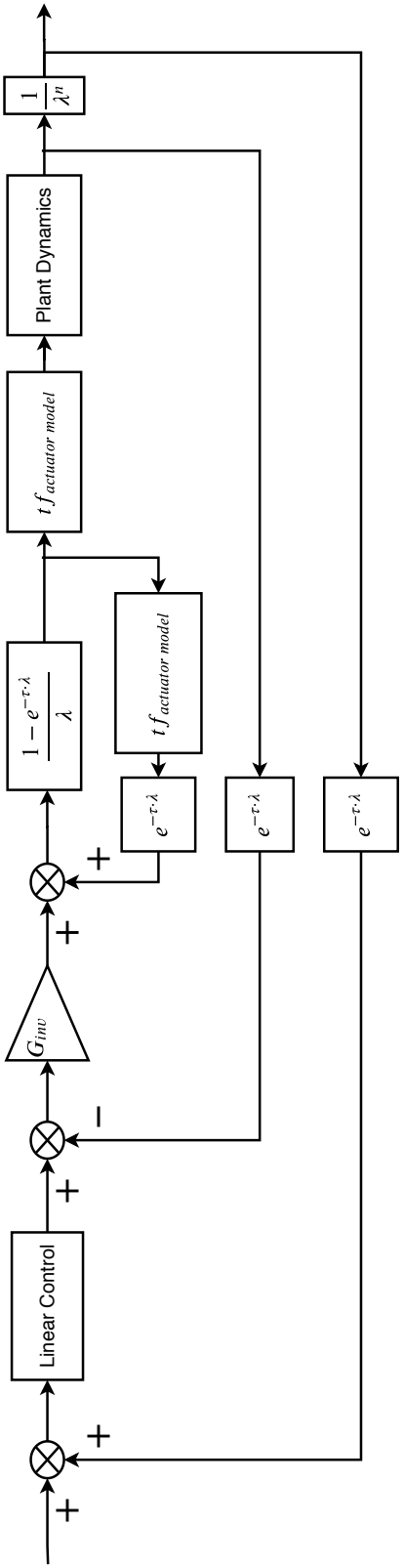

Fig. 21: Block diagram of INDI-controlled system with zero-order hold filter.

[12] A. Dorobantu, P. Seiler, and G. J. Balas, "Time-delay margin analysis for an adaptive controller," *Journal of Guidance, Control, and Dynamics*, vol. 35, no. 5, pp. 1418–1425, 2012.

[13] A. M. Pacheco, "Time delay margin analysis for model reference adaptive flight control laws," Master's thesis, Delft University of Technology, nov 2018.

[14] R. van 't Veld, E.-J. Van Kampen, and Q. P. Chu, "Stability and Robustness Analysis and Improvements for Incremental Nonlinear Dynamic Inversion Control," 2018.

[15] E. Smeur, *Incremental Control for Hybrid Micro Air Vehicles*. PhD thesis, Delft University of Technology, nov 2018.

[16] Y. Huang, D. M. Pool, O. Stroosma, and Q. Chu, "Long-stroke hydraulic robot motion control with incremental nonlinear dynamic inversion," *IEEE/ASME Transactions on Mechatronics*, 2019.

[17] J. Koschorke, "Advanced flight control design and evaluation: An application of time delayed incremental backstepping," Master's thesis, Delft University of Technology, jun 2012.

[18] F. Grondman, G. Looye, R. O. Kuchar, Q. P. Chu, and E.-J. Van Kampen, "Design and Flight Testing of Incremental Nonlinear Dynamic Inversion-based Control Laws for a Passenger Aircraft," 2018.

[19] A. Seuret, F. Gouaisbaut, and L. Baudouin, "D1. 1-overview of lyapunov methods for time-delay systems," 2016.

[20] A. Papachristodoulou, M. M. Peet, and S.-I. Niculescu, "Stability analysis of linear systems with time-varying delays: Delay uncertainty and quenching," in *2007 46th IEEE Conference on Decision and Control*, pp. 2117–2122, IEEE, 2007.

[21] R. Sipahi, *Mastering Frequency Domain Techniques for the Stability Analysis of LTI Time Delay Systems*, vol. 20. SIAM, 2019.

[22] K. Gu, J. Chen, and V. L. Kharitonov, *Stability of time-delay systems*. Springer Science & Business Media, 2003.

[23] R. Sipahi and S.-I. Niculescu, "Stability of car following with human memory effects and automatic headway compensation," *Philosophical Transactions of the Royal Society A: Mathematical, Physical and Engineering Sciences*, vol. 368, no. 1928, pp. 4563–4583, 2010.

[24] K. Gu and S.-I. Niculescu, "Survey on recent results in the stability and control of time-delay systems," *Journal of dynamic systems, measurement, and control*, vol. 125, no. 2, pp. 158–165, 2003.

[25] A. Fioravanti, *H analysis and control of time-delay systems by methods in frequency domain*. PhD thesis, Paris 11, 2011.

[26] E. Fridman, *Introduction to time-delay systems: Analysis and control*. Springer, 2014.

[27] G. M. SCHOEN, *Stability and Stabilization of Time-Delay Systems*. PhD thesis, SWISS FEDERAL INSTITUTE OF TECHNOLOGY ZURICH, 1995.

[28] X.-G. Li, S.-I. Niculescu, and A. Cela, *Analytic curve frequency-sweeping stability tests for systems with commensurate delays*. Springer, 2015.

[29] W. Michiels and S.-I. Niculescu, *Stability, control, and computation for time-delay systems: an eigenvalue-based approach*, vol. 27. Siam, 2014.

[30] G. J. Silva, A. Datta, and S. P. Bhattacharyya, *PID controllers for time-delay systems*. Springer Science & Business Media, 2007.

[31] J. Chen, P. Fu, and S.-I. Niculescu, "When will zeros of time-delay systems cross imaginary axis?," in *2007 European Control Conference (ECC)*, pp. 5631–5638, IEEE, 2007.

[32] K. Gu, A. C. Luo, and S.-I. Niculescu, "Discretized lyapunov functional for systems with distributed delay," in *1999 European Control Conference (ECC)*, pp. 3649–3654, IEEE, 1999.

[33] E. Fridman, "Descriptor discretized lyapunov functional method: Analysis and design," *IEEE Transactions on Automatic control*, vol. 51, no. 5, pp. 890–897, 2006.

[34] K. Gu, "A further refinement of discretized lyapunov functional method for the stability of time-delay systems," *International Journal of Control*, vol. 74, no. 10, pp. 967–976, 2001.

[35] K. Gu, "Refined discretized lyapunov functional method for systems with multiple delays," *International Journal of Robust and Nonlinear Control: IFAC-Affiliated Journal*, vol. 13, no. 11, pp. 1017–1033, 2003.

[36] A. Seuret and F. Gouaisbaut, "Complete quadratic lyapunov functionals using bessel-legendre inequality," in *2014 European Control Conference (ECC)*, pp. 448–453, IEEE, 2014.

[37] A. Seuret and F. Gouaisbaut, "Hierarchy of lmi conditions for the stability analysis of time-delay systems," *Systems & Control Letters*, vol. 81, pp. 1–7, 2015.

[38] S. Skogestad and I. Postlethwaite, *Multivariable feedback control: analysis and design*, vol. 2. Wiley New York, 2007.

[39] M. Fu, A. W. Olbrot, and M. P. Polis, "Robust stability for time-delay systems: the edge theorem and graphical tests," *IEEE Transactions on Automatic Control*, vol. 34, no. 8, pp. 813–820, 1989.

[40] M. Fu, A. W. Olbrot, and M. P. Polis, "The edge theorem and graphical tests for robust stability of neutral time-delay systems," *Automatica*, vol. 27, no. 4, pp. 739–741, 1991.

[41] İ. Tuzcu, "A computational approach to stability of polytopic families of quasi-polynomials with single delay," *International Journal of Robust and Nonlinear Control*, vol. 20, no. 17, pp. 1981–1992, 2010.

[42] B. R. Barmish, *New tools for robustness of linear systems*. Macmilllan, 1994.

[43] R. S. Sanchez Pena, *Robust analysis of feedback systems with parametric and dynamic structured uncertainty*. PhD thesis, California Institute of Technology, 1989.

[44] K. Walton and J. Marshall, "Direct method for tds stability analysis," in *IEE Proceedings D-Control Theory and Applications*, vol. 134, pp. 101–107, IET, 1987.

[45] X.-G. Li, S.-I. Niculescu, A. Çela, H.-H. Wang, and T.-Y. Cai, "On τ-decomposition frequency-sweeping test for a class of time-delay systems. part i: Simple imaginary roots case," *IFAC Proceedings Volumes*, vol. 45, no. 14, pp. 132–137, 2012.

[46] X.-G. Li, S.-I. Niculescu, A. Çela, H.-H. Wang, and T.-Y. Cai, "On τ-decomposition frequency-sweeping test for a class of time-delay systems. part ii: Multiple roots case," *IFAC Proceedings Volumes*, vol. 45, no. 14, pp. 138–143, 2012.

[47] X.-G. Li, S.-I. Niculescu, and A. Çela, "An iterative frequency-sweeping approach for stability analysis of linear systems with multiple delays," *IMA Journal of Mathematical Control and Information*, vol. 36, no. 02, pp. 379–398, 2017.

II

Preliminary Study

Part of Previously Graded Content.

This page was intentionally left blank.

2

Nonlinear Control

This chapter will give a review of the model-based nonlinear control method, Nonlinear Dynamic Inversion (NDI), as well as its incremental form, Incremental Nonlinear Dynamic Inversion (INDI). As the main focus of this thesis is on incremental control techniques, advancements and implementations of INDI will be provided as well.

The structure of the chapter is as follows. First, the principles of NDI will be explained in section 2.1, and the extension of NDI into INDI, in its several variants, will be discussed in section 2.2. This section concludes with a survey of academic publications on INDI.

2.1 Nonlinear Dynamic Inversion

Nonlinear Dynamic Inversion (NDI), which is also commonly known as feedback linearization, is a nonlinear control technique. It relies on inverting the plant dynamics in order to cancel the nonlinearities in the system, either fully or partially. As opposed to traditional linearization techniques, NDI reaps the benefit that the linearization is usually applicable, if not globally, to a larger region than in the case of Jacobian linearization, for instance.

The first discussion is on the feedback linearization of systems in the controllability canonical form (also referred to as the companion form). This is a good entering point for the discussions because the controllability canonical form is required for feedback linearization. Thus, beginning with a system that is already in the "correct" form helps to intuitively convey the main idea behind the control technique.

The discussions in the following parts on NDI get progressively more involved. After introducing feedback linearization, the discussion that follows generalizes to the cases when the system provided is not in the controllability canonical form. Since the form is important for the inversion of the dynamics, the means to transform the system into the companion form will receive their due attention. This discussion includes a presentation of mathematical topics such as diffeomorphisms, Lie derivatives, and the Frobenius theorem.

Besides whether or not the system is in the controllability canonical form, another complication appears. Depending on the system's output equation, it may be the case that the input-output relation does not fully linearize the system. This means that a part of the system is unobservable. This part is adequately referred to as the internal dynamics. The consideration of internal dynamics is important because the stability of the internal dynamics is necessary for the effectiveness of NDI in solving the stabilization or tracking problem.

While input-state linearization is, by definition, a full linearization, i.e. one that does not lead to any internal dynamics, input-output linearization accommodates the possibility that there may be internal dynamics in the system. This makes input-output linearization the encompassing topic among the presented topics. Being the most general of the three, input-output linearization will be discussed for the MIMO case as well.

The structure of this section is as follows. First, the application of NDI to systems with a controllability canonical form will be shown in section 2.1.1. Input-state linearization will be dealt with in section 2.1.2, and the mathematical concepts will first be introduced in this subsection as well. Several of these concepts will be encountered again in the subsection that follows, section 2.1.3, which discusses input-output linearization. As mentioned earlier, since input-output linearization offers the most general discussion on NDI, the MIMO case will be covered in that subsection.

2.1.1 NDI and the Controllability Canonical Form

As previously mentioned, a convenient way to convey the gist of NDI is to discuss its application on systems that have the controllability canonical form which is also known as the companion form. A general representation of system dynamics in

canonical form is shown in eq. (2.1). As seen from the equation, a key feature of the controllability canonical form is that there are no derivatives of the control input.

$$x^{(n)} = f(\mathbf{x}) + b(\mathbf{x})u \tag{2.1}$$

In order to represent eq. (2.1) in a state-space form, the equation is augmented with equations of the form $x^{(r)} = \frac{d}{dt}x^{(r-1)}$ for $r < n$. This leads to eq. (2.2).

$$\frac{d}{dt}\begin{bmatrix} x_1 \\ \vdots \\ x_{n-1} \\ x_n \end{bmatrix} = \begin{bmatrix} x_2 \\ \vdots \\ x_n \\ b(\mathbf{x}) + a(\mathbf{x})u \end{bmatrix} \tag{2.2}$$

The nonlinearities that appear in the bottom row, on the right-hand side of eq. (2.2) need to eliminated. In order to do that, the control input is selected to have the form shown in eq. (2.3).

$$u = a^{-1}(\mathbf{x})[v - b(\mathbf{x})] \tag{2.3}$$

In other words, the variable v, which is referred to as the virtual control input, is defined to be equal to the expression shown in eq. (2.4).

$$v \triangleq a(\mathbf{x})[\mathbf{u} + b(\mathbf{x})] \tag{2.4}$$

Substituting the expression for u, eq. (2.3), into eq. (2.2) leads to the linear input-output relation shown in eq. (2.5).

$$\frac{d}{dt}\begin{bmatrix} x_1 \\ x_2 \\ \vdots \\ x_{n-1} \\ x_n \end{bmatrix} = \begin{bmatrix} 0 & 1 & 0 & \cdots & 0 \\ 0 & 0 & 1 & \cdots & 0 \\ \vdots & \vdots & & \ddots & \vdots \\ 0 & 0 & 0 & \cdots & 1 \\ 0 & 0 & 0 & \cdots & 0 \end{bmatrix}\begin{bmatrix} x_1 \\ x_2 \\ \vdots \\ x_{n-1} \\ x_n \end{bmatrix} + \begin{bmatrix} 0 \\ 0 \\ \vdots \\ 0 \\ 1 \end{bmatrix} v = \begin{bmatrix} x_2 \\ \vdots \\ x_n \\ v \end{bmatrix} \tag{2.5}$$

The linearization leads to the multiple integrator form in the bottom row of eq. (2.5), which is shown for convenience in eq. (2.6).

$$\frac{dx_n}{dt} = v \tag{2.6}$$

After the linearization of the dynamics in the inner-loop, it remains to design an outer-loop linear controller. For stabilization problems which are also referred to as regulation problems, the virtual control takes the form shown in eq. (2.7).

$$v = -k_0 x - k_1 \frac{dx}{dt} - k_2 \frac{d^2x}{dt^2} - \cdots - k_{n-1}\frac{d^{n-1}x}{dt^{n-1}} \tag{2.7}$$

The reason for taking this form becomes clear after substituting the expression for v from eq. (2.7) into eq. (2.6), which leads to the closed-loop system shown in eq. (2.8).

$$\frac{d^n x}{dt^n} + k_{n-1}\frac{d^{n-1}x}{dt^{n-1}} + \cdots + k_2\frac{d^2x}{dt^2} + k_1\frac{dx}{dt} + k_0 x = 0 \tag{2.8}$$

It can be seen that, through as suitable choice of the gains $k_0, k_1, \cdots, k_{n-1}$ based on linear control design techniques (such as root locus, pole placement, and bode plots), the closed-loop system can be made to be asymptotically stable. Consequently, this means that the variable that needs to be stabilized tends to zero.
As for tracking problems, the outer-loop linear control takes the form shown in eq. (2.9).

$$v = -k_0(x - x_d) - k_1\frac{d(x - x_d)}{dt} - k_2\frac{d^2(x - x_d)}{dt^2} - \cdots - k_{n-1}\frac{d^{n-1}(x - x_d)}{dt^{n-1}} + \frac{d^n x_d}{dt^n} \tag{2.9}$$

which leads to the following closed-loop system:

$$\frac{d^n x}{dt^n} - \frac{d^n x_d}{dt^n} = -k_0 e - k_1\frac{de}{dt} - k_2\frac{d^2e}{dt^2} - \cdots - k_{n-1}\frac{d^{n-1}e}{dt^{n-1}} = \frac{d^n e}{dt^n} \tag{2.10}$$

Alternatively, the closed-loop system can be written in terms of the tracking error as shown in eq. (2.11).

$$\frac{d^n e}{dt^n} + k_{n-1}\frac{d^{n-1}e}{dt^{n-1}} + \cdots + k_2\frac{d^2e}{dt^2} + k_1\frac{de}{dt} + k_0 e = 0 \tag{2.11}$$

Similar to the case of the stabilization control problem, a suitable choice of the gains $[k_0, k_1, k_2, ..., k_{n-1}]$ ensures that a stable closed-loop system is obtained and that the tracking error tends to zero.

2.1.2 Input-State Linearization

Input-state linearization is a two-step approach. The first step is to transform the inputs and states in order to fully linearize the system, and the second step is to design a suitable controller for the linearized dynamics. For the first step, the feasibility of the state and input transformations requires certain conditions to be satisfied. In the following, these conditions as well as the steps involved in the transformations will be discussed. As for the choice of the control gains, the same guidelines presented in the previous subsection apply here again.

Consider the input-state equation, with a single input, shown in eq. (2.12).

$$\dot{\mathbf{x}} = \mathbf{f}(\mathbf{x}, u) \tag{2.12}$$

For the input transformation to be possible, the input-state equation should be affine in the control input, which is the case for the input-state equation shown in eq. (2.13). Note that the vector fields $\boldsymbol{f}$ and $\boldsymbol{g}$ in the equation are smooth, meaning that they are infinitely differentiable.

$$\dot{\mathbf{x}} = \mathbf{f}(\mathbf{x}) + \mathbf{g}(\mathbf{x})\, u \tag{2.13}$$

More general than the applicability of an input transformation to eq. (2.13), the input transformation is also possible for systems of the form shown in eq. (2.14), where the scalar function t is an invertible function. Note, that, here too, the vector fields are smooth.

$$\dot{\mathbf{x}} = \mathbf{f}(\mathbf{x}) + \mathbf{g}(\mathbf{x})\, t[u + \phi(\mathbf{x})] \tag{2.14}$$

The rationale behind this generalization can be seen through a replacement of the expression $t[u+\phi(\mathbf{x})]$, with some temporary variable w, which returns the form of eq. (2.13). As the function w is invertible, one can design for the variable w and then determine the control input variable u based on the relation $u = t^{-1}(w) - \phi(\mathbf{x})$.

Before moving on to discussing the conditions for the state transformation, the definition of state-linearization is presented to cement the previously discussed concepts and to bridge to the discussion on the conditions for state transformation.

Definition 2.1 (Input-state Linearization): *The system shown in eq.* (2.13) *is considered to be input-state linearizable if there is a diffeomorphism $T : \Omega \to \mathbb{R}^n$ which is applied upon the state vector to obtain the new state variables $\mathbf{z} = \mathbf{T}(\mathbf{x})$, and if there is a nonlinear input transformation given by eq.* (2.15)

$$u = \alpha(\mathbf{x}) + \beta(\mathbf{x})\, v \tag{2.15}$$

such that together these transformations lead to a linear time-invariant relation

$$\dot{\mathbf{z}} = \mathbf{A}\mathbf{z} + \mathbf{b}v \tag{2.16}$$

such that

$$\mathbf{A} = \begin{bmatrix} 0 & 1 & 0 & ..0 \\ 0 & 0 & 1 & .. \\ . & . & .. & \\ . & . & .. & \\ . & . & .. & \\ 0 & 0 & 0 & .1 \\ 0 & 0 & ..0 & \end{bmatrix} \quad \mathbf{b} = \begin{bmatrix} 0 \\ 0 \\ . \\ . \\ 0 \\ 1 \end{bmatrix} \tag{2.17}$$

Note, that A and b are in the linear companion form [14].

Starting with the form for the input-state equation in eq. (2.13), the following theorem presents the conditions for a feasible state transformation.

Theorem 2.1 (Conditions for Input-state Linearization [14]): *The nonlinear system of the form considered in eq.* (2.13) *is input-state linearizable if and only if, there exists a region $\boldsymbol{\Omega}$ such that the following conditions hold:*

- *the vector fields $\left\{\mathbf{g}, ad_{\mathbf{f}}\mathbf{g}, \ldots, ad_{\mathbf{f}}^{n-1}\mathbf{g}\right\}$ are linearly independent in $\boldsymbol{\Omega}$, where $ad_{\mathbf{f}}\mathbf{g}$ denotes the Lie bracket of $\boldsymbol{f}$ and $\boldsymbol{g}$, the definition of which is given in Definition 2.3.*

- *the set* $\left\{\mathbf{g}, ad_{\mathbf{f}}\mathbf{g}, \ldots, ad_{\mathbf{f}}^{n-2}\mathbf{g}\right\}$ *is involutive in* $\mathbf{\Omega}$*, where the involutive property is explained in Definition 2.4.*

The complete proof can be found in [14]. However, for completeness, the intuition behind those conditions will be presented. Since the goal of the transformation $\mathbf{z} = \mathbf{T}(\mathbf{x})$ is to bring the system into the controllability canonical form, it is known that after the transformation is performed (if feasible at all), the control input u will only appear in the final equation of eq. (2.18).

$$\begin{aligned} \dot{z}_1 &= \tfrac{\partial T_1}{\partial \mathbf{x}}\mathbf{f} + \tfrac{\partial T_1}{\partial \mathbf{x}}\mathbf{g}u = T_2 \\ \dot{z}_2 &= \tfrac{\partial T_2}{\partial \mathbf{x}}\mathbf{f} + \tfrac{\partial T_2}{\partial \mathbf{x}}\mathbf{g}u = T_3 \\ &\cdots \\ \dot{z}_n &= \tfrac{\partial T_n}{\partial \mathbf{x}}\mathbf{f} + \tfrac{\partial T_n}{\partial \mathbf{x}}\mathbf{g}u = v \end{aligned} \tag{2.18}$$

Since it is desired that only the last equation depend on the control input, it is known that $T_1, \ldots, T_n$ are independent of u, and only v depends on u. In order to simplify the notation, one may use the Lie derivatives, defined as follows.

Definition 2.2 (Lie Derivative [14]): *Let h be a smooth scalar function and* $\boldsymbol{f}$ *a smooth vector field. The Lie derivative of h with respect to* $\mathbf{f}$ *is a vector field that is defined according to eq.* (2.19).

$$L_{\mathbf{f}}h = \nabla h\mathbf{f} = \sum_{i=1}^{n} \frac{\partial h(\mathbf{x})}{\partial x_i} f_i(\mathbf{x}) \tag{2.19}$$

Higher orders of the Lie derivative are obtained, recursively, as shown in eq. (2.20):

$$L_{\mathbf{f}}^{k}h(\mathbf{x}) = L_{\mathbf{f}}\left[L_{\mathbf{f}}^{k-1}h(\mathbf{x})\right] = \nabla\left[L_{\mathbf{f}}^{k-1}h(\mathbf{x})\right]\mathbf{f}(\mathbf{x}) \tag{2.20}$$

Thus, the k^{th} *Lie derivative can be traced back to the* 0^{th} *Lie derivative which is simply equal to the function whose Lie derivative it is desired to compute, as shown in eq.* (2.21).

$$L_{\mathbf{f}}^{0}h(\mathbf{x}) = h(\mathbf{x}) \tag{2.21}$$

As for the case when the Lie derivative is with respect to another vector field, the calculation goes as follows:

$$L_{\mathbf{g}}L_{\mathbf{f}}h = \nabla(L_{\mathbf{f}}h)\mathbf{g} \tag{2.22}$$

Based on this definition, the partial differential equations in eq. (2.18) can be rewritten using Lie derivatives, and the result is shown in eq. (2.23).

$$\begin{aligned} L_{\mathbf{f}}T_1 + L_{\mathbf{g}}T_1 u &= T_2 \\ L_{\mathbf{f}}T_2 + L_{\mathbf{g}}T_2 u &= T_3 \\ &\cdots \\ L_{\mathbf{f}}T_n + L_{\mathbf{g}}T_n u &= v \end{aligned} \tag{2.23}$$

Since the control input only appears in the bottom-most equation, it is deduced that:

$$\begin{aligned} &L_{\mathbf{g}}T_1 = L_{\mathbf{g}}T_2 = \ldots. = L_{\mathbf{g}}T_{n-1} = 0 \quad && L_{\mathbf{g}}T_n \neq 0 \\ &L_{\mathbf{f}}T_i = T_{i+1} && i = 1, 2, \ldots, n-1 \end{aligned} \tag{2.24}$$

Definition 2.3 (Lie Bracket [14]): *For two given vector fields* $\boldsymbol{f}$ *and* $\boldsymbol{g}$*, defined on* $\mathbb{R}^n$*, the Lie bracket of* $\boldsymbol{f}$ *and* $\boldsymbol{g}$*, which is often denoted by* $ad_{\mathbf{f}}\mathbf{g}$*, is defined according to eq.* (2.25).

$$[\mathbf{f}, \mathbf{g}] = \nabla\mathbf{g}\mathbf{f} - \nabla\mathbf{f}\mathbf{g} = L_{\mathbf{f}}\mathbf{g} - L_{\mathbf{g}}\mathbf{f} \tag{2.25}$$

Moreover, higher orders of the Lie bracket are obtained recursively according to eq. (2.26).

$$ad_{\mathbf{f}}^{i}\mathbf{g} = [\mathbf{f}, ad_{\mathbf{f}}^{i-1}\mathbf{g}] \quad i = 1, 2, \cdots \tag{2.26}$$

and knowing that:

$$ad_{\mathbf{f}}^{0}\mathbf{g} = \mathbf{g} \tag{2.27}$$

Equation (2.28) describes the Jacobi identity, which is one of the properties of the Lie Bracket.

$$\begin{aligned} & L_{ad_{\mathbf{f}}\mathbf{g}}h = L_{\mathbf{f}}L_{\mathbf{g}}h - L_{\mathbf{g}}L_{\mathbf{f}}h \\ \iff & \nabla h[\mathbf{f},\mathbf{g}] = \nabla(L_{\mathbf{g}}h)\mathbf{f} - \nabla(L_{\mathbf{f}}h)\mathbf{g} \end{aligned} \tag{2.28}$$

The Jacobi identity can be used to rewrite the constraints in eq. (2.24) only in terms of T_1, which is part of the overall diffeomorphism $T(\mathbf{x})$. This is done as follows.

$$\nabla T_1[\mathbf{f},\mathbf{g}] = \nabla(L_{\mathbf{g}}T_1)\mathbf{f} - \nabla(L_{\mathbf{f}}T_1)\mathbf{g} \tag{2.29}$$

According to eq. (2.24), $L_{\mathbf{g}}T_1 = 0$ and $L_{\mathbf{f}}T_1 = T_2$, thus:

$$\begin{aligned} \nabla T_1[\mathbf{f},\mathbf{g}] &= \nabla(0)\mathbf{f} - \nabla(T_2)\mathbf{g} \\ &= 0 - L_{\mathbf{g}}T_2 = 0 \end{aligned} \tag{2.30}$$

This finding can be generalized to the result in eq. (2.31).

$$\nabla T_1 ad_{\mathbf{f}}^{k}\mathbf{g} = 0 \quad k = 0,1,2,\ldots,n-2 \tag{2.31}$$

It can also be shown that this property is not valid when k = n-1, i.e.

$$\nabla T_1 ad_{\mathbf{f}}^{n-1}\mathbf{g} \neq 0 \tag{2.32}$$

Together, eq. (2.31) and eq. (2.32) are the equivalent constraints to those of eq. (2.24). The result in eq. (2.31) shows a system of differential equations with an unknown variable which is T_1. According to the Frobenius theorem, an unknown function defined as the solution of a set of partial differential equations can be obtained if and only if the vector fields involved in this set of differential equations are involutive. In words, the involutive property means that the Lie Bracket of any chosen pair from the set $\{\mathbf{f}_1,\mathbf{f}_2,\ldots,\mathbf{f}_m\}$ can be written as the linear combination all of the vector fields in that set. This is formally described as follows:

Definition 2.4 (Involutive Property): *A linearly independent set of vector fields $\{\mathbf{f}_1,\mathbf{f}_2,\ldots,\mathbf{f}_m\}$ on $\mathbb{R}^n$ is said to be involutive if, and only if, there are scalar functions $\alpha_{ijk}:\mathbb{R}^n \to \mathbb{R}$ such that:*

$$\left[\mathbf{f}_i,\mathbf{f}_j\right](\mathbf{x}) = \sum_{k=1}^{m} \alpha_{ijk}(\mathbf{x})\mathbf{f}_k(\mathbf{x}) \quad \forall i,j \tag{2.33}$$

where $\left[\mathbf{f}_i,\mathbf{f}_j\right]$ denotes the Lie bracket of $\mathbf{f}_i$ and $\mathbf{f}_j$.

If the conditions for input-state linearization, according to the theorem, are satisfied, it follows to try to find T_1 such that eq. (2.31) and eq. (2.32) are satisfied. Moreover, from the feasibility analysis presented above, it can be deduced that the state transformation is $\boldsymbol{z} = T(\boldsymbol{x}) = (T_1\ L_{\boldsymbol{f}}T_1 \cdots L_{\boldsymbol{f}}^{n-1}T_1)^T$, and the input transformation is of the form:

$$u = \alpha(\mathbf{x}) + \beta(\mathbf{x}) \cdot v \tag{2.34}$$

where:

$$\alpha(\mathbf{x}) = -\frac{L_{\mathbf{f}}z_1}{L_{\mathbf{g}}L_{\mathbf{f}}^{n-1}z_1} \tag{2.35}$$

$$\beta(\mathbf{x}) = \frac{1}{L_{\mathbf{g}}L_{\mathbf{f}}^{n-1}z_1} \tag{2.36}$$

As mentioned in the introduction of this section, input-state linearization is a specific case of input-output linearization where full linearization is achieved. Lemma 2.1 formally states the relation between input-state linearization and input-output linearization.

Lemma 2.1 (Input-state Linearization as a special case of Input-output Linearization [14]): *An n^{th}-order nonlinear system is input-state linearizable if, and only if, there exists a function $\lambda(x)$ such that the input-output linearization with $\lambda(x)$ as output function has relative degree n.*

This Lemma brings attention to the concept of the relative degree which is formally defined for a SISO system as shown in the following.

Definition 2.5 (Relative degree of a SISO system): *The SISO system is said to have a relative degree r in a region Ω if $\forall \mathbf{x} \in \Omega$*

$$\begin{aligned} &L_{\mathbf{g}} L_{\mathbf{f}}^{j} h(\mathbf{x}) = 0 \qquad 0 \leq i < r-1 \\ &L_{\mathbf{g}} L_{\mathbf{f}}^{r-1} h(\mathbf{x}) \neq 0 \end{aligned} \tag{2.37}$$

As for the case of a MIMO system, the definition is slightly more involved, and it reads:

Definition 2.6 (Relative degree for MIMO system): *The MIMO system is said to have relative degree $(r_1, \cdots, r_m)$ at x_0 if there exists a neighborhood Ω of $\mathbf{x_0}$ such that $\forall \mathbf{x} \in \Omega$*

$$L_{\mathbf{g}_i} L_{\mathbf{f}}^{k} h_j(\mathbf{x}) = 0 \quad 0 \leq k < r_i - 1 \tag{2.38}$$

and that the decoupling matrix shown in eq. (2.59) is non-singular. Moreover, the total relative degree of the system is defined according to eq. (2.39).

$$r = r_1 + \cdots + r_m \tag{2.39}$$

In the following part, the input-output linearization is discussed. It is mentioned what additional considerations need to be taken into account in comparison with input-state linearization. Moreover, the MIMO case will also be discussed there.

2.1.3 Input-Output Linearization

As in the case of input-state linearization, the procedure for input-output linearization consists of performing state and input transformations first which are followed by designing a linear controller for the linearized dynamics. Section 2.1.3.1 will discuss the SISO case, and the discussion on the MIMO case which is more involved will follow in section 2.1.3.2.

2.1.3.1 Single Input Single Output Systems

The starting point for input-output linearization is the input-state-output equations, shown for the SISO case in eq. (2.40).

$$\begin{aligned} \dot{\mathbf{x}} &= \mathbf{f}(\mathbf{x}, u) \\ y &= h(\mathbf{x}) \end{aligned} \tag{2.40}$$

Similar to the case of input-state linearization, the system dynamics have to be affine in the control input u. Therefore, input-output linearization is more specifically applicable to eq. (2.41), for the SISO case.

$$\begin{aligned} \dot{\mathbf{x}} &= \mathbf{f}(\mathbf{x}) + \mathbf{g}(\mathbf{x})\, u \\ y &= h(\mathbf{x}) \end{aligned} \tag{2.41}$$

Since the system output information is fed back and relied upon to invert the dynamics, an explicit relation between the input and the output of the system is needed. However, the output equation may not explicitly be in terms of the input. In order to obtain an explicit relation between the output and the input, the output equation is differentiated until the input variable u appears. For the system in eq. (2.41), taking the derivative of the output equation with respect, according to the chain rule, to time gives eq. (2.42).

$$\dot{y} = \frac{\partial h(\mathbf{x})}{\partial \mathbf{x}} \cdot \dot{\mathbf{x}} = \frac{\partial h(\mathbf{x})}{\partial \mathbf{x}} \cdot (\mathbf{f}(\mathbf{x}) + \mathbf{g}(\mathbf{x})\, u) \tag{2.42}$$

As the derivative of a scalar function with respect to a vector is nothing else than the gradient of that scalar function relative to that vector, eq. (2.42) is equivalent to eq. (2.43).

$$\dot{y} = \nabla h(\mathbf{f} + \mathbf{g} u) \tag{2.43}$$

Making use of the definition of the Lie derivative (Definition 2.2), eq. (2.43) can be rewritten as eq. (2.44).

$$\dot{y} = L_{\mathbf{f}} h(\mathbf{x}) + L_{\mathbf{g}} h(\mathbf{x})\, u \tag{2.44}$$

If $L_{\mathbf{g}} h(\mathbf{x}) = 0$, which means that the term involving the control input vanishes, the output equation needs to differentiated again. Moreover, the derivative is taken repeatedly until the control input appears in the expression. A general expression for the ith derivative of the output equation is derived, and the result for that is shown in eq. (2.45).

$$y^{(i)} = L_{\mathbf{f}}^{i} h(\mathbf{x}) + L_{\mathbf{g}} L_{\mathbf{f}}^{i-1} h(\mathbf{x})\, u \tag{2.45}$$

This expression hints that similar to the input-state linearization, the state transformation that needs to be performed will involve $(T_1\, L_{\boldsymbol{f}} T_1 \cdots L_{\boldsymbol{f}}^{r-1} T_1)^T$. However, different from the case of input-state linearization, the exponent r may have a value that is less than n, and the remaining $n - r$ terms of the diffeomorphism may still need to be determined. More on that is presented in the following two subsections for each of the SISO and the MIMO cases.

Building on the fact that the order of the output derivative at which the control term appears (r) may be less than the order of the system (n), the transformation of states that needs to be performed (from the state vector $\mathbf{x}$ to the state vector $\mathbf{z}$) takes the form shown in eq. (2.46),

$$\mathbf{z} = \mathbf{T}(\mathbf{x}) = \begin{bmatrix} T_1(\mathbf{x}) \\ T_2(\mathbf{x}) \\ \vdots \\ T_r(\mathbf{x}) \\ T_{r+1}(\mathbf{x}) \\ \vdots \\ T_n(\mathbf{x}) \end{bmatrix} \tag{2.46}$$

where the functions $T_1(\mathbf{x})$, $T_2(\mathbf{x})$, ..., $T_r(\mathbf{x})$ are defined according to eq. (2.47).

$$\begin{aligned} T_1(\mathbf{x}) &= h(\mathbf{x}) \\ T_2(\mathbf{x}) &= L_f h(\mathbf{x}) \\ \cdots &= \cdots \\ T_r(\mathbf{x}) &= L_f^{r-1} h(\mathbf{x}) \end{aligned} \tag{2.47}$$

and $T_{r+1}(\mathbf{x}), ..., T_n(\mathbf{x})$ are chosen such that $L_g T_i(\mathbf{x}) = 0$ (for all $r + 1 \leq i \leq n$).

Applying this state transformation leads to the system shown in eq. (2.48).

$$\begin{aligned} \dot{z}_1 &= z_2 \\ \dot{z}_2 &= z_3 \\ &\cdots \\ \dot{z}_{r-1} &= z_r \\ \dot{z}_r &= b(\mathbf{z}) + a(\mathbf{z})\, u \\ \dot{z}_{r+1} &= q_{r+1}(\mathbf{z}) \\ &\cdots \\ \dot{z}_n &= q_n(\mathbf{z}) \end{aligned} \tag{2.48}$$

where

$$a(\mathbf{z}) = L_g L_f^{r-1} h(\mathbf{x}) = L_g L_f^{r-1} h\left[\mathbf{T}^{-1}(\mathbf{z})\right], \quad b(\mathbf{z}) = L_f^r h(\mathbf{x}) = L_f^r h\left[\mathbf{T}^{-1}(\mathbf{z})\right] \tag{2.49}$$

and

$$q_i(\mathbf{x}) = L_f T_i(\mathbf{x}) + L_g T_i(\mathbf{x})\, u \tag{2.50}$$

Similar to what was done earlier, it is now possible to completely linearize the first r equations by setting the virtual control equal to the right hand side of the rth differential equation in the system.

$$\begin{aligned} \dot{z}_1 &= z_2 \\ \dot{z}_2 &= z_3 \\ &\cdots \\ \dot{z}_{r-1} &= z_r \\ \dot{z}_r &= \nu \end{aligned} \tag{2.51}$$

2.1.3.2 Multiple Input Multiple Output Systems

In the MIMO case, a similar discussion ensues as that in the SISO case. For the MIMO case, the starting point is eq. (2.52) where the input and output are now vectors.

$$\begin{aligned}\dot{\mathbf{x}} &= \mathbf{f}(\mathbf{x},\mathbf{u})\\ \mathbf{y} &= \mathbf{h}(\mathbf{x})\end{aligned} \tag{2.52}$$

The system needs to be affine in the input. Thus, the discussion is limited to systems of the form given in eq. (2.53),

$$\begin{aligned}\dot{\mathbf{x}} &= \mathbf{f}(\mathbf{x}) + \mathbf{G}(\mathbf{x})\mathbf{u}\\ \mathbf{y} &= \mathbf{h}(\mathbf{x})\end{aligned} \tag{2.53}$$

where $\mathbf{x} \in \mathbb{R}^n$ is the state vector, $\mathbf{u} \in \mathbb{R}^m$ is the input vector, $\mathbf{f} : \mathbb{R}^n \to \mathbb{R}^m, \mathbf{h} : \mathbb{R}^n \to \mathbb{R}^m$ are smooth vector fields and $\mathbb{G} : \mathbb{R}^n \to \mathbb{R}^{n\times m}$ is a smooth function. Moreover, both of the vectors $\mathbf{f}(\mathbf{x})$ and $\mathbf{h}(\mathbf{x})$ are m-dimensional:

$$\mathbf{f}(\mathbf{x}) = \left[f_1(\mathbf{x}), f_2(\mathbf{x}), \cdots, f_m(\mathbf{x})\right], \quad \mathbf{h}(\mathbf{x}) = \left[h_1(\mathbf{x}), h_2(\mathbf{x}), \cdots, h_m(\mathbf{x})\right] \tag{2.54}$$

The transformation applied in the MIMO case is the same as the transformation shown in eq. (2.46), but this transformation is applied to each output function $h_i(x)$.

$$\begin{aligned}T_1^i(\mathbf{x}) &= L_f^0 h_i(\mathbf{x}) = h_i(\mathbf{x})\\ T_2^i(\mathbf{x}) &= L_f^1 h_i(\mathbf{x})\\ &\cdots\\ T_{r_i}^i(\mathbf{x}) &= L_f^{r_i-1} h_i(\mathbf{x})\end{aligned} \tag{2.55}$$

The result of the state transformation for one of the output functions $h_i(x)$ is shown in eq. (2.56).

$$\begin{aligned}&\dot{T}_1^i(\mathbf{x}) = T_2^i(\mathbf{x})\\ &\cdots\\ &\dot{T}_{r_i-1}^i(\mathbf{x}) = T_{r_i}^i(\mathbf{x})\\ &\dot{T}_{r_i}^i(\mathbf{x}) = L_f^r h_i(\mathbf{x}) + \textstyle\sum_{j=1}^m L_{g_j} L_f^{r-1} h_i(\mathbf{x})\, u_j\end{aligned} \tag{2.56}$$

Moreover, considering all output functions, i.e. $1 \le i \le m$, this leads to the following result:

$$\mathbf{u} = A^{-1}(\mathbf{x})\left[\boldsymbol{\nu}(\mathbf{x}) - \mathbf{b}(\mathbf{x})\right] \tag{2.57}$$

where

$$\nu(\mathbf{x}) = \begin{bmatrix} \dot{T}_{\mathrm{r}}^1 \\ \dot{T}_{r_2}^2 \\ \vdots \\ \dot{T}_{r_m}^m \end{bmatrix} \quad \mathbf{b}(\mathbf{x}) = \begin{bmatrix} L_f^{\mathrm{r}} h_1(\mathbf{x}) \\ L_f^{r_2} h_2(\mathbf{x}) \\ \vdots \\ L_f^{r_m} h_m(\mathbf{x}) \end{bmatrix} \tag{2.58}$$

and

$$A(\mathbf{x}) = \begin{bmatrix} L_{g_1} L_f^{r_1-1} h_1(\mathbf{x}) & L_{g_2} L_f^{r_1-1} h_1(\mathbf{x}) & \cdots & L_{g_m} L_f^{\mathrm{r}_1-1} h_1(\mathbf{x}) \\ L_{g_1} L_f^{r_2-1} h_2(\mathbf{x}) & L_{g_2} L_f^{r_2-1} h_2(\mathbf{x}) & \cdots & L_{g_m} L_f^{\mathrm{r}_2-1} h_2(\mathbf{x}) \\ & & & \\ L_{g_1} L_f^{r_m-1} h_m(\mathbf{x}) & L_{g_2} L_f^{r_m-1} h_m(\mathbf{x}) & \cdots & L_{g_m} L_f^{\mathrm{r}_m-1} h_m(\mathbf{x}) \end{bmatrix} \tag{2.59}$$

Moreover, as in the SISO, the equations up to r_i are linearized for each $i \in [1, 2, \cdots, m]$. Additionally, the resultant equations are decoupled. That is, there is a virtual control input corresponding to each input. More generally, the controllability canonical form is established for every input. This is illustrated by the complete input-output linearization for each $i \in [1, 2, \cdots, m]$, as shown in eq. (2.60).

$$\begin{aligned}&\dot{T}_1^i(\mathbf{x}) = T_2^i(\mathbf{x})\\ &\cdots\\ &\dot{T}_{r_i-1}^i(\mathbf{x}) = T_{r_i}^i(\mathbf{x})\\ &\dot{T}_{r_i}^i(\mathbf{x}) = v_i\end{aligned} \tag{2.60}$$

2.1.4 Additional Considerations

When the relative degree is smaller than the degree of the system, there will be internal dynamics. The presence of internal dynamics means that part of the system dynamics is unobservable. Thus, it is important to check the stability of the internal dynamics analytically.

As studying the stability of internal dynamics is not always an easy task, an alternative is to examine the stability of the zero dynamics of the system. The zero dynamics are the internal dynamics of the control system when the input is such that the output of the system is zero [14].

It should be noted that the stability of the zero dynamics is only a guarantee of local stability. If the zero dynamics of a system are asymptotically stable, the (nonlinear) system is described as an asymptotically minimum phase system. In the case of a linear system, the system is said to be minimum phase.

Perhaps, one of the most limiting aspects of NDI is its full dependency on the model of the system being controlled and its requirement of the full knowledge of the states of the system. If the system dynamics are not known precisely, an estimate of these unknown parts of the model have to be made through some system identification techniques. Moreover, in the case that the latter requirement cannot be fulfilled (if the states cannot be directly and fully obtained), alternative measures need to be implemented in the closed loop system. One possibility is to implement a nonlinear observer which is a deterministic estimator. Another option is to implement a nonlinear state estimator which is a stochastic option.

Another limitation of NDI is it that it can be applied to systems that have the same number of inputs and outputs. In situations where this is not the case, control allocation problems arise that need to be solved.

Moreover, NDI is suitable for systems affine in the control input. While they can still be applied to systems that are not affine in control, it becomes a more cumbersome process as nonlinear solvers would be needed to formulate the expression for the controller.

Furthermore, care should be taken during the inversion that singularities are checked for. The results are then only valid when the singularities are not encountered. Thus, the inversion in the inner loop alongside the linear compensation in the outer loop are not always applicable globally [14].

In the presence of internal dynamics, the effectiveness of the feedback linearization control technique hangs upon the stability of those internal dynamics, in the sense of Bounded Input Bounded Output stability. Since the system is only partly linearized, if the internal dynamics happen to be unstable, a different output equation should be chosen that would lead to stable internal dynamics, if possible. Otherwise, a different control technique should be utilized [14].

2.2 Incremental Nonlinear Dynamic Inversion

The INDI control approach emerged as a more robust variant of NDI by alleviating the dependency control approach on the plant model. This is realized by linearizing the system about the current state and control input of every sample period. The incremental form that arises allows to feed back sensor measurements. As will be seen in the following, for INDI, only the knowledge of the value of the control effectiveness matrix is needed. Moreover, three different formulations of INDI will be presented here.

2.2.1 Continuous-time Formulation

For the derivation of INDI control, the system in eq. (2.53) which is affine in the control is considered. The equation is linearized as shown in eq. (2.61).

$$\dot{\mathbf{x}} \approx \dot{\mathbf{x}}_0 + \mathbf{G}\left(\mathbf{x}_0\right)\left(\mathbf{u}-\mathbf{u}_0\right) + \left.\frac{\partial[f(\mathbf{x})+\mathbf{G}(\mathbf{x})\mathbf{u}]}{\partial \mathbf{x}}\right|_0 \left(\mathbf{x}-\mathbf{x}_0\right) + \mathbf{O}\left[\left(\mathbf{x}-\mathbf{x}_0\right)^2\right] \tag{2.61}$$

The higher order terms in the linearized system dynamics are often neglected, and this leads to the form in eq. (2.61):

$$\dot{\mathbf{x}} \approx \dot{\mathbf{x}}_0 + \mathbf{G}\left(\mathbf{x}_0\right)\left(\mathbf{u}-\mathbf{u}_0\right) + \left.\frac{\partial[f(\mathbf{x})+\mathbf{G}(\mathbf{x})\mathbf{u}]}{\partial \mathbf{x}}\right|_0 \left(\mathbf{x}-\mathbf{x}_0\right) \tag{2.62}$$

In the usual derivation of INDI, time-scale separation is assumed. This assumptions means that the actuator dynamics are quite fast, and that the evolution of the state variables is quite slow in comparison. This assumption allows to neglect the term involving the change in state. This leaves eq. (2.63).

$$\dot{\mathbf{x}} \approx \dot{\mathbf{x}}_0 + \mathbf{G}\left(\mathbf{x}_0\right)\left(\mathbf{u}-\mathbf{u}_0\right) = \dot{\mathbf{x}} \approx \dot{\mathbf{x}}_0 + \mathbf{G}\left(\mathbf{x}_0\right)\Delta\mathbf{u} \tag{2.63}$$

After the linearization, the virtual control ν can replace $\dot{\mathbf{x}}$ and the inversion of the dynamics is performed. Thereafter, the incremental control is obtained.

$$\Delta \mathbf{u} = \hat{\mathbf{G}}^{-1}\left(\mathbf{v} - \dot{\mathbf{x}}_0\right) \tag{2.64}$$

Thus, the final control law is given by eq. (2.65).

$$\mathbf{u} = \mathbf{u}_0 + \hat{\mathbf{G}^{-1}}\left(\mathbf{v} - \dot{\mathbf{x}}_0\right) \tag{2.65}$$

2.2.2 Continuous-time Formulation Including Internal Dynamics

Despite the demonstrated effectiveness of INDI, the original formulation of INDI control makes use of time-scale separation and omits higher-order terms. Furthermore, it can only be applied to systems of relative degree one. That is why, Wang et al. derived a new formulation of INDI, which does not assume time-scale separation, which takes into consideration the internal dynamics, and which is applicable to systems of any relative degree. For the complete derivation of the new formulation, the reader is referred to [12].

2.2.3 Discrete-time Formulation

Obtaining the discrete-time formulation of INDI can be done through discretizing the continuous system the linearizing the result, or through reversing the order of these two steps. Van 't Veld has shown that either order leads to the same end result [28]. In the following, the approach where discretization is applied first is presented.

$$\mathbf{x}_{k+1} = \mathbf{x}_k + \int_{t_k}^{t_{k+1}} f(\mathbf{x}, \mathbf{u})\, dt \tag{2.66}$$

If $f(\mathbf{x}, \mathbf{u})$ is assumed to be constant between two instances of time, the right-hand side of eq. (2.66) can be simplified, and this simplification yields:

$$\mathbf{x}_{k+1} \approx \mathbf{x}_k + (t_{k+1} - t_k)\mathbf{f}\left(\mathbf{x}_k, \mathbf{u}_k\right) = \mathbf{x}_k + \Delta t \mathbf{f}\left(\mathbf{x}_k, \mathbf{u}_k\right) \tag{2.67}$$

Rearranging eq. (2.67) leads to the following:

$$\frac{\mathbf{x}_{k+1} - \mathbf{x}_k}{\Delta t} = \mathbf{f}\left(\mathbf{x}_k, \mathbf{u}_k\right) \tag{2.68}$$

In order to avoid the evaluation of $f(\mathbf{x}, \mathbf{u})$ which may be computationally intensive (if f is a complicated function), $f(\mathbf{x}, \mathbf{u})$ can instead be linearized about the state and input values pertaining to the timestep t_{k-1}.

$$\frac{x_{k+1} - \mathbf{x}_k}{\Delta t} \approx \mathbf{f}\left(\mathbf{x}_{k-1}, \mathbf{u}_{k-1}\right) + \left.\frac{\partial \mathbf{f}(\mathbf{x}, \mathbf{u})}{\partial \mathbf{x}}\right|_{\substack{\mathbf{x}=\mathbf{x}_{k-1}, \\ \mathbf{u}=\mathbf{u}_{k-1}}} \left(\mathbf{x}_k - \mathbf{x}_{k-1}\right) + \left.\frac{\partial f(\mathbf{x}, \mathbf{u})}{\partial \mathbf{u}}\right|_{\substack{\mathbf{x}=\mathbf{x}_{k-1}, \\ \mathbf{u}=\mathbf{u}_{k-1}}} \left(\mathbf{u}_k - \mathbf{u}_{k-1}\right) \tag{2.69}$$

Let

$$F\left(\mathbf{x}_{k-1}, \mathbf{u}_{k-1}\right) \triangleq \left.\frac{\partial \mathbf{f}(\mathbf{x}, \mathbf{u})}{\partial \mathbf{x}}\right|_{\substack{\mathbf{x}=\mathbf{x}_{k-1}, \\ \mathbf{u}=\mathbf{u}_{k-1}}} \tag{2.70}$$

$$G\left(\mathbf{x}_{k-1}, \mathbf{u}_{k-1}\right) \triangleq \left.\frac{\partial \mathbf{f}(\mathbf{x}, \mathbf{u})}{\partial \mathbf{u}}\right|_{\substack{\mathbf{x}=\mathbf{x}_{k-1}, \\ \mathbf{u}=\mathbf{u}_{k-1}}} \tag{2.71}$$

This turns eq. (2.69) into

$$\frac{x_{k+1} - \mathbf{x}_k}{\Delta t} \approx \mathbf{f}\left(\mathbf{x}_{k-1}, \mathbf{u}_{k-1}\right) + F\left(\mathbf{x}_{k-1}, \mathbf{u}_{k-1}\right)\left(\mathbf{x}_k - \mathbf{x}_{k-1}\right) + G\left(\mathbf{x}_{k-1}, \mathbf{u}_{k-1}\right)\left(\mathbf{u}_k - \mathbf{u}_{k-1}\right) \tag{2.72}$$

By adjusting the subscripts in eq. (2.68) appropriately, an expression to replace $\mathbf{f}\left(\mathbf{x}_{k-1}, \mathbf{u}_{k-1}\right)$ is obtained. This replacement turns eq. (2.72) into eq. (2.73).

$$\frac{x_{k+1} - \mathbf{x}_k}{\Delta t} \approx \frac{\mathbf{x}_k - \mathbf{x}_{k-1}}{\Delta t} + F\left(\mathbf{x}_{k-1}, \mathbf{u}_{k-1}\right)\left(\mathbf{x}_k - \mathbf{x}_{k-1}\right) + G\left(\mathbf{x}_{k-1}, \mathbf{u}_{k-1}\right)\left(\mathbf{u}_k - \mathbf{u}_{k-1}\right) \tag{2.73}$$

Applying the time-scale separation principle to eq. (2.73) leads to:

$$\frac{\mathbf{x}_{k+1} - \mathbf{x}_k}{\Delta t} \approx \frac{\mathbf{x}_k - \mathbf{x}_{k-1}}{\Delta t} + G\left(\mathbf{x}_{k-1}, \mathbf{u}_{k-1}\right)\left(\mathbf{u}_k - \mathbf{u}_{k-1}\right) \tag{2.74}$$

Inverting eq. (2.73) leads to

$$\mathbf{u}_k = \mathbf{u}_{k-1} + G^{-1}\left(\mathbf{x}_{k-1}, \mathbf{u}_{k-1}\right)\left(\nu_k - \frac{\mathbf{x}_k - \mathbf{x}_{k-1}}{\Delta t}\right) \tag{2.75}$$

where ν_k is defined in eq. (2.76).

$$\nu_k = \frac{\mathbf{x}_{k+1} - \mathbf{x}_k}{\Delta t} \tag{2.76}$$

2.2.4 Literature Survey of INDI

The birth of the idea of INDI already began in the 1990s. Several terms were used to refer to it including "simplified nonlinear dynamic inversion", "modified nonlinear dynamic inversion", and "implicitly nonlinear dynamic inversion" [37–39]. The concept of INDI was reintroduced by Sieberling et al. in 2010 [27]. It emerged as a control approach that would allow resilience to model mismatch, and this is attained through relying on sensor measurements. The application of INDI presented in the paper was for the control of a UAV with a T tail and rear-mounted engines. Moreover, it was first assumed that the measurements of the angular accelerations were available and could be fed back directly, but angular acceleration measurements are not always readily available. Thus, the authors also made use of a linear predictive filter to obtain the angular acceleration from the angular velocity measurements. The robustness of the control approach was demonstrated through reduced sensitivity to aerodynamic model mismatch, center of gravity mismatch and inertia mismatch [27].

Several applications of INDI, to different platforms, followed Sieberling et al.'s pioneering work. Falkena et al. applied INDI to the control of small aircraft due to the rising interest in personal aerial vehicles [40]. An application that shortly followed was the development of an INDI controller for spacecraft attitude control [41]. Thereafter, the INDI control of a Reusable Launch Vehicle (RLV) was implemented and tested in simulation [42]. INDI was shown to be eligible for the control of the AD-33 helicopter based on the feedback of acceleration measurements. The resultant controller was tested and proven, in simulation, to be capable of tracking commanded references efficiently [43]. Yet another platform onto which an INDI controller was applied was a tilt rotor Unmanned Aerial Vehicle (UAV). The significance of this application lies in the fact that tilt rotor UAVs have a large flight envelope whose dynamics are highly nonlinear throughout the envelope. Nonetheless, the paper demonstrates through simulation the effectiveness of INDI in controlling this platform [44]. Lin et al. present the implementation of INDI for the attitude control of an autogyro [45]. INDI was also applied in the attitude control of a Vertical/Short Takeoff and Landing (V/STOL) aircraft across all of its flight envelope [46]. Liu et al. also used INDI for the control of a Vertical Takeoff and Landing (VTOL) UAV [47]. Moreover, INDI was applied successfully for the first time onboard a CS-25 certified aircraft [48].

Apart from aerial vehicles, INDI was successfully used with flight simulators. Specifically, Huang et al. have shown that INDI can be used for the inner-loop control of motion systems for flight simulation [49–51]. While the simulator's hydraulic actuators achieve high precision, they also add a number of challenges. Their dynamics are highly nonlinear. Moreover, they make the control system highly susceptible to disturbances for reasons including nonlinear friction in hydraulic actuation, the possibility of oil leakage, as well unmodelled dynamics. Because of its inherent robustness to uncertainties, INDI has shown big improvements in the tracking accuracy in comparison to previously used techniques for motion control [1, 52]. This is clearly seen from fig. 2.1, where INDI with 50% model mismatch outperforms NDI with 10% model mismatch.

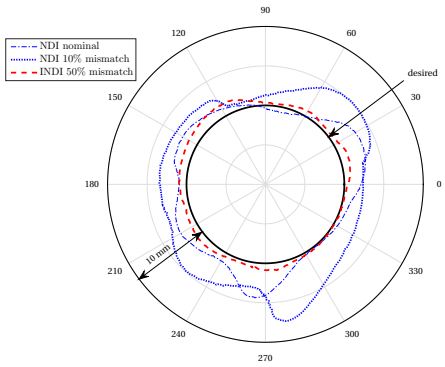

Figure 2.1: Effectiveness of INDI in comparison to NDI handling model mismatches [1]

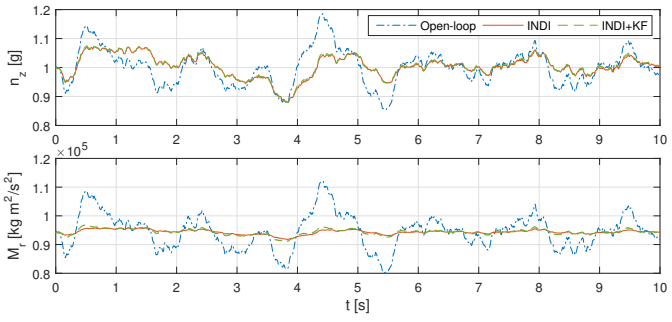

Figure 2.2: Effect of INDI in alleviating vertical load factor and the root bending moment [2]

Besides its versatile applicability to different platforms, INDI has tackled several specific control applications. For example, in one of the examples already mentioned, which was the use of INDI in the control of a small aircraft, INDI was used as part

of a flight envelope protection control system, although the paper showed that the strategy based on INDI was not the very best one for the task [40].Pavel et al. have demonstrated the use of INDI as part of the Stability Augmentation System (SAS) of an Apache AH-64 helicopter [53]. INDI was also used as part of the control during take-off of the quadrotor. This application is important because during take-off a lot of dynamic effects take place such as the ground effect.

Another success of INDI was in its effectiveness as a Fault-tolerant Control (FTC) technique. For example, Lu et al. had proposed the use of INDI for the control of a quadrotor in the case of losing a rotor, which was demonstrated through simulation [54]. Another example of the application of INDI for fault-tolerant control is in aircraft trajectory control. It has been shown that a trajectory controller based on INDI is able to cope well with model uncertainties and actuator faults [55]. In another example of adaptive and fault-tolerant control, INDI was used in the control of an aircraft with a partly failing active high-lift system [56].

One of the main strengths of INDI is its greater overall robustness in comparison to NDI. This encompasses robustness to model uncertainties as well as the capacity for disturbance rejection. The former was demonstrated by Smeur et al when they showed that INDI handle gusts well, both through a wind tunnel experiment and an outdoor experiment [3]. The comparison of the tracking performance of INDI in comparison to that of PID is shown in fig. 2.3 and fig. 2.4. Another disturbance rejection application was performed in [57]. This was done by adding INDI to the outer loop control.

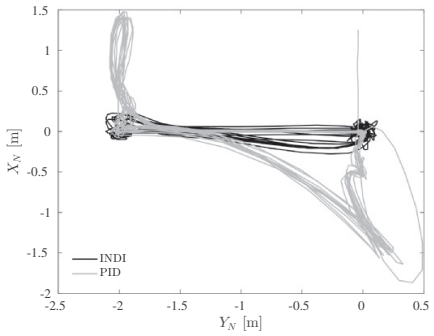

Figure 2.3: Top view of the experiment which allows to compare the performance of INDI to that of PID in the task of flying under the influence of gusts [3]

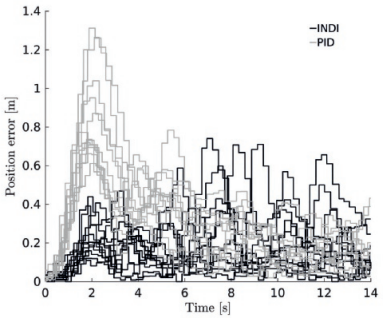

Figure 2.4: Comparison of the horizontal position error of INDI to that of PID in the task of flying under the influence of gusts [3]

The increasing use of lighter and more flexible structures poses another control challenge which INDI has adequately dealt with. The challenge comes from the fact that the eigenfrequencies of the structure and the rigid-body modes become close. Therefore, the presence of turbulence may excite the rigid-body dynamics as well as the structural dynamics and can induce their interaction. Wang et al. presented an INDI Gust Load Alleviation (GLA) controller that is specifically for quasi-rigid aircraft [2, 58].

A recent and interesting control application of INDI was demonstrated by Pollack et al. which involved the use of INDI for servo current control. That is, INDI was used to provide the current control inputs to the electro-mechanical actuators. The success of this application was proven through simulation as well as many flight tests. Moreover, this integrated approach allows to harness the power of INDI and to leverage the benefits of FBW systems which inclu direct haptic feedback as well as passive and active load alleviation in the presence of gust loads [59].

In relation to control architecture, INDI is often used in inner loop control. In [60], INDI was used for the angular acceleration control of a quadrotor, and in the outer loop NDI, was used for the attitude control. This architecture enabled accurate tracking of position, velocity, acceleration, jerk, snap, as well as yaw angle, yaw rate, and yaw acceleration. The RMS attained for the position was 4 cm [60]. In [61], the control of the quadrotor system consists of three loops. In this architecture, the two outer loops used NDI, and INDI was used in the innermost-loop. It should be noted that in this example, the innermost-loop comprised of dynamics in a non-affine form which means that NDI cannot be used for that loop because, as mentioned earlier, NDI requires a controllability canonical form. However, INDI can handle a non-affine form which is indeed an advantage of INDI over NDI.

Another advantage of INDI in relation to control architecture is that the use of INDI in a cascaded control structure ensures that internal dynamics are avoided. However, it should be mentioned that the cascaded structure makes stability guarantees difficult to prove [18].

One of the prominent challenges of INDI is handling measurement and actuator delays. In the problem of controlling the

attitude with INDI, the angular acceleration is in the feedback loop. Usually when measurements of the angular acceleration are available, they are quite noisy, and filtering the measurements leads to the introduction of a time-delays. When measurement of the angular acceleration are unavailable, the angular acceleration is estimated from measurements of the angular rate, and that would usually require the use of a filter (due to the noise in the gyroscope output as well as the additional noise obtained from differentiation of the angular rate measurements). In the case of either method, since a filter is applied, there is the need to deal with time delays that arise. Previously, and as mentioned earlier, the issue of the measurement delays has been dealt with predictive filtering. However, this approach requires further modeling [27]. An alternative approach would be to make use of multiple accelerometer measurements [62]. However, that is a cumbersome and complicated method to apply as pointed out in [63]. As an alternative solution, Smeur et al. were able to take into account the time delay happening as a result of filtering the gyroscope measurements, by applying the same filter to the input [63]. This leads to the delay of the input by the same amount at which the feedback signal is delayed because of filtering the measurements. Moreover, filtering the input leads to a transfer function from the virtual control to the angular rate measurement and all that remains is the actuator dynamics. Clearly, this transfer function does not contain the measurement delays any longer.

Cakiroglu et al. used an angular accelerometer sensor for acceleration measurements needed for feedback rather than obtaining the acceleration from differentiating the angular rate measurements [64].

Su et al. have proposed a modified version of INDI which is able to handle time-delays arising from measurements. As was in the case of [63], this approach called Finite Time Convergence Incremental Nonlinear Dynamic Inversion (FINDI) does not propose a new method for obtaining the angular acceleration accurately. Rather, the novelty of the method lies in reducing the effect of the time-delay on performance, and this is done by incorporating command differential signals into the outer-loop linear controller [65].

Another main concern for INDI is dealing with time-varying control effectiveness matrix. Smeur et al. address this challenge by estimating the control effectiveness, which lead to an adaptive variant of INDI [63].

Actuator saturation is a threat to stability, and INDI is also vulnerable to this threat. When control allocation is applied to a platform where INDI is used as a controller, this leads to signficant interaction between the control allocation frame and the dynamics of the actuators which is usually detrimental to performance. In their work, Li et al. present a way to compensate for actuator saturation in this case [66]. Moreover, Van 't Veld et al. have applied Pseudo-Control Hedging (PCH) to deal with actuator saturation [19].

Augmenting INDI with adaptive control techniques to enhance the robustness is needed because the formulation of INDI relies on the time-scale separation assumption as well as the omission of higher-order terms. This means that perturbation terms remain present in the closed-loop system. It is those remnants that compromise the effectiveness of the incremental method. To address this problem, adaptive augmentation is used to determine parametric uncertainties in the system to make the INDI controller more robust.

This page was intentionally left blank.

3

Sampled-data Systems

Many control systems nowadays make use of digital computers or digital microprocessors to perform control computations. This conversion has its advantages. In general, digital computers can be more accurate because digital signals are not as susceptible to noise and power supply drift as is the case for analog signals. In relation to this, implementation errors are more likely to occur when analog computers are used because performing calculations based on analog signals requires that the analog signals are manipulated using resistors and capacitors, whose properties may change over time. Another key advantage of digital controllers over analog controllers is their flexibility. While the control is implemented in hardware for the case of an analog controller (making it difficult and cumbersome to modify), it is implemented in software or firmware for the case of a digital controller, which makes adjusting the implementation of the control laws much simpler. Furthermore, digital controllers are economical because the cost of digital controllers has been continuously decreasing [5].

The use of digital computers introduces discrete signals into the control system. Since there are often also continuous signals in the control system, for instance as outputs of the controlled plant, the system has a hybrid nature. In order for control to be possible in a hybrid system, suitable conversion techniques that transform the signals from digital to continuous and vice versa, are needed. These conversions are performed by analog-to-digital converters and digital-to-analog converters.

Essential to those conversion techniques are two processes: sampling and data holding. In an analog-to-digital converter, a signal is sampled, and then it is digitized (a process known as quanitization). It is because of the sampling that the control system is, specifically, referred to as a sampled-data system [4]. As for the case of a digital-to-analog converter, the analog signal is computed as a weighted sum of the digital bits. Thereafter, the signal is held for the duration of the sampling period, in order for a piecewise continuous signal to be available. The sample and hold processes show how the sampling period affects the signals in the control system and gives a hint on why the sampling period may have an influence on the performance of the control system [6].

The analysis of sampled-data systems is usually considered to be harder than that of systems that consist of purely continuous signals or purely discrete signals. In order to perform an analysis of a sampled-data system that is aligned with the physical reality, both the continuous and discrete nature of the signals need to considered, and the conversion that occurs between the signals needs to be accounted for [4].

In this chapter, suitable models for sampled-data systems will be discussed, with a focus on systems that are entirely continuous. First the model of the digital computer will be presented in section 3.1. Thereafter, a number of models will be discussed in section 3.2.

3.1 Model of the Digital Computer

In this section, the modeling of a digital computer will be presented. A generic example of a basic digital control system is shown in fig. 3.1. A more specific example is shown in fig. 3.2, showing a (sampled-data) engine control system.

The digital-to-analog converters and the analog-to-digital converters are seen in both diagrams, fig. 3.1 and fig. 3.2, and as mentioned ealier, that is because the conversion techniques are essential in a digital control systems. Therefore, they will be discussed in section 3.1.1 and section 3.1.2.

3.1.1 Analog-to-Digital Conversion

In contrast to digital-to-analog conversion, analog-to-digital conversion consists of two steps and does not occur instantaneously. This means that there will be a delay between the time that the analog input is received and that at which the digital

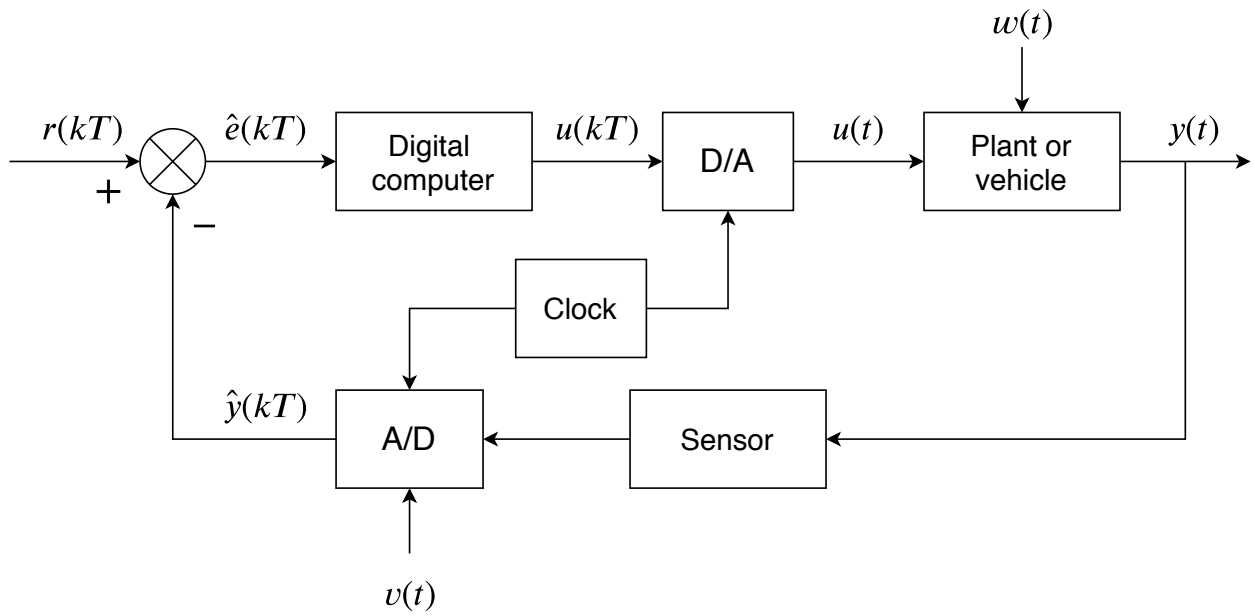

Figure 3.1: General Block Diagram of a Digital Control System [4]

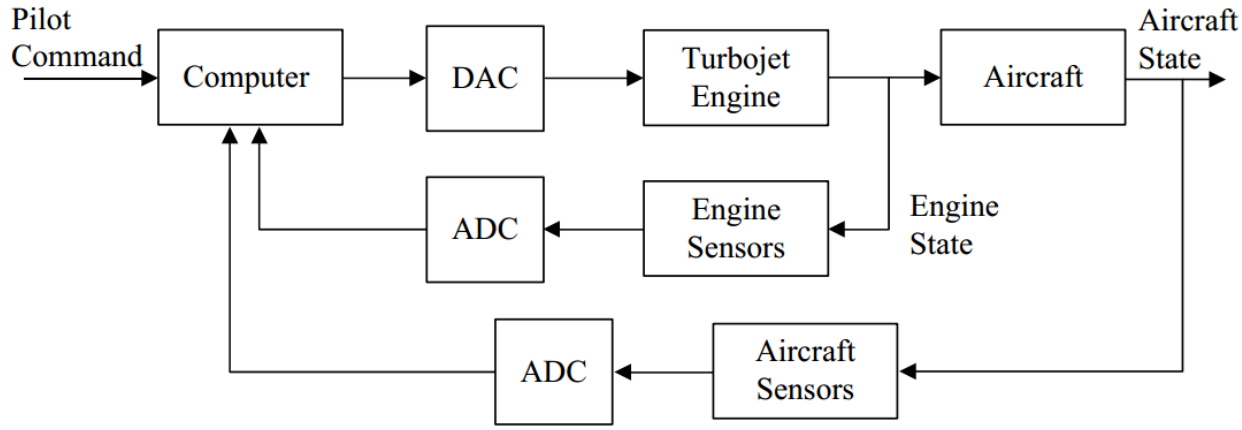

Figure 3.2: Engine Control System [5].

output is obtained. The two steps involved are the conversion to a sampled signal followed by a conversion of the sampled signal to a binary signal [6].

The first step involved is to sample the analog signal. The (non-ideal) sampling generally occurs through a finite pulse-width sampler, with the width of the pulses denoted by T_W. A special case of the finite pulse-width sampler is the ideal sampler, where the width of the pulses tends to zero, and the pulses become delta Dirac functions. In general, the operation of the finite pulse-width sampler can be understood from fig. 3.3.

The equation for the sampled waveform is shown in eq. (3.1).

$$f^*_{T_W}(t) = f(t)s(t) = f(t)\sum_{k=-\infty}^{\infty} u(t-kT) - u(t-kT-T_W) \tag{3.1}$$

It is clear that obtaining the Laplace transform of this signal would be difficult, due to the product of two signals in the time domain. However, if it is assumed that T_W is much smaller than the sampling period T, then a simplication can be made. Specifically, it will be assumed that $f(t)$ is constant over the span of a sampling interval. This means that $f(t) = f(kT)$ can be assumed, and eq. (3.1) can be transformed in eq. (3.2) [6].

$$f^*_{T_W}(t) = \sum_{k=-\infty}^{\infty} f(kT)\left[u(t-kT) - u\left(t-kT-T_W\right)\right] \tag{3.2}$$

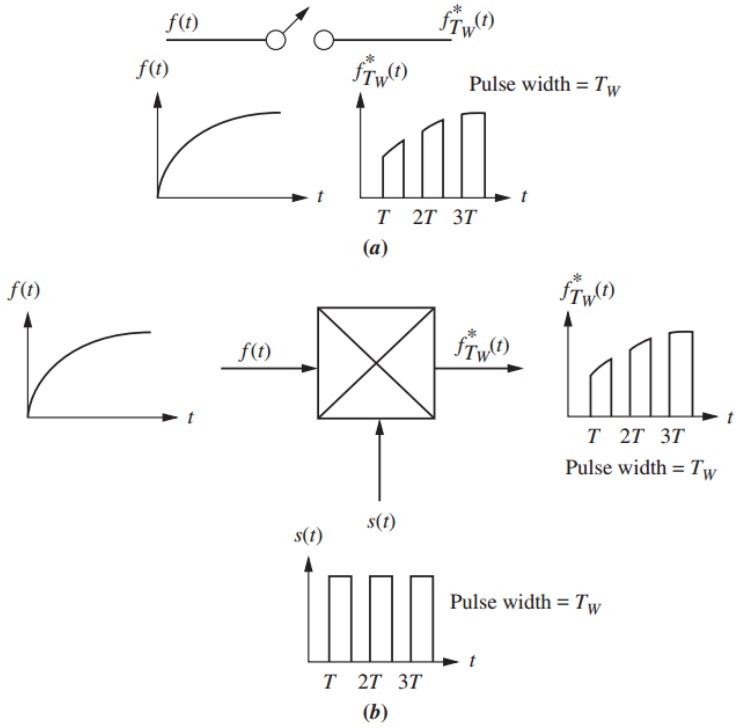

Figure 3.3: Diagram showing the operation of the sampler [6]

Now that the $f(t)$ is replaced by a piecewise constant function $f(kT)$, taking the Laplace transform of $f^*_{T_W}(t)$ is no longer a complex task. The Laplace transform of eq. (3.2) is shown in eq. (3.3).

$$F^*_{T_W}(s) = \sum_{k=-\infty}^{\infty} f(kT)\left[\frac{e^{-kTs}}{s} - \frac{e^{-kTs-T_{ws}}}{s}\right] = \sum_{k=-\infty}^{\infty} f(kT)\left[\frac{1-e^{-T_{ws}}}{s}\right]e^{-kTs} \tag{3.3}$$

Reusing the assumption of T_W being small, and making a first order approximation of the exponential term based on its series expansion leads to the expression for $F^*_{T_W}(s)$ shown in eq. (3.4).

$$F^*_{T_W}(s) = \sum_{k=-\infty}^{\infty} f(kT)\left[\frac{T_W s}{s}\right]e^{-kTs} = \sum_{k=-\infty}^{\infty} f(kT)\,T_W e^{-kTs} \tag{3.4}$$

Taking the inverse Laplace transform of eq. (3.4) leads to eq. (3.5).

$$f^*_{T_W}(t) = T_W \sum_{k=-\infty}^{\infty} f(kT)\delta(t-kT) \tag{3.5}$$

In the case of ideal impulse sampling, the equation for sampling in the time-domain is the one shown in eq. (3.6).

$$f^*_{T_W}(t) = \sum_{k=-\infty}^{\infty} f(kT)\delta(t-kT) \tag{3.6}$$

As mentioned earlier, the second step in the digital-to-analog conversion is the quantization step. In order to perform this step, the dynamic range of the sampled-signals needs to be determined first. The obtained range is then divided into a number of discrete levels. Finally, a digital number is assigned to each of the discrete levels [6].

3.1.2 Digital-to-Analog Conversion

Digital-to-analog conversion is a one-step procedure that occurs almost instantaneously. The analog output is obtained through computing a weighted sum of the bits of the digital input. This can be explained through the example digital-to-analog converter shown in fig. 3.4. Consider the case where the binary number is 110. Based on the weights shown in the blocks of the figure, the output analog voltage will be 6 volts [6]. Note, that the switches in fig. 3.4 are "on" whenever a bit with the value of 1 is encountered and closed whenever a bit with the value of 0 is encountered.

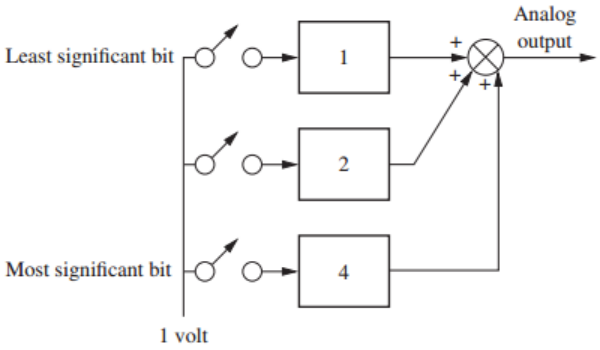

Figure 3.4: Example of a digital-to-analog converter [6].

After this analog value is obtained, then the signal is held for the duration of the sample period. This is also referred to as data-reconstruction. The data-reconstruction can be based on a Zero-Order-Hold (ZOH), which is described in eq. (3.7) [5].

$$\{u(k)\} \xrightarrow{ZOH} u(t) = u(k), kT \leq t < (k+1)T, \quad k = 0, 1, 2, \ldots \tag{3.7}$$

There are alternatives to the ZOH filter. This includes the first-order hold and the second-order hold. While the former performs linear interpolation between the sample points, the latter interpolates the data using parabolas. However, the ZOH is most commonly used [5], and it is this data-extrapolation technique that will be considered for the rest of this report.

In the case of ZOH, the signal is held constant for the duration of the sample period until a new digital signal is provided by the computer. The working of the ZOH is illustrated through fig. 3.5.

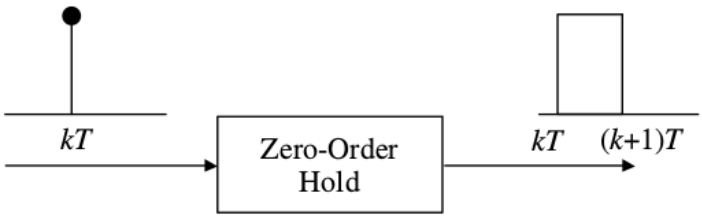

Figure 3.5: Effect of a zero-order hold filter [5]

From this figure, it can be seen that the impulse response of a ZOH is a step function. In order to get the transfer function corresponding to the zero-order hold, the Laplace transform of the elements in fig. 3.5 need to be taken. The Laplace transform of an impulse is unity. This means that the transfer function of the ZOH is equal to the Laplace transform of the pulse with the width T. The pulse is equivalent to the difference of two heaviside functions $H(t)$ and $H(t-T)$. Since the Laplace transform of a heaviside function is $\frac{1}{s}$ and the Laplace transform of a heaviside function with a delay is $\frac{1}{s} \cdot e^{-s \cdot T}$, then the transfer function of a ZOH is given by eq. (3.8) [5].

$$G_{ZOH}(s) = \frac{1 - e^{-sT}}{s} \tag{3.8}$$

3.2 Modeling of Sampled-data Systems

Digital control systems can be modelled in several ways [7]. Before presenting a number of these models, the means to check the fidelity of the models needs to be mentioned. In brief, this was done based on a Fourier analysis of a Simulink®model that is assumed to be an accurate representation of the control system, which involves a discrete controller as well as a ZOH block. For information on the Fourier routine that was implemented to perform this analysis, the reader is referred to [7].

There were five models that were studied by Noijen. The first one involved a continuous form of the digital controller. A representative diagram of this model is shown in fig. 3.6. Conversely, all the analog components of the system can be discretized. Then, the overall discrete transfer function can be analyzed. A model that is similar to the baseline model is the one shown in fig. 3.7. However, of course, this model is fully continuous but includes the ZOH filter. Another model comprised of

adding delays in the feedback signals to represent the pure delay that occurs due to sampling. A variant of the previous model is to include the delay in the main loop. The resultant model is shown in fig. 3.9.

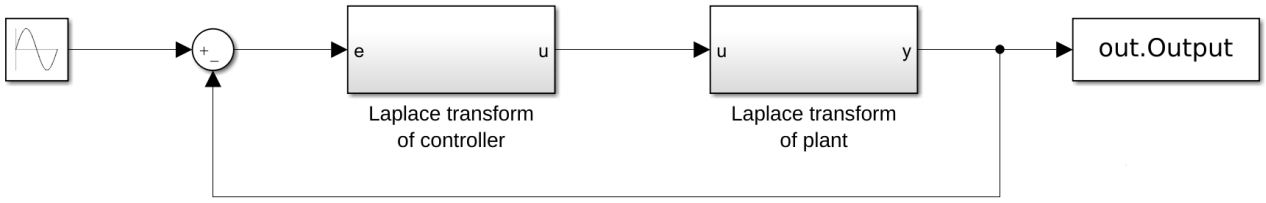

Figure 3.6: Continuous model of a sampled-data systems obtained by using the continuous form of the controller [7]

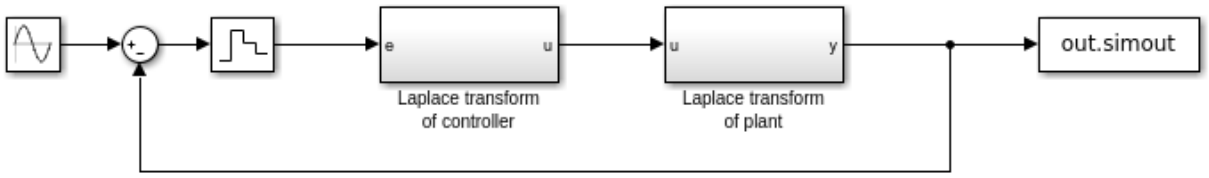

Figure 3.7: Sampled-data model [7]

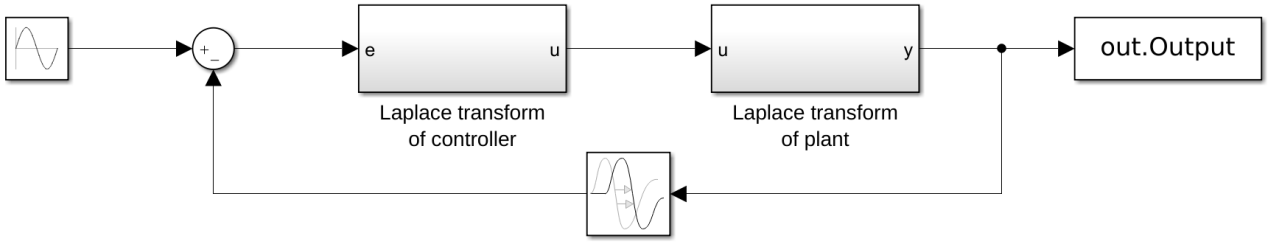

Figure 3.8: Analog controller and components with delay corresponding to the sampling period in the feedback signal [7].

According to the discussion by Noijen, the models with the highest fidelity are the ones shown in fig. 3.7 and fig. 3.9. Based on this discussion as well as the one from the previous chapter, a suitable model of the control system is shown in fig. 3.10. Note that, for stabilization problems fig. 3.9 would be equivalent to fig. 3.8. This means that another model which is suitable to model the system is the one that is shown in fig. 3.11.

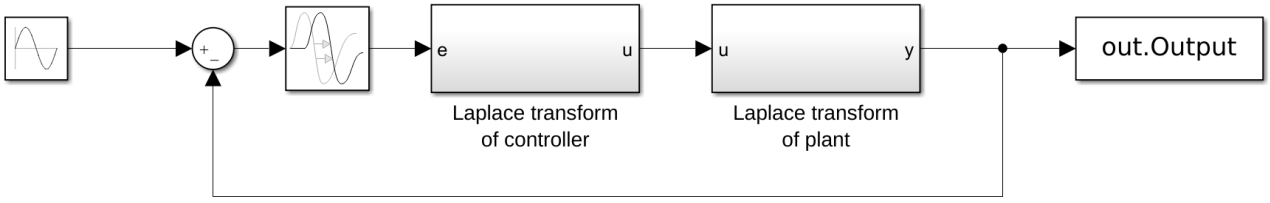

Figure 3.9: Analog controller and components with delay corresponding to the sampling period in the main loop [7].

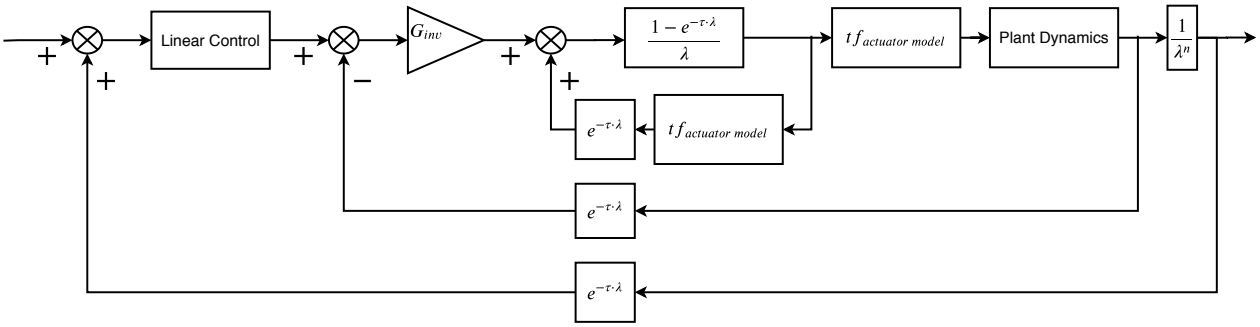

Figure 3.10: Block diagram of a control system relying on INDI control(with n-th order inversion) and including feedback delays as well as a zero-order hold filter.

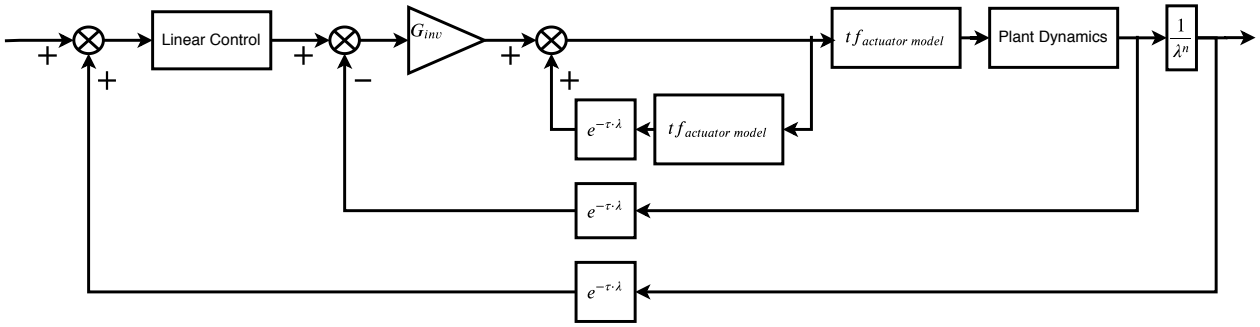

Figure 3.11: Block diagram of a control system relying on INDI control(with n-th order inversion) and including feedback delays.

4

Introduction to Time-delay Systems

Processes in real systems do not occur instantaneously. This is due to transport and propagation phenomena as well aftereffect phenomena within the components in the system, the sources of which are multifaceted. As a result, time-delays arise in those systems. There are several ways to refer to such systems including TDSs, hereditary systems, and systems with aftereffects [25].

Interest in the TDSs over the past few decades is reflected in the tremendous amount of research that has been performed on the subject. Several reasons for this interest have been postulated by Richard [31], including the fact that the analysis of time-delays is an applied problem (time-delays are always present) and the effect of time-delays on a system's stability and performance.

This chapter is dedicated to giving an introduction to the class of TDSs. The first section discusses the effect of delays on stability. Then, the ways to represent the TDSs are shown in section 4.2. Thereafter, the taxonomy for the classification of TDSs will be presented in section 4.3. Finally, a discussion on the spectral properties of TDSs is given.

4.1 Effects of Delay on Stability

It comes as no surprise that some of the initial studies on TDSs, as early as in the 1930s, were focused on the effects of delays on stability of a TDSs. It may be intuitively guessed that the presence of delays may induce instability in a control system. For example, when a controller makes use of past information about the states in a system, the output it provides may be unsuitable for the current state of the system. The tardiness in the information availability to the controller is due to any delays occuring in the closed-loop system such as the delays in the propagation of information between the elements in the control system, the time needed for a sensor to return a signal (sensor delay), or the reaction-time of actuators (actuator delay), as well as the digital nature of the controller. Moreover, even if it is idealized that the information is delivered instantaneously to the controller, delays occuring at the level of the controller also make the output of the controller unsuitable and with the potential to destabilize the system.

However, there is a dual effect to the nature of TDSs [67]. It may also be the case that time-delays may restore stability to a system. This may occur in the case of oscillatory systems. Given the possibility of a stabilizing effect, time-delays have been intentionally introduced into a control system to stabilize it.

There are also examples where the presence of delays does not affect the system's stability, irrespectively of how large the delay may become. This is known as the case of delay-independent (in)stability. this is a (un)fortunate property of the system considered.

In general, it is not always practical to analyze or design a system for delay-independent stability, as those results are often excessively conservative. Instead, and in alignment with the research objective of this thesis, it is more reasonable to search for the stability regions in the delay-space of the control system. That is why, the focus will be on delay-dependent stability.

It should be noted, however, that some of the discussions on delay-independent stability are sometimes relevant or are pre-requisites for the derivation of delay-dependent stability results, and they will be discussed in this light. The discussions on both the approaches for delay-independent and delay-dependent stability analysis will be returned to in chapter 5 and chapter 6.

4.2 Representation of Time-delay Systems

Dugard et al. discuss three ways to represent TDSs mathematically: as differential equations on abstract space [68] (as cited in [25, 69]), as differential equations on functional spaces i.e. as functional differential equations [70] (as cited in [25, 69]), and as differential equations over rings or operators [71] (as cited in [25, 69]).

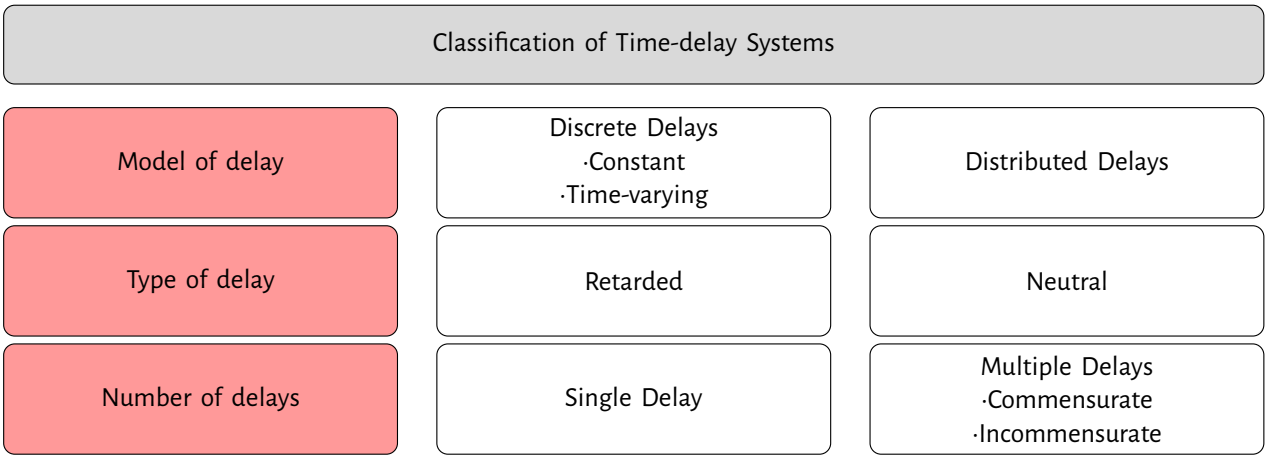

Figure 4.1: Classification of Time-delay Systems

However, TDS s are usually described by functional differential equations. In exception of the discussion on the matrix pencil approach for the determination of the characteristic equations in a certain right half plane (in section 5.2.2), the other two representations will not be encountered in this report. As a result, only the functional differential representation will be discussed in the subsequent paragraphs.

Equation (4.1) shows a functional differential equation that represents a generic TDS [72].

$$\begin{cases} \dot{x}(t) = f\left(t, x(t), x_t, u_t\right) & \\ x_{t_0} = \phi(\theta), & \forall\theta \in \left[t_0 - \tau, t_0\right] \\ u_{t_0} = \zeta(\theta), & \forall\theta \in \left[t_0 - \tau, t_0\right] \end{cases} \tag{4.1}$$

In this equation, ϕ and ξ denote the initial conditions for the state and the input, respectively. Moreover, τ denotes a time-delay, and as such $\tau > 0$. As for x_t, it is defined according to eq. (4.2):

$$x_t : \begin{cases} [-\tau, 0] \to \mathbb{R}^n \\ \theta \mapsto x_t(\theta) = x(t+\theta) \end{cases} \tag{4.2}$$

and u_t is defined according to eq. (4.3):

$$u_t : \begin{cases} [-\tau, 0] \to \mathbb{R}^n \\ \theta \mapsto u_t(\theta) = u(t+\theta) \end{cases} \tag{4.3}$$

The notation x_t and u_t corresponding to the definitions in eq. (4.2) and eq. (4.3) is referred to as the Shimanov notation. Moreover, it is clear that eq. (4.1) shows the dependence of the functional differential equation on current as well as past states and inputs.

4.3 Classification of Time-delay Systems

In this section, TDSs are described and categorized based on a number of dimensions. Of particular relevance are the model of the delay, the number of delays in the systems, and the type of delays in the system. The categories as well as the possible options for each of category are summarized in fig. 4.1.

4.3.1 Model of Delay: Discrete or Distributed

Following the taxonomy shown in fig. 4.1, it can be seen that there are two main ways to model delays: either as discrete (also referred to as point-wise delays) or distributed delays. States with discrete delays in their arguments such as $x(t-\tau)$ can be understood as values from a specific moment in the past which is in this case $t-\tau$. Furthermore, referring again to the taxonomy, it is seen that a discrete delay may either be constant or vary with time.

The choice of whether to model a time-delay as fixed or as time-varying is important for the validity of the results. When the analyses of systems with discrete delays are compared with those of systems with time-varying delays, the phenomenon of quenching is witnessed. That is, quenching happens at certain time-delays at which the system with discrete time-delays is stable but for which when the time-delays are assumed to be time-varying, stability is lost (or vice versa, having stable delay intervals for the case of time-varying delays for which the TDS with discrete delays is no longer stable) [73].

As for distributed delays, use is made of values from an interval of time occuring in the past $[-\tau_1, -\tau_2]$, where $\tau_1 > \tau_2 \geq 0$. This interval is then weighed with a kernel. It is this information that is incorporated into the dynamics [74]. An example of a system with distributed delay is shown in eq. (4.4) [75].

$$\dot{x}(t) = \int_{-r}^{0} c(\theta) x(t+\theta) d\theta \tag{4.4}$$

It should be remarked that the information captured by modeling the dependence on past information through distributed delays is a more complex but richer representation. Distributed delays are able to incorporate "memory" of a sequence occuring in the past which is more insightful than just looking at discrete points in the past.

Examples of using distributed delays in the description of a TDS is in the case of the delay response of human drivers. Physically, the interpretation for the use of distributed delays rather than discrete delays is that drivers make use of a cumulative continuous stream of past information they have perceived to take a control action [76]. Distributed delays are also used to describe the time delays occuring in stochastic thermodynamics, specifically the dynamics of a particle inside a heat reservoir with memory effects [77].

Besides their use in the system representation, distributed time-delays are also important in the derivation of delay-dependent stability criteria in the time-domain, for TDSs with point-wise delays. This will be seen in chapter 6.

4.3.2 Type of Delay: Retarded or Neutral

An important aspect is how the delay influences the states or the derivatives of the states in the system [74]. There are three main ways in which delays influence the states or the derivatives of the states in the system. Those are retarded type TDSs, neutral type TDSs, and advanced type TDSs. It is important to make this distinction between the types because the type has important implications on the properties of the system, on the necessary conditions for their stability, and consequently, on the approaches for stability analysis. In the following, it is explained how to differentiate between those three types.

In the case of retarded TDSs, the highest order derivative in the system is not affected by time-delays. The general form of the retarded type TDS is given by the functional differential equation in eq. (4.5) [78].

$$\dot{x}(t) = f\left(t, x_t\right) \tag{4.5}$$

A generic example of a retarded TDS is eq. (4.6).

$$\dot{x}(t) = A_0 x(t) + \sum_{i=1}^{m} A_i x\left(t - \tau_i\right) \tag{4.6}$$

However, for neutral TDSs, there are two terms with the highest-order derivative, one that does depend on the time-delay and another that does not. The general form of the neutral type TDS is given by the functional differential equation in eq. (4.7) [78].

$$\dot{x}(t) = f\left(t, x_t, \dot{x}_t\right) \tag{4.7}$$

A generic example of neutral time-delay system is eq. (4.8), where the term indicated with the underbrace is commonly referred to as the delay-difference operator.

$$\frac{d}{dt}\left(\underbrace{x(t) + \sum_{k=1}^{m} Cx\left(t - \tau_k\right)}_{\text{Delay-difference operator}}\right) = A_0 x(t) + \sum_{i=1}^{m} A_i x\left(t - \tau_i\right) \tag{4.8}$$

Moreover, the equation based on the delay-difference operator (also known as the discrete kernel operator [78]), shown in eq. (4.9), is that of associated delay-difference equation. The stability of this equation is tied to that of the neutral TDS as will be discussed later.

$$x(t) + \sum_{k=1}^{m} Cx\left(t - \tau_k\right) = 0 \tag{4.9}$$

As for the case where there is only one term for the highest-order derivative and this term depends on the time-delay, this case characterizes an advanced type TDS [74, 78, 79].

The distinction between the three types is further clarified with the examples of the scalar systems shown in eq. (4.10) and eq. (4.11) (as taken from [22]) and eq. (4.12). From eq. (4.10), it can be seen that the highest order derivative which is a second

order derivative does not depend on the state, but the first order derivative does. Thus, although there are state derivatives that depend on the delays in the system, this is a retarded type TDS.

$$\ddot{x}(t) = a\dot{x}(t-h) + bx(t), \quad x(t) \in \mathbb{R} \tag{4.10}$$

As for eq. (4.11), it can be seen that the highest-order derivative does also depend on the time-delay: $\ddot{x}(t-h)$. Therefore, this system is of neutral type.

$$\ddot{x}(t) = a\ddot{x}(t-h) + bx(t), \quad x(t) \in \mathbb{R} \tag{4.11}$$

Moreover, if the case where the $\ddot{x}(t)$ of eq. (4.11) is no longer part of the equation is encountered, as in the case shown in eq. (4.12), since the highest order derivative depends on the time-delay $a\ddot{x}(t-h)$, this is an advanced type TDS.

$$a\ddot{x}(t-h) + bx(t) + \dot{x}(t) = 0, \quad x(t) \in \mathbb{R} \tag{4.12}$$

It should be noted however that, for the sake of engineering applications, the advanced type is not as relevant [78]. The reason for this is that, in an advanced type TDS, the quantity described by the dynamics depends on its future values [80]. Since the dependence of a state on future values is not physically possible, only the retarded and the neutral types will be discussed in the parts to follow.

One main difference between retarded TDSs and neutral TDSs is the smoothness of solutions of the system. While for the case retarded TDSs, the solutions become smoother with the passing of time, such a smoothing effect does not always occur in the case of neutral TDS.

Another difference occurs in the spectral properties of the TDSs. In the case of retarded TDSs, it is guaranteed that there will be a finite number of roots to the right side of any vertical line drawn in the complex plane. However, in the case of neutral TDSs, there may be an infinite number of unstable roots. The stability of the delay-difference operator however induces the number of unstable roots for the neutral TDS to become finite. However, the disussion on the spectral properties will be further developed in section 4.4.

4.3.3 Number of Delays: Single or Multiple Delays

The final part of the taxonomy shown in fig. 4.1 deals with the number of delays in the system. The two categories here are the case of single delay in the system or multiple delays. If there are multiple delays in the system, it may be the case of either commensurate delays (when the delays are multiple of a certain baseline delay) or incommensurate delays [74].

It should be noted that a slightly confusing terminology has been adopted in the literature to describe systems with commensurate delays. Despite there being multiple delays in such a system, the system is referred to as a single delay system. In order to determine what multiple of the baseline delay occur in the system, the commensurate degree (denoted by L) is introduced. Therefore, the terms $x_1(t-\tau), x_2(t-2\tau)$ and $x_3(t-3\tau)$ present in the system, the commensurate degree is $L = 3$. As for the case of a system with a single delay, the commensurate degree is $L = 1$.

Dealing with multiple-delay systems is often much more complicated than that of the single-delay systems. One key challenge is the computational complexity which in the case of the stability analysis of multiple-delay systems is $\mathcal{NP}$-hard. Here, $\mathcal{NP}$ stands for non-deterministic polynomial time. However, it should be noted that $\mathcal{NP}$-hard problems constitute a completely different set of problems than that of $\mathcal{NP}$ problems. For both classes of problems, it is not possible to obtain a solution that is tractable and scalable with the size of the problem. Here, tractable means that the problem can be solved in polynomial time even in worst-case scenarios. The key difference between $\mathcal{NP}$ and $\mathcal{NP}$-hard problems is that for $\mathcal{NP}$ problems verifying a postulated solution is possible using a polynomial-time algorithm while for $\mathcal{NP}$-hard problems, it isn't. This makes $\mathcal{NP}$-hard problems the toughest class of problems to deal with.

To give an intuition of why this problem is $\mathcal{NP}$-hard, consider the stability analysis of a system with two distinct delays. This problem may be considered as the stability analysis of a system with commensurate delays but whereby all possible ratios between the two delays are attempted. Clearly, this makes it an intractable problem [74]. A formal proof of $\mathcal{NP}$-hardness of stability analysis in the case of incommensurate delays is provided by Gu et al. in [75].

4.4 Spectral Properties of Time-delay Systems

It is important to discuss the spectral properties of TDSs, as the spectral properties provide useful insights for the stability analysis techniques that will be explained later. Some of the spectral properties of retarded TDSs and of neutral TDSs will be individually discussed. However, before this discussion ensues, there are main properties that are applicable to the spectra of both retarded and neutral TDSs that need to be mentioned.

First and foremost, TDSs have infinitely many roots, and this is one of the aspects that reflect the infinite dimensional nature of TDSs. This property is easily seen from examining the characteristic quasipolynomial of any TDS. The Laplace transform

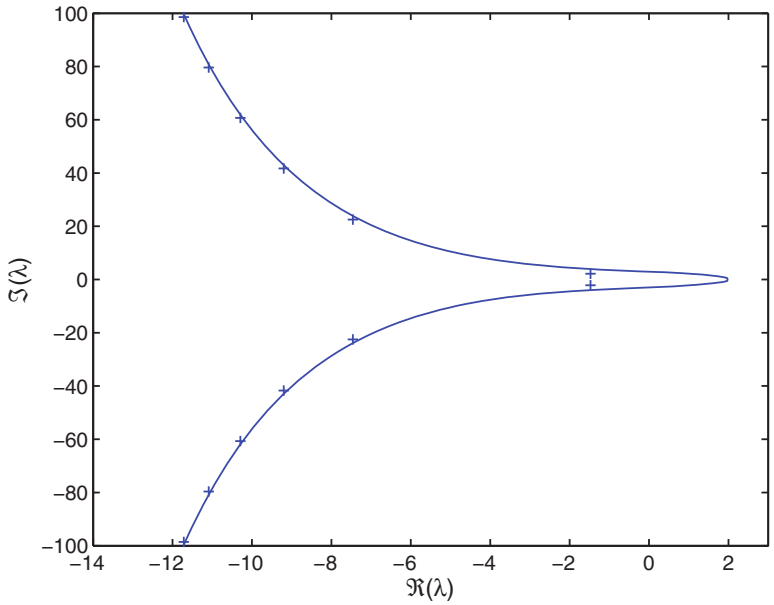

Figure 4.2: Example curve envelope of the spectrum of a TDS [8].

of delayed terms such as $x(t-\tau)$ leads to exponential terms in the characteristic equation. Since the exponential function is a transcendental function, its presence in the characteristic equation leads to an infinite number of zeros [8, 9].

Another important property of the spectrum of both retarded and neutral type TDSs is that when the coefficients of the quasipolynomial are real, the spectrum is symmetric with respect to the x-axis. This is applicable in the case of both retarded and neutral TDSs.

4.4.1 Spectral Properties of Retarded Time-delay Systems

Despite there being infinitely many characteristic roots, usually there is a finite number of unstable roots. For retarded systems, this is always applicable. As for neutral systems, this is guaranteed when the delay-difference operator is stable [8]. Conversely, when the delay-difference operator is unstable, there can appear infinitely many unstable roots for the neutral TDS [31].

For retarded TDSs, if there is a sequence of roots whose magnitude tends to $+\infty$, then the real part of those roots tends to $-\infty$.[8]. This is in alignment with the property that retarded systems have a finite number of unstable roots. That is, if the magnitude is getting increasingly large and it is known that the number of unstable roots has to be finite, then it must be that those roots are tending towards the extremes of the other half-plane. If there exists a sequence $\{\lambda_k\}$ of characteristic roots of the retarded system such that $\lim_{k\to\infty} \Re\left(\lambda_k\right) \to -\infty$ [8].

Additionally, there is a finite number of roots within any vertical strip in the complex plane. The vertical strip is formally expressed in eq. (4.13) where $\alpha, \beta \in \mathbb{R}$ and $\alpha < \beta$.

$$\{\lambda \in \mathbb{C} : \alpha < \Re(\lambda) < \beta\} \tag{4.13}$$

A special case of this property occurs when this vertical strip is narrowed down to an infinitesimally thin strip about the imaginary axis. Thus, it is deduced that the number of eigenvalues on the imaginary axis is always finite.

Another property is that there is a vertical line to the left-side of which will be all the roots of the retarded TDS. Let this vertical line be represented with $x = \gamma$. Formally, this is described with eq. (4.14).

$$\{\lambda \in \mathbb{C} : \Re(\lambda) < \gamma\} \tag{4.14}$$

An even stronger case of the latter is the proposition that yields the envelope curve of the spectrum. For the retarded TDS described by eq. (4.6), the envelope is described by eq. (4.15). The proof for this proposition is provided by Michiels et al. in [8]. An example of such an envelope is shown in fig. 4.2.

$$|\lambda| \leq \left\|A_0\right\|_2 + \sum_{i=1}^{m} \left\|A_i\right\|_2 e^{-\Re(\lambda)\tau_i} \tag{4.15}$$

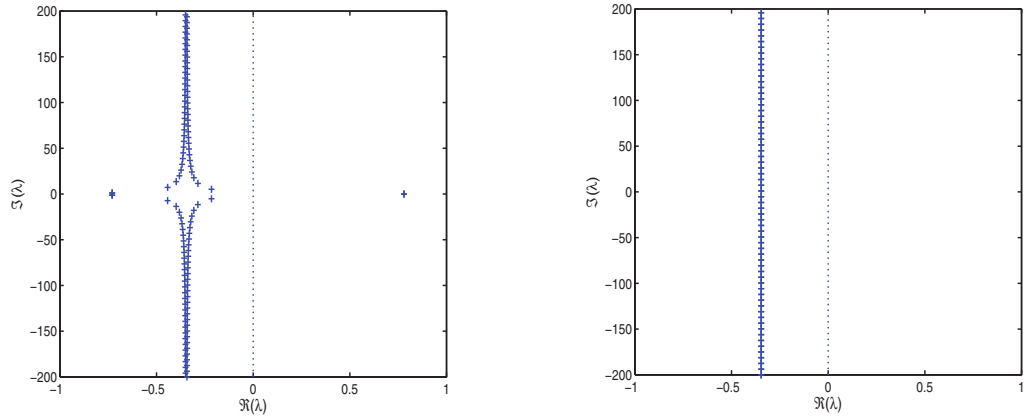

(a) Spectrum of the neutral type TDS [8].

(b) Spectrum of the corresponding delay-difference equation [8].

Figure 4.3: Spectrum of a neutral type TDS and that of the corresponding delay-difference equation.

The envelope curve provides very nice information regarding the location of the critical imaginary roots which are the roots of the characteristic equation that occur on the imaginary axis of the complex plane. Knowing about the presence and location of the critical imaginary roots is important because, for retarded systems, the gain or loss of stability is related to the crossing of the imaginary axis. Being imaginary roots, λ in eq. (4.15) can be replaced with $j\omega$. Moreover, the real part of the characteristic root is zero i.e. $\mathfrak{N}(j\omega) = 0$. This leads to eq. (4.16) [8].

$$
\begin{aligned}
|j\omega| &\leq \left\|A_0\right\|_2 + \sum_{i=1}^{m} \left\|A_i\right\|_2 e^0 \\
\implies |\omega| &\leq \left\|A_0\right\|_2 + \sum_{i=1}^{m} \left\|A_i\right\|_2 \\
\implies |\omega| &\leq \sum_{i=0}^{m} \left\|A_i\right\|_2
\end{aligned} \tag{4.16}
$$

From eq. (4.16), it is clear that there is an interval over the imaginary axis of finite width that is guaranteed to contain the critical imaginary roots. It can also be noted, based on this inequality, that this interval is independent of the delay values [8].

The spectra of retarded TDSs also possess nice continuity properties. That is, the characteristic roots behave continuously with respect to the variations of system matrices and delays. Additionally, the spectral abscissa, which is the largest real part available from the roots in the spectrum i.e. $\max_i \left\{\mathrm{Re}\left(\lambda_i\right)\right\}$, is also continuous with respect to these variations.

4.4.2 Spectral Properties of Neutral Time-delay Systems

The properties of the spectrum of the associated delay-difference equation, shown in eq. (4.9), heavily dictate those of the spectrum of the neutral type TDS. It is also this aspect that leads to the additionaly necessary stability condition for the exponential stability of the null solution of the neutral type TDS, which is the exponential stability of the null solution of the delay-difference equation [8].

An important aspect of the relation between the spectrum of the neutral type TDS and that of the associated delay difference equation is that the real part of the sequence of characteristic roots $\left\{\lambda_n\right\}_{n\geq 1}$ of the neutral type TDS (eq. (4.8)) tends to the limit of that of the delay-difference equation, denoted by ζ. Moreover, the imaginary part of the sequence of characteristic roots tends to infinity; thus, the neutral TDS is said to have vertical asymptotic chains [81]. Both of these characteristics are expressed in eq. (4.17).

$$
\lim_{n\to\infty} \Re\left(\lambda_n\right) = \zeta, \quad \lim_{n\to\infty} = \Im\left(\lambda_n\right) = \infty \tag{4.17}
$$

An example spectrum demonstrating these properties is shown in fig. 4.3. Examining the spectrum of the neutral TDS shown in fig. 9.1a, it is seen that the sequence of eigenvalues tends to the vertical line at around -0.35, which happens to be location of where all the roots of the delay-difference equation are located, as seen in fig. 9.1h.

Another property is that neutral type time-delay equation has a finite number of roots that are in the right-half plane and that are to the right of the spectral abscissa of the delay-difference equation, which is denoted by c_D. This again can be seen

from fig. 9.1a where it can be seen that there is only one root in the right half-plane, which also happens to be on the right-hand side of the spectral abscissa of the characteristic roots of the delay-difference operator which occurs at about -0.35.

Small perturbations can remove the stability of the delay-difference equation, which is known as the delay sensitivity problem of the delay-difference equation. This susceptibility to small perturbations is eliminated when the delay-difference equation is strongly stable, which is ensured when condition eq. (4.18) is satisfied. In this case, it can also be said that the delay-difference operator is strongly stable.

$$\sum_{k=1}^{m} \|C\| < 1 \tag{4.18}$$

When the strong stability of the delay-difference operator is ensured, the loss or gain of stability, as in the case of retarded TDSs, is related to crossing the imaginary axis in the complex plane. This ties to the fact that, as mentioned earlier, the strong stability of the delay-difference operator induces a finite number of unstable roots.

This page was intentionally left blank.

5

Frequency-domain Techniques

Frequency-domain techniques are often preferred for their simplicity, and they can be often computationally efficient [75]. The discussion in this chapter is devoted to giving an overview of frequency-domain techniques for analyzing the stability of Linear Time-invariant (LTI) TDSs. Due to the vast amount of literature on the subject matter, a comprehensive review of all the academic contributions is not possible within the scope of this thesis. However, in this chapter, the attempt was to assemble a thorough discussion of more recent frequency-domain techniques.

The development of frequency domain techniques for the stability analysis of LTI TDSs emerged as early as the 1949 with the work of Chebotarev and Neimark [82, 83]. Moreover, the study of zeros of quasipolynomials was investigated by Pontryagin in 1955. However, the first systematic application of frequency-domain methods on TDSs was performed by Bellman and Cooke [79, 84]. Beyond these classical results, a number of more recent and more versatile techniques emerged, and as mentioned, the focus will be on discussing these methods. These techniques will be grouped into three main categories, which are the delay-independent stability techniques discussed in section 5.1, the spectrum computation techniques that will be discussed in section 5.2, and the techniques that determine the critical pairs and study asymptotic behaviour to analyze delay-dependent stability. The latter are discussed in section 5.3. A number of concluding remarks are presented in section 5.4.

5.1 Frequency Sweeping Tests for Delay-independent Stability

It was previously mentioned that the main interest is in discussing delay-dependent stability. However, when analyzing for delay-dependent stability, it is possible that hyperbolic cases are encountered. This means that the system is either stable or unstable irrespective of the value of the delays occurring in the system. For such cases, it may be useful to verify the analysis with a number of delay-independent stability tests. That is why, some tests for delay-independent stability that have been encountered in the literature will be presented. Namely, the results for TDSs with single delay (Theorem 5.1 and Theorem 5.2), for TDSs with commensurate delays (Theorem 5.3 and Theorem 5.4), and for TDSs with incommensurate delays (Theorem 5.5) will be presented. These stability results can be tested using frequency sweeping tests.

For a TDS with a single delay of retarded type as the one shown in eq. (5.1),

$$\dot{x}(t) = A_0 x(t) + A_1 x(t-\tau), \quad \tau \geq 0 \tag{5.1}$$

the following delay-independent result has been derived in the literature [75].

Theorem 5.1 (Delay-independent Stability Test for TDS with a Single Delay [75]): *The system eq.* (5.1) *is stable independent of delay if and only if*

1. A_0 *is stable.*
2. $A_0 + A_1$ *is stable.*
3. $\rho\left(\left(j\omega I - A_0\right)^{-1} A_1\right) < 1, \quad \forall \omega > 0$ *where* $\rho(\cdot)$ *denotes the spectral radius of a matrix.*

This result is equivalent to the one shown in Theorem 5.2.

Theorem 5.2 (Delay-independent Stability Test for TDS with a Single Delay[75]): *The system eq.* (5.1) *is stable independent of delay if and only if*

1. A_0 *is stable.*
2. $A_0 + A_1$ *is stable.*
3. $\underline{\rho}\left(j\omega I - A_0, A_1\right) > 1, \quad \forall \omega > 0.$

As for a TDS with commensurate delays shown in eq. (5.2),

$$\dot{x}(t) = A_0 x(t) + \sum_{k=1}^{m} A_k x(t - k\tau), \quad \tau \geq 0 \tag{5.2}$$

the following stability result was obtained:

Theorem 5.3 (Delay-independent Stability Test for TDS with Commensurate Delays [75]): *The system eq.* (5.2) *is stable independent of delay if and only if*

1. A_0 *is stable.*
2. $A_0 + \sum_{k=1}^{m} A_k$ *is stable.*
3. $\rho\left(M_m(j\omega)\right) < 1, \quad \forall \omega > 0.$ *where*

$$M_m(s) := \begin{pmatrix} \left(sI - A_0\right)^{-1} A_1 & \cdots & \left(sI - A_0\right)^{-1} A_{m-1} & \left(sI - A_0\right)^{-1} A_m \\ I & \cdots & 0 & 0 \\ \vdots & \ddots & \vdots & \vdots \\ 0 & \cdots & I & 0 \end{pmatrix} \tag{5.3}$$

Remark 5.1: *If the system with commensurate delays is expressed as differential-difference equation*

$$y^{(n)}(t) + \sum_{i=0}^{n-1} \sum_{k=0}^{q} a_{ki} y^{(i)}(t - k\tau) = 0, \quad \tau \geq 0 \tag{5.4}$$

it can be transformed into the form of eq. (5.2) *by taking the matrices* A_0 *and* A_1 *in eq.* (5.2) *as follows:*

$$A_0 = \begin{pmatrix} 0 & 1 & \cdots & 0 \\ \vdots & \vdots & \ddots & \vdots \\ 0 & 0 & \cdots & 1 \\ -a_{00} & -a_{01} & \cdots & -a_{0,n-1} \end{pmatrix} \tag{5.5}$$

$$A_k = \begin{pmatrix} 0 & 0 & \cdots & 0 \\ \vdots & \vdots & \cdots & \vdots \\ 0 & 0 & \cdots & 0 \\ -a_{k0} & -a_{k1} & \cdots & -a_{k,n-1} \end{pmatrix} \tag{5.6}$$

Applying the transformation mentioned in Remark 5.1 to Theorem 5.3, the following theorem is obtained:

Theorem 5.4 (Delay-independent Stability Test for TDS with Commensurate Delays[75]): *The system eq.* (5.4) *is stable independent of delay if and only if*

1. $a_0(s)$ *is stable*
2. $a_0(s) + \sum_{k=1}^{q} a_k(s)$ *is stable*

3. $\rho\left(M_a(j\omega)\right) < 1, \quad \forall \omega > 0$ *where*

$$M_a(s) := \begin{pmatrix} -\frac{a_1(s)}{a_0(s)} & \cdots & -\frac{a_{q-1}(s)}{a_0(s)} & -\frac{a_q(s)}{a_0(s)} \\ 1 & \cdots & 0 & 0 \\ \vdots & \ddots & \vdots & \vdots \\ 0 & \cdots & 1 & 0 \end{pmatrix} \tag{5.7}$$

As for a system with incommensurate delays shown in eq. (5.8),

$$\dot{x}(t) = A_0 x(t) + \sum_{i=1}^{m} A_i x\left(t - \tau_i\right), \quad \tau_i \geq 0 \tag{5.8}$$

the following stability result is applicable:

Theorem 5.5 (Delay-independent Stability for TDS with Incommensurate Delays): *Let $r_k \geq 0, k = 1, 2, \cdots, m$ be independent, incommensurate delays. Then the system eq.* (5.8) *is independent of delay if and only if*

1. A_0 *is stable*
2. $A_0 + A_1$ *is stable*
3. $\mu_{\mathbb{X}_m}(M(j\omega)) < 1, \quad \forall \omega > 0$ *where*

$$M(s) := \begin{bmatrix} I \\ \vdots \\ I \end{bmatrix} \left(sI - A_0\right)^{-1} \begin{bmatrix} A_1 & \cdots & A_m \end{bmatrix} \tag{5.9}$$

5.2 Spectrum Computation

A well-known approach for studying the stability of an LTI system described in the frequency domain is to determine the eigenvalues of that system. However, as expressed previously, since TDSs belong to the class of infinite dimensional systems and have infinitely-many roots [68], it is impractical to try to obtain all the eigenvalues of the system, and in the following, two approaches to deal with this issue are presented.

The first one is to approximate the transcendental terms in the characteristic equation which are the exponential terms with finite-dimensional approximations. This leads to an finite-dimensional approximation of the overall system, for which a finite number of roots may be obtained.

The second option is to only investigate the eigenvalues belonging to a certain right half-plane. This is appropriate because the number of roots in this case will be finite (For retarded TDSs, this is always applicable; whereas, for neutral TDSs, this holds when the delay-difference operator is strongly stable). Determining those eigenvalues is done through the discretization of the solution operator first, which leads to a matrix pencil approximation of the solution operator. Thus, the operator eigenvalue problem is transformed to that of a matrix eigenvalue problem which can be numerically solved [8, 85].

5.2.1 Finite-dimensional Approximation

As mentioned in the introduction of this section, it is possible to approximate the exponential terms with truncated power series or rational approximations thereof. In general, the rational approximations of an exponential term are of the form shown in eq. (5.10), where p is a polynomial that does not have any roots that belong to the right half-plane [31].

$$\mathrm{e}^{-\tau s} \approx \frac{p(-\tau s)}{p(\tau s)} \tag{5.10}$$

An example of a finite-dimensional approximation of the exponential term is a first order Taylor series approximation, which is shown in eq. (5.11).

$$e^{-\tau s} \approx 1 - \tau s \tag{5.11}$$

Other examples of finite-dimensional approximations include Padé approximations, the Laguerre-Fourier series, and the Kautz series [31].

In the case of finite-dimensional approximations, the resultant stability regions are approximations of the true stability regions [81]. A discussion on this limitation, specifically in the case of taking Padé approximation of the exponential terms, is presented in [81].

5.2.2 Spectral Discretization

The main idea behind this approach is to first perform a spectral discretization of the solution operator, which will be explained shortly, in order to transform the eigenvalue problem into a discretized eigenvalue problem. The resultant matrix pencil can be solved for to determine the characteristic roots in a certain right half plane. The results are often crude, but they can be refined by using Newton's method on the characteristic equation. The refinement is necessary because the goal here is to robustly determine the characteristic roots of the system that belong to the a certain right half plane [8].

Before discussing the discretization procedure that leads to the final matrix pencils whose solution yields the characteristic roots, the concepts of a solution operator and infinitesimal operator need to be understood first. Before, presenting the mathematical definition of the solution operator and infinitesimal generator, it is first important to give an overview of how it is in general possible to determine the solution of a TDS.

Consider the retarded TDS shown in eq. (5.8), with the initial condition defined on an interval $\left[-\tau_m, 0\right]$ as shown in eq. (5.12).

$$\phi \in \mathscr{C}\left(\left[-\tau_m, 0\right], \mathbb{R}^n\right) \tag{5.12}$$

The solution of a TDS can be determined using the method of steps. Specifically, the initial condition eq. (5.12) can replace the delayed terms in the equation of the retarded TDS. This leads to an ordinary differential equation, seen in eq. (5.13), with the initial condition being $\xi_1(0) = x(0) = \phi(0)$.

$$\dot{\xi}_1(t) = A_0\xi_1(t) + \sum_{i=1}^{m} A_i\phi\left(t-\tau_i\right) \tag{5.13}$$

The solution of this initial value problem is the state of the system for the interval $\left[0, \tau_m\right]$, or a "piece of the trajectory" of the system pertaining to that interval of time-delays. This is repeated for following time-steps. In other words, in order to obtain the state for the interval $\left[\tau_m, 2\tau_m\right]$, it is required to obtain the solution of eq. (5.14) with the initial condition $\xi_2(\tau_m)$ which was obtained by evaluating the previously obtained solution ξ_1 at τ_m, i.e. $\xi_2(\tau_m) = x(\tau_m) = \xi_1(\tau_m)$.

$$\dot{\xi}_2(t) = A_0\xi_2(t) + \sum_{i=1}^{m} A_i\xi_1\left(t-\tau_i\right) \tag{5.14}$$

This procedure can be repeated for as many intervals as desired. That is because for the case of retarded TDSs, the solution becomes smoother, the more pieces of the trajectories are solved for.

Through the method of steps, it can be seen that obtaining the solution for the TDS is constructed by obtaining these so-called forwards solutions, ξ_k, which represent parts of the trajectory of the TDS. An operator has been defined to denote this mapping. Since the method of steps allows to obtain the solution of the TDS, the operator is called the solution operator $\mathscr{T}(t)$. The mapping itself from the initial conditions to the state of the system at time t denoted by $x_t(\phi)(\theta) = x(\phi)(t+\theta)$, using the solution operator, is mathematically described in eq. (5.15).

$$x_t(\phi)(\theta) = x(\phi)(t+\theta) = (\mathscr{T}(t)\phi)(\theta), \quad \theta \in \left[-\tau_m, 0\right] \tag{5.15}$$

The infinitesimal generator $\mathscr{A}$ of the solution operator $\mathscr{T}$ is defined in eq. (5.16).

$$\begin{gathered}\mathscr{D}(\mathscr{A}) = \left\{\phi \in \mathscr{C}\left(\left[-\tau_m, 0\right], \mathbb{R}^n\right) : \frac{d\phi}{d\theta} \in \mathscr{C}\left(\left[-\tau_m, 0\right], \mathbb{R}^n\right) \phi(0) = A_0\phi(0) + \textstyle\sum_{k=1}^{m} A_k\phi\left(-\tau_k\right)\right\} \\ \mathscr{A}\phi = \frac{d\phi}{d\theta}\end{gathered} \tag{5.16}$$

Based on this definition, it is possible to write the relation $\mathscr{A}\phi = \frac{d\phi}{d\theta}$ in the form of an eigenvalue problem, as seen in eq. (5.17).

$$\mathscr{A}\phi = \lambda\phi, \quad \lambda \in \mathbb{C}, \phi \in \mathscr{C}\left(\left[-\tau_{\max}, 0\right], \mathbb{R}^n\right), \phi \neq 0 \tag{5.17}$$

The importance of the infinitesimal generator is that it allows for a different representation of the TDS, specifically as an abstract ordinary differential equation, which subscribes to the catergory of represenation of TDSs on abstract spaces, as mentioned in section 4.2. As seen from eq. (5.16), the representation based on the infinitesimal generator allows to interpret the problem as an eigenvalue problem.

While the initial formulation of the eigenvalue problem was a nonlinear but finite-dimensional one, the new formulation is an equivalent linear but infinte-dimensional eigenvalue problem. Thus, instead of obtaining the roots of the characteristic equation of the TDS, λ is solved for in eq. (5.17). However, in order to solve for that, the infinitesimal generator has to be discretized because the discretization allows to approximate the infinitesimal generator with a matrix, which means that the eigenvalue problem can be solved numerically. The first step in this direction is to discretize the interval $\left[-\tau_m, 0\right]$,

$$\Omega_N = \left\{\theta_{N,i}, i = 1, \ldots, N+1\right\} \tag{5.18}$$

such that

$$-\tau_m \leq \theta_{N,1} < \cdots < \theta_{N,N+1} = 0 \tag{5.19}$$

Then, the discretized version of the continuous initial condition ϕ, which is denoted by $\mathbf{x}$, consists of elements where each of these elements, denoted by $\mathbf{x}_i$, is described by eq. (5.20).

$$\mathbf{x}_i = \phi\left(\theta_{N,i}\right) \in \mathbb{C}^n, \quad i = 1, \ldots, N+1 \tag{5.20}$$

Note that, $\mathbf{x}$ represents the discretization of the range of the continuous function ϕ defined on the domain $\left[-\tau_m, 0\right]$. With the discretized domain (eq. (5.19)) and the discretized range (eq. (5.20)) established, it is possible to determine the unique polynomial mapping between them which is denoted by $\mathscr{L}_N\mathbf{x}, \mathbf{x} \in X_N$. This means that:

$$\left(\mathscr{L}_N\mathbf{x}\right)\left(\theta_{N,i}\right) = \mathbf{x}_i, \quad i = 1, \ldots, N+1 \tag{5.21}$$

It is now possible to write the equivalent of eq. (5.16) using the discretized counterparts. This leads to:

$$\begin{aligned} \left(\mathbf{A}_N\mathbf{x}\right)_i &= \left(\mathscr{L}_N\mathbf{x}\right)'\left(\theta_{N,i}\right), \quad i = 1, \ldots, N \\ \left(\mathbf{A}_N\mathbf{x}\right)_{N+1} &= A_0\left(\mathscr{L}_N\mathbf{x}\right)(0) + \textstyle\sum_{k=1}^{m} A_k\left(\mathscr{L}_N\mathbf{x}\right)\left(-\tau_k\right) \end{aligned} \tag{5.22}$$

In order to obtain the expression for the entries of $\mathbf{A}_N$, the Lagrange polynomials are used as a basis.

$$\mathbf{A}_N = \begin{bmatrix} a_{1,1} & \cdots & a_{1,N+1} \\ \vdots & \ddots & \vdots \\ a_{N+1,1} & \cdots & a_{N+1,N+1} \end{bmatrix} \in \mathbb{C}^{n(N+1)\times n(N+1)} \tag{5.23}$$

$$a_{il} = \begin{cases} \ell_l'\left(\theta_{N,i}\right) I_n, & l \in \{1, \ldots, N+1\}, \quad i \in \{1, \ldots, N\} \\ \sum_{k=0}^{m} A_k \ell_l\left(-\tau_k\right) & l \in \{1, \ldots, N+1\}, \quad i = N+1 \end{cases} \tag{5.24}$$

The concept of a forward solution, which is encountered in the method of steps, appears here again even for the discretized variant of the problem.

$$\mathbf{A}_N\mathbf{x} = \lambda\mathbf{x}, \quad \lambda \in \mathbb{C}, \quad \mathbf{x} \in \mathbb{C}^{n(N+1)}, \quad \mathbf{x} \neq 0 \tag{5.25}$$

5.2.2.1 Retarded Time-delay System

The choice of the grid for the interval $\left[-\tau_m, 0\right]$ (eq. (5.18) and eq. (5.19)) has not yet been defined. One possibility shown in eq. (5.26) has been seen in the literature [8].

$$\theta_{N,i} = \frac{\tau_m}{2}\left(\alpha_{N,i} - 1\right), \quad \alpha_{N,i} = -\cos\frac{\pi i}{N+1}, \quad i = 1, \ldots, N+1 \tag{5.26}$$

It has been proven that, with this choice, spectral convergence is guaranteed. Moreover, the discretization leads to the eigenvalue problem of the form in eq. (5.27), which involves a linear matrix pencil (Σ_N, Π_N),

$$\left(\Sigma_N - \lambda\Pi_N\right)\mathbf{c} = 0, \quad \lambda \in \mathbb{C}, \quad \mathbf{c} \in \mathbb{C}^{(N+1)n}, \quad \mathbf{c} \neq 0 \tag{5.27}$$

where

$$\Pi_N = \frac{\tau_m}{4}\begin{bmatrix} \frac{4}{\tau_m} & \frac{4}{\tau_m} & \frac{4}{\tau_m} & \cdots & & \cdots & \frac{4}{\tau_m} \\ 2 & 0 & -1 & & & & \\ & \frac{1}{2} & 0 & -\frac{1}{2} & & & \\ & & \frac{1}{3} & 0 & \ddots & & \\ & & & \frac{1}{4} & \ddots & -\frac{1}{N-2} & \\ & & & & \ddots & 0 & -\frac{1}{N-1} \\ & & & & & \frac{1}{N} & 0 \end{bmatrix} \otimes I_n \tag{5.28}$$

and

$$\Sigma_N = \begin{bmatrix} R_0 & R_1 & \cdots & R_N \\ & I_n & & \\ & & \ddots & \\ & & & I_n \end{bmatrix} \tag{5.29}$$

where

$$R_i = A_0 + \sum_{k=1}^{m} A_k T_i\left(-2\frac{\tau_k}{\tau_m} + 1\right), \quad i = 0, \ldots, N \tag{5.30}$$

and T_i are Chebyshev polynomials of the first kind, which are defined by recursive relations.

Furthermore, the process of determining the discretization points is automated through an algorithm which is described in detail in [8]. The selection of the number of discretization points is a central aspect because a large number of discretization points leads to a significant increase in the computation needed, yet if the number of discretization points is too small, the accuracy of the estimated characteristic roots may be very poor such that even the corrections based on Newton's method are futile and do not converge [8].

5.2.2.2 Neutral Time-delay System

The overall procedure to calculating the characteristic roots in the case of neutral type TDS based on a spectral discretization is provided in the work of Breda et al. [86]. Their results show that the computation of the characteristic roots is done through solving for the roots of eq. (5.31).

$$\det\left\{\lambda\begin{bmatrix} E^{(1)} & 0 \\ 0 & -A_0^{(22)} \end{bmatrix} - \sum_{i=0}^{m}\begin{bmatrix} A_i^{(11)} & A_i^{(12)} \\ 0 & 0 \end{bmatrix} p_N\left(-\tau_i;\lambda\right) - \begin{bmatrix} 0 & 0 \\ A_0^{(21)} & 0 \end{bmatrix} p'_N(0;\lambda) - \sum_{i=1}^{m}\begin{bmatrix} 0 & 0 \\ A_i^{(21)} & A_i^{(22)} \end{bmatrix} p'_N\left(-\tau_i;\lambda\right)\right\} \tag{5.31}$$

where p_N is a degree N polynomial defined in eq. (5.32).

$$\begin{cases} p_N(0;\lambda) = 1 \\ p'_N\left(\theta_{N,i};\lambda\right) = \lambda p_N\left(\theta_{N,i};\lambda\right), 1 \le i \le N \end{cases} \tag{5.32}$$

However, it is known that the roots of neutral time-delay equation are the same as those of the corresponding DDAE, in expection of the case of the presence of zero as a root. The form of the DDAE is shown in eq. (5.33).

$$E\dot{x}(t) = A_0 x(t) + \sum_{i=1}^{m} A_i x\left(t - \tau_i\right) \tag{5.33}$$

Therefore, the spectral discretization can be applied to the DDAE instead. Solving for the roots of DDAE involves solving for the matrix pencil $(\mathbf{E}_N, \mathbf{A}_N)$, i.e. solving for:

$$\left(\lambda\mathbf{E}_N - \mathbf{A}_N\right)\mathbf{x} = 0 \tag{5.34}$$

where $\mathbf{A}_N$ is defined according to eq. (5.23) and eq. (5.24), and E_N is defined in eq. (5.35).

$$\mathbf{E}_N = \begin{bmatrix} I_{nN} & 0 \\ 0 & E \end{bmatrix} \tag{5.35}$$

Moreover, it was also shown that solving for the characteristic roots of the DDAE led to smaller errors. That is why, it is preferred to use the matrix pencil $(\mathbf{E}_N, \mathbf{A}_N)$ to determine the characteristic roots of the neutral TDS that belong to some half-plane such that $\Re(z) > \alpha$ for some finite α.

5.3 Critical Pairs and Root Tendency

The paradigm presented in this section circumvents the determination of the eigenvalues of the closed-loop system. In order to do so, some of the spectral properties and stability properties of TDSs that had been discussed in chapter 4 are harnessed. Specifically, one spectral property is that there is a finite number of characteristic roots in the right half-plane for retarded TDSs and for neutral TDSs with strongly stable delay-difference operators. Recall also, that this property bore the stability property: that the gain or loss of stability of these systems is determined by the crossing of the imaginary axis. Therefore, the stability problem now is turned into one of counting the number of unstable roots as the time-delay(s) is/are varied. This is done based on determining the crossings with the imaginary axis and determining the time-delays at which these crossings occur. The combinations of the critical imaginary roots with their associated time-delays are known as critical pairs. With the delay intervals or regions (for the case of multiple delays) established, it remains to determine whether the intervals/regions are stable or not.

5.3.1 Determining the Critical Pairs

As mentioned in the introduction of this section, the first part is to determine the critical pairs of the TDS. There are several methods in the literature that show how this can be done, and those will be discussed in the following. It should be noted, that for all the methods that will be discussed in this subsection, it is assumed that $\lambda = 0$ is not a root of the characteristic quasipolynomial because this degenrate case implies that the system may not be asymptotically stable [9, 11].

5.3.1.1 Direct Method

The direct method was developed by Walton and Marshal for TDSs that have a single delay [87]. At the core of this approach is the elimination of the exponential term in the TDS, which is why it is referred to as the direct method. In the following, it will be explained how this elimination is done. The steps that follow and that lead to the determination of the critical imaginary roots and their corresponding critical time-delays will also be explained.

For an LTI system with a single time-delay, the characteristic equation takes the form shown in eq. (5.36).

$$f\left(\lambda, e^{-\tau\lambda}\right) = P(\lambda) + Q(\lambda)e^{-\tau\lambda} \tag{5.36}$$

According to the conjugate symmetry property, if a quasipolynomial has a root at some complex value λ, then the conjugate characteristic equation has a root at the conjugate of λ.

Thus, if the characteristic equation has a root at $j\omega$,

$$P(j\omega) + Q(j\omega)e^{-j\tau\omega} = 0 \tag{5.37}$$

then the following holds true as well.

$$P(-j\omega) + Q(-j\omega)e^{j\tau\omega} = 0 \tag{5.38}$$

Those two equations, eq. (5.37) eq. (5.38), can then be combined by eliminating $e^{j\tau\omega}$ to obtain the polynomial eq. (5.39), which is referred to as the magnitude equation.

$$\left|P(j\omega)\right|^2 - \left|Q(j\omega)\right|^2 = 0 \tag{5.39}$$

Let $\theta_i = \tau_i \cdot \omega_i$. Then, based on eq. (5.37),

$$e^{-j\theta_i} = -1 \cdot \left(\frac{P(j\omega)}{Q(j\omega)}\right) \Longrightarrow e^{j\theta_i} = -1 \cdot \left(\frac{Q(j\omega)}{P(j\omega)}\right) \Longrightarrow \angle e^{j\theta_i} = \angle -1 + \angle\left(\frac{Q(j\omega)}{P(j\omega)}\right) \tag{5.40}$$

$$\theta_i = \begin{cases} \angle\frac{Q(j\omega_i)}{P(j\omega)} + \pi, & 0 \leq \angle\frac{Q(j\omega_i)}{P(j\omega)} \leq \pi \\ \angle\frac{Q(j\omega_i)}{P(j\omega)} - \pi, & \pi < \angle\frac{Q(j\omega_i)}{P(j\omega)} \leq 2\pi \end{cases} \tag{5.41}$$

Since the ω_i values are obtained from solving for the roots of eq. (5.39), and that the θ_i values are obtainable with eq. (5.41), the set of τ_i values, the set of critical times, can be computed.

5.3.1.2 Bilinear Transformation: Pseudo-delay Techniques

In this method, the exponential term is replaced using a bilinear transformation. It should be noted that these substitutions are exact and are not approximations (in contrast to the finite dimensional approximations discussed in section 5.2.1). After the transformation, the new characteristic equation is expected to be easier to analyze. However, it should also be noted that applying this approach is not guaranteed to be an easy task.

One of the earliest and most notable pseudo-delay techniques relies on the Rekasius substitution [88], shown in eq. (5.42). It is the variable T in the equation that is referred to as the pseudo-delay [25].

$$\mathrm{e}^{-j\omega\tau} = \frac{1 - j\omega T}{1 + j\omega T}, \quad T > 0 \tag{5.42}$$

It was noticed that the Rekasius substitution in fact only maps $[0, \infty]$ onto a semi-circle [89]. For the mapping to cover an entire circle, the values of T need to be both positive and negative. As a result, another type of bilinear substitution was proposed, shown in eq. (5.43), which is similar to the Rekasius substitution. This transformation involves the square of the term in the Rekasius substitution. As a result, it simplifies the analysis to only the consideration of $T > 0$ [90].

$$e^{-j\omega\tau} = \left(\frac{1 - j\omega T}{1 + j\omega T}\right)^2, \quad T > 0 \tag{5.43}$$

Olgac and Sipahi used the Rekasius substitution to determine the critical imaginary roots [91]. In order for the transformation to be exact at the imaginary axis, the phase and magnitude of the right hand side of the transformation have to be equal to those of the left hand side. This may lead to conditions that need to be satisfied to ensure the exactness. These conditions will be determined for the case of the Rekasius substitution.

It can be seen that the condition for equal magnitudes is readily satisfied.

$$\left|e^{-j\tau\omega}\right| = 1, \quad \left|\frac{1 - j\omega T}{1 + j\omega T}\right| = \frac{\sqrt{1 + (-T\omega)^2}}{\sqrt{1 + (T\omega)^2}} = 1 \tag{5.44}$$

As for the phases to be equal, the following derivation leads to a condition that needs to be ensured, which is in the form of a relation between τ and ω and T [74].

$$\begin{aligned} &\angle e^{-j\tau\omega} = -\tau\omega, \quad \angle\left(\frac{1 - j\omega T}{1 + j\omega T}\right) = \angle(1 - j\omega T) - \angle(1 + j\omega T) \\ \implies &-\tau\omega = \tan^{-1}(-\omega T) - \tan^{-1}(\omega T) \\ \implies &\tau_\ell = \frac{2}{\omega}\left(\tan^{-1}(\omega T) \mp \ell\pi\right) \end{aligned} \tag{5.45}$$

Consider the characteristic equation of a TDS shown in eq. (5.46).

$$f\left(\lambda; e^{-\tau\lambda}\right) := \sum_{k=0}^{n} P_k(\lambda) e^{-k\tau\lambda} \tag{5.46}$$

If the Rekasius transformation is applied to this characteristic equation, the following is obtained:

$$\tilde{F}(s; T) := \sum_{k=0}^{n} P_k(s) \left(\frac{1 - Ts}{1 + Ts}\right)^k \tag{5.47}$$

For easier handling, by multiplying with the polynomial term in the denominator that has the highest order, i.e. $(1 + sT)^n$, the terms in the denominator are cancelled out. The result is the polynomial shown in eq. (5.48).

$$F(\lambda; T) := (1 + T\lambda)^n \tilde{F}(\lambda; T) = \sum_{k=0}^{n} P_k(\lambda)(1 - T\lambda)^k (1 + T\lambda)^{n-k} \tag{5.48}$$

Of course, it should be checked whether the multiplied terms lead to any additional roots, i.e. to check whether $1 + T\lambda = 0$ leads to be any feasible solution. Since the analysis concerns the case of the intersection with the imaginary axis, the expression that needs to be checked becomes $1 + T \cdot j\omega = 0$. It is desired that this expression does not have any feasible roots because they would be artificial roots that are not the roots of the original characteristic equation that was considered. However, it is clear that the expression $1 + T \cdot j\omega = 0$ will never be satisfied for real values of T and ω. Thus, it can be concluded that the roots of the $F(\lambda; T)$ are the same as those of $\tilde{F}(\lambda; T)$.

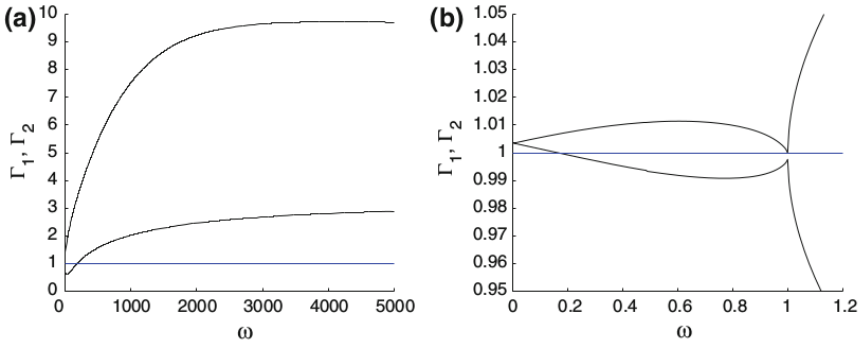

Figure 5.1: Example Frequency Sweeping Curves (zoomed-out view on the left and zoomed-in view on the right side) [9]

With the appropriate bivariate polynomial established, it remains to determine the crossings of $F(\lambda; T)$ with the imaginary axis. Since the characteristic equation has been transformed into a bivariate polynomial, it is possible to use the stability tests for multivariable polynomials. This includes finding the values that satisfy the Routh Hurwitz criterion or through the simultaneous solution of real and imaginary parts of the bivariate complex polynomial $F(j\omega; T)$ [75].

5.3.1.3 Frequency Sweeping Tests

The idea behind the frequency sweeping tests is generic and is easy to apply in several contexts. As such, the frequency sweeping tests will be encountered in several parts of this chapter. The gist of frequency sweeping is to vary the frequency and to check for a certain parameter or condition that may give insights about either delay-independent or delay-dependent stability. In the context of critical pairs and root tendency, frequency sweeping can be used to derive the critical imaginary roots as well as the asymptotic behaviour of critical pairs.

In frequency sweeping, there is neither a need to replace the exponential terms nor to eliminate them. It is usually easy to implement, but in certain situations the problem may not be solvable in a finite number of computations. Another drawback of frequency sweeping tests is that the precision of the results depends on the choice of the frequency grid. In certain situations, insufficient resolution may lead to missed detection of critical pairs.

Frequency Sweeping Curves One of the ways to detect critical imaginary roots is through the frequency sweeping curves. The construction of frequency sweeping curve(s) is as follows. The frequencies in a certain range with a certain step size are iterated over. For each frequency, the value(s) for z are determined, where z is defined as $z = e^{-j\omega\tau}$. Thereafter, the magnitude(s) of the z value(s) are obtained. These values are plotted against the values of ω at which they were obtained. Note that each z expression corresponds to one frequency sweeping plot. The critical imaginary roots are the intersections with the horizontal line $\Gamma = 1$.

This can be illustrated with the following example, shown in fig. 5.1. From these curves, three intersections with the horizontal line at one can be spotted, which are at $\omega = \{0.1638, 1, 182.6684\}$. Those are the critical imaginary roots of the analyzed system.

It can be seen that frequency sweeping can be done programmatically as well. The risk of this, however, is that an automated procedure eliminates the human's role in determining the critical imaginary roots. This means that if the steps used in the frequency sweeps are too large, that some roots may be missed.

In order to make use of the automated determination of the critical imaginary roots through programmatic frequency sweeping and avoid problems of undetected roots, the frequency sweeping curves can be generated as well, which can be later checked to verify whether all the critical imaginary roots have been determined. If the possibility of missed roots is noticed, the analysis is repeated using smaller frequency steps.

Frequency-dependent matrix pencils

Frequency-sweeping tests can also be applied to solve for frequency-dependent matrix pencils which would determine the critical imaginary roots. The following three theorems are delay-dependent results for systems with single delay, systems with commensurate delays, and systems with commensurate delays expressed as differential-difference equations (eq. (5.4)), respectively.

Theorem 5.6 (Stability dependent on delay [92]): *Suppose that the system described in eq.* (5.1) *is stable at* $\tau = 0$. *Let*

$$\operatorname{rank}\left(A_1\right) = q \tag{5.49}$$

Furthermore, define

$$\bar{\tau}_i := \begin{cases} \min_{\substack{1\le k\le n \\ \omega_k}} \frac{\theta_k^i}{\omega_k^k} & \text{if } \lambda_i\left(j\omega_k^i I - A_0, A_1\right) = e^{-j\theta_k^i} \\ & \text{for some } \omega_k^i \in (0,\infty), \theta_k^i \in [0, 2\pi] \\ \infty & \text{if } \underline{\rho}\left(j\omega I - A_0, A_1\right) > 1, \forall \omega \in (0,\infty) \end{cases} \tag{5.50}$$

Then,

$$\bar{\tau} := \min_{1\le i\le q} \bar{\tau}_i \tag{5.51}$$

That is, the system described in eq. (5.1) *is stable for all* $\tau \in [0, \bar{\tau})$ *but becomes unstable for* $\tau = \bar{\tau}$.

Theorem 5.7 ([75]): *Suppose that the system eq.* (5.2) *is stable at* $\tau = 0$, *and let* $q = \operatorname{rank}\left(A_m\right)$. *Furthermore, define*

$$\bar{\tau}_i := \begin{cases} \min_{1\le k\le n} \frac{\theta_i^i}{\omega_k^*} & \text{if } \lambda_i\left(G\left(j\omega_k^i\right), H\left(j\omega_k^i\right)\right) = e^{-j\theta_k^i} \\ & \text{for some } \omega_k^i \in (0,\infty), \theta_k^i \in [0, 2\pi] \\ \infty & \text{if } \underline{\rho}(G(j\omega), H(j\omega)) > 1, \forall \omega \in (0,\infty) \end{cases} \tag{5.52}$$

where

$$G(s) := \begin{pmatrix} 0 & I & \cdots & 0 \\ \vdots & \vdots & \ddots & \vdots \\ 0 & 0 & \cdots & I \\ -\left(sI - A_0\right) & A_1 & \cdots & A_{m-1} \end{pmatrix} \tag{5.53}$$

and

$$H(s) := \operatorname{diag}\begin{pmatrix} I & \cdots & I & -A_m \end{pmatrix} \tag{5.54}$$

Then,

$$\bar{\tau} := \min_{1\le i\le q+n(m-1)} \bar{\tau}_i \tag{5.55}$$

the system eq. (5.2) *is stable for all* $\tau \in [0, \bar{\tau})$ *but becomes unstable at* $\tau = \bar{\tau}$

Theorem 5.8 ([75]): *Suppose that the system eq.* (5.4) *is stable at* $\tau = 0$. *Define*

$$\bar{\tau}_i := \begin{cases} \min_{\substack{1\le k\le n \\ \omega_k}} \frac{\theta_k^i}{\omega_k} & \text{if } \lambda_i\left(G_a\left(j\omega_k^i\right), H_a\left(j\omega_k^i\right)\right) = e^{-j\theta_k^i} \\ \min_{1\le k\le n} \frac{\theta_k^i}{\omega_k} & \text{for some } \omega_k^i \in (0,\infty), \theta_k^i \in [0, 2\pi] \\ \infty & \text{if } \underline{\rho}\left(G_a(j\omega), H_a(j\omega)\right) > 1, \forall \omega \in (0,\infty) \end{cases} \tag{5.56}$$

where

$$G_a(s) := \begin{pmatrix} 0 & 1 & \cdots & 0 \\ \vdots & \vdots & \ddots & \vdots \\ 0 & 0 & \cdots & 1 \\ -a_0(s) & -a_1(s) & \cdots & -a_{q-1}(s) \end{pmatrix} \tag{5.57}$$

and

$$H_a(s) := \operatorname{diag}\begin{pmatrix} 1 & 1 & \cdots & a_q(s) \end{pmatrix} \tag{5.58}$$

Then,

$$\bar{\tau} := \min_{1\le i\le q} \bar{\tau}_i \tag{5.59}$$

The system eq. (5.2) *is stable for all* $\tau \in [0, \bar{\tau})$ *but becomes unstable at* $\tau = \bar{\tau}$

5.3.1.4 Constant Matrix Stability Tests

Matrix-pencil approaches emerged as a more computationally efficient alternative to several previous methods that relied on symbolic calculation to determine the time-delay margin. Besides computational efficiency, precision was also an issue for some of the methods, namely the frequency-sweeping approach, as mentioned earlier. In the case of the frequency-sweeping approach, the precision of the results is dependent on the chosen step-size of the frequency sweeps.

The main idea behind the use of matrix-pencil approach to determine the critical imaginary roots is to compute the eigenvalues and the generalized eigenvalues of constant matrices. Due to this numerical scheme, the matrix-pencil approaches are computationally efficient. Additionally, they may also be completed in a finite number of steps.

To the knowledge of the author, the analysis of constant matrices and matrix-pencils in order to determine critical imaginary pairs was first proposed by Chen et. al. [93]. The resultant constant matrices here are based off the frequency-dependent matrices discussed in the previous section of frequency sweeping approaches [94].

The method based on constant matrix stability tests is applicable to LTI systems. It allows to effectively determine the critical imaginary roots and the corresponding critical imaginary delays. It is a two step procedure. First, the generalized eigenvalues of a constant matrix pencil are computed, and then the eigenvalues of a constant matrix are computed in the second step.

Retarded TDSs To the knowledge of the author, the first attempt to use the matrix pencil approach to determine the delay margin of a linear retarded TDS was made by Chen et al. [93]. In their paper, several theorems are proposed and proven. The purpose of these theorems is to be able to compute the delay margin for two classes of models: the differential-difference equations and the differential-difference equations in state-space form.

The goal of this technique, as is the case for the other techniques discussed in section 5.3.1, is to determine the critical imaginary roots. As was encountered before, the characteristic equation of a TDS can be interpreted as a bivariate polynomial, by replacing the exponential terms with a new variable ($z = e^{-\tau\lambda}$), or with a bilinear transformation involving a new variable as was the case in section 5.3.1.2. This means that finding the zero-crossings of the characteristic bivariate polynomial, denoted by $f(s,z)$, amounts to finding the values for s and z such that $(s,z) \in \partial\mathbb{C}_+ \times \partial\mathbb{D}$.

Consider, for example, the characteristic equation eq. (5.60):

$$p\left(s, e^{-\tau s}\right) := \sum_{k=0}^{n} a_k(s) e^{-k\tau s} = 0 \tag{5.60}$$

If the expression $e^{-\tau\lambda}$ is replaced with a variable z, the following bivariate polynomial would be obtained:

$$p\left(s,z\right) := \sum_{k=0}^{n} a_k(s) z = 0 \tag{5.61}$$

If the parameter $s = j\omega$ is fixed to some value such that $\omega \in (0,\infty)$ (since it is required that $s \in \partial\mathbb{C}_+$), then the bivariate polynomial reduces to a function of a single variable z, as seen in eq. (5.62).

$$p(z) = a_0 z^n + a_1 z^{n-1} + \cdots + a_n, \quad a_0 \neq 0 \tag{5.62}$$

Now, it should be determined whether eq. (5.62) has any the solution such that $|z| = 1$, as it was established that the zero crossing corresponds to $z \in \partial\mathbb{D}$.

The Orlando Formula which relates the roots of $p(z)$ to the determinant of the Schur-Cohn matrix provides the link between the problem of determining the zero-crossings of the characteristic quasipolynomial and obtaining a constant matrix test. The following Lemma shows this relation:

Theorem 5.9 (Orlando Formula [75, 95]): *Let $z_i, i = 1, \quad \cdots, n$ be the roots of the complex polynomial $p(z) = \sum_{k=0}^{n} a_k z^k$ whose corresponding Schur-Cohn-Fujiwara matrix is denoted by H. Then,*

$$\det(H) = |a_n|^{2n} \prod_{i,j=1}^{n} \left(1 - z_i \bar{z}_j\right) \tag{5.63}$$

Since complex conjugates have the same magnitude, and it is desired to determine z such that $|z| = 1$, then $|\bar{z}| = 1$. This makes the right-hand side of eq. (5.63) equal to 0. This means that the Schur-Cohn-Fujiwara matrix H is required to be singular for determining a zero crossing, i.e. $\det(H) = 0$.

Now that it is established that $\det(H) = 0$ is the condition that needs to be ensured in order to determine the critical pairs, the next step would be to try to express the $\det(H)$ in terms of the coefficients of the polynomial $p(z)$. In order to proceed further, the definition of the Schur-Cohn-Fujiwara matrix needs to be given, which is seen in eq. (5.64).

$$H = q(S)^H q(S) - p(S)^H p(S) \tag{5.64}$$

In the equation, a number of new elements appear. The operator $(\cdot)^H$ denotes the Hermitian transpose, which means that the matrix is first transposed, then the conjugate of the entries of the transpose matrix are determined. Moreover, S in eq. (5.64) which is called the shift matrix and whose definition is shown in eq. (5.65), has nonzero entries only on the superdiagonal. It is referred to as the shift matrix because pre-multiplying by this matrix leads to the shift of the elements of the multiplicand by one entry location upwards.

$$S = \begin{bmatrix} 0 & 1 & 0 & \cdots & 0 \\ 0 & 0 & 1 & \cdots & 0 \\ 0 & \cdots & 0 & \ddots & \cdots \\ 0 & \cdots & 0 & \cdots & 1 \\ 0 & 0 & 0 & \cdots & 0 \end{bmatrix} \tag{5.65}$$

Moreover, the term q in eq. (5.64) is the "complex reverse" polynomial associated with $p(z)$ or simply the conjugate polynomial of $p(z)$, and its definition is given in eq. (5.66).

$$q(z) = z^n p(1/z) = \bar{a}_n z^n + \bar{a}_{n-1} z^{n-1} + \cdots + \bar{a}_0 \tag{5.66}$$

In principle, now it may be attempted to start expressing $\det(H)$ in terms of a_k. However, there is an important Lemma that relates the determinant of the Schur-Cohn-Fujiwara to the determinant of the Schur-Cohn matrix, which makes it worthwhile to check for the possibility of a diversion to a simpler derivation of a stability criterion. The Schur-Cohn matrix (the test matrix for the Schur-Cohn criterion) is defined in eq. (5.67)

$$\Delta := \begin{pmatrix} p^T(S) & \left(\bar{p}^T(S)\right)^H \\ \bar{p}^T(S) & \left(p^T(S)\right)^H \end{pmatrix} \tag{5.67}$$

Moreover, the relation between the determinants of the two matrices is shown in eq. (5.68).

$$\det(H) = (-1)^n \det(\Delta) \tag{5.68}$$

This relation is proven based on the Schur determinant complement which is shown in eq. (5.69) [75].

$$\det\begin{pmatrix} A & B \\ C & D \end{pmatrix} = \det(D) \det\left(A - BD^{-1}C\right) \tag{5.69}$$

The proof of the relation eq. (5.68) looks like this:

$$\begin{aligned} \det(H) &= \det\left(\bar{p}^H(S)\bar{p}(S) - p^H(S)p(S)\right) \\ &= \det\left(\bar{p}^H(S)\bar{p}(S)p^{-1}(S) - p^H(S)\right)\det(p(S)) \\ &= (-1)^n \det\left(p^H(S) - \bar{p}^H(S)p^{-1}(S)\bar{p}(S)\right)\det(p(S)) \\ &= (-1)^n \det\begin{pmatrix} p(S) & \bar{p}(S) \\ \bar{p}^H(S) & p^H(S) \end{pmatrix} \\ &= (-1)^n \det\begin{pmatrix} p^H(S) & p^H(S) \end{pmatrix}^H \\ &= (-1)^n \det\begin{pmatrix} p^T(S) & \left(\bar{p}^T(S)\right)^H \\ \bar{p}^T(S) & \left(p^T(S)\right)^H \end{pmatrix} \end{aligned} \tag{5.70}$$

Thus, now, it is instead possible to try to obtain a stability criterion based on $\det(\Delta) = 0$. Therefore, the next steps are about expressing $\det(\Delta)$ with the coefficients of $p(z)$. Based on the definition of the Schur-Cohn matrix in eq. (5.67), the terms

$p^T(S)$ and $\left(\bar{p}^T(S)\right)^H$ and $\bar{p}^T(S)$ and $\left(p^T(S)\right)^H$ need to be determined. Beginning with $p(S)$, and based on eq. (5.62), $p(S)$ will correspond to:

$$\mathrm{p(S)} = a_0\mathrm{S^n} + a_1\mathrm{S^{n-1}} + \cdots + a_\mathrm{n}\mathrm{I} \tag{5.71}$$

As explained earlier, a shift matrix leads to a shift in the entries of the matrix by an entry location upwards. That is why, if the shift matrix is raised to a certain power, let it be denoted by k, the resultant matrix corresponds to a matrix of the same size with the entries shifted upwards by k entries. It should be noted, however, that the non-zero entries may rotate depending on the value of k. Thus, the following expression for $p(S)$ is obtained.

$$p(S) = \begin{bmatrix} a_n & a_{n-1} & \cdots & a_1 \\ 0 & a_\mathrm{n} & \cdots & a_2 \\ . & . & \cdots & . \\ 0 & 0 & \cdots & a_n \end{bmatrix} \tag{5.72}$$

Note that $\left(\bar{p}^T(S)\right)^H = p(S)$. Thus,

$$p^T(S) = \begin{pmatrix} a_0 & 0 & \cdots & 0 \\ a_1 & a_0 & \cdots & 0 \\ \vdots & \vdots & \ddots & \vdots \\ a_{n-1} & a_{n-2} & \cdots & a_0 \end{pmatrix}, \quad \left(\bar{p}^T(S)\right)^H = \begin{pmatrix} a_n & a_{n-1} & \cdots & a_1 \\ 0 & a_n & \cdots & a_2 \\ \vdots & \vdots & \ddots & \vdots \\ 0 & 0 & \cdots & a_n \end{pmatrix} \tag{5.73}$$

Applying the Schur determinant complement identity (eq. (5.69)) to the Schur-Cohn matrix Δ leads to eq. (5.74).

$$\det(\Delta) = \det\begin{pmatrix} p^T(S) & \left(\bar{p}^T(S)\right)^H \\ \bar{p}^T(S) & \left(p^T(S)\right)^H \end{pmatrix} = \det\left(\left(p^T(S)\right)^H\right)\det\left(p^T(S) - \left(\bar{p}^T(S)\right)^H\left(\left(p^T(S)\right)^H\right)^{-1}\bar{p}^T(S)\right) \tag{5.74}$$

Knowing that $\left(\bar{p}^T(S)\right)^H = p(S)$ leads to the following simplifications:

$$\det(\Delta) = \det\left(\left(p^T(S)\right)^H\right)\det\left(p^T(S) - \left(\bar{p}^T(S)\right)^H\left(\left(p^T(S)\right)^H\right)^{-1}\bar{p}^T(S)\right) \tag{5.75}$$

$$= \det\left(\left(p^T(S)\right)^H\right)\det\left(p^T(S) - \left(\bar{p}^T(S)\right)^H\left(\left(p^T(S)\right)^H\right)^{-1}\bar{p}^T(S)\right) \tag{5.76}$$

Note that, $\det(\Delta)$ corresponds to a polynomial in ω. The positive real solutions of this equation are the values of ω for which a z that belongs to the unit circle may be found. As the value for ω is obtained, the corresponding values for z may be determined from solving for $p(s,z) = 0$.

Moreover, a consequence of Schur's complement for the determinant is the following Lemma.

Lemma 5.1 (Consequence of the Schur Complement Identity [75]): *For any $z \in \mathbb{C}$ and $P_k \in \mathbb{C}^{n\times n}$, $k = 0, 1, \cdots, m$*

$$\det\left(\sum_{k=0}^{m} P_k z^k\right) = \det\left\{ z\begin{pmatrix} I & & \\ & \ddots & \\ & & I \\ & & P_m \end{pmatrix} - \begin{pmatrix} 0 & I & \cdots & 0 \\ \vdots & \vdots & \ddots & \vdots \\ 0 & 0 & \cdots & I \\ -P_0 & -P_1 & \cdots & -P_{m-1} \end{pmatrix}\right\} \tag{5.77}$$

This discussion leads to the following theorem, which was derived in [93].

Theorem 5.10 ([93]):
Consider a retarded TDS described by the differential-difference equation shown in eq. (5.78),

$$y^{(n)}(t) + \sum_{i=0}^{n-1} \sum_{k=0}^{q} a_{ki} y^{(i)}(t - k\tau) = 0 \tag{5.78}$$

and whose characteristic equation is given by eq. (5.79).

$$\begin{aligned} a\left(s, e^{-hs}\right) &= \sum_{k=0}^{q} a_k(s) e^{-khs} \\ a_0(s) &= s^n + \sum_{i=0}^{n-1} a_{0i} s^i \\ a_k(s) &= \sum_{i=0}^{n-1} a_{ki} s^i, \quad k = 1, \cdots, q \end{aligned} \tag{5.79}$$

$$T_n := 0, \quad H_n := \begin{bmatrix} 0 & \cdots & 0 & 1 \\ 0 & \cdots & 1 & 0 \\ \vdots & \iddots & \iddots & \vdots \\ 1 & \cdots & 0 & 0 \end{bmatrix} \tag{5.80}$$

$$T_i := \begin{bmatrix} a_{q\prime} & a_{q-1,i} & \cdots & a_{1i} \\ 0 & a_{qi} & \cdots & a_{2i} \\ \vdots & \ddots & \ddots & \vdots \\ 0 & 0 & \cdots & a_{qi} \end{bmatrix} \tag{5.81}$$

$$H_i := \begin{bmatrix} 0 & \cdots & 0 & a_{0i} \\ 0 & \cdots & a_{0i} & a_{1i} \\ \vdots & \iddots & \iddots & \vdots \\ a_{0i} & \cdots & a_{q-2,i} & a_{q-1,i} \end{bmatrix} \tag{5.82}$$

$$P, \quad := \begin{bmatrix} (-j)^{\mathrm{i}} T_{\mathrm{i}} & (j)^i H_i \\ (-j)^i H_{\mathrm{i}}^T & (j)^{\mathrm{i}} T_{\mathrm{i}}^T \end{bmatrix} \tag{5.83}$$

$$P := \begin{bmatrix} 0 & I & \cdots & 0 \\ \vdots & \vdots & \ddots & \vdots \\ 0 & 0 & \cdots & I \\ -P_n^{-1} P_0 & -P_n^{-1} P_1 & \cdots & -P_n^{-1} P_{n-1} \end{bmatrix} \tag{5.84}$$

$$F(s) := \begin{bmatrix} 0 & 1 & \cdots & 0 \\ \vdots & \vdots & \ddots & \vdots \\ 0 & 0 & \cdots & 1 \\ -a_0(s) & -a_1(s) & \cdots & -a_{q-1}(s) \end{bmatrix} \tag{5.85}$$

$$G(s) \quad := \operatorname{diag}\begin{pmatrix} 1 & \cdots & 1 & a_q(s) \end{pmatrix} \tag{5.86}$$

$$\tau^* := \min_{1 \le k \le 2nq} \frac{\alpha_k}{\omega_k} \tag{5.87}$$

where ω_k belongs to the set of eigenvalues of the matrix P and α_k belongs to the set of eigenvalues of the matrix pencil $(F(j\omega_k), G(j\omega_k))$.

As mentioned in the introduction of this part on constant matrix stability tests, the overall procedure for the implementation of the above theorem consists of two steps. The first step is to determine the generalized eigenvalues of a constant matrix, and the second step is to determine the eigenvalues of another constant matrix. Note that, the theorem makes the assumption that the system is stable when there are no delays present. .

As for the stability results corresponding to the equivalent state-space form, it is presented in the following. Consider the state-space form shown in eq. (5.88),

$$\dot{x}(t) = A_0 x(t) + \sum_{k=1}^{q} A_k x(t - k\tau), \quad h \geq 0 \tag{5.88}$$

where $A_k \in \mathbb{R}^{n \times n}$ are real matrices and τ denotes the time-delay, the result is presented in Theorem 5.11.

Theorem 5.11 ([93]):
Let the matrices $B_k \in \mathbb{R}^{n^2}, \quad k = 0, 1, \cdots, 2q$ be defined as:

$$\begin{aligned} B_{q-k} &= I \otimes A_k^T, k = 1, \cdots, q \\ B_q &= A_0 \oplus A_0^T \\ B_{q+k} &= A_k \otimes I, k = 1, \cdots, q \end{aligned} \tag{5.89}$$

Let the matrices U and V be defined as:

$$U := \begin{bmatrix} I & & & \\ & \ddots & & \\ & & I & \\ & & & B_{2q} \end{bmatrix} \tag{5.90}$$

and

$$V := \begin{bmatrix} 0 & I & \cdots & 0 \\ \vdots & \vdots & \ddots & \vdots \\ 0 & 0 & \cdots & I \\ -B_0 & -B_1 & \cdots & -B_{2q-1} \end{bmatrix} \tag{5.91}$$

If there is not at least one generalized eigenvalue of this pair of matrices, $\sigma(U, V)$, whose magnitude is equal to 1, then the TDS is stable for all $h \in [0, \infty]$. Otherwise, the time-delay margin is given by

$$\tau^* := \min_{1 \leq k \leq 2n^2 q} \frac{\alpha_k}{\omega_k} \tag{5.92}$$

where $\alpha_k \in [0, 2\pi]$ and $e^{-j\alpha_k} \in \sigma(U, V)$ and $j\omega \in \sigma\left(\sum_{m=0}^{q} A_m e^{-jm\alpha_k}\right)$.

As can be seen from the theorem, some important operations for this approach appear, which are the Kronecker product and the Kronecker summation. The Kronecker product is the extension of the outer product, or the cross product, to matrices [74].

$$c_{\alpha\beta} = a_{ij} b_{kl} \tag{5.93}$$

where

$$\begin{aligned} \alpha &\equiv p(i-1) + k \\ \beta &\equiv q(j-1) + l \end{aligned} \tag{5.94}$$

As for the Kronecker summation, it is defined in terms of the Kronecker product:

$$\mathrm{A} \oplus \mathrm{B} = \mathrm{A} \otimes \mathrm{I}_b + \mathrm{I}_a \otimes \mathrm{B} \tag{5.95}$$

This approach was extended to compute multiple stability intervals by Niculescu et al. [96].

Neutral TDSs with Commensurate Delays This methodology was extended to the case of neutral TDSs by Fu et al. [97]. As discussed in chapter 4, the stability analysis of neutral TDS involves an additional necessary requirement for stability, which is the stability of the delay-difference operator.

As in the case of the previous discussion, two theorems were proposed in the work of Fu et al., one for the differential-difference form and one for the corresponding state-space form [97]. The reader is referred to [97] for those two theorems, as well as their proofs which are similar to the proofs of the theorems proposed by Chen et al. [93].

5.3.2 Asymptotic Behaviour of the Critical Imaginary Roots

While the methods discussed in the previous part indicate where the stability switches may occur, they do not indicate whether the switch, if at all present, is to stability or instability. Without this information, the stability regions cannot be determined.

By studying the tendencies of the critical imaginary roots, one is able to keep track of the number of unstable roots and consequently, infer the information about the presence and the type of stability switch (whether it is towards stability or towards instability). Those tendencies are referred to as the asymptotic behaviour of the critical imaginary root. The asymptotic behaviour can be studied either graphically or analytically. The advantage of the graphical approach is its simplicity; whereas, the advantage of the analytical approach is that it allows for automation.

In the next two parts, solving the problem of determining the asymptotic behaviour of the critical imaginary root using each of the the graphical and the analytical approaches will be discussed, and in this order. Note that, the asymptotic behaviour is analyzed at a specific critical pair. As there are infinitely many critical pairs, it may seem intractable to analyze the asymptotic behaviour at all critical time-delays. However, this issue was addressed when the invariance property was proven for systems with commensurate delays in [9] and later on for incommensurate delays in [11]. This property implies that the asymptotic behaviour at all critical time-delays associated with a certain critical imaginary root is the same. Therefore, it suffices to study the asymptotic behaviour of a critical imaginary root at one of the infinitely many time-delays associated with. This, along with the fact that there is a finite number of crossings with the imaginary axis, means that there are only a finite number of cases for which the asymptotic behaviour will need to be studied.

5.3.2.1 Frequency Sweeping Tests

Through frequency-sweeping tests, the sign of $|z| - 1$ close to the determined critical imaginary roots is studied. If the sign changes from negative to positive, this means that the crossing direction is from the left half-plane to the right half-plane. Conversely, when the sign changes from positive to negative, the crossing direction is into the stable left half-plane. Graphically, the former condition corresponds to the frequency sweeping curve crossing the horizontal line $\Gamma = 1$ from below. As for the latter case, the crossing is from top to bottom.

However, it should be noted that the frequency sweeping curves can show some complex features even when the case of simple critical imaginary roots is encountered [9]. This makes it difficult, in certain cases, to infer the asymptotic behaviour from the frequency sweeping test. An example case was shown by [9].

For the case of neutral TDSs, the stability of the delay-difference operator can also be examined graphically. The means to do this is to check that for very large values of ω, the frequency sweeping curve is still higher than the horizontal line $\Gamma = 1$.

5.3.2.2 Eigenvalue Pertubation-based Approach and Puiseux Series

The crossing direction of an imaginary root is defined as the sign of the change in the value of eigenvalues around the imaginary axis with respect to an increase in the time-delay. This is shown in eq. (5.96).

$$CDIR = \text{sign}\left[\frac{d\lambda}{d\tau}\right]_{\lambda=\omega_{C,i}} \tag{5.96}$$

To the knowledge of the author, Chen et al. were the first to use an eigenvalue perturbation-based approach to determine the asymptotic behaviour of the critical imaginary roots and to consequently determine the regions of stability [98].

If a critical imaginary root is simple, then the asymptotic behaviour can be studied based on the implicit function theorem from which it holds that expression for $\frac{d\lambda}{d\tau}$ can be determined with eq. (5.97).

$$\frac{d\lambda}{d\tau} = -\frac{f_\tau}{f_\lambda} \tag{5.97}$$

However, when the multiplicity of the root is larger than 1, then the implicit function theorem no longer applies. In this case, an alternative is to study the asymptotic behaviour through a series expansion of the relation between a time-delay τ and the characteristic root λ. Since the Puiseux series allows to describe the local behaviour of a power series, the asymptotic behaviour can be studied through n Puiseux series, where n is an important index that will be explained in the following paragraphs [9]. To the knowledge of the author, Chen et al. were the first to use an eigenvalue perturbation-based approach to determine the asymptotic behaviour of the critical imaginary roots and to consequently determine the regions of stability [98].

The procedure for obtaining the Puiseux series is summarized with algorithm 1, obtained from [9]. However, before proceeding with presenting the algorithm, there are two important non-negative indices that need to be discussed, the indices n and g, that are associated with a critical pair $(\lambda_a, \tau_{a,k})$. The index n is defined according to eq. (5.98).

$$f_{\lambda^0} = \cdots = f_{\lambda^{n-1}} = 0, f_{\lambda^n} \neq 0 \tag{5.98}$$

From this definition, it can be seen that the index n corresponds to the multiplicity of a critical pair. As for the index g, it is defined according to eq. (5.99).

$$f_{\tau^0} = \cdots = f_{\tau^{g-1}} = 0, f_{\tau^g} \neq 0 \tag{5.99}$$

It should be noted that both of the indices are guaranteed to be bounded if the critical imaginary root to which they are associated is not zero [9]. Moreover, one of the properties is that the index g is constant for all $\tau_{\alpha,k}$. However, the index n can possibly vary with $\tau_{\alpha,k}$.

Now that the definitions of those two important indices have been established, the algorithm for obtaining the Puiseux series of a quasipolynomial at a critical pair can be presented, and it reads as shown in algorithm 1.

Algorithm 1 Algorithm to determine the Puiseux series [9]

procedure GETPUISEUXSERIES($f(\lambda,\tau), n, g$)
  $\alpha_0 \leftarrow 0$
  $\beta_0 \leftarrow g$
  while True **do**
    $\mu \leftarrow \max\left\{\frac{\beta_0-\beta}{\alpha-\alpha_0} > 0 : L_{\alpha\beta} \neq 0, \alpha > \alpha_0, \beta < \beta_0\right\}$ ▷ Note that $L_{il} = \frac{f_{\lambda i}\tau^l}{(i+l)!}\begin{pmatrix} i+l \\ i \end{pmatrix}\begin{pmatrix} i+l \\ i \end{pmatrix}$
    if μ exists **then**
      Determine all nonzero $L_{\alpha\beta}$ such that $\frac{\beta_0-\beta}{\alpha-\alpha_0} = \mu$
      Form the set $\left\{L_{\alpha_1\beta_1}(\Delta\lambda)^{\alpha_1}(\Delta\tau)^{\beta_1}, L_{\alpha_2\beta_2}(\Delta\lambda)^{\alpha_2}(\Delta\tau)^{\beta_2}, \ldots\right\}$ such that $\alpha_1 > \alpha_2 > \ldots$
      Determine coefficients satisfying the equation $L_{\alpha_1\beta_1}C^{\alpha_1-\alpha_0} + L_{\alpha_2\beta_2}C^{\alpha_2-\alpha_0} + \cdots + L_{\alpha_0\beta_0} = 0$ ▷ denoted $\widetilde{C}_{\mu,l}$
      $\Delta\lambda \leftarrow \widetilde{C}_{\mu,l}(\Delta\tau)^\mu + o\left((\Delta\tau)^\mu\right), l = 1, \ldots, \alpha_1 - \alpha_0$
      $\alpha_0 \leftarrow \alpha_1$
      $\beta_0 \leftarrow \beta_1$
    else
      return $\Delta\lambda(\Delta\tau)$
    end if
  end while
end procedure

Once the Puiseux series $\Delta\lambda(\Delta\tau)$ are obtained, the effect of $\Delta\tau = +\epsilon$ and $\Delta\tau = -\epsilon$ on the real part of $\Delta\lambda$ can be determined. Based on this, it is possible to tell what the asymptotic behaviour is when the time-delay changes from $\tau_\alpha - \epsilon$ to $\tau_\alpha + \epsilon$.

However, in some cases which are referred to as degenerate cases, the resultant Puiseux series involves only an imaginary term. This means that the first order Puiseux series is insufficient. In order to address this issue, higher order Puiseux series need to be determined, which is done by applying algorithm 1, iteratively [9].

5.3.3 Stability Regions in the Delay Space

After having determined the critical pairs and the asymptotic behaviour associated with them, it finally remains to determine the stability regions in the delay space of the TDS. This entails monitoring the change in the number of unstable roots and keeping track of the number of unstable roots pertaining to the time-delay intervals. The change in the number of unstable roots is mathematically described in eq. (5.100) [9].

$$\Delta NU_\alpha(\beta) \triangleq NU_\alpha\left(\beta^+\right) - NU_\alpha\left(\beta^-\right) \tag{5.100}$$

The notation $\Delta NU_\alpha(\beta)$ signifies the change in the number of unstable roots that is associated with the critical pair (α, β), with α being the critical imaginary root and β being the associated critical time-delay. As shown from eq. (5.100), $\Delta NU_\alpha(\beta)$ corresponds to the change that occurs when the time-delay is increased from β^- to β^+.

Remark 5.2 (Remark on the Analytic Curve Frequency Sweeping Approach): *In principle, the analytic curve frequency sweeping approach, described in [9], is nothing more than the frequency sweeping approach used to determine the critical pairs from section 5.3.1.3 combined with the eigenvalue perturbation-based approach (and the use of series expansions) to study the asymptotic behaviour (possibly also combined with the verification of the analysis on the asymptotic behaviour through*

examining frequency sweeping curves). It has been presented in this section in such a segmented fashion in order to emphasize the three main steps of the outlined approach which are to determine the critical pairs, to study the asymptotic behaviour of a critical pair and, finally, to determine the stability regions in the delay space. Through this structure, it is possible to group all the relevant techniques that can be used to execute either of these three steps.

Another, yet unrelated, note needs to be made regarding this approach. It hosts a special feature. Specifically, as formally described in the book [9], the approach has also been augmented to solve for the complete stability problem of TDSs with commensurate delays. What is meant by complete stability is that the ultimate stability is also addressed, which is the stability of the system when the time-delay tends to infinity. The study of complete stability often is not of practical relevance as engineers often strive to minimize the occurrence of delays in control systems. Consequently, the order of magnitude of the time-delays in a system is usually known. However, in case such an analysis is needed, the aspects that need to be considered to check for ultimate stability can be reviewed from the 9^{th} chapter of the book [9].

5.3.4 Iterative Frequency Sweeping Approach

The iterative Frequency Sweeping Approach [11] is an extension of the analytic curve frequency sweeping approach [9], and it allows to the study the complete stability of a TDS with multiple incommesurate delays. The gist of the approach is to analyze the stability with respect to a delay vector, denoted by $\overrightarrow{\tau^{\#}} = \left(\tau_1^{\#}, \ldots, \tau_L^{\#}\right)$ (where the # indicates that a value is fixed), sequentially. At each step, one of the delay parameters is "freed" while the others are kept fixed. The following will explain the steps of this approach more clearly.

Consider the characteristic quasipolynomial of a TDS with incommensurate delays which is given in eq. (5.101).

$$f(\lambda, \vec{\tau}) = \det\left(\lambda I - A - \sum_{\ell=1}^{L} B_\ell e^{-\tau_\ell \lambda}\right) \tag{5.101}$$

Before proceeding with the steps of the algorithm, some notation needs to be established. For convenience, the time-delay vector $\vec{\tau}$, of length L, can be represented according to eq. (5.102),

$$\vec{\tau} = \sum_{\ell=1}^{L} \tau_\ell \delta(\ell) \tag{5.102}$$

where $\delta(\ell)$ is given by eq. (5.103).

$$\delta_i(\ell) = \begin{cases} 0, \text{ if } i \neq \ell \\ 1, \text{ if } i = \ell \end{cases} \tag{5.103}$$

This new notation is useful for the concept of freeing one time-delay component and fixing the others, which will be seen in the following.

Let the index of a time-delay component in the time-delay vector that is free be denoted by χ, i.e. $\tau_\chi (\chi \in \{1, \ldots, L\})$ is the free component in the vector, and the rest of the elements ($\ell \neq x$) are fixed. The previously introduced notation in eq. (5.102) and eq. (5.103) allows to write the delay vector as follows.

$$\vec{\tau} = \tau_\chi \delta(\chi) + F_\chi \tag{5.104}$$

where

$$F_\chi = \sum_{\ell \neq \chi} \tau_\ell^{\#} \delta(\ell) \tag{5.105}$$

With the notation clarified, it is possible to proceed to the steps of the algorithm, which are shown in algorithm 2.

Based on this algorithm, it is seen that in order to check for the stability in a region, the stability of many such delay vectors need to be checked. This is in alignment with what was mentioned before, that when the delays are incommensurate, the problem becomes very difficult to solve and is considered to have an $\mathcal{NP}$-hard computational complexity [74, 75, 99].

Algorithm 2 Algorithm to perform the iterative frequency sweeping approach [11]

procedure ITERATIVEFREQUENCYSWEEPINGAPPROACH($f(\lambda, \vec{\tau})$)
  $F_1 \leftarrow F_1 = (0, \ldots, 0)$
  for $\chi \leftarrow 1, L$ **do**
    $NU\left(F_\chi + \varepsilon\delta(\chi)\right) \leftarrow NU\left(F_\chi\right)$+ the number of values in $\mathbb{C}_+$ of the Puiseux series for all the corresponding CIRs when $\tau_\chi = 0$ with $\Delta\tau_\chi = +\varepsilon$ ▷ It is assumed that $f(\lambda, \vec{\tau})$ does not have CIRs when $\tau_\chi = 0$
    Plot the frequency sweeping curves denoted by $\Gamma_{\chi,i}(\omega), i = 1, \ldots, q_\chi$, obtained from $p\left(\lambda, \tau_\chi, F_\chi\right) = 0$
    $F_\chi \leftarrow F_{\chi-1} + \tau^{\#}_{\chi-1}\delta(\chi - 1)$
  end for
  if $f(\lambda, \vec{\tau})$ has no CIRs when $\vec{\tau} = \vec{\tau^{\#}}$ **then**
    if NU = 0 **then**
      isStableBool ← True
    else
      isStableBool ← False
    end if
    return $NU(\vec{\tau^{\#}})$, isStableBool
  else
    Plot the frequency sweeping curves, denoted by $\Gamma^{\#}_{\ell,i}(\omega), i = 1', \ldots, q_\ell, \ell = 1, \ldots, L$, pertaining to $p\left(\lambda, \tau_\ell, F^{\#}_\ell\right) = 0$ with $F^{\#}_\ell = \sum_{\kappa \neq \ell} \tau^{\#}_\kappa \delta(\kappa)$
    Analyze the asymptotic behaviour when $\vec{\tau} = \vec{\tau^{\#}}$ with respect to each delay element in the delay vector.
    return whether increasing or decreasing a delay element τ_ℓ would stabilize the system
  end if
end procedure

5.4 Concluding Remarks

To conclude, this chapter set out to present a number of techniques that can be used for the stability analysis of TDSs in the frequency domain. Of the methods for the analysis of delay-dependent stability, two main directions were identified: one that relies on discretization of either the transcendental terms or of the spectrum, and another that involves identifying the pairs of frequencies and time-delays, referred to as critical pairs, for which stability crossing occurs and studying their asymptotic behaviour. Of the two, the latter set of approaches is preferred, and in the following, it will be explained why.

In the class of spectrum computation approaches, the method relying on finite-dimensional approximation has already been denounced as a method because of the need to ensure that the determined stability regions do not enclose the actual stability regions.

With regards to the spectral discretization method, while an elegant method, it has its drawbacks. One issue is that this method is computationally intensive. A related concern is that the convergence of the numerical scheme depends on the chosen number of discretization points, and a suitable choice of this parameter is a trade-off between computational intensiveness and accuracy. However, as previously mentioned, a procedure for the determination of the discretization points has been developed by Michiels et al. which partially alleviates this concern [8].

However, the second group of methods offers the possibility for much simpler, more versatile techniques that are devoid of the possibility of this type of complications. That is why, the second group is preferred.

The methods subscribing to the preferred group involve three main steps. The first of these steps is to determine the critical pairs of the TDS. This is followed by determining the asymptotic behaviour associated with these pairs. Finally, the stability regions are established through sorting the critical time-delays and book-keeping the number of unstable roots in between the critical time-delays. For the third step, there aren't any choices to be made. As for the second step, there is no need to choose between or the other.

For the first step, four methods were discussed: the direct method, pseudo-delay techniques, frequency sweeping approaches, and constant matrix stability tests. The main limitation of the direct method is that it is only applicable to systems with single delays. As for the pseudo-delay techniques, they are more versatile, but they may be more difficult to automate due to the need to check conditions such as the presence of artificial roots as well as to ensure stability conditions based on a Routh Hurwitz table, for example. The frequency sweeping approaches are simple in comparison to the other methods, but they face the issue that a crude step size in the frequency sweeps may lead to missed roots. Finally, the constant matrix stability tests offer the advantages of computational efficiency and precision which makes them a seeming best option. However, to the knowledge of the author, such tests have not yet been derived for the case of TDSs with incommensurate delays. However,

for the frequency sweeping approach, such an extension has been derived, and in the interest of choosing a method that can be later applied to the case of TDSs with incommensurate delays, the frequency sweeping approach (and specifically the analytic curve frequency sweeping approach) is promoted as the method that will be used for the stability analysis of the TDSs in the frequency domain.

6

Lyapunov's Second Method

The Lyapunov notion of stability is a powerful one; however, classical Lyapunov theory cannot be directly applied to TDSs. There are two main extensions of Lyapunov's second method that have been developed for TDSs, which are the Lyapunov-Krasovskii (LK) and Lyapunov-Razumikhin (LR) approaches. The evolution of the stability results based on the Razumikhin and Krasovskii approaches will be delineated in this chapter, for the case of linear TDSs. Furthermore, although the interest is in delay-dependent stability, both delay-independent and delay-dependent stability will be discussed. This is because, as will be seen, the delay-independent stability results prove to be instrumental to some of the delay-dependent results.

The structure of the chapter is as follows. First, the extensions of the Lyapunov theory to the case of TDSs is presented in section 6.1. Thereafter, a number of important tools for deriving stability conditions in the time-domain, namely, model transformations and integral inequalities, are presented in section 6.2 and section 6.3, respectively. Next, several stability results based on the LR theorem are derived in section 6.4. Section 6.5 discusses stability results that are based on the LK theorem. In section 6.6, the discretized Lyapunov functional method is discussed, and some interesting stability results are presented. Finally, a number of concluding remarks are made in section 6.7.

6.1 Extensions of Lyapunov Theory for Time-delay Systems

The classical Lyapunov theory does not directly apply to TDSs because the delayed states in the TDS may violate the monotonic decrease of a Lyapunov function, which is a requirement for Lyapunov functions in the classical Lypanunov theory [100]. This shortcoming created the need to extend the classical Lyapunov theory to make it applicable to the study of the stability of TDSs in the time-domain, which is the topic of this section. Section 6.1.1 presents a number of stability definitions for TDSs, and section 6.1.2 and section 6.1.3 discuss the theoretical extensions of Lyapunov theory to TDSs.

6.1.1 Stability Definitions for the Case of Time-delay Systems

The notion of stability, for the case of a TDS, concerns how much the system trajectory deviates from a system solution. While the main interest is in studying the stability of non-trivial solutions of a TDS, through a change of variables, it is possible to transform the stability analysis to that of the trivial solution. Furthermore, in the case of linear systems, the stability of the trivial solution can be used to deduce the stability of all other solutions [22].

The definitions of stability themselves do not differ from those of non-autonomous systems without delay [75]. In the case of non-autonomous systems, there is a dependence on the initial time. That is why, the initial time is included in the definition of stability for non-autonomous systems [14]. In general, it is desirable that the stability is robust to the initial time, and this aspect of the stability concept is known as uniformity.

The trivial solution is said to be **uniformly stable** in the initial time t_0 "if $\forall\, t_0 \in \mathbb{R}$ and $\forall \epsilon < 0$ there exists some $\delta(\epsilon) > 0$ such that $\|x_{t_0}\|_C < \delta(\epsilon)$ for all $t \geq t_0$". A solution is said to be **uniformly asymptotically stable** if "it is uniformly stable and there exists $\delta_a > 0$ such that for any $\eta > 0$ there exists a $T(\delta_a, \eta)$ such that $\|x_{t_0}\|_C < \delta_a$ implies $|x(t)| < \eta$ for all $t > t_0 + T(\delta_a, \eta)$ and $t_0 \in \mathbb{R}$". Finally, a solution is said to be **globally uniformly asymptotically stable** if "δ_a can be an arbitrarily large, finite number" [22]. Those concepts of stability will be encountered in both the LK theorem and the LR theorem.

6.1.2 Lyapunov-Krasovskii Theorem

In the case of a delay-free system, the Lyapunov function expression involves the state of the system, because it is desired to see how much the state deviates from the trivial solution. In a similar fashion, for TDSs, the state should be part of the Lyapunov expression [101]. However, the difference between TDSs and systems free of delay is that the state in the case of a TDS is not

a vector at an instant t. It is instead a function taken over an interval whose width is the time-delay, i.e. over the interval [t-τ,t] [72]. That is why, the Lyapunov term involves x_t rather than x(t).

Following this intuition gives a hunch of why Krasovskii's extension of Lyapunov's second method for TDSs involves functionals. This extension is formally presented through the LK stability theorem, which reads:

Theorem 6.1 (Lyapunov-Krasovskii Stability Theorem [75]): *Suppose that the function*

$$f : \mathbb{R}_{\geq t_0} \times C\left([-\tau, 0], \mathbb{R}^n\right) \rightarrow \mathbb{R}^n \tag{6.1}$$

in eq. (6.10) *maps* $\mathbb{R}_{\geq t_0}\times$ *(bounded sets of* $C\left([-\tau,0],\mathbb{R}^n\right)$ *into bounded sets of* $\mathbb{R}^n$*, and* $u, v, w : \mathbb{R}_{\geq 0} \rightarrow \mathbb{R}_{\geq 0}$ *are continuous nondecreasing functions,* $u(s)$ *and* $v(s)$ *are positive for* $s > 0$*, and* $u(0) = v(0) = 0$.
Assume further that there exists a continuous differentiable functional

$$V : \mathbb{R} \times C\left([-\tau, 0], \mathbb{R}^n\right) \rightarrow \mathbb{R} \tag{6.2}$$

such that

$$u(\|\phi(0)\|) \leq V(t, \phi) \leq v\left(\|\phi\|_c\right) \tag{6.3}$$

and

$$\dot{V}(t, \phi) := \limsup_{\epsilon \rightarrow 0^+} \left[V\left(t + \epsilon, x_{t+\epsilon}(t, \phi)\right) - V(t, \phi) \right] \leq -w(\|\phi(0)\|) \tag{6.4}$$

Then, the trivial solution of eq. (6.10) *is uniformly stable. Moreover, if* $w(s) > 0$ *for* $s > 0$*, then it is uniformly asymptotically stable. If, in addition,* $\lim_{s \rightarrow +\infty} u(s) = +\infty$*, then it is globally uniformly asymptotically stable.*

6.1.3 Lyapunov-Razumikhin Theorem

The idea behind the LR theorem emerged as a way to avoid having to deal with functionals and to use functions instead [101]. This is done by choosing a function $V(x)$ such that $V(x) < \max_{\theta \in [-\tau, 0]} V(x(t+\theta))$. Based on the LK theorem, the functional $V(x(t+\theta))$ should not grow and should have a negative-semidefinite derivative. Based on the relation, $V(x) < \max_{\theta \in [-\tau, 0]} V(x(t+\theta))$, only that the function $V(x)$ has a negative derivative when it is equal to the functional needs to be ensured. The theorem is formally stated as follows:

Theorem 6.2 (Lyapunov-Razumikhin Stability Theorem [75]): *Suppose that the function*

$$f : \mathbb{R}_{\geq t_0} \times C\left([-\tau, 0], \mathbb{R}^n\right) \rightarrow \mathbb{R}^n \tag{6.5}$$

in eq. (6.10) *maps* $\mathbb{R}_{\geq t_0}\times$ *(bounded sets of* $C\left([-\tau,0],\mathbb{R}^n\right)$ *into bounded sets of* $\mathbb{R}^n$*, and* $u, v, w : \mathbb{R}_{\geq 0} \rightarrow \mathbb{R}_{\geq 0}$ *are continuous nondecreasing functions,* $u(s)$ *and* $v(s)$ *are positive for* $s > 0$*, and* $u(0) = v(0) = 0$.
Assume further that there exists a continuous differentiable function

$$V : \mathbb{R} \times \mathbb{R}^n \rightarrow \mathbb{R} \tag{6.6}$$

verifying

$$u(\|x\|) \leq V(t, x) \leq v(\|x\|), \quad \text{for } t \geq t_0 \text{ and } x \in \mathbb{R}^n \tag{6.7}$$

and such that the derivative of V along the solution of eq. (6.10) *satisfies*

$$\dot{V}(t, x(t)) \leq -w(\|x(t)\|) \text{ whenever } V(t+\theta, x(t+\theta)) \leq V(t, x(t)) \tag{6.8}$$

for all $\theta \in [-\tau, 0]$*. Then, the system eq.* (6.10) *is uniformly stable.*

If, moreover, $w(s) > 0$ *for* $s > 0$ *and there exists a continuous nondecreasing function* $p(s) > S$ *for* $s > 0$ *such that the condition eq.* (6.8) *is strengthened to*

$$\dot{V}(t, x(t)) \leq -w(\|x(t)\|) \text{ if } V(t+\theta, x(t+\theta)) \leq p(V(t, x(t))) \tag{6.9}$$

for all $\theta \in [-\tau, 0]$*, then the system eq.* (6.10) *is uniformly asymptotically stable. If, in addition,* $\lim_{s \rightarrow +\infty} u(s) = +\infty$ *then the system eq.* (6.10) *is globally uniformly asymptotically stable.*

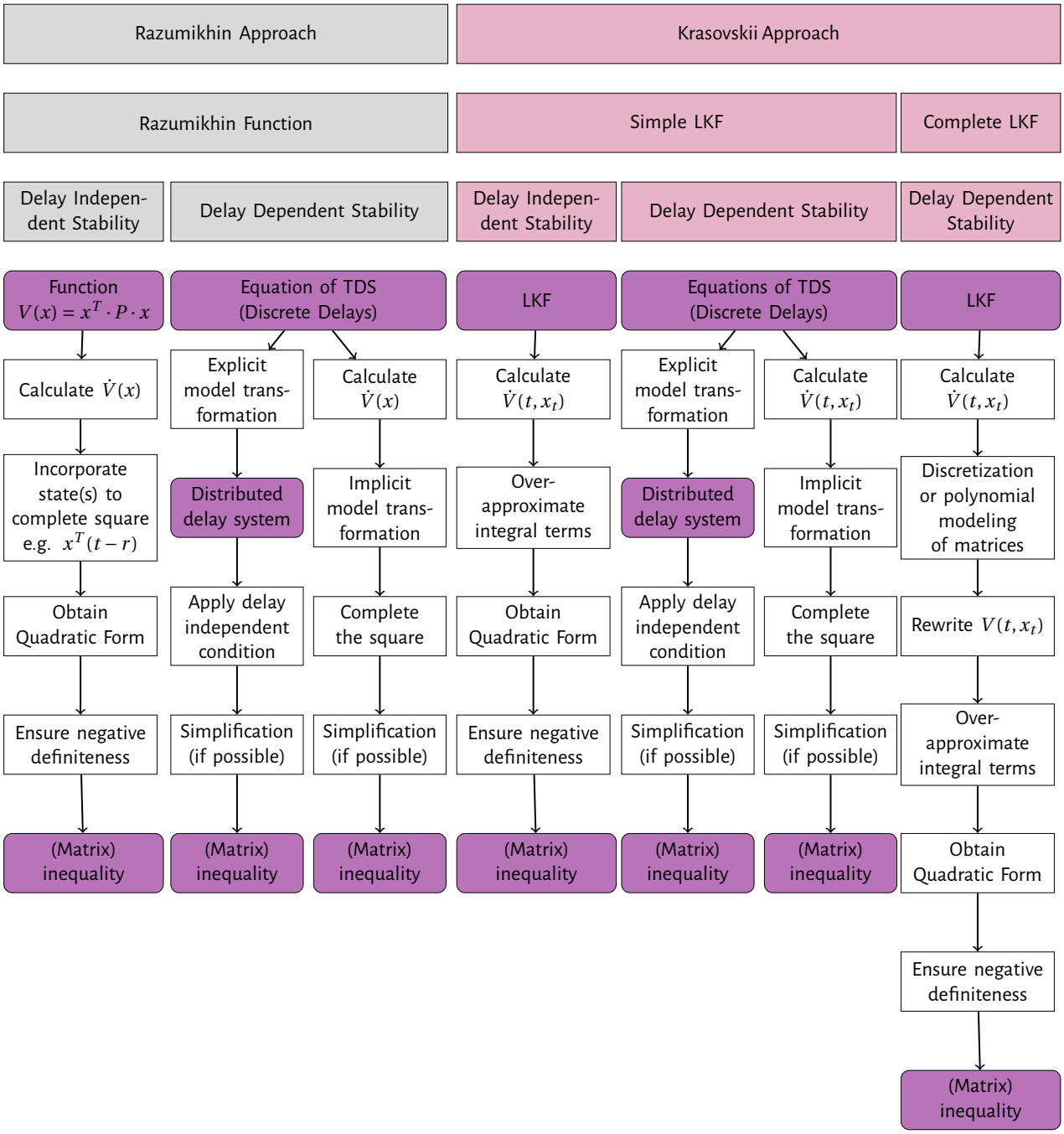

Figure 6.1: Overview of derivation steps for stability results that are based on Lyapunov's Second Method for Time-delay Systems

6.2 Model Transformations and Comparison Systems

Model transformations are an important tool in the analysis of TDSs. The transformation could turn the TDS into another type of system. The resultant model is called the comparison model (or comparison system). Usually, the comparison model is supposed to be easier to analyze, and from analyzing the stability of the comparison model, some conclusions about the stability of the original system should be deduced.

It should be mentioned that model transformations are often utilized with many analysis techniques. This includes several robust stability analysis techniques such as Linear Fractional Transformation (LFT), and Integral Quadratic Constraint (IQC). Moreover, model transformations can be combined with the general time-domain analysis approaches of TDSs, such as the LK and LR approaches [102].

One main complication that arises with the application of model transformations is that possible additional dynamics may appear. This is important because in case there are additional dynamics and the comparison model is unstable, it is not possible to make conclusions about the stability of the original system (as the instability may originate from the additional dynamics) [102].

In the following, three model transformations will be discussed: Newton-Leibniz Transformation, Parametrized Newton-Leibniz Transformation, and the Descriptor Model Transformation. For each case, the presence of additional dynamics is analyzed in [102]. This is done by examining the characteristic equation of the comparison models. Only the findings of the analysis on the additional dynamics will be presented here. For the following discussions in this section, the LTI TDS with a constant time-delay, as described in eq. (6.10), will be considered.

$$\begin{aligned} \dot{x}(t) &= A_0 x(t) + A_1 x(t-\tau) \\ x(\theta) &= \varphi(\theta), \quad \theta \in [-\tau, 0] \end{aligned} \tag{6.10}$$

6.2.1 Newton-Leibniz Transformation

The Newton-Leibniz transformation is the first model transformation to be used in the analysis of TDS [103]. As the name of the transformation suggests, the Newton-Leibniz transformation is based on the Newton-Leibniz formula, shown in eq. (6.11).

$$x(t-\tau) = x(t) - \int_{t-\tau}^{t} \dot{x}(\theta)\, d\theta \tag{6.11}$$

Substituting eq. (6.11) into eq. (6.10), produces the comparison model, shown in eq. (6.12).

$$\dot{x}(t) = \left(A_0 + A_1\right) x(t) - A_1 \int_{t-\tau}^{t} \left[A_0 x(s) + A_1 x(s-\tau)\right] ds \tag{6.12}$$

In the case of this comparison model, there are additional dynamics, which only depend on the system. Because of the additional dynamics, the stability of the original system is ensured in the cases where the eigenvalues of the matrix A_1 lie on the negative real axis. Otherwise, the comparison model does not help in making inferences about the stability of the original system [102].

6.2.2 Parametrized Newton-Leibniz Transformation

This transformatiton is a more general form of the Newton-Leibniz transformation. It introduces a free parameter $C \in \mathbb{R}^{n \times n}$, and this parameter is multiplied throughout the Newton-Leibniz formula (eq. (6.11)) which yields eq. (6.13).

$$Cx(t-\tau) = Cx(t) - C \int_{t-\tau}^{t} \dot{x}(\theta)\, d\theta \tag{6.13}$$

Applying this model transformation to the system dynamics (eq. (6.10)) leads to eq. (6.14).

$$\dot{x}(t) = (A_0 + C)x(t) + \left(A_1 - C\right) x(t-\tau) - C \int_{t-\tau}^{t} \left[A_0 x(s) + A_1 x(s-\tau)\right] ds \tag{6.14}$$

The analysis in [102] shows the characteristic equation of the system as well as its factorization into the characteristic equations corresponding to the original dynamics and to the additional dynamics. The result shows that the parameter C appears in the characteristic equation of the additional dynamics:

$$\Delta_a(s) := \det\left(I - C\frac{1 - e^{-s\tau}}{s}\right) \tag{6.15}$$

From this characteristic equation, it becomes clear that a convenient choice of the parameter C can be made to ensure that the additional dynamics are stable, which would sustain the usefulness of the comparison system for analyzing the original TDS [102].

6.2.3 Descriptor Model Transformation

The desriptor model transformation was first introduced by Fridman [104]. The main idea behind this transformation is to augment the state with the derivative of the state vector, i.e. the new state vector becomes $\left[\begin{array}{cc} x^\top(t), \dot{x}^\top(t) \end{array}\right]^\top$ [105]. For example, if this transformation is to be applied to a simple TDS such as the system in eq. (6.10), leads to the comparison system shown in eq. (6.16).

$$\begin{aligned} E\frac{d}{dt}\left[\begin{array}{c} x(t) \\ \dot{x}(t) \end{array}\right] &= \left[\begin{array}{cc} 0 & I \\ A_0 & -I \end{array}\right]\left[\begin{array}{c} x(t) \\ \dot{x}(t) \end{array}\right] + \left[\begin{array}{c} 0 \\ A_1 \end{array}\right] x(t-\tau) \\ E &= \left[\begin{array}{cc} I & 0 \\ 0 & 0 \end{array}\right] \end{aligned} \tag{6.16}$$

Briat shows that this comparison model has the same characteristic equation as that of the original system (eq. (6.10)) which means that it does not introduce any additional dynamics. However, this is at the cost of needing more complex tools for analyzing stability of the more complicated comparison model.

6.3 Integral Inequalities

Integral inequalities are an essential part of deriving stability conditions based on the LK approach. Since the LK functionals involve integrals, some integrals may remain as a part of the functional derivatives. As the expression for the derivative of the Lyapunov-functional needs to be expressed in a quadratic form in order to enforce the negative definite condition upon it, the remnant integrals need to be replaced with quadratic terms. This replacement cannot be done exactly, so, instead, integral inequalities are resorted to.

Many examples of integral inequalities exist in the literature [106–111]. Being inequalities, they inherently introduce conservatism into the analysis. Therefore, there has been an interest in trying to discover integral inequalities that are decreasingly conservative. Following the order of their proposal in the literature, some of the most known integral inequalities include Jensen's inequality, Wirtinger-based integral inequality, as well as Bessel-Legendre integral inequality [106, 107, 110].

To the knowledge of the author, the first application of an integral inequality to the derivation of stability criteria for TDSs was made by Gu [106]. The integral inequality proposed, referred to as Jensen's inequality, is shown in eq. (6.17).

Theorem 6.3 (Jensen's Inequality [106]):

$$\gamma\int_0^\gamma x^\top(u)Rx(u)du \geq \left(\int_0^\gamma x(u)du\right)^\top R\left(\int_{-\tau}^0 x(u)du\right)^\top M\left(\int_0^\gamma x(u)du\right) \tag{6.17}$$

When applied to a TDS, the bounds are changed to $[-\tau, 0]$, and the inequality is rewritten into eq. (6.18).

$$\tau\int_{-\tau}^0 x^\top(u)Rx(u)du \geq \left(\int_{-\tau}^0 x(u)du\right)^\top R\left(\int_{-\tau}^0 x(u)du\right) \tag{6.18}$$

As for the Wirtinger-based integral inequality, it was proposed by Seuret et al.[107]. As implied by the name, the integral inequality is based on Wirtinger's inequality, an inequality that has been previously used in other applications in automatic control [72]. This inequality is shown in eq. (6.19) which demonstrates how the inequality relates the integral of the derivative of a function to the integral of the function.

$$\int_{-\tau}^0 \dot{z}^\top(u)R\dot{z}(u)\mathrm{d}u \geq \frac{\pi^2}{h^2}\int_{-\tau}^0 z^\top(u)Rz(u)\mathrm{d}u \tag{6.19}$$

Theorem 6.4 (Wirtinger-based Inequality [107]):

$$\int_{-\tau}^0 x^\top(u)Rx(u)\mathrm{d}u \geq \frac{1}{\tau}\left[\begin{array}{c} \Omega_0(x) \\ \Omega_1(x) \end{array}\right]^\top \left[\begin{array}{c} R \\ \frac{\pi^2}{4}R \end{array}\right]\left[\begin{array}{c} \Omega_0(x) \\ \Omega_1(x) \end{array}\right] \tag{6.20}$$

where

$$\begin{aligned} \Omega_0(x) &= \textstyle\int_{-\tau}^0 x(u)\mathrm{d}u \\ \Omega_1(x) &= \textstyle\int_{-\tau}^0 x(u)\mathrm{d}u - \frac{2}{\tau}\int_{-\tau}^0\int_{-\tau}^u x(s)\mathrm{d}s\mathrm{d}u \end{aligned} \tag{6.21}$$

Seuret and Gouaisbaut proposed an integral inequality whose conservativeness can be made arbitrarily small, through the choice of a suitable N (see eq. (6.22)). This integral inequality is referred to as the Bessel-Legendre inequality, and it is shown in eq. (6.22) [110, 112].

Theorem 6.5 (Bessel-Legendre Inequality [110]):

$$\int_{-\tau}^{0} x(u)Rx(u)\mathrm{d}u \geq \frac{1}{\tau}\begin{bmatrix}\Omega_0\\ \vdots\\ \Omega_N\end{bmatrix}^{\top} R_N \begin{bmatrix}\Omega_0\\ \vdots\\ \Omega_N\end{bmatrix} \tag{6.22}$$

where

$$\begin{aligned} R_N &= \mathrm{diag}(R, 3R, \ldots, (2N+1)R)\\ \Omega_k &= \int_{-\tau}^{0} L_k(u)x(u)\mathrm{d}u, \text{ for all } k \in \mathbb{N}\end{aligned} \tag{6.23}$$

6.4 Lyapunov-Razumikhin Approach

According to the discussions in the literature, the LR approach often leads to more conservative results than the LK approach. However, the derivation of LR stability results is often simpler [75]. The following subsections discuss the steps of this approach.

As will be the case for the LK approach, it is important to discuss the steps of obtaining both delay-independent and delay-dependent stability criteria. This is because the delay-dependent results sometimes make use of delay-independent stability conditions derived (which happens when an explicit model transformation is applied).

6.4.1 Delay-independent Stability

The first step in the LR approach is the choice of a LR function. A commonly used function has the quadratic form $x^{\top}\cdot P\cdot x$. The corresponding expression for $\dot{V}(x)$ is given by:

$$\dot{V}(x) = 2\cdot x^{\top}\cdot P\cdot \dot{x} \tag{6.24}$$

Ultimately, the goal is to establish a quadratic form for $\dot{V}(x)$ or an upper bound on $\dot{V}(x)$ that is in a quadratic form. Then, ensuring the negative definiteness of the matrices involved ensures the negative definiteness the negative definiteness of the expression for $V(x)$ or the upper bound on $\dot{V}(x)$. This will guarantee that the Lyapunov derivative condition is satisfied.

The approach to construct the quadratic form will be more clearly explained with examples. Section 6.4.1.1 presents an example derivation for the case of a TDS with discrete delays, and section 6.4.1.2 briefly presents an example for the case of a TDS with distributed delays.

6.4.1.1 Retarded Time-delay System with Discrete Delays

Consider a TDS with a single discrete delay (eq. (6.10)). The availability of the system dynamics allows to replace the expression for $\dot{x}$ in eq. (6.24). The result of the replacement is shown in eq. (6.25).

$$\dot{V}(x(t)) = 2\cdot x^{\top}\cdot P\cdot [A_0x(t) + A_1x(t-\tau)] \tag{6.25}$$

However, eq. (6.25) does not include all the terms needed to obtain the quadratic form, so they need to be added somehow. One way to achieve this is through the following steps. Consider some constant p such that eq. (6.26) holds.

$$V(x(t+\theta)) < pV(x(t)) \text{ for all } -\tau \leq \theta \leq 0 \tag{6.26}$$

A re-arrangement of the expression and its subsequent multiplication by some positive $\alpha > 0$ leads to eq. (6.27).

$$\alpha\left(pV(x(t)) - V(x(t+\theta))\right) = \alpha\left(p\cdot x^{\top}(t)\cdot P\cdot x(t) - x^{\top}(t-\tau)\cdot P\cdot x(t-\tau)\right) > 0 \tag{6.27}$$

Being a positive expression, $\alpha\left(p\cdot x^{\top}(t)\cdot P\cdot x(t) - x^{\top}(t-\tau)\cdot P\cdot x(t-\tau)\right)$ helps establish an upper bound for $\dot{V}(x(t))$:

$$\dot{V}(x(t)) \leq \dot{V}(x(t)) + \alpha\left(p\cdot x^{\top}(t)\cdot P\cdot x(t) - x^{\top}(t-\tau)\cdot P\cdot x(t-\tau)\right) \tag{6.28}$$

The upper bound, in its more elaborate form, is shown in eq. (6.29).

$$2 \cdot x^\top \cdot P \cdot A_0 x(t) + 2 \cdot x^\top \cdot P \cdot A_1 x(t-\tau) + \alpha \left(p \cdot x^\top(t) \cdot P \cdot x(t) - x^\top(t-\tau) \cdot P \cdot x(t-\tau) \right) \tag{6.29}$$

Moreover, this expression can be written as the product of the transpose of the state vector, some matrix M, and the state vector, i.e. $\begin{bmatrix} x^\top(t) & x^\top(t-\tau) \end{bmatrix} \cdot M \cdot \begin{bmatrix} x(t) \\ x(t-\tau) \end{bmatrix}$ where

$$M = \begin{bmatrix} 2PA_0 + \alpha pP & 2PA_1 \\ 0 & -\alpha P \end{bmatrix} \tag{6.30}$$

To make the matrix M symmetric, the operation in eq. (6.31) is applied.

$$\bar{M} = \frac{M + M^\top}{2} \tag{6.31}$$

The following demonstrates an important aspect regarding matrix transposition. Consider a matrix N that is composed of sub-matrices N_1, N_2, N_3 and N_4:

$$N = \begin{bmatrix} N_1 & N_2 \\ N_3 & N_4 \end{bmatrix} \tag{6.32}$$

The transpose of matrix N is given by eq. (6.33).

$$N^\top = \begin{bmatrix} N_1^\top & N_3^\top \\ N_2^\top & N_4^\top \end{bmatrix} \tag{6.33}$$

Applying this to obtain the transpose of M shown in eq. (6.30) leads to eq. (6.34).

$$M^\top = \begin{bmatrix} \alpha pP^\top + 2A_0^\top P^\top & 0 \\ 2A_1^\top P^\top & -\alpha P^\top \end{bmatrix} \tag{6.34}$$

Since P is symmetric, $P = P^\top$. Thus, replacing eq. (6.34) in eq. (6.31) and simplifying leads to eq. (6.35).

$$\bar{M} = \begin{bmatrix} PA_0 + A_0^\top P + \alpha pP & PA_1 \\ A_1^\top P & -\alpha P \end{bmatrix} \tag{6.35}$$

To satisfy the Lyapunov derivative criterion, eq. (6.36) needs to be satisfied.

$$\begin{bmatrix} x^\top(t) & x^\top(t-\tau) \end{bmatrix} \cdot \begin{bmatrix} PA_0 + A_0^\top P + \alpha pP & PA_1 \\ A_1^\top P & -\alpha P \end{bmatrix} \cdot \begin{bmatrix} x(t) \\ x(t-\tau) \end{bmatrix} < 0 \tag{6.36}$$

Therefore, the final stability result is that the negative definiteness of $\bar{M}$ needs to be guaranteed.

$$\bar{M} = \begin{bmatrix} PA_0 + A_0^\top P + \alpha pP & PA_1 \\ A_1^\top P & -\alpha P \end{bmatrix} < 0 \tag{6.37}$$

6.4.1.2 Retarded Time-delay System with Distributed Delays

Now, consider a system with distributed time-delays such as the one shown in eq. (6.38).

$$\dot{x}(t) = A_0(t)x(t) + \int_{-r(t)}^{0} A(t,\theta)x(t+\tau(t,\theta))d\theta \tag{6.38}$$

Replacing the system dynamics into the expression for $\dot{V}(x)$ in eq. (6.24) leads to eq. (6.39).

$$\dot{V}(x(t)) = 2x^\top(t)P \left[A_0 x(t) + \int_{-\tau}^{0} A(\theta)x(t+\theta)d\theta \right] \tag{6.39}$$

The procedure that was applied in the case of the system with a discrete delay is applied again, and this finally leads to the stability result seen in eq. (6.40).

$$\begin{gathered} PA_0 + A_0^\top P + \int_{-\tau}^{0} R(\theta)\,d\theta < 0 \\ \begin{pmatrix} \alpha(\theta)P - R(\theta) & PA(\theta) \\ A^\top(\theta)P & -\alpha(\theta)P \end{pmatrix} < 0 \text{ for } 0 \le \theta \le r \end{gathered} \tag{6.40}$$

Notice that this stability result is not a single matrix inequality. It is possible to perform operations to combine the two inequalities into a single matrix inequality. However, these additional steps are omitted from the discussion, and the interested reader is referred to the book of Gu et al. for more information regarding these steps [75].

6.4.2 Delay-dependent Stability

This subsection presents two methods that lead to delay-dependent stability results that are based on the LR approach. Both methods involve a form of model transformation, which is performed either on the system dynamics or on the expression for $\dot{V}(x)$.

The first method involves transforming the original TDS with the discrete delays into a system with distributed delays. This is known as "explicit model transformation", and it is an important step because it induces the appearance of time-delays in the inequalities that emerge. The step following the transformation is to apply the delay-independent results derived for systems with distributed delays onto the transformed system. The outcome of this step is usually in quadratic form, so any further simplifications are optional. These inequalities may be matrix inequalities or equation inequalities, or a combination thereof.

As for the second method, the transformation is applied to the expression of $\dot{V}(x)$, rather than to the TDS. Namely, this transformation helps in establishing the quadratic form. It may be, however, still necessary to perform additional manipulations to obtain the needed quadratic form.

The workings of the approaches are demonstrated through their application to an example of a TDS with a discrete time-delay (eq. (6.10)). Section 6.4.2.1 presents the application of the approach that relies on the explicit model transformation, and section 6.4.2.2 presents the application of the method that uses the implicit model transformation. Moreover, the overview of the steps of those two methods is presented in fig. 6.1.

6.4.2.1 Retarded Time-delay System with Discrete Delays: Explicit Model Transformation

As mentioned, the first step is to apply an explicit model transformation to the TDS. Specifically, the Newton-Leibniz transformation (see section 6.2) will be applied here. The model transformation leads to distributed time-delays in the system dynamics, as shown in eq. (6.41).

$$\begin{aligned} \dot{x}(t) &= A_0 x(t) + A_1 x(t-\tau) \\ &= A_0 x(t) + A_1 \left[x(t) - \int_{t-\tau}^{t} \dot{x}(\theta)\,d\theta \right] \\ &= A_0 x(t) + A_1 \left[x(t) - \int_{t-\tau}^{t} \left(A_0 x(\theta) + A_1 x(\theta-\tau) \right) d\theta \right] \\ &= \left[A_0 + A_1 \right] x(t) + \int_{-\tau}^{0} \left[-A_1 A_0 x(t+\theta) - A_1 A_1 x(t-\tau+\theta) \right] d\theta \end{aligned} \tag{6.41}$$

As shown in fig. 6.1, it follows to apply the delay independent stability conditions derived for the case of system with distributed delays. Those results were obtained in the previous parts. Specifically, the conditions shown in eq. (6.40) will be applied. However, before this can be done, eq. (6.41) has to be put in the form of the system for which eq. (6.40) was derived, i.e. for the system with distributed delays $\dot{x}(t) = A_0 x(t) + \int_{-\tau}^{0} A(\theta) x(t+\theta)\,d\theta$. By comparing to the form shown in eq. (6.41), it can be seen that for the first term, a new matrix needs to be defined, $\bar{A}$, which is equal to $A_0 + A_1$. As for the integral terms, it can be seen that there are two state delays $x(t+\theta)$ and $x(t-\tau+\theta)$, whereas in the equation for which the stability condition was derived, there is only one term which is $x(t+\theta)$. To deal with this, a change of variable on the term involving $x(t-\tau+\theta)$ needs to be performed. The outcome of this step is shown in eq. (6.44). Finally, since the bounds of the integrals are not overlapping, this may written as cases. This is shown in eq. (6.45).

$$\dot{x}(t) = \left[A_0 + A_1\right] x(t) + \int_{-\tau}^{0} \left[-A_1 A_0 x(t+\theta) - A_1 A_1 x(t-\tau+\theta)\right] d\theta \tag{6.42}$$

$$= \left[A_0 + A_1\right] x(t) + \int_{-\tau}^{0} -A_1 A_0 x(t+\theta) d\theta + \int_{-\tau}^{0} -A_1 A_1 x(t \underbrace{-\tau+\theta}_{\text{Let } s=-\tau+\theta}) d\theta \tag{6.43}$$

$$= \left[A_0 + A_1\right] x(t) + \int_{-\tau}^{0} -A_1 A_0 x(t+\theta) d\theta + \int_{-2\tau}^{-\tau} -A_1 A_1 x(t+\theta) d\theta \tag{6.44}$$

$$= \begin{cases} \underbrace{\left[A_0 + A_1\right]}_{\bar{A}} x(t) + \int_{-\tau}^{0} \underbrace{-A_1 A_0}_{\bar{A}(\theta)} x(t+\theta) d\theta & \theta \in [-\tau, 0] \\ \underbrace{\left[A_0 + A_1\right]}_{\bar{A}} x(t) + \int_{-2\tau}^{-\tau} \underbrace{-A_1 A_1}_{\bar{A}(\theta)} x(t+\theta) d\theta & \theta \in [-2\tau, -\tau) \end{cases} \tag{6.45}$$

This result is summarized with the notation in eq. (6.46).

$$\begin{cases} \bar{A}_0 = A_0 + A_1 \\ \bar{A}(\theta) = -A_1 A_0, \theta \in [-\tau, 0] \\ \bar{A}(\theta) = -A_1 A_1, \theta \in [-2\tau, -\tau) \end{cases} \tag{6.46}$$

Finally, after applying eq. (6.40) to the system eq. (6.45) leads to the stability result shown in eq. (6.47).

$$\begin{gathered} P\left(A_0 + A_1\right) + \left(A_0 + A_1\right)^\top P + \tau\left(R_0 + R_1\right) < 0 \\ \begin{pmatrix} \alpha_k P - R_k & -P A_1 A_k \\ -A_k^\top A_1^\top P & -\alpha_k P \end{pmatrix} < 0, k = 0, 1 \end{gathered} \tag{6.47}$$

6.4.2.2 Retarded Time-delay System with Discrete Delays: Implicit Model Transformation

As previously mentioned, the first step in this method, after having determined the time derivative of the Razumikhin function $\dot{V}(x)$ (see eq. (6.25)), is to apply the implicit model transformation. For that, consider matrices X, Y, and Z such that $X^\top = X, Y, Z^\top = Z$ and $\begin{pmatrix} X & Y \\ Y^\top & Z \end{pmatrix} > 0$. Since the matrix is positive definite, then by definition, the quadratic form involving the matrix is positive. Furthermore, the integral of that expression is expected to be positive as well:

$$\int_{-\tau}^{0} \begin{pmatrix} x^\top(t) & \frac{d}{d\theta} x^\top(t+\theta) \end{pmatrix} \begin{pmatrix} X & Y \\ Y^\top & Z \end{pmatrix} \begin{pmatrix} x(t) \\ \frac{d}{d\theta} x(t+\theta) \end{pmatrix} d\theta \ > 0 \tag{6.48}$$

Being positive, adding eq. (6.48) (which is the implicit transformation referred to here) to the expression for $\dot{V}(x)$ leads to an upper bound on $\dot{V}(x)$.

$$\begin{aligned} \dot{V}(x) =& 2x^\top(t) P \left[A_0 x(t) + A_1 x(t-\tau)\right] \\ \leq& 2x^\top(t) P \left[A_0 x(t) + A_1 x(t-\tau)\right] \\ &+ \int_{-\tau}^{0} \begin{pmatrix} x^\top(t) & \frac{d}{d\theta} x^\top(t+\theta) \end{pmatrix} \\ &\begin{pmatrix} X & Y \\ Y^\top & Z \end{pmatrix} \begin{pmatrix} x(t) \\ \frac{d}{d\theta} x(t+\theta) \end{pmatrix} d\theta \end{aligned} \tag{6.49}$$

If the matrix multiplication inside the integral in eq. (6.49), i.e. eq. (6.48), is expanded, this leads to:

$$\begin{aligned} &\int_{-\tau}^{0} \begin{pmatrix} x^\top(t) & \frac{d}{d\theta} x^\top(t+\theta) \end{pmatrix} \begin{pmatrix} X & Y \\ Y^\top & Z \end{pmatrix} \begin{pmatrix} x(t) \\ \frac{d}{d\theta} x(t+\theta) \end{pmatrix} \\ &= \int_{-\tau}^{0} \left(\underbrace{x^\top(t) X x(t)}_{\text{Term 1}} + \underbrace{x^\top(t) \cdot Y \cdot \frac{d}{d\theta} x(t+\theta)}_{\text{Term 2}} + \underbrace{\frac{d}{d\theta} x^\top(t+\theta) \cdot Y^\top \cdot x(t)}_{\text{Term 3}} + \underbrace{\frac{d}{d\theta} x^\top(t+\theta) \cdot Z \cdot \frac{d}{d\theta} x(t+\theta)}_{\text{Term 4}} \right) d\theta \end{aligned} \tag{6.50}$$

From eq. (6.50), it can be seen that term 1 may be directly pulled out of the integral, as the integral is with respect to θ, and the term itself is only a function of t.

$$\int_{-\tau}^{0} x^\top(t) X x(t) d\theta = x^\top(t) X x(t) \cdot (0 - (-\tau)) = r \cdot x^\top(t) X x(t) \tag{6.51}$$

As for term 2, using Leibniz' rule for differentiation under the integral sign, it is possible to evaluate the integral of term 2 with respect to θ.

$$\begin{aligned}
&\int_{-\tau}^{0} x^\top(t) \cdot Y \cdot \frac{d}{d\theta} x(t+\theta) d\theta \\
&= x^\top(t) \cdot Y \cdot \int_{-\tau}^{0} \frac{d}{d\theta} x(t+\theta) d\theta \\
&= x^\top(t) \cdot Y \cdot \Big(x(t+\theta)\Big)\Big|_{-\tau}^{0} \\
&= x^\top(t) \cdot Y \cdot \Big(x(t) - x(t-\tau)\Big) \\
&= x^\top(t) \cdot Y \cdot x(t) - x^\top(t) \cdot Y \cdot x(t-\tau)
\end{aligned} \tag{6.52}$$

Similarly, for term 3, this leads to:

$$\begin{aligned}
&\int_{-\tau}^{0} \frac{d}{d\theta} x^\top(t+\theta) \cdot Y^\top \cdot x(t) \\
&= \Big(x^\top(t) - x^\top(t-\tau)\Big) \cdot Y^\top \cdot x(t) \\
&= x^\top(t) \cdot Y^\top \cdot x(t) - x^\top(t-\tau) \cdot Y^\top \cdot x(t)
\end{aligned} \tag{6.53}$$

As for term 4, it will not be possible to take it out of the integral. However, the chain rule can be applied to the expression for $\frac{d}{d\theta} x(t+\theta)$, and this leads to eq. (6.54).

$$\begin{aligned}
\frac{d}{d\theta} x(\underbrace{t+\theta}_{\text{Let } U = t+\theta}) &= \frac{d}{dU} x(U) \cdot \frac{d}{d\theta} U \\
&= \frac{d}{dU} x(U) \\
&= A_0 x(U) + A_1 \cdot x(U-\tau) \\
&= A_0 x(t+\theta) + A_1 \cdot x(t+\theta-\tau)
\end{aligned} \tag{6.54}$$

Incorporating this result into the expression for term 4 leads to eq. (6.56).

$$\begin{aligned}
&\int_{-\tau}^{0} \frac{d}{d\theta} x^\top(t+\theta) \cdot Z \cdot \frac{d}{d\theta} x(t+\theta) d\theta \\
&= \int_{-\tau}^{0} [A_0 x(t+\theta) + A_1 \cdot x(t+\theta-\tau)]^\top \cdot Z \cdot [A_0 x(t+\theta) + A_1 \cdot x(t+\theta-\tau)] d\theta \\
&= \int_{-\tau}^{0} [x^\top(t+\theta) \cdot A_0^\top + x^\top(t+\theta-\tau) \cdot A_1^\top] \cdot Z \cdot [A_0 x(t+\theta) + A_1 \cdot x(t+\theta-\tau)] d\theta \\
&= \int_{-\tau}^{0} \Big(x^\top(t+\theta) \cdot A_0^\top Z A_0 \cdot x(t+\theta) + x^\top(t+\theta) \cdot A_0^\top Z A_1 \cdot x(t+\theta-\tau) + x^\top(t+\theta-\tau) \cdot A_1^\top Z A_0 \cdot x(t+\theta) + x^\top(t+\theta-\tau) \cdot A_1^\top Z A_1 \cdot x(t+\theta-\tau)\Big) d\theta \qquad (6.55) \\
&= \int_{-\tau}^{0} [x^\top(t+\theta) x^\top(t+\theta-\tau)] \begin{pmatrix} A_0^\top Z A_0 & A_0^\top Z A_1 \\ A_1^\top Z A_0 & A_1^\top Z A_1 \end{pmatrix} \begin{pmatrix} x(t+\theta) \\ x(t+\theta-\tau) \end{pmatrix} d\theta \qquad (6.56)
\end{aligned}$$

Define the vector $x_{tr}(\theta)$:

$$x_{tr}(\theta) = \begin{pmatrix} x(t+\theta) \\ x(t+\theta-\tau) \end{pmatrix} \tag{6.57}$$

Thus, $x_{tr}(0)$ is

$$x_{tr}(0) = \begin{pmatrix} x(t) \\ x(t-\tau) \end{pmatrix} \tag{6.58}$$

Thus, the expression for term 4 can be simplified into eq. (6.59).

$$\int_{-\tau}^{0} x_{tr}^{\top}(\theta)\begin{pmatrix} A_0^{\top}ZA_0 & A_0^{\top}ZA_1 \\ A_1^{\top}ZA_0 & A_1^{\top}ZA_1 \end{pmatrix} x_{tr}(\theta)d\theta \tag{6.59}$$

So far, the upper bound for the $\dot{V}(x)$ is given by

$$\begin{aligned} &2x^{\top}(t)PA_0x(t) + 2x^{\top}(t)PA_1x(t-\tau) + r\cdot x^{\top}(t)\cdot X\cdot x(t) + x^{\top}(t)\cdot Y\cdot x(t) - x^{\top}(t)\cdot Y\cdot x(t-\tau) + x^{\top}(t)\cdot Y^{\top}\cdot x(t) - x^{\top}(t-\tau)\cdot Y^{\top}\cdot x(t) \\ &+\int_{-\tau}^{0} x_{tr}^{\top}(\theta)\begin{pmatrix} A_0^{\top}ZA_0 & A_0^{\top}ZA_1 \\ A_1^{\top}ZA_0 & A_1^{\top}ZA_1 \end{pmatrix} x_{tr}(\theta)d\theta \\ &= x_{tr}^{\top}(0)\cdot\begin{pmatrix} 2PA_0 + Y + Y^{\top} + rX & 2PA_1 - Y \\ -Y^{\top} & 0 \end{pmatrix}\cdot x_{tr}(0) + \int_{-\tau}^{0} x_{tr}^{\top}(\theta)\begin{pmatrix} A_0^{\top}ZA_0 & A_0^{\top}ZA_1 \\ A_1^{\top}ZA_0 & A_1^{\top}ZA_1 \end{pmatrix} x_{tr}(\theta)d\theta \end{aligned} \tag{6.60}$$

For computational purposes, it is often desirable that the matrices occurring in eq. (6.60) are symmetric. The second matrix of eq. (6.60) is clearly symmetric, so only the symmetric version of the first matrix occurring in eq. (6.60) needs to be obtained. This is done using eq. (6.30) and eq. (6.31):

$$\begin{aligned} &\frac{1}{2}\cdot\left(\begin{pmatrix} 2PA_0 + Y + Y^{\top} + rX & 2PA_1 - Y \\ -Y^{\top} & 0 \end{pmatrix} + \begin{pmatrix} 2A_0^{\top}P^{\top} + Y + Y^{\top} + rX^{\top} & -Y \\ 2A_1^{\top}P^{\top} - Y^{\top} & 0 \end{pmatrix}\right) \\ &= \begin{pmatrix} A_0^{\top}P + PA_0 + Y + Y^{\top} + rX & PA_1 - Y \\ -Y^{\top} + A_1^{\top}P & 0 \end{pmatrix} \end{aligned} \tag{6.61}$$

Thus, the expression for the upper bound of $\dot{V}(x)$ becomes

$$x_{tr}^{\top}(0)\cdot\begin{pmatrix} A_0^{\top}P + PA_0 + Y + Y^{\top} + rX & PA_1 - Y \\ -Y^{\top} + A_1^{\top}P & 0 \end{pmatrix}\cdot x_{tr}(0) + \int_{-\tau}^{0} x_{tr}^{\top}(\theta)\begin{pmatrix} A_0^{\top}ZA_0 & A_0^{\top}ZA_1 \\ A_1^{\top}ZA_0 & A_1^{\top}ZA_1 \end{pmatrix} x_{tr}(\theta)d\theta \tag{6.62}$$

From eq. (6.62), it can be seen that there is a zero in the fourth entry of the first matrix. The presence of the diagonal terms needs to be ensured in order to guarantee that the problem with the matrix inequality is not ill-posed.

This is done by making use of the LR equation. That is, it can be assumed that for some $p > 1$, eq. (6.63) holds.

$$V(x(t+\theta)) < pV(x(t)) \text{ for all } -2\tau \le \theta \le 0 \tag{6.63}$$

Thus, for some positive α (which is to be determined in the final stability criterion),

$$\alpha\left[px^{\top}(t)Px(t) - x^{\top}(t-\tau)Px(t-\tau)\right] > 0 \tag{6.64}$$

So overall, eq. (6.63) can be added.

$$\begin{aligned} &\alpha\left[px^{\top}(t)Px(t) - x^{\top}(t-\tau)Px(t-\tau)\right] \\ &+\alpha_0\int_{-\tau}^{0}\left[px^{\top}(t)Px(t) - x^{\top}(t+\theta)Px(t+\theta)\right]d\theta \\ &+\alpha_1\int_{-\tau}^{0}\left[px^{\top}(t)Px(t) - x^{\top}(t+\theta-\tau)Px(t+\theta-\tau)\right]d\theta \ge 0 \\ &\quad \text{for } \alpha \ge 0, \alpha_0 \ge 0, \alpha_1 \ge 0 \end{aligned} \tag{6.65}$$

Again, some terms can be pulled out from the integrals in eq. (6.65), and this leads to the additive term eq. (6.66).

$$\begin{aligned} &\left[\alpha + (\alpha_0 + \alpha_1)r\right]px^{\top}(t)Px(t) - \alpha x^{\top}(t-\tau)Px(t-\tau) \\ &+\alpha_0\int_{-\tau}^{0}\left[-x^{\top}(t+\theta)Px(t+\theta)\right]d\theta \\ &+\alpha_1\int_{-\tau}^{0}\left[-x^{\top}(t+\theta-\tau)Px(t+\theta-\tau)\right]d\theta \ge 0 \\ &\quad \text{for } \alpha \ge 0, \alpha_0 \ge 0, \alpha_1 \ge 0 \end{aligned} \tag{6.66}$$

Adding eq. (6.66) to eq. (6.62) leads to the final results shown in eq. (6.67),

$$\begin{pmatrix} \Delta + \left(\alpha + \alpha_0 r + \alpha_1 r\right) P & PA_1 - Y \\ \left(PA_1 - Y\right)^\top & -\alpha P \end{pmatrix} < 0$$
$$\begin{pmatrix} A_0^\top Z A_0 - \alpha_0 P & A_0^\top Z A_1 \\ A_1^\top Z A_0 & A_1^\top Z A_1 - \alpha_1 P \end{pmatrix} < 0 \tag{6.67}$$

where

$$\Delta = PA_0 + A_0^\top P + rX + Y + Y^\top \tag{6.68}$$

6.5 Lyapunov-Krasovskii Approach

The first step is to select a suitable LK functional. For asymptotic stability, this functional is required to satisfy two conditions which are the Lyapunov positive functional criterion and the Lyapunov derivative condition.

In the literature that appeared earlier on, Lyapunov functionals that were sufficient but not necessary for stability were proposed. These are now known as simple LK functionals. Sufficiency of a stability condition means that if that condition is satisfied, stability is guaranteed. However, if one knows that the stability is satisfied, then that does not mean that the aforementioned condition is satisfied. This means that the stability conditions obtained from using the simple LK functionals are conservative.

In order to address the conservativeness that arises because of this class of functionals, new LK functionals were constructed based on prescribed desired derivatives. The resultant functionals are known as complete LK functionals. They provide sufficient and necessary condition for stability of the TDS. This means that, provided there is a tractable way to solve for parameters of the complete LK functional, the exact analytical solution for the stability intervals of a system can be obtained using this functional.

Thus, ultimately, the relation between the simple and the complete functionals is that the simple functionals are specific and simplified cases of the complete LK functionals. The "incompleteness" of the simple LK functionals leads to conservativeness.

As mentioned, the main drawback of the complete LK functionals is that they are very difficult to determine the parameters of the functionals that would satisfy the Lyapunov derivative condition. As a solution to this problem, a discretization technique was introduced. This discretization technique involves modeling the parameters of the complete LK functionals. They can be modeled as piecewise linear functions, or as sum-of-squares polynomials. Recently, there has been other polynomial used as a basis such as the Legendre polynomials.

First, the stability results based on the simple LK functionals will be discussed. Then, the complete LK functionals as well as the discretization method will be discussed.

6.5.1 Simple Lyapunov-Krasovskii Functional: Delay-independent Stability

As mentioned in the introduction of this section, simple LK functionals lead to conservative stability results. However, they preceded the complete Lyapunov functionals, and as mentioned, solving for the parameters of the LK functional can be a lot easier for the case of simple LK functionals. That is why, the derivation of delay-independent stability results based on simple LK will be presented in this subsection.

6.5.1.1 Retarded Time-delay System with Discrete Delays

Following the steps outlined in fig. 6.1, first, a LK functional is proposed. For the retarded type system with discrete delays eq. (6.10), the functional in eq. (6.69) is proposed.

$$V\left(x_t\right) = x^\top(t) P x(t) + \int_{t-\tau}^{t} x^\top(\theta) S x(\theta) d\theta \tag{6.69}$$

Taking the derivative of this functional and while making use of the fundamental theorem of calculus leads to the result shown in eq. (6.70).

$$\begin{aligned}
\dot{V}(x_t) &= 2\cdot x^\top(t)P\dot{x}(t) + \frac{d}{dt}\int_{t-\tau}^{t} x^\top(\theta)Sx(\theta)d\theta \\
&= 2\cdot x^\top(t)PA_0x(t) + 2\cdot x^\top(t)PA_1x(t-\tau)] + x^\top(t)Sx(t) - x^\top(t-\tau)Sx(t-\tau) \\
&= \begin{pmatrix} x^\top(t) & x^\top(t-\tau) \end{pmatrix}\begin{pmatrix} 2PA_0+S & 2PA_1 \\ 0 & -S \end{pmatrix}\begin{pmatrix} x(t) \\ x(t-\tau) \end{pmatrix} \\
&= \begin{pmatrix} x^\top(t) & x^\top(t-\tau) \end{pmatrix}\begin{pmatrix} A_0^\top P + PA_0 + S & PA_1 \\ A_1^\top P & -S \end{pmatrix}\begin{pmatrix} x(t) \\ x(t-\tau) \end{pmatrix}
\end{aligned} \tag{6.70}$$

As was done in the derivation of some of the previous stability results, the last step in eq. (6.70) was to make the matrix symmetric. In order to ensure stability, this matrix needs to be negative definite. Thus, the stability condition reduces to eq. (6.71).

$$\begin{pmatrix} PA_0 + A_0^\top P + S & PA_1 \\ A_1^\top P & -S \end{pmatrix} < 0 \tag{6.71}$$

It is seen that the matrix inequality does not depend on the time-delay. Hence, it is a delay-independent condition. Moreover, as for the procedure steps, it is seen in the derivation that there were no remaining integrals in the derivative eq. (6.70), and there was no need for an integral inequality.

6.5.1.2 Retarded Time-delay System with Distributed Delays

For a system with distributed delays, a simple functional of a similar structure to that of eq. (6.69) is proposed, which is the one shown in eq. (6.72).

$$V(x_t) = x_t^\top(0)Px_t(0) + \int_{-\tau}^{0}\left[\int_{\theta}^{0} x_t^\top(\theta)S(\theta)x_t(\theta)d\theta\right]d\theta \tag{6.72}$$

The derivative of eq. (6.72) is obtained in eq. (6.73). Similar to what was done before, here again, Leibniz' integral rule, which allows to interchange the order of differentiation and integration, i.e. $\frac{d}{dx}\int_a^b f(x,t)dt = \int_a^b \frac{\partial}{\partial x}f(x,t)dt$, is used. Next, the fundamental theorem of calculus, which states that if $F(x) = \int_a^x f(t)dt$ then $F'(x) = f(x)$, may also be used.

$$\begin{aligned}
V(x_t) &= 2x_t^\top(0)P\dot{x}_t(0) + \frac{d}{dt}\int_{-\tau}^{0}\left[\int_{\theta}^{0} x_t^\top(\theta)S(\theta)x_t(\theta)d\theta\right]d\theta \\
&= 2x_t^\top(0)P\dot{x}_t(0) + \int_{-\tau}^{0}\frac{d}{dt}\left[\int_{\theta}^{0} x_t^\top(\theta)S(\theta)x_t(\theta)d\theta\right]d\theta \\
&= 2x_t^\top(0)P\dot{x}_t(0) + \int_{-\tau}^{0}\left[x_t^\top(0)S(\theta)x_t(0)\right] - \left[x_t^\top(\theta)S(\theta)x_t(\theta)\right]d\theta \\
&= 2x_t^\top(0)P\left[A_0x_t(0) + \int_{-\tau}^{0}A(\theta)x_t(\theta)d\theta\right] + \int_{-\tau}^{0}x_t^\top(0)S(\theta)x_t(0)d\theta - \int_{-\tau}^{0}x_t^\top(\theta)S(\theta)x_t(\theta)d\theta \\
&= 2x_t^\top(0)PA_0x_t(0) + 2x_t^\top(0)P\int_{-\tau}^{0}A(\theta)x_t(\theta)d\theta + x_t^\top(0)\left[\int_{-\tau}^{0}S(\theta)d\theta\right]x_t(0) - \int_{-\tau}^{0}x_t^\top(\theta)S(\theta)x_t(\theta)d\theta \\
&= x_t^\top(0)\left[PA_0 + A_0^\top P\int_{-\tau}^{0}S(\theta)d\theta\right]x_t(0) + 2x_t^\top(0)P\int_{-\tau}^{0}A(\theta)x_t(\theta)d\theta - \int_{-\tau}^{0}x_t^\top(\theta)S(\theta)x_t(\theta)d\theta \\
&= x_t^\top(0)\left[PA_0 + A_0^\top P\int_{-\tau}^{0}S(\theta)d\theta\right]x_t(0) + \int_{-\tau}^{0}\left(2x_t^\top(0)PA(\theta)x_t(\theta) - x_t^\top(\theta)S(\theta)x_t(\theta)\right)d\theta \\
&= x_t^\top(0)\underbrace{\left[PA_0 + A_0^\top P\int_{-\tau}^{0}S(\theta)d\theta\right]}x_t(0) + \int_{-\tau}^{0}\begin{pmatrix} x_t^\top(0) & x_t^\top(\theta) \end{pmatrix}\underbrace{\begin{pmatrix} S(\theta)-R(\theta) & PA(\theta) \\ A^\top(\theta)P & -S(\theta) \end{pmatrix}}\begin{pmatrix} x_t(0) \\ x_t(\theta) \end{pmatrix}d\theta
\end{aligned} \tag{6.73}$$

Thus, in order to ensure that eq. (6.73) is negative, the negative-definiteness of the terms indicated with the underbrace in eq. (6.73) needs to be ensured. These resultant conditions are shown in eq. (6.74).

$$\begin{gathered} PA_0 + A_0^\top P + \int_{-\tau}^{0} R(\theta)d\theta < 0 \\ \begin{pmatrix} S(\theta) - R(\theta) & PA(\theta) \\ A^\top(\theta)P & -S(\theta) \end{pmatrix} < 0, \quad \theta \in [-\tau, 0] \end{gathered} \tag{6.74}$$

6.5.2 Simple LKF: Delay-dependent Stability

Analogous to the discussion in section 6.4.2, there are two pipelines for obtaining delay-dependent stability results based on the LR approach. The first one relies on an explicit transformation; whereas, the second one relies on an implicit transformation.

6.5.2.1 Retarded Time-delay System with Discrete Delays: Explicit Model Transformation

Applying the Leibniz Newton model transformation to the TDS with the discrete delays then applying the delay-independent stability results for the case of distributed time-delays in eq. (6.74) leads to the stability condition in eq. (6.75).

The stability results is shown in eq. (6.75)

$$\begin{gathered} \left[P\left(A_0 + A_1\right) + \left(A_0 + A_1\right)^\top P\right] + r\left(R_0 + R_1\right) < 0 \\ \begin{pmatrix} S_k - R_k & -PA_1A_k \\ -A_k^\top A_1^\top P & -S_k \end{pmatrix} < 0, k = 0, 1 \end{gathered} \tag{6.75}$$

6.5.2.2 Retarded Time-delay System with Discrete Delays: Implicit Model Transformation

The starting point for the analysis is the functional in eq. (6.76).

$$V(x_t) = x_t^\top(0)Px_t(0) + \int_{-\tau}^{0}\int_{\theta}^{0} f^\top\left(x_{t\theta}\right)Zf\left(x_{t\theta}\right)d\theta d\theta + \int_{-\tau}^{0} x_t^\top(\theta)Sx_t(\theta)d\theta \tag{6.76}$$

The next step is to calculate the derivative of the functional $\dot{V}(x_t)$.

$$\begin{aligned} \dot{V}(x_t) &= 2x_t^\top(0)P\dot{x}_t(0) + \frac{d}{dt}\int_{-\tau}^{0}\int_{\theta}^{0} f^\top\left(x_{t\theta}\right)Zf\left(x_{t\theta}\right)d\theta d\theta + \frac{d}{dt}\int_{-\tau}^{0} x_t^\top(\theta)Sx_t(\theta)d\theta \\ &= 2x_t^\top(0)P\dot{x}_t(0) + \int_{-\tau}^{0}\frac{d}{dt}\int_{\theta}^{0} f^\top\left(x_{t\theta}\right)Zf\left(x_{t\theta}\right)d\theta d\theta + \frac{d}{dt}\int_{-\tau}^{0} x_t^\top(\theta)Sx_t(\theta)d\theta \\ &= 2x_t^\top(0)PA_0x_t(0) + 2x_t^\top(0)P\int_{-\tau}^{0} A(\theta)x_t(\theta)d\theta + \int_{-\tau}^{0}\left[f^\top(x_t)Zf(x_t) - f^\top\left(x_{t\theta}\right)Zf\left(x_{t\theta}\right)\right]d\theta + x_t^\top(0)Sx_t(0) - x_t^\top(-\tau)Sx_t(-\tau) \end{aligned} \tag{6.77}$$

The final stability result is

$$\begin{pmatrix} \hat{N} & PA_1 - Y & -A_0^\top Y^\top \\ A_1^\top P - Y^\top & -S & -A_1^\top Y^\top \\ -YA_0 & -YA_1 & -\frac{1}{r}X \end{pmatrix} < 0 \tag{6.78}$$

where

$$\hat{N} = PA_0 + A_0P + S + rX + Y + Y^\top \tag{6.79}$$

6.5.3 Complete Lyapunov-Krasovskii Functional

The complete type LK functionals were first introduced by Kharitonov and Zhabko [113]. They pointed out that up until that point the functionals that had been proposed in the literature only admitted a lower cubic bound, instead of a quadratic lower bound. This shortcoming makes them inadequate for TDSs with uncertainty. This is because for a robust analysis, the derivative of the Lyapunov functionals should depend on the past and present states, when in the case of the functionals that have preceded their work, the derivatives only dependend on the present states [114].

However, for exponential stability, it is important to have a lower quadratic bound, according to the following theorem, as taken from Kharitonov's book [115].

Theorem 6.6 ([115]): *A TDS is exponentially stable if there exists a functional which is a piece-wise continuous, which is formally written as:*

$$v : PC\left([-\tau, 0], R^n\right) \rightarrow R \tag{6.80}$$

This functional is supposed to satisfy the following two conditions. The first one is that for some α_1 and α_2

$$\alpha_1 \|\varphi(0)\|^2 \leq v(\varphi) \leq \alpha_2 \|\varphi\|_\tau^2, \quad \varphi \in PC\left([-\tau, 0], R^n\right) \tag{6.81}$$

Moreover, the second condition is that for some $\beta > 0$, the following inequality is satisfied along the trajectories of the system.

$$\frac{\mathrm{d}}{\mathrm{d}t} v\left(x_t\right) \leq -\beta \|x(t)\|^2, \quad t \geq 0 \tag{6.82}$$

Therefore, they introduced functionals that admit upper and lower quadratic bounds, which are termed functionals of the complete type. Furthermore, a criterion that guarantees exponential stability means that it is one that minimizes conservatism. This means that the stability criteria based on the Complete LK functionals are necessary and sufficient for stability [116, 117].

The starting point to constructing complete LK functionals is the prescribed derivative of the functional. While the derivation of these functionals is beyond the scope of this research, being familiar with some results of the complete Lyapunov functionals in important. Therefore, in the following, some results of derived complete Lyapunov functionals are presented. Moreover, as the main focus in this thesis will be on the discrete delays, only the complete functionals pertaining to such systems will be presented.

Time-delay Systems of Retarded Type The derivation of quadratic LK functional of the complete type for a retarded TDS is detailed in [114], and the resultant complete LK functional is the following:

$$\begin{aligned} V\left(x_t\right) =& x^\top(t) P x(t) + 2x^\top(t) \int_{-\tau}^{0} Q(\theta) x_t(\theta) \mathrm{d}\theta \\ &+ \int_{-\tau}^{0} \int_{-\tau}^{0} x_t^\top\left(\theta_1\right) T\left(\theta_1, \theta_2\right) x_t\left(\theta_2\right) \mathrm{d}\theta_1 \mathrm{d}\theta_2 \\ &+ \int_{-\tau}^{0} x_t^\top(\theta) S(\theta) x_t(\theta) \mathrm{d}\theta \end{aligned}$$

It should be noted that the functional eq. (6.83) is also applicable to systems with multiple delays as discussed in Proposition 7.4 on page 236 of the book [75]. However, in this case, the matrices will have discontinuities when θ_1 and θ_2 are equal to $-\tau_i, i = 1, 2, \ldots, K-1$. However, the equivalent complete quadratic Lyapunov functional for the case of retarded TDS with multiple delays, shown in eq. (6.83), circumvents having to deal with these discontinuities [75].

$$\begin{aligned} V\left(x_t\right) =& x_t^T(0) P x_t(0) + 2 \sum_{i=1}^{K} x_t^T(0) \int_{-\tau_i}^{0} Q^i(\theta) x_t(\theta) d\theta \\ &+ \sum_{i=1}^{K} \int_{-\tau_i}^{0} x_t^T(\theta) S^i(\theta) x_t(\theta) d\theta \\ &+ \sum_{i=1}^{K} \sum_{j=1}^{K} \int_{-\tau_i}^{0} \left[\int_{-\tau_j}^{0} x_t^T(\theta) R^{ij}(\theta, \eta) x_t(\eta) d\eta \right] d\theta \end{aligned} \tag{6.83}$$

Neutral Type with Single Delay As for the case of a neutral TDS, the complete Lyapunov functional which was proposed by Xu-guang et al. [118], and the result is shown in the following.

$$
\begin{aligned}
V\left(x_t\right) = &\left[x(t) - Cx\left(t-\tau\right)\right]^\top \cdot P \cdot \left[x(t) - Cx\left(t-\tau\right)\right] + 2 \cdot \left[x(t) - Cx\left(t-\tau\right)\right]^\top \int_{-\tau}^{0} Q(\theta) x_t(\theta) \mathrm{d}\theta \\
&+ \int_{-\tau}^{0} \int_{-\tau}^{0} x_t^\top\left(\theta_1\right) T\left(\theta_1, \theta_2\right) x_t\left(\theta_2\right) \mathrm{d}\theta_1 \mathrm{d}\theta_2 \\
&+ \int_{-\tau}^{0} x_t^\top(\theta) S(\theta) x_t(\theta) \mathrm{d}\theta \\
&+ \int_{-\tau}^{0} \dot{x}_t^\top(\theta) S(\theta) \dot{x}_t(\theta) \mathrm{d}\theta
\end{aligned} \tag{6.84}
$$

6.6 Discretized Lyapunov Functional Method

As mentioned earlier, solving for the parameters of the complete LK functional can be an intractable problem for systems with a high dimension, and a method that was developed to deal with this problem is the discretized Lyapunov functional method. The main idea behind the discretized Lyapunov functional method is to discretize the parameters that need to be determined. The discretization allows to write the Lyapunov functional as well as its derivative in the form of a matrix inequalities. This reformulation is often easier to solve than the original problem. For example, in the case of linear discretization, the resultant stability results are in the form of linear matrix inequalities which allows to leverage the bounty of available numerical algorithms that solve for linear matrix inequalities.

In the following parts, the steps of the discretized Lyapunov functional method will be explained, and some stability results based on implementing this method are presented thereafter.

The first step of this method is to discretize the matrices of the functional that is being used. The discretization of the matrices of the Lyapunov functionals can take different forms. This includes piecewise-linear discretization, polynomial discretization, as well as discretization based on special basis functions such as the Legendre basis [73, 110, 119–121]. The former two discretization techniques have been used with the complete Lyapunov functionals as the initial intention was to determine the matrices of the complete Lyapunov functionals.

However, the increased interest in effective methods for discretization gave leeway to using the discretization technique to reduce the complexity and conservatism (based on a suitable discretization technique), which was not the initial intention of the discretized Lyapunov functional method. This meant that the discretization could be used to reduce the complete Lyapunov functionals to simple Lyapunov functionals which could still lead to matrix inequalities whose solution tends to the analytical results. This was demonstrated by Seuret and Gouaisbaut [110].

The step after that is to rewrite the Lyapunov functional, replacing the integrals with summations, which is due to the discretization that was made. Thereafter, a number of manipulations may need to be performed in order to put the functional in an appropriate form in order to enforce the positive definiteness condition. That is followed by the usual procedure to obtain the expression for the derivative of the functional. A combination of a number of manipulations to put the derivative expression in quadratic form and imposing the negative definiteness condition on the expression of $\dot{V}$ leads to the stability results in the form of matrix inequalities.

As an example, the piecewise-linear discretization will be presented. The delay segment is divided into N equal parts. This means that the square formed by $[-\tau, 0] \times [-\tau, 0]$ is divided into $N \times N$ smaller squares. In the case of the squares, they are further sub-divided into two triangles. Moreover, the matrices are assumed to be linear within a segment or within a traingular region. Thus, this discretization of matrices Q, S, and R is mathematically described as shown in eq. (6.85) and eq. (6.86).

$$
\begin{aligned}
Q\left(\theta_p + \alpha h\right) &= Q^{(p)}(\alpha) = (1-\alpha) Q_p + \alpha Q_{p-1} \\
S\left(\theta_p + \alpha h\right) &= S^{(p)}(\alpha) = (1-\alpha) S_p + \alpha S_{p-1}
\end{aligned} \tag{6.85}
$$

$$
\begin{aligned}
&R\left(\theta_p + \alpha h, \theta_q + \beta h\right) \\
=&R^{(pq)}(\alpha, \beta) \\
=&\begin{cases} (1-\alpha) R_{pq} + \beta R_{p-1,q-1} + (\alpha - \beta) R_{p-1,q}, & \alpha \geq \beta \\ (1-\beta) R_{pq} + \alpha R_{p-1,q-1} + (\beta - \alpha) R_{p,q-1}, & \alpha < \beta \end{cases}
\end{aligned} \tag{6.86}
$$

For an elaboration on the other steps of the procedure using this discretization scheme, the reader is referred to [75, 121].

Several such matrix inequalities based on the discretized Lyapunov functional method have been derived in the literature [105, 121–123]. However, recently there has been a set of matrix inequalities that are particularly efficient in comparison to other stability results in this category. The derivation of those results is based on the Bessel-Legendre inequality (see Theorem 6.5) as well as the use of Legendre polynomials (see Definition 6.1) as basis for the discretization [110, 112].

Definition 6.1 (Legendre Polynomial [110]): *The Legendre polynomials considered over the interval* $[-\tau, 0]$ *are defined by:*

$$\forall k \in \mathbb{N}, \quad L_k(u) = (-1)^k \sum_{l=0}^{k} p_l^k \left(\frac{u+\tau}{\tau}\right)^l \tag{6.87}$$

with $p_l^k = (-1)^l \binom{k}{l} \binom{k+l}{l}$.

In the following, a review of the steps to derive the stability results obtained in [110] are presented. The starting point for the derivation is the LK functional which is a complete LK Functional for a retarded TDS, shown in eq. (6.88), where P is a symmetric and positive-definite matrix. As for Q, S, and T, they are differentiable matrices. This functional was first proposed by Kharitonov and Zhabko [113].

$$V\left(x_t\right) = x^\top(t)Px(t) + 2x^\top(t)\int_{-\tau}^{0} Q(\theta)x_t(\theta)\mathrm{d}\theta + \int_{-\tau}^{0}\int_{-\tau}^{0} x_t\left(\theta_1\right) T\left(\theta_1,\theta_2\right) x_t\left(\theta_2\right)\mathrm{d}\theta_1\mathrm{d}\theta_2 + \int_{-\tau}^{0} x_t^\top(\theta)S(\theta)x_t(\theta)\mathrm{d}\theta \tag{6.88}$$

The matrices Q and T are discretized with the Legendre basis, as seen in eq. (6.89).

$$Q(\theta) = \sum_{i=0}^{N} Q_i L_i(\theta), \quad T(\theta, s) = \sum_{i=0}^{N}\sum_{j=0}^{N} L_i(\theta)L_j(s)T_{ij} \tag{6.89}$$

As for matrix S, it is assumed to be piecewise linear and is discretized linearly, as seen in eq. (6.90).

$$S(\theta) = S + (\tau + \theta)R \tag{6.90}$$

These discretization steps lead to a new form of the LK functional seen in eq. (6.91).

$$V_N\left(x_t\right) = \tilde{x}_N^\top(t)P_N\tilde{x}_N(t) + \int_{t-\tau}^{t} x^\top(s)(S + (\tau - t + s)R)x(s)\mathrm{d}s \tag{6.91}$$

where

$$P_N = \begin{bmatrix} P & Q_0 & \dots & Q_N \\ Q_0^\top & T_{00} & \dots & T_{0N} \\ \vdots & \vdots & & \vdots \\ Q_N^\top & T_{N0} & \dots & T_{NN} \end{bmatrix} \tag{6.92}$$

and

$$\tilde{x}_N(t) = \begin{bmatrix} x_t(0) \\ \int_{-\tau}^{0} L_0(s)x_t(s)\mathrm{d}s \\ \vdots \\ \int_{-\tau}^{0} L_N(s)x_t(s)\mathrm{d}s \end{bmatrix}, \quad N \geq 0 \tag{6.93}$$

Expanding the right-most term in eq. (6.91) leads to eq. (6.94).

$$\begin{aligned} V_N\left(x_t\right) &= \tilde{x}_N^\top(t)P_N\tilde{x}_N(t) + \int_{t-\tau}^{t} x^\top(s)(S + (\tau - t + s)R)x(s)\mathrm{d}s \\ &= \tilde{x}_N^\top(t)P_N\tilde{x}_N(t) + \int_{t-\tau}^{t} x^\top(s)Sx(s)\mathrm{d}s + \int_{t-\tau}^{t} (\tau - t + s)x^\top(s)Rx(s)\mathrm{d}s \end{aligned} \tag{6.94}$$

The positive definiteness of this functional needs to be guaranteed. To do that, the matrices P_N, S, and R can be constrained to be positive definite. However, it is better to try to combine the terms involved to reduce the conservativeness, and the opportunity to use the Bessel-Legendre inequality to do that presents itself. The Bessel-Lengendre inequality, obtained from [110], dictates that eq. (6.95) holds.

$$\int_{-\tau}^{0} x^\top(s)Sx(s)\mathrm{d}s \geq \frac{1}{\tau}\begin{bmatrix} \int_{-\tau}^{0} L_0(s)x(s)\mathrm{d}s \\ \vdots \\ \int_{-\tau}^{0} L_N(s)x(s)\mathrm{d}s \end{bmatrix}^\top \mathrm{diag}(S, 3S, \dots, (2N+1)S) \begin{bmatrix} \int_{-\tau}^{0} L_0(s)x(s)\mathrm{d}s \\ \vdots \\ \int_{-\tau}^{0} L_N(s)x(s)\mathrm{d}s \end{bmatrix} \tag{6.95}$$

Moreover, if the vectors involved in the inequality with $x_t(0)$ are augmented, eq. (6.96) is obtained.

$$\int_{-\tau}^{0} x^\top(s)Sx(s)\mathrm{d}s \geq \frac{1}{\tau}\begin{bmatrix} x_t(0) \\ \int_{-\tau}^{0} L_0(s)x(s)\mathrm{d}s \\ \vdots \\ \int_{-\tau}^{0} L_N(s)x(s)\mathrm{d}s \end{bmatrix}^\top \mathrm{diag}(0,S,3S,\ldots,(2N+1)S)\begin{bmatrix} x_t(0) \\ \int_{-\tau}^{0} L_0(s)x(s)\mathrm{d}s \\ \vdots \\ \int_{-\tau}^{0} L_N(s)x(s)\mathrm{d}s \end{bmatrix} \tag{6.96}$$

Thus,

$$\int_{-\tau}^{0} x^\top(s)Sx(s)\mathrm{d}s \geq \frac{1}{\tau}\tilde{x}_N^\top(t)\,\mathrm{diag}(0,S,3S,\ldots,(2N+1)S)\tilde{x}_N(t) \tag{6.97}$$

However, in the expression for $V_N\left(x_t\right)$, there are different integral bounds, namely the integral is $\int_{t-\tau}^{t} x^\top(s)Sx(s)\mathrm{d}s$ rather than $\int_{-\tau}^{0} x^\top(s)Sx(s)\mathrm{d}s$. This can be resolved through a change of variables. Let $q = s - t$. The differential obtained from this transformation is $dq = ds$, and the lower and upper bounds are now $t-\tau$ and t, respectively. Thus, $\int_{-\tau}^{0} x^\top(s)Sx(s)\mathrm{d}s = \int_{t-\tau}^{t} x^\top(s)Sx(s)\mathrm{d}s$. Taking that into account, and applying the resultant inequality to eq. (6.94) allows to obtain a lower bound on $V_N\left(x_t\right)$ which is shown in eq. (6.98),

$$V_N\left(x_t\right) \geq \tilde{x}_N^\top(t)\Phi_N^+(\tau)\tilde{x}_N(t) + \int_{t-\tau}^{t}(\tau - t + s)x^\top(s)Rx(s)\mathrm{d}s \tag{6.98}$$

where

$$\Phi_N^+(\tau) := P_N + \frac{1}{\tau}\,\mathrm{diag}(0,S,3S,\ldots,(2N+1)S) \tag{6.99}$$

Based on eq. (6.98) and eq. (6.99), in order to ensure the positive definiteness of the expression for $V_N\left(x_t\right)$ as a whole, matrices $\Phi_N^+(\tau)$, R, and S are required to be positive definite.

The next step is to obtain the expression for the derivative of the Lyapunov functionals, i.e. $\dot{V}_N\left(x_t\right)$. In doing so, Leibniz' rule for differentiation under the integral sign is used, i.e. $\frac{d}{dx}\left(\int_{a(x)}^{b(x)} f(x,t)dt\right) = f(x,b(x))\cdot\frac{d}{dx}b(x) - f(x,a(x))\cdot\frac{d}{dx}a(x) + \int_{a(x)}^{b(x)}\frac{\partial}{\partial x}f(x,t)dt$ in order to evaluate $\frac{d}{dt}\left(\int_{t-\tau}^{t}\underbrace{x^\top(s)[S+(\tau-t+s)R]x(s)}_{f(t,s)}ds\right)$:

$$\begin{aligned}
&\frac{d}{dt}\left(\int_{t-\tau}^{t}\underbrace{x^\top(s)[S+(\tau-t+s)R]x(s)}_{f(t,s)}ds\right)\\
&= f(t,t)\frac{d}{dt}(t) - f(t,t-\tau)\frac{d}{dt}(t-\tau) + + \int_{t-\tau}^{t}\frac{d}{dt}f(t,s)ds\\
&= x^\top(t)[S+(\tau-t+t)R]x(t)\cdot 1 - x^\top(t-\tau)[S+(\tau-t+t-\tau)R]x(t-\tau)\cdot 1\\
&+ \int_{t-\tau}^{t}\frac{\partial}{\partial t}\left[x^\top(s)Sx(s) + x^\top(s)(\tau-t+s)Rx(s)\right]ds\\
&= x^\top(t)[S+(\tau-t+t)R]x(t) - x^\top(t-\tau)[S+(\tau-t+t-\tau)R]x(t-\tau)\\
&+ \int_{t-\tau}^{t}(-1)x^\top(s)Rx(s)ds\\
&= x_t^\top(0)(S+\tau R)x_t(0) - x_t^\top(-\tau)Sx_t(-\tau) + \int_{\theta=-\tau}^{\theta=0}(-1)\cdot x_t^T(\theta)Rx_t(\theta)d\theta
\end{aligned} \tag{6.100}$$

This leads to eq. (6.101).

$$\begin{aligned}
\dot{V}_N\left(x_t\right) &= 2\tilde{x}_N^\top(t)P_N\dot{\tilde{x}}_N(t) + x^\top(t)(S+(\tau-t+t)R)x(t) - x^\top(t-\tau)(S+(\tau-t+t-\tau)R)x(t-\tau) - \int_{-\tau}^{0}x_t^\top(s)Rx_t(s)\mathrm{d}s\\
&= 2\tilde{x}_N^\top(t)P_N\dot{\tilde{x}}_N(t) + x^\top(t)(S+\tau R)x(t) - x^\top(t-\tau)Sx(t-\tau) - \int_{-\tau}^{0}x^\top(t+s)Rx(t+s)\mathrm{d}s
\end{aligned} \tag{6.101}$$

Recalling the Shimanov notation $x_t(\theta) \triangleq x(t+\theta)$, the expression for $\dot{V}_N\left(x_t\right)$ is rewritten as:

$$\dot{V}_N\left(x_t\right) = 2\tilde{x}_N^\top(t)P_N\dot{\tilde{x}}_N(t) + x_t^\top(0)(S+\tau R)x_t(0) - x_t^\top(-\tau)Sx_t(-\tau) - \int_{-\tau}^{0} x_t^\top(s)Rx_t(s)\mathrm{d}s \tag{6.102}$$

As in the cases before, here again, ultimately, the goal is to be able to get to a quadratic form for $\dot{V}_N\left(x_t\right)$ or for an upper bound of $\dot{V}_N\left(x_t\right)$, in order to enforce negative definiteness on the resultant matrix in the vector version of the quadratic form.

So, if the expression for the augmented state $\tilde{x}_N(t)$, from eq. (6.93), is replaced in eq. (6.102).

$$\dot{V}_N\left(x_t\right) = 2\begin{bmatrix} x_t(0) \\ \int_{-\tau}^{0} L_0(s)x_t(s)\mathrm{d}s \\ \vdots \\ \int_{-\tau}^{0} L_N(s)x_t(s)\mathrm{d}s \end{bmatrix}^\top P_N \begin{bmatrix} \dot{x}_t(0) \\ \int_{-\tau}^{0} L_0(s)\dot{x}_t(s)\mathrm{d}s \\ \vdots \\ \int_{-\tau}^{0} L_N(s)\dot{x}_t(s)\mathrm{d}s \end{bmatrix} + x_t^\top(0)(S+\tau R)x_t(0) - x_t^\top(-\tau)Sx_t(-\tau) - \int_{-\tau}^{0} x_t^\top(s)Rx_t(s)\mathrm{d}s \tag{6.103}$$

It is desired that this expression is in written in quadratic form or is compared to a expression (which is greater than $\dot{V}_N\left(x_t\right)$) that is in quadratic form. In order to do so, it becomes clear that the derivative expressions need to be replaced. Moreover, a state that includes the elements of $\tilde{x}_N(t)$ as well as $x_t(-\tau)$. For that, the vector $\tilde{x}_N(t)$ is augmented with $x_t(-\tau)$ is needed. This new state vector is denoted by $\theta_N(t)$ and is shown in eq. (6.104).

$$\theta_N(t) = \begin{bmatrix} x_t(0) \\ x_t(-\tau) \\ \frac{1}{\tau}\int_{-\tau}^{0} L_0(s)x_t(s)\mathrm{d}s \\ \vdots \\ \frac{1}{\tau}\int_{-\tau}^{0} L_N(s)x_t(s)\mathrm{d}s \end{bmatrix}, \quad N \geq 0 \tag{6.104}$$

With regards to replacing the derivative terms in eq. (6.103), first, $\dot{x}_t(0)$ is considered:

$$\dot{x}_t(0) = A_0x_t(0) + A_1x_t(-\tau) \tag{6.105}$$

As for the terms $\int_{-\tau}^{0} L_k(s)\dot{x}_t(s)\mathrm{d}s$, integration by parts leads to:

$$\int_{-\tau}^{0} L_k(s)\dot{x}_t(s)\mathrm{d}s = L_k(s)\dot{x}_t(s)\Big|_{-\tau}^{0} - \int_{-\tau}^{0} \dot{L}_k(s)x_t(s)\mathrm{d}s \tag{6.106}$$

However, from the properties of Legendre polynomials is that:

$$\frac{\mathrm{d}}{\mathrm{d}u}L_k(u) = \sum_{i=0}^{k-1}\frac{(2i+1)}{\tau}\left(1-(-1)^{k+i}\right)L_i(u) \text{ if } k \geq 1 \tag{6.107}$$

Thus,

$$\int_{-\tau}^{0} L_k(s)\dot{x}_t(s)\mathrm{d}s = x_t(0) - (-1)^k x_t(-\tau) - \sum_{i=0}^{k-1}\gamma_{Nk}^i\int_{-\tau}^{0} L_i(u)x(u)\mathrm{d}u = \Gamma_N(k)\theta_N(t) \tag{6.108}$$

Applying this to the terms of $\dot{\tilde{x}}_N(t)$ results in the relation eq. (6.109) between $\dot{\tilde{x}}_N(t)$ and $\theta_N(t)$:

$$\dot{\tilde{x}}_N(t) = H_N(\tau)\theta_N(t) \tag{6.109}$$

where

$$H_N = \begin{bmatrix} F_N^\top & \Gamma_N^\top(0) & \Gamma_N^\top(1) & \cdots & \Gamma_N^\top(N) \end{bmatrix}^\top \tag{6.110}$$

As for the relation between $\tilde{x}_N(t)$ and $\theta_N(t)$, it is described by:

$$\tilde{x}_N(t) = G_N(\tau)\theta_N(t) \tag{6.111}$$

where

$$G_N(\tau) = \begin{bmatrix} I_n & 0_n & 0_{n,n(N+1)} \\ 0_{n(N+1),n} & 0_{n(N+1),n} & \tau I_{n(N+1)} \end{bmatrix} \tag{6.112}$$

At this stage, the first three terms of eq. (6.103) can be combined altogether:

$$\theta_N^\top(t)\Phi_{N0}(\tau)\theta_N(t) \tag{6.113}$$

where

$$\Phi_{N0}(\tau) = \mathrm{He}\left(G_N^\top(\tau)P_N H_N\right) + \mathrm{diag}\left\{S + hR, -S, 0_{(N+1)n}\right\} \tag{6.114}$$

and the operator He is used for obtaining a symmetric version of a matrix. For example, the effect of applying the operator on a matrix A can be seen in eq. (6.115).

$$\mathrm{He}(A) = A_0 + A^\top \tag{6.115}$$

Based on the Bessel-Legendre inequality, and the definition of $\theta_N(t)$, eq. (6.116) holds.

$$-\int_{-\tau}^{0} x_t^\top(s)Rx_t(s)\mathrm{d}s \leq -\frac{1}{\tau}\theta_N^\top(t)\,\mathrm{diag}\left(0,0,R_N\right)\theta_N(t) \tag{6.116}$$

Lastly, based on the distributive property of matrix multiplication, eq. (6.117) is obtained.

$$\dot{V}_N\left(x_t\right) \leq \theta_N^\top(t)\left(\Phi_{N0}(\tau) - \frac{1}{\tau}\,\mathrm{diag}\left(0,0,R_N\right)\right)\theta_N(t) \tag{6.117}$$

Therefore, the negative definiteness of $\dot{V}_N\left(x_t\right)$ is ensured when eq. (6.118) is satisfied.

$$\Phi_N^-(\tau) = \Phi_{N0}(\tau) - \frac{1}{\tau}\,\mathrm{diag}\left(0,0,R_N\right) < 0 \tag{6.118}$$

This concludes the review of the derivation, and those stability results are summarized in the following theorem.

Theorem 6.7 ([110]): *For a given integer $N \geq 1$ and a constant a delay τ, assume that there exist a matrix $P_N \in \mathbb{S}_{(N+1)n}$ and two matrices $S, R \in \mathbb{S}_n^+$ such that the following LMIs are satisfied*

$$\Phi_N^+(\tau) := P_N + \frac{1}{\tau}\,\mathrm{diag}(0, S, 3S, \ldots, (2N+1)S) > 0$$

and

$$\Phi_N^-(\tau) = \Phi_{N0}(\tau) - \frac{1}{\tau}\,\mathrm{diag}\left(0,0,R_N\right) < 0$$

Moreover, a similar stability result (derived in [112]) is shown in Theorem 6.8.

Theorem 6.8 ([112]): *For a given N and a constant delay τ, assume that there exist a matrix $P_N \in \mathbb{S}_{(N+1)n}$ and two matrices*

$S, R \in \mathbb{S}_n^+$ such that

$$\Theta_N(\tau) = \begin{cases} P_N \succ 0, & \text{if } N = 0 \\ P_N + \frac{1}{\tau} \begin{bmatrix} 0 & & & \\ & S & & \\ & & \ddots & \\ & & & (2N-1)S \end{bmatrix} \succ 0, & \text{if } N > 0 \end{cases}$$

$$\Phi_N(\tau) = \Phi_{N0}(\tau) - \begin{bmatrix} \Gamma_N(0) \\ \vdots \\ \Gamma_N(N) \end{bmatrix}^\top \begin{bmatrix} R & & & \\ & 3R & & \\ & & \ddots & \\ & & & (2N+1)R \end{bmatrix} \begin{bmatrix} \Gamma_N(0) \\ \vdots \\ \Gamma_N(N) \end{bmatrix} \prec 0 \tag{6.119}$$

$$\Phi_{N0}(\tau) = \mathrm{He}\left(G_N^\top(\tau) P_N H_N\right) + \tilde{S}_N + (\tau)^2 F_N^\top R F_N$$

$$\tilde{S}_N = \mathrm{diag}\{S, -S, 0_{Nn}\}$$

$$S_N = \mathrm{diag}\{S, 3S, \ldots, (2N+1)S\}$$

$$F_N = \begin{bmatrix} A_0 & A_1 & 0_{n,nN} \end{bmatrix}$$

$$G_N(\tau) = \begin{bmatrix} I_n & 0_n & 0_{n,nN} \\ 0_{nN,n} & 0_{nN,n} & \tau I_{nN} \end{bmatrix}$$

$$H_N = \left[F_N^\top \Gamma_N^\top(0)\, \Gamma_N^\top(1) \ldots \Gamma_N^\top(N-1)\right]^\top$$

where $\Gamma_N(k)$ for all $k = 0, \ldots, N$ are defined as follows:

$$\Gamma_N(k) = \begin{cases} [I \; -I], & \text{if} \quad N = 0 \\ I\,(-1)^{k+1} I\, \gamma_{Nk}^0 I \ldots \gamma_{Nk}^{N-1} I\Big], & \text{if} \quad N > 0 \end{cases}$$

$$\gamma_{Nk}^i = \begin{cases} -(2i+1)\left(1 - (-1)^{k+i}\right), & \text{if } i \le k \\ 0, & \text{if } i > k \end{cases} \tag{6.120}$$

The stability intervals of the retarded TDS with a single delay (eq. (6.10)) are the values of time-delay for which eq. (6.119) is satisfied.

6.7 Concluding Remarks

There are many stability results that have been proposed in the literature for the stability analysis of TDSs in the time domain. However, since it is desired to have time-domain stability results that would corroborate the results obtained from the frequency domain analysis (which are exact results), the set of candidate stability results is narrowed down to the results that are based off the discretized Lyapunov functional method. The reason for this is that, for increasing N, the solutions of these matrix inequalities tend to the exact results.

Interesting stability results were developed in [110], and a review of the steps to derive these results has been presented in the earlier section. As they rely on the discretization of the Lyapunov functional and an effective integral inequality, the stability result that emerged is able to obtain the analytical results efficiently. As a consequence, it is this stability result that will be used for the stability analysis of retarded TDSs with a single delays in the time-domain. Note, that with regards to stability results for neutral-type TDS, as for the case of retarded TDS, there have been several (though noticeably fewer) results that have been derived in the literature that are based on the discretized Lyapunov functional method. To mention a few, the reader is referred to the work of Han et al. [124–126], the results of Fridman [105], as well as those of Li et al. [127].

However, due to the efficiency of the stability results based on the Bessel Legendre inequality as well as the discretization based on taking the Legendre polynomials as a basis, it was fitting to try to derive similar results for the case of the neutral-type TDS. The derivation of these results as well as their application to examples from the literature can be seen in chapter 10.

The discussions in this chapter have been focused on the steps of the derivation of stability results in the time domain.

However, so far, it has not been mentioned how to obtain the stable time-delay intervals from the presented matrix inequalities. The following final remarks are reserved for that. First, the means to obtain a solution for Linear Matrix Inequality (LMI)s is discussed. This is followed by a quick discussion on obtaining solutions for more complicated matrix inequalities such as Bilinear Matrix Inequality (BMI)s.

Many of the stability results that are obtained in the time domain are in the form of LMIs. This is usually advantageous because LMIs are known to be convex problems, and many efficient algorithms have been developed in order to solve them efficiently. Widely-known algorithms that are used to solve LMIs are the ellipsoid algorithm and the interior point method. However, a discussion on those algorithms is beyond the scope of this research, and the interested reader is referred to the survey of van Antwerp and Braatz for an overview of the workings of those methods [128].

Not only are there many existent efficient algorithms to solve LMIs, there are several numerical software tools that have implemented these algorithms and can be used to solve the LMIs. This includes MATLAB®'s LMI Control Toolbox, LMITOOL, and YALMIP [128, 129]. The latter is the most recent of the three and has been often resorted to in the TDS community. Additionally, YALMIP has the ability to solve for several kinds of optimization problems, including heuristics for global optimization, the need for which, in solving matrix inequalities such as the ones defined in eq. (6.119) and eq. (6.120), will become clear shortly [129]. Therefore, it is this tool that will be used for the implementations in this research.

As may have been noticed from the previously presented results, not all are in the form of LMIs. Rather, they are in the form of the more general BMIs which are a category of nonlinear matrix inequalities. That is the case for eq. (6.119) and eq. (6.120). Solving for these matrix inequalities is in essence more difficult than solving for LMIs. This is because nonlinear matrix inequalities are nonconvex problems, and their computational complexity is $\mathcal{NP}$-hard [128, 130]. While this does not necessarily mean that there may not be practical solutions to these problems, it implies that it is usually very unlikely that there is an algorithm that can solve the inequality in polynomial-time [128]. In other words, the $\mathcal{NP}$-hardness means that, depending on the size of the problem, there are no guarantees on the boundedness of the time needed to obtain a suitable solution.

In general, as solving a BMI is a nonconvex problem, global optimization is needed as a part of the solution pipeline. The global optimization can be performed through heuristic techniques such as branch and bound algorithms. In fact, many branch and bound algorithms have been developed for solving BMI problems [128]. Thus, effectively, the branch and bound algorithm is responsible for selecting different time-delays. Thereafter, a convex solver solves for the resultant LMI at those selected time-delays to check whether the stability conditions are satisfied. Together those solvers provide a candidate solution scheme. However, as mentioned earlier, stable time-delay intervals will have already been obtained from the application of a frequency-domain method. This means that the feasibility of the matrix inequalities can be checked for those time-delay intervals, as a form of verification of those results.

7

Pendulum Control System

In this chapter, the stability techniques that have been selected from the earlier chapters will be applied to a control system comprising of a damped pendulum and an INDI controller. First, the techniques from the frequency domain will be discussed. Of those, the implemented techniques to determine the critical pairs include the direct method and the frequency sweeping approach (both graphically and programmatically). As for the analysis of the asymptotic behaviour, this is done both graphically and analytically, through the use of series. As for the time-domain technique, the matrix inequalities presented in section 6.6, based off a discretized Lyapunov functional method are implemented. Finally, a number of a simulation runs are performed to verify the obtained results.

The structure of the chapter is as follows. The expressions for the controllers are determined first. Before delving into the INDI control of the pendulum control system, the NDI control law of the system is derived. This is done in section 7.1. Thereafter, the INDI control of the damped pendulum is discussed in section 7.2. With the completion of the discussion on the suitable controller expressions, the discussion on the stability analyses ensues in section 7.3, where the mentioned chosen stability methods are applied to the INDI-controlled damped pendulum.

7.1 Nonlinear Dynamic Inversion (NDI) Control

The forced pendulum with friction is modeled by eq. (7.1),

$$\ddot{\theta} + \frac{b}{I}\dot{\theta} + \frac{mgl}{I}\sin\theta = u \tag{7.1}$$

where θ denotes the angular deflection of the pendulum (reference chosen to be the bottom position), u is the input to the system, I is the moment of inertia of the pendulum, b is the damping coefficient of the pendulum, l is the length of the pendulum, and m is the mass of the pendulum. This second order equation, eq. (7.1), can be transformed into a system of two first-order equations. By setting $x_1 = \theta$ and $x_2 = \dot{\theta}$, eq. (7.2) is obtained.

$$\begin{aligned} \dot{x_1} &= x_2 \\ \dot{x_2} &= u - \frac{b}{I}x_2 - \frac{mgl}{I}\sin(x_1) \end{aligned} \tag{7.2}$$

Linearizing this system of equations about $(x_{1,0}, x_{2,0})$ leads to the following system of equations:

$$\begin{aligned} \dot{x_1} &= x_2 \\ \dot{x_2} &= u - \frac{b}{I}x_2 - \frac{mgl}{I}\sin(x_1) - \frac{mgl}{I}\cdot cos(x_{1,0})(x_1 - x_{1,0}) \end{aligned} \tag{7.3}$$

It can be seen from eq. (7.3) that $x_{2,0}$ gets canceled in the linearization process and that only the remnant $x_{1,0}$ is relevant for the linearized dynamics.

Based on the discussion in chapter 2, in order to perform IO linearization, a suitable choice of the output variable needs to be made. An important concern related to making this choice are the internal dynamics. Specifically, the choice of output should ensure that the control system either does not have any internal dynamics or if it does, that the internal dynamics are

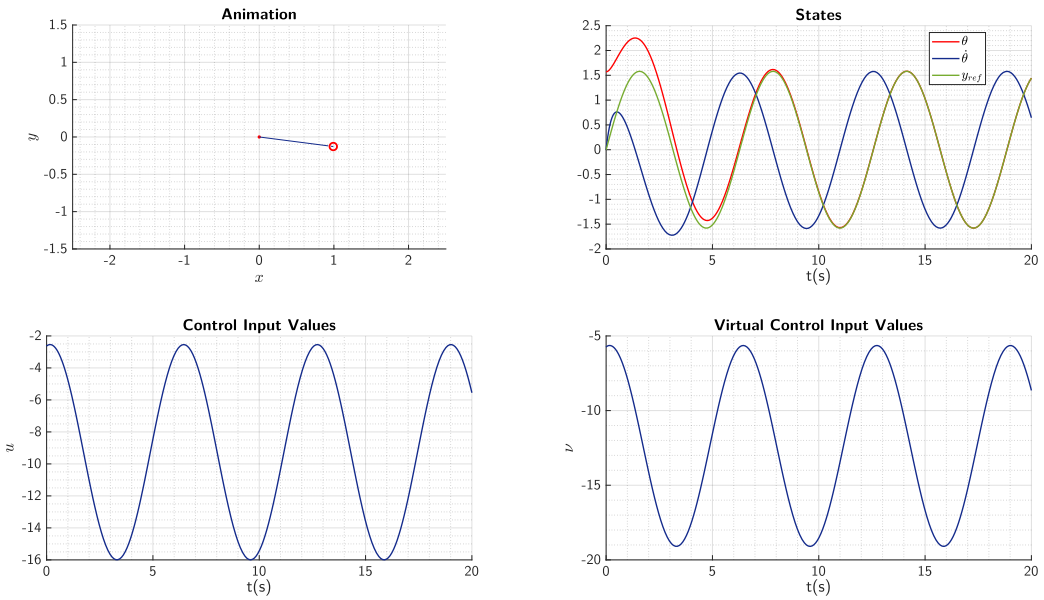

Figure 7.1: NDI Implementation Results

stable. To elaborate on the importance of ensuring the latter, the presence of internal dynamics means that full controllability is not guaranteed, in exception of the cases where it is known that the internal dynamics are stable.

First, the consequences of taking the output to be x_2 are examined. From this choice, it can be seen that there are internal dynamics since a single differentiation of the output equation leads to the appearance of the control input, meaning that the relative degree of the system is equal to 1 which is less than the order of the system, which is 2.

If the output is, instead, taken to be $y = x_1$, then the output needs to be differentiated twice in order for the control input to appear, as shown below.

$$\ddot{y} = \dot{x_1} = \dot{x_2} = u - \frac{b}{I}x_2 - \frac{mgl}{I}\sin(x_1) \tag{7.4}$$

Knowing that the system is second order, this means that the relative degree of the system is zero and the closed-loop system does not have any internal dynamics, which further means that the system is fully controllable. As a result, the output is selected to be x_1.

In order to linearize the dynamics, the virtual control input is defined according to eq. (7.5).

$$\nu = u - \frac{b}{I}x_2 - \frac{mgl}{I}\sin(x_1) \tag{7.5}$$

Moreover, for a tracking task, the virtual control is designed based on eq. (7.6).

$$\nu = \ddot{y}_{ref} + K_p(y_{ref} - y) + K_d(\dot{y_{ref}} - \dot{y}) \tag{7.6}$$

Combining eq. (7.5) and eq. (7.6) leads to the control law shown in eq. (7.7)

$$u = \ddot{y}_{ref} + K_p(y_{ref} - y) + K_d(\dot{y_{ref}} - \dot{y}) + \frac{b}{I}x_2 + \frac{mgl}{I}\sin(x_1) \tag{7.7}$$

In order to test its effectiveness, this controller has been implemented with the gains $K_p = 25$ and $K_d = 7$, and the simulation results of the application of this controller on a damped pendulum, for a sinusoidal reference signal, are shown in fig. 7.1. It is clear from the figure that the error converges to zero at around 6 seconds.

7.2 Incremental Nonlinear Dynamic Inversion (INDI) Control

As discussed before, in INDI, linearization is performed about the current state and control input. In the case of the system shown in eq. (7.1), linearizing eq. (7.4) followed by applying the time-scale separation principle leads to:

Table 7.1: Parameters used in the implementation of the INDI control of the pendulum control system.

m (kg)	b (kg/s)	l (m)	I (kgm^2)	$x_{1,0}$ (rad)	$x_{2,0}$ (rad/s)	u_0 (rad/s^2)	K_p	K_d	Actuator model	Sensor model 1	Sensor model 2
0.3	0.1	1	1	0.1	0	1	25	7	$\frac{1}{s+20}$	1	1

$$\ddot{y} = \ddot{y}_0 + \beta(x_0)\Delta u + \delta(z, \Delta t) \tag{7.8}$$

where $\delta(z, \Delta t)$ denotes the higher order terms. These terms can usually be neglected which reduces eq. (7.8) to:

$$\ddot{y} = \ddot{y}_0 + \Delta u \tag{7.9}$$

As in the case of NDI, the virtual control is chosen equal to $\ddot{y}$. Thus,

$$\Delta u = \nu - \ddot{y}_0 \tag{7.10}$$

Since a tracking problem is considered, the outer-loop linear control is again set to be as in eq. (7.6), which leads to the following incremental control law.

$$\Delta u = \ddot{y}_{ref} + K_p(y_{ref} - y) + K_d(\dot{y}_{ref} - \dot{y}) - \ddot{y}_0 \tag{7.11}$$

This means that the control law is

$$u = \Delta u + u_0 = \ddot{y}_{ref} + K_p(y_{ref} - y) + K_d(\dot{y}_{ref} - \dot{y}) - \ddot{y}_0 + u_0 \tag{7.12}$$

The block diagram of the control system that applies this INDI control is shown in fig. 7.2 (and an equivalent block diagram is shown in fig. 7.3). Based on this structure and the manipulation of transfer functions, it is possible to obtain the closed-loop formulation for the system dynamics in the frequency domain, for which later a time-domain realization is set up. Each of these will be needed for the application of the stability analysis methods.

7.3 Stability Regions in the Delay Space of the Pendulum Control System

In the following, the stability analysis of the INDI-controlled damped pendulum, whose parameters are shown in table 7.1, will be discussed. First, the analyses in the frequency domain will be discussed. This is followed by a discussion on the analysis in the time-domain. A number of simulation tests validate the results.

7.3.1 Frequency-domain Techniques

Two frequency domain techniques will be used to analyze the stability of the control system at hand. The first approach, which is called the direct method, is used to determine the critical pairs. Thereafter, the root tendency is analyzed analytically. As for the second approach, the frequency sweeping approach, the analysis is done entirely graphically.

7.3.1.1 Direct Method

It can be seen that the characteristic equation can be grouped into two different parts:

$$P(\lambda) + Q(\lambda) \cdot e^{-\tau \cdot \lambda} = 0 \tag{7.13}$$

If the equation is rearranged, this leads to

$$e^{-\tau \cdot \lambda} = \frac{-P(\lambda)}{Q(\lambda)} \tag{7.14}$$

Since the interest is in the intersection with the y-axis in the pole-zero map, then λ can be replaced by $j\omega$, and $\|e^{-\tau \cdot j\omega}\|$ is 1. This leads to the magnitude equation

$$\|P(j\omega)\| - \|Q(j\omega)\| = 0 \tag{7.15}$$

Thus, solving for the magnitude equation leads to the critical angular frequency values, each denoted by $\omega_{C,i}$. For the case of the pendulum control system considered, this leads to two critical imaginary roots which are 1.3207 rad/s and 2.0534

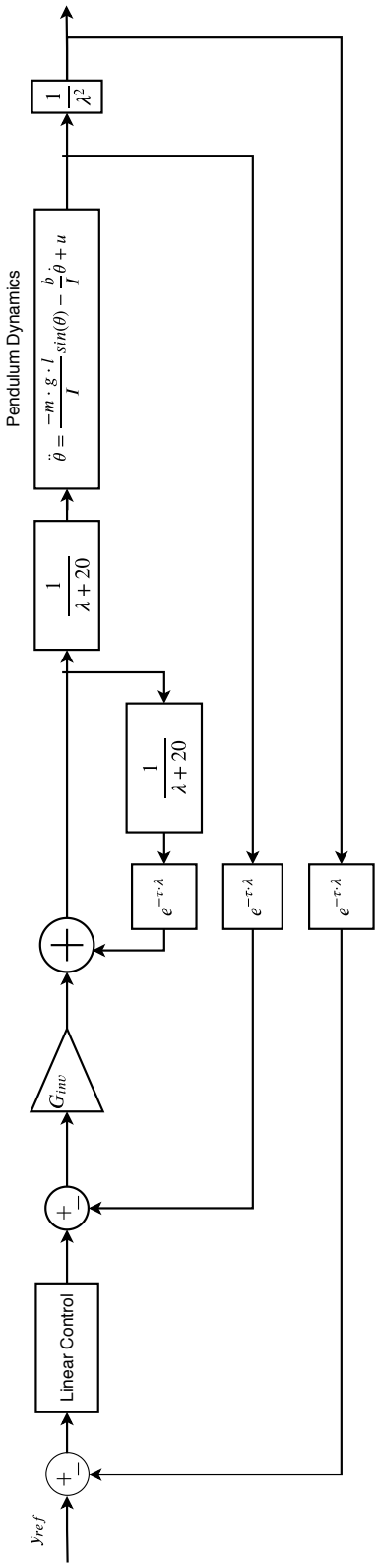

Figure 7.2: Block diagram of INDI control of damped pendulum.

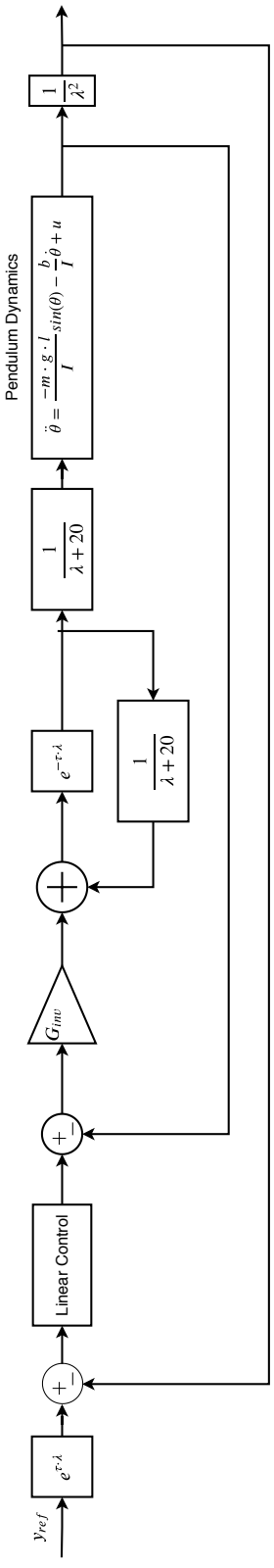

Figure 7.3: Equivalent block diagram of INDI control of damped pendulum.

rad/s. Actually, it should be noted is that there will also be crossings at -1.3207 rad/s and -2.0534 rad/s as well, due to symmetry property of the spectrum as discussed in section 5.3.1.1. However, for a simpler discussion, only the positive frequencies will be discussed, and this simplification will be compensated for in the final part in the determination of the stability sequence [9].

Now, to solve for the critical time-delays, the argument of $e^{-\tau \cdot j\omega}$ is used.

$$\arg(e^{-\tau \cdot j\omega_{C,i}}) = -\tau \cdot \omega_{C,i} \tag{7.16}$$

But based on eq. (7.14), $\arg(e^{-\tau \cdot j\omega_{C,i}})$ is also equal to

$$\arg(e^{-\tau \cdot j\omega_{C,i}}) = \arg\left(\frac{-P(j\omega_{C,i})}{Q(j\omega_{C,i})}\right) + 2\pi k \tag{7.17}$$

Thus,

$$\tau = \frac{1}{-\omega_{C,i}} \cdot \left(\arg\left(\frac{-P(j\omega_{C,i})}{Q(j\omega_{C,i})}\right) + 2\pi k\right) \tag{7.18}$$

This leads to the expressions for the

$$\tau_{\omega_{C,1}=1.3207\text{ rad/s}} = -2.216270 + 4.757412 \cdot k \tag{7.19}$$

$$\tau_{\omega_{C,2}=2.0534\text{ rad/s}} = 0.305067 + 3.059841 \cdot k \tag{7.20}$$

It becomes clear that due to the variable k, that for every critical frequency $\omega_{C,i}$, there correspond infinitely many critical time-delays.

The last part is to determine the stability intervals. This consists of three main steps, the first of which is determine the number of unstable roots when the time-delay is zero. The step that follows is to determine the Crossing Direction of Imaginary Root (CDIR) associated with the critical roots. Finally, the critical time-delays are sorted in increasing order, and the book-keeping of the number of unstable roots is performed for the intervals between the critical time-delays. This is done based on the CDIR determined.

Thus, first, the stability of the control system without any time-delays is studied. For the case of the pendulum control system, based on the input values mentioned above, the 3 roots obtained at $\tau = 0$ are: -19.71, - 0.1963 - 2.013i, and - 0.1963 + 2.013i. These three roots are all stable, therefore the starting count is zero.

The CDIR can be obtained based on eq. (5.96) and eq. (5.97) which for convenience is repeated in eq. (7.21). As mentioned in section 5.3.2.2, this is only applicable when the CIRs are simple [131, 132].

$$CDIR = \text{sign}\left[\frac{d\lambda}{d\tau}\right]_{\lambda=\omega_{C,i}} = \text{sign}\left[-\frac{f_\tau}{f_\lambda}\right]_{\lambda=\omega_{C,i}} \tag{7.21}$$

Moreover, as discussed in chapter 4, according to the invariance property, for all critical time-delay pertaining to a certain crossing-frequency the crossing direction will be the same [9]. For the case of the pendulum control system, based on eq. (7.21), the CDIR corresponding to 1.3207 rad/s is -1. That is, whenever there is a crossing at 1.3207 rad/s, if the time-delay is increased further this particular pole will move to the left-half plane. As for the critical angular frequency 2.0534, the CDIR is +1.

Once the CDIRs are established, it remains to perform thorough book-keeping. The critical time-delays are sorted in increasing order as shown in the first column of table 7.2. The starting score is equal to the number of unstable roots when there are no delays in the systems, which was determined to be zero. For the result of the scores, every time a critical time-delay with a CDIR of +1 is encountered, the score is increased by 2 (this corresponds to a +1 for the positive frequency crossing and another +1 for the conjugate CIR). Conversely, when a critical time-delay with a CDIR of -1 is encountered, the score is decreased by 2. This leads to the scores shown in the second column of table 7.2.

This leads to a constant score between the different critical time-delays. For the pendulum, the result looks like the result shown in table 7.2. From this table, it can be seen that the score will be zero for the intervals [0,0.305069] and [2.541144, 3.364915] seconds. Therefore, those are the stability intervals.

7.3.1.2 Analytic Curve Frequency Sweeping Approach

Unfortunately, not all characteristic equations that will be encountered will be of the form shown in eq. (7.13) and may be more complicated, thereby making the direct method inapplicable. Therefore, the more general Frequency Sweeping Approach is resorted to. As discussed in chapter 5, frequency sweeping can be used to *graphically* determine the critical angular frequencies,

Table 7.2: Stability Sequence for Pendulum Control System

Critical Time-delay Intervals (s)	Number of Unstable Roots
[0 , 0.305069]	0
[0.305069 , 2.541144]	2
[2.541144 , 3.364915]	0
[3.364915 , 6.424762]	2
[6.424762 , 7.298558]	4
[7.298558 , 9.484609]	2
[9.484609 , 12.055972]	4
[12.055972 , 12.544459]	2
[12.544459 , 15.604303]	4
[15.604303 , 16.813387]	6
[16.813387 , 18.664149]	4
[18.664149 , 21.570801]	6
[21.570801 , 21.723996]	4
[21.723996 , 24.783843]	6
[24.783843 , 26.328215]	8
[26.328215 , 27.843690]	6

as well as to graphically determine the roots tendencies. For the case of the pendulum control system at hand, applying the frequency sweeping approach serves as a form of verification of the analytical computations.

As explained before, the first step of the approach is to introduce the variable z that replaces the $e^{-\tau\cdot\lambda}$. Moreover, since the concern is with the intersections with the imaginary axis, to replace λ by $j\omega$. This leads to the following bivariate equation for the pendulum:

$$a0\cdot j\omega + a1\cdot z + a2\cdot j\omega\cdot z + a3\cdot(j\omega)^2 + a4\cdot(j\omega)^3 + a5 = 0 \tag{7.22}$$

The sweeping frequency curves are constructed by "sweeping" the frequency, and at each frequency, substituting in eq. (7.22) computing the values of z, and plotting the magnitude of that. In the case of the pendulum, there is only one frequency sweeping curve with two intersections with y=1. The curve is shown in fig. 7.4. It is clear that the two intersection points confirm that the critical angular velocities are 1.3207 and 2.0534 rad/s.

As for the asymptotic behaviour, this can be determined by examining the frequency sweeping curves, for which it can be seen that the CDIR is -1 for $\omega = 1.3207$ rad/s and CDIR is +1 for $\omega = 2.0534$ rad/s. These are deduced based on the slope of the curve at their intersection with the horizontal line at 1.

The asymptotic behaviour can also be determined based upon a pertubation-based approach or in other words, constructing the Puiseux series at a certain critical pair. The procedure to do is an implementation of the pseudocode shown in algorithm 1.

For the critical pair (1.3207j,- 2.216269937965585141505854449941 5 + 4.75741193760923979569288745574 09 · k), the following series is obtained:

$$\Delta\lambda = (-0.246395 - 0.284083\cdot j)\cdot\Delta\tau + o(\Delta\tau) \tag{7.23}$$

Since $\Delta\tau$ in eq. (7.23) does not have a fractional power, the series is in fact a special form of the Puiseux series and is in fact a Taylor series. This is expected because the critical roots are simple. Moreover, based on this Taylor series, it can be seen that a small positive increase in τ, i.e. $\Delta\tau = +\epsilon$ leads to a decrease in the real part of λ which means that the CDIR is -1.

As for the critical pair (2.0534j,0.3050669909787054426088629214 2673 + 3.059841342520988872411095859 7726 · k), the following series is obtained:

$$\Delta\lambda = (0.665318 - 0.123293\cdot j)\cdot\Delta\tau + o(\Delta\tau) \tag{7.24}$$

Here, again, since the CIR is a simple root, the series in eq. (7.24) is a Taylor series. Moreover, based on this obtained series, it can be seen that for $\Delta\tau = +\epsilon$, that the real part of $\Delta\lambda$ will be positive, which means that the CDIR is +1.

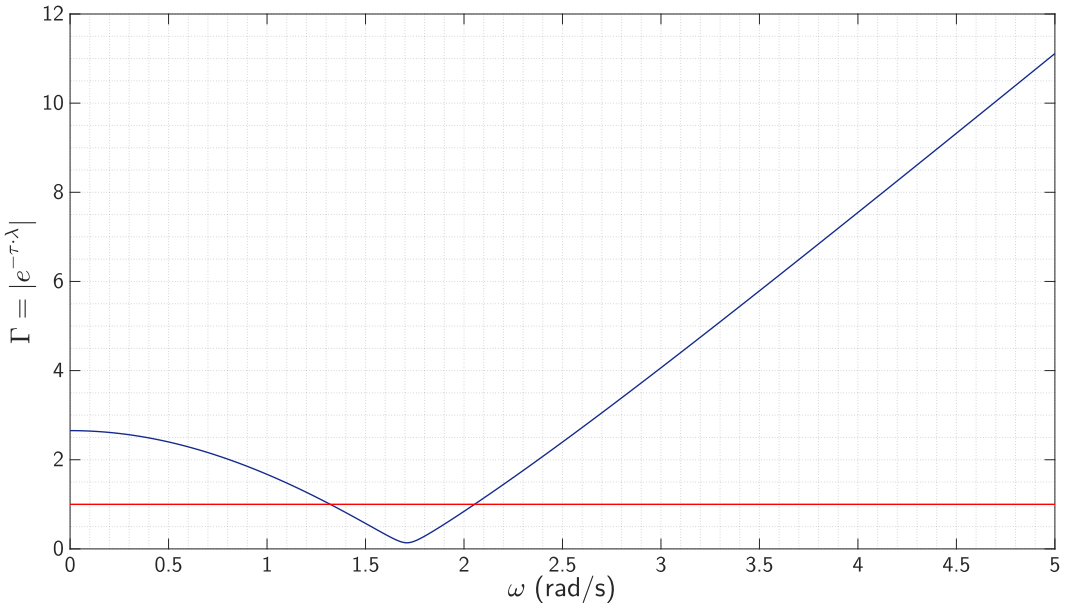

Figure 7.4: Frequency sweeping curve for the pendulum control system

This can also be verified by examining the frequency sweeping curves. From the curve in fig. 7.4, it can be confirmed that the CDIR is -1 for $\omega_{C,1} = 1.3207$ rad/s and the CDIR is +1 for $\omega_{C,2} = 2.0534$ rad/s. This is deduced based on the slope of the curve at their intersection with the horizontal line $\Gamma = 1$, whereby a positive slope corresponds to a CDIR equal to +1, and a negative slope corresponds to a CDIR equal to -1.

Since the obtained critical imaginary roots and the critical time-delays are the same, the stability sequence will also be the same, and the same stable time-delay regions are obtained: [0,0.305069] and [2.541144, 3.364915] seconds.

7.3.2 Lyapunov-based Approach

Now, the time-domain approach will be used to further verify the results obtained from the frequency domain analyses. Specifically, the LMIs described in eq. (6.119) and eq. (6.120) will be used. They are used to study the stability of systems of the form:

$$\begin{cases} \dot{x}(t) = A_0 x(t) + A_1 x(t-\tau), & \forall\, t \geq 0 \\ x(t) = \phi(t), & \forall\, t \in [-\tau, 0] \end{cases} \tag{7.25}$$

Thus, the matrices A_0 and A_1 have to be determined for the pendulum control system. As it is easier to determine the

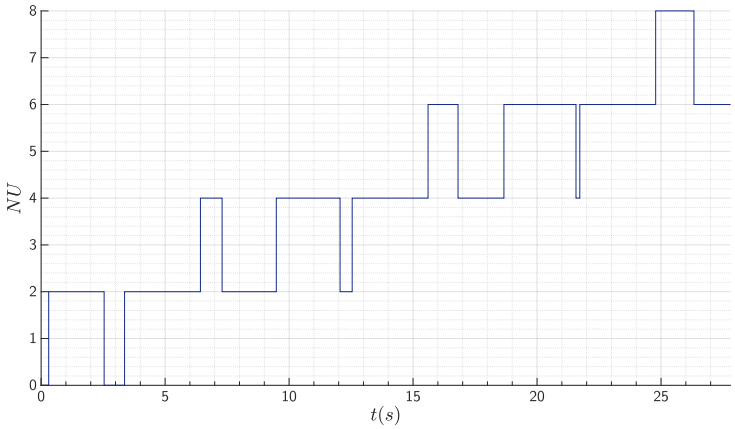

Figure 7.5: Plot of the number of unstable roots versus time for the considered pendulum control system.

overall system representation for an LTI system in the frequency domain, the characteristic equation of the pendulum control system (that had been already determined for the above analyses) is made use of to obtain an equivalent description in the time domain, which entails applying the inverse Laplace transform to the control system's characteristic equation. The obtained differential equation is of the form shown in eq. (7.26), with $a_1 \ldots a_2$ and b_0, b_1 being the appropriate coefficients.

$$\overline{x} + a_0 \cdot x + a_1 \cdot \dot{x} + a_2 \cdot \ddot{x} + b_0 \cdot x(t-\tau) + b_1 \cdot \dot{x}(t-\tau) = 0 \tag{7.26}$$

It is clear from the structure of eq. (7.26) that the pendulum is a retarded type TDS. The highest order of derivative of y without time-delay is 3; whereas the order of derivative including a time-delay is 1. Since the former is strictly greater than the latter, the system is a retarded system.

In order to obtain a state space representation from the differential equation eq. (7.26), a state vector denoted by $\tilde{z} = \left[x,\ \dot{x},\ \ddot{x}\right]^\top$ is proposed. Re-writing eq. (7.26) in terms of $\tilde{z}$ leads to eq. (7.27).

$$\begin{cases} \dot{\tilde{z}} & = A_0\tilde{z} + A_1\tilde{z}(t-\tau) \\ A_0 & = \begin{bmatrix} 0 & 1 & 0 \\ 0 & 0 & 1 \\ -a_0 & -a_1 & -a_2 \end{bmatrix} \\ A_1 & = \begin{bmatrix} 0 & 0 & 0 \\ 0 & 0 & 0 \\ -b_0 & -b_1 & 0 \end{bmatrix} \end{cases} \tag{7.27}$$

Since eq. (7.27) has the form that is suitable for the stability results in eq. (6.119) and eq. (6.120), it is possible to proceed to the step of solving for the matrix inequalities for the determined A_0 and A_1 matrices of the pendulum control system. Although, an efficient way to solve those matrix inequalities (which happen to be bilinear matrix inequalities) has not been found, it is still possible to check the feasibility of the solution of the matrix inequalities for different values of time-delay.

Checking for the first interval [0,0.305069]s The correctness of the first stability interval, [0,0.305069]s, can be verified by checking the feasibility of the solution of the matrix inequalities in eq. (6.119) and eq. (6.120) for the entirety of this interval. Moreover, once the limit of the first interval is reached, the set of matrix inequalities no longer has a feasible solution, not until the second stability interval. This is clear from fig. 7.6, where the residuals of V and $\dot{V}$ constraints both reach zero at what is visibly around 0.305 s.

For finer results on the upper bound of this stability interval, starting with τ = 0.3s and taking increments of 0.0001s, the matrix inequalities are feasible up to 0.3050s. N ≥ 1 is sufficient to obtain this result. If the steps are taken to be 0.000001, N≥ 3 is sufficient to obtain 0.305068 as the largest number that makes the matrix inequalities feasible (for the first stability interval). The value of N that is sufficient to obtain a certain precision is also dependent on the constraints set for the matrix inequalities.

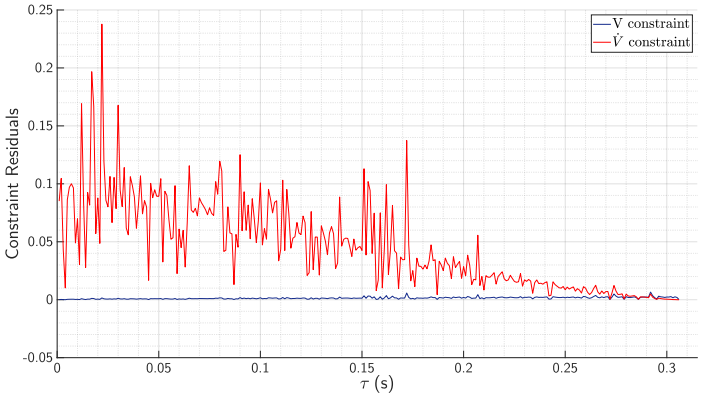

Figure 7.6: Plot showing the evolution of the constraint residuals for the Lyapunov functional condition and the Lyapunov functional derivative condition.

Checking for the second interval [2.541144,3.364915]s A similar procedure is applied to check the second stability interval. To do so, checking the feasibility of the matrix inequalities is broken down into two tests. Both tests start by checking the feasibility of some interior point for the interval, say 3s. One test would apply delay decrements to this initial starting delay, and the other would apply delay increments. The results of those tests in terms of constraint residuals, for the Lyapunov functional constraint and the Lyapunov functional derivative constraint, are shown in fig. 7.7 and fig. 7.8, respectively. It is seen from fig. 7.7 that the solution of the set of matrix inequalities does not have a feasible solution for values that are smaller than around 2.54s (and which are larger than 0.305069s) because the $\dot{V}$ constraint residual had already reached zero at this limit. In fig. 7.8, it is seen how the plots of the constraint residuals terminate at around 3.365s.

To attain the bound 2.541144s with a precision of 6 decimal points (2.541144s as 2.541143s is already in the infeasible region), if one starts with a value larger than 2.541144s and takes decrements with step size 0.000001s, the value of 2.541144s is attained with N≥ 8.

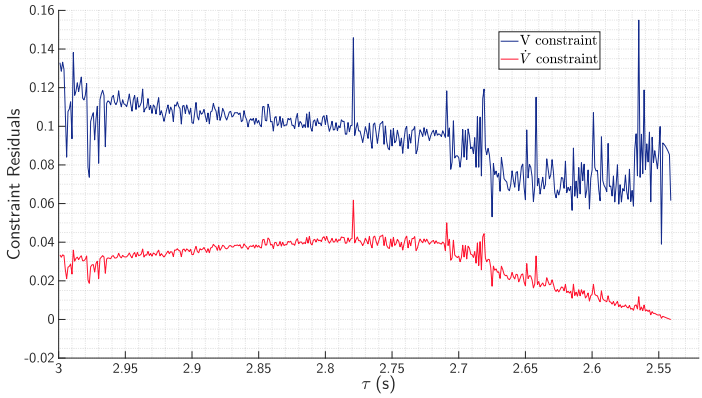

Figure 7.7: Plot showing the evolution of the constraint residuals for the Lyapunov functional condition and the Lyapunov functional derivative condition.

The bound 3.364915s can be checked in the same manner that was used for the upper bound of the first stability interval, through delay increments. To attain a value of 3.364915s, N≥ 8 is needed.

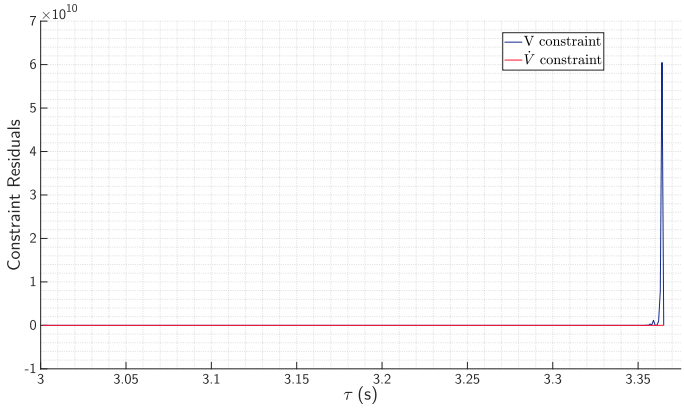

Figure 7.8: Plot showing the evolution of the constraint residuals for the Lyapunov functional condition and the Lyapunov functional derivative condition.

7.3.3 Verification with the Simulink Model

Based on simulation (which includes the nonlinear pendulum plant) and based on the same initial conditions, gains and all the parameters that were used in the previous analysis (as well as running at a rate of 10,000Hz), the system appears to be stable for the intervals [0,0.3] and [2.5,3.4]. Stability is lost for a time-delay of 0.31 seconds, which is in accordance with the results obtained from the frequency sweeping approach.

The response to a 0 reference (stabilization) leads to the outputs shown in fig. 7.9a, fig. 7.9b, fig. 7.9c, fig. 7.9d, fig. 7.9e, fig. 7.9f, fig. 7.9g, and fig. 7.9h. The results concur with the stability intervals obtained.

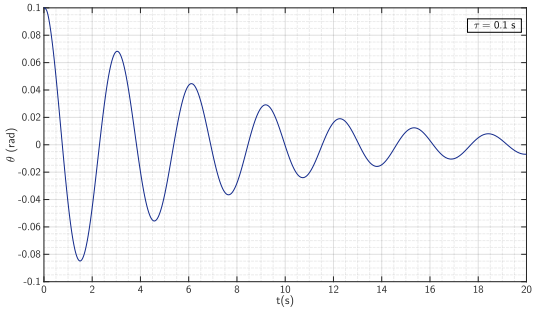

(a) Response corresponding to a delay of 0.10s for the first 20s.

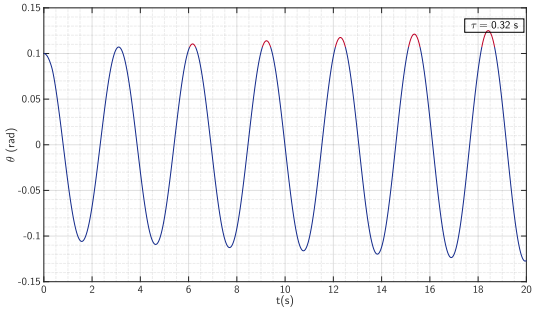

(b) Response corresponding to a delay of 0.32s for the first 20s.

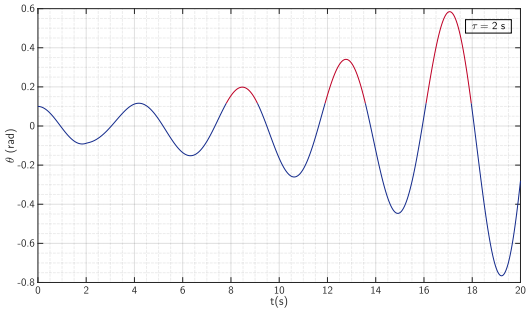

(c) Response corresponding to a delay of 2s for the first 20s.

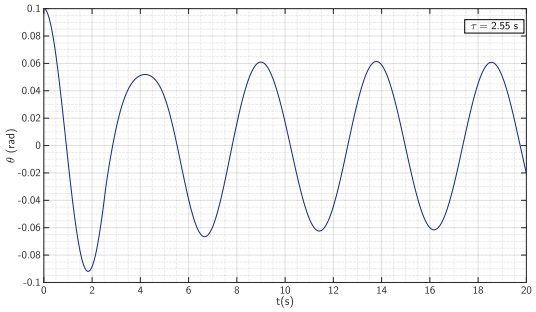

(d) Response corresponding to a delay of 2.55s for the first 20s.

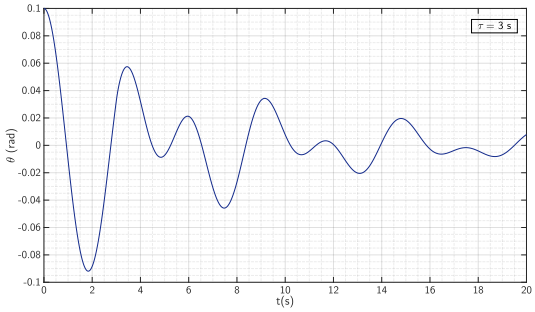

(e) Response corresponding to a delay of 3s for the first 20s.

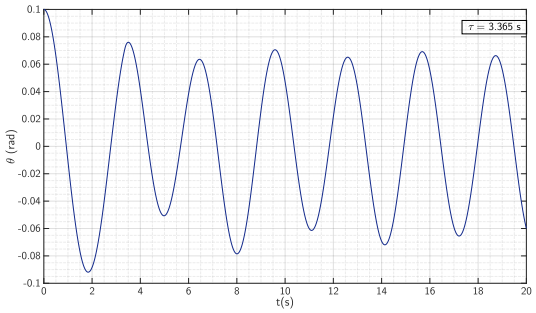

(f) Response corresponding to a delay of 3.365s for the first 40s.

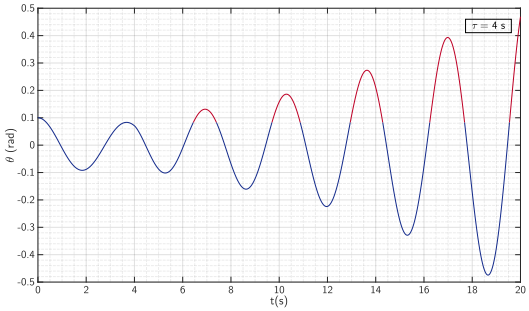

(g) Response corresponding to a delay of 4s for the first 20s.

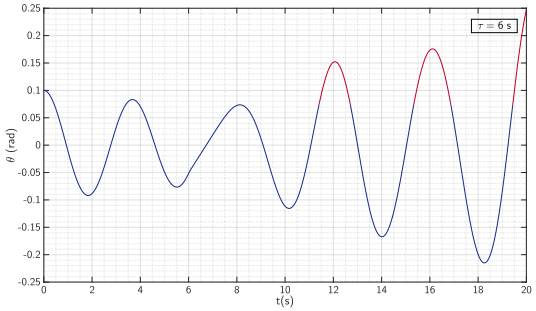

(h) Response corresponding to a delay of 6s for the first 20s.

Figure 7.9: Plots of the response of the pendulum control system, shown for the first 20 s, for different time-delays.

III

Robust Stability Analysis

For real-world applications, it is practically impossible to describe a system precisely. Uncertainties in the linear system representation occur due to many reasons. These include approximate or incorrect knowledge about certain parameters in the system. Another source of uncertainty is the linearization of system dynamics; some parameters may be time-varying because of nonlinearities in the actual system dynamics or because of different operating conditions. Furthermore, the limited measurement accuracy of sensors introduces uncertainties in the signals in the system. In some situations, despite having accurate insight about the plant model, it may be preferred to deal with a deliberately simplified version of the model and to represent the parts that were neglected with uncertainties [133].

Considering the inevitable presence of uncertainties in practice, it is important to make the analysis robust to such uncertainties. Doing so involves a two-part procedure. The first part is to characterize the uncertainty, and the second part is to analyze for robust stability given the established uncertainty representation.

It should be noted that, in the case of TDSs, uncertainties may arise in two main ways: either as uncertainties in the coefficients or as uncertainties in the time-delay parameters themselves. While it has been expressed in the literature that the analysis of the latter is a harder problem, for the case of the problem analyzed in this thesis, the research aim is to determine the time-delays for which the stability of the control system is ensured while considering uncertainties in the knowledge about the modelled parts of the system, rather than assessing the stability for time-delay intervals that are known a priori. Therefore, in this thesis, the concern is with uncertainties in the coefficient matrices (in the case of the time domain) or the coefficient vectors of the quasipolynomials (in the case of the frequency domain).

Chapter 8 is related to the first part, whereby how to characterize the uncertainty will be dealt with. It will be seen that of the issues tied to uncertainty characterization are conservatism and mathematical tractability. In chapter 9, a number of theorems and principles that can be used for robust stability analysis of TDS are presented, and how these methods relate to the uncertainty structures and other paradigms of uncertainty characterization is discussed.

This page was intentionally left blank.

8

Uncertainty Characterization

In this chapter,the concern is with parametric uncertainty, rather than dynamic uncertainty. There are two main paradigms encountered with parametric uncertainty. In one of the paradigms, the uncertainty characterization is based on each uncertainty parameter varying within a known interval. Depending on the way of the occurrence of the uncertainties parameters in the equation that is studied, this leads to a number of uncertainty structures. The second paradigm offers the possibility of grouping the uncertain parameters and assuming a norm-bounded variation on certain element in the equation of the system. In the rest of this chapter, the concepts pertaining to those two paradigms are discussed. The discussion presented in this chapter mainly follows the discussions in [10, 75, 133].

8.1 Uncertainty Bounding Set and the Family of Systems

In the literature on robust stability analysis, uncertainty bounding sets, typically denoted by the letter Q, that are either in the form of boxes or spheres are usually encountered [10]. However, Barmish also expresses that it is not very critical which of the two options is chosen. For this thesis, uncertainty bounding sets that are in the form of hypercubes are assumed, which is described by eq. (8.1).

$$Q = \left\{ q \in \mathbf{R}^{\ell} : q_i^- \leq q_i \leq q_i^+ \text{ for } i = 1, 2, \ldots, \ell \right\} \tag{8.1}$$

The uncertainty bounding set serves only as a description of the uncertain variables. Thus, it is only when this set is combined together with the uncertain function, that the concept of the family of systems is obtained.

8.2 A Hierarchy of Uncertainty Structures

When considering a function with coefficients that have independent uncertainty, then depending on how these parameters appear in the function, the function may adhere to one of many uncertainty structures. Examples of parametric uncertainty structures include independent uncertainty structure, affine uncertainty structure, multilinear uncertainty structure, and polynomic uncertainty structure. More specifically, these types form a hierarchy whereby the independent uncertainty structure is a subset of affine uncertainty structure, which is a subset of multilinear uncertainty structure, and which, in turn, is a subset of polynomic uncertainty structure, i.e. independent $\subset$ affine $\subset$ multilinear $\subset$ polynomic [10].

This is important to note because robust stability analysis methods that are applicable to systems with uncertainty structures that are lower in the hierarchy usually are no longer directly applicable to the systems with uncertainty structures that are higher in the hierarchy. For example, vertex results, which are applicable to the cases where independent uncertainty is encountered, no longer hold for systems with an affine uncertainty structure.

8.2.1 Independent Uncertainty Structure

As mentioned in the introduction of this section, the independent uncertainty structure is the lowest in the hierarchy. In words, a system has an independent uncertainty structure if each uncertain variable in the uncertainty set appears only in one of the coefficients of the system equation [10]. In the frequency domain, interval quasipolynomials take the form shown in eq. (8.2).

$$I(s) = \left\{ s^n + \sum_{k=0}^{n-1} \left(\sum_{l=0}^{m} \alpha_{kl} s^k \right) e^{-\beta_l s} | \alpha_{kl} \in \left[\alpha_{kl}, \bar{\alpha}_{kl} \right] \in \mathbb{R} \right\} \quad k = 0, \ldots, n-1; l = 0, \ldots, m \tag{8.2}$$

8.2.2 Affine Linear Uncertainty Structure

An affine linear uncertainty structure which is also known as a polytopic uncertainty structure occurs when the uncertain variables appear affine in the coefficients. This structure leads to a family that is polytopic. A polytope is the convex hull of a set of points, where a convex hull of some set C is the smallest convex set that contains the elements of the set C. Furthermore, a set is convex if any line connecting any two points in the set is contained within that set. Every point p in a polytope P can be generated as the convex combination of the vertices of P. A convex combination is by definition the linear combination of points where the sum of their coefficients is equal to 1. Thus, an uncertain quasipolynomial with an affine linear uncertainty structure has the form shown in eq. (8.3),

$$F(s) = \left\{ \sum_{l=1}^{T} \mu_l f_l(s) | \mu_l \geq 0, \sum_{l=1}^{T} \mu_l = 1 \right\} \tag{8.3}$$

where f_l are the vertex quasipolynomials of this family.

In the time domain, the familiy with affine linear uncertainty structure is described in eq. (8.4),

$$\Omega = \left\{ \sum_{k=1}^{n_v} \alpha_k \omega^{(k)} | \alpha_k \geq 0, k = 1,2,\ldots,n_v; \sum_{k=1}^{n_v} \alpha_k = 1 \right\} \tag{8.4}$$

as the convex combination of ω^k, where ω^k is a pair of vertex matrices as shown in eq. (8.5).

$$\omega^{(k)} = \left(A_0^{(k)}, A_1^{(k)} \right), \quad k = 1,2,\ldots,n_v \tag{8.5}$$

The number of vertices can be easily calculated. Given that there are n_p uncertain parameters, due to the upper and lower bounds on each parameter, the number of vertices can be determined based on $n_v = 2^{n_p}$.

8.2.3 Multilinear Uncertainty Structure

As for the case of multilinear uncertainty structure, it arises when every coefficient in the uncertain function is multilinear, which means that if only one element of the vector q is kept free and the rest of the uncertain variables are fixed, that coefficient would be affine in that free uncertain variable [10].

In the time domain, the multilinear uncertainty structure manifests as interval/independent matrices. This is a consequence of the transformation that occurs when converting from a state-space representation to that of a characteristic function representation or vice versa. Furthermore, the family is mathematically described according to eq. (8.6), where the operator co denotes the operation of obtaining the convex hull.

$$\Omega \subset \mathrm{co} \left\{ \omega^{(i)}, i = 1,2,\ldots,n_v \right\} \tag{8.6}$$

As presented in [75], in the time domain, and as will be discussed again in the next chapter, the case of sub-polytopic or multilinear uncertainty is comparatively easy to handle. That is, it can be said that the studied system is stable when the matrix inequalities are satisfied for all the vertices. However, in cases when the vertices are too many which happens in the case of "combinatorial explosion" of the extreme values of the uncertain parameters, describing the uncertainty using this paradigm is no longer favourable. Rather, in these cases, it is preferred to describe uncertainties in a norm-bounded form, which is discussed in section 8.3.

8.2.4 Polynomic Uncertainty Structure

A polynomic uncertainty structure occurs when every coefficient in the uncertain function is polynomial in the elements of the uncertain variables. This makes this uncertainty structure the most inclusive of the above mentioned structured. Of course, it should be noted that there are more general uncertainty structures, but these are not relevant within the context of the stability of LTI control systems.

8.3 Norm-bounded Uncertainty

As mentioned in the introduction of the chapter, the second of the two paradigms of parametric uncertainty that are discussed in this chapter is norm-bounded uncertainty. In the case of norm-bounded uncertainty, the general representation is to have the nominal value of the system matrices and add an uncertainty to it. For example, in the case of a retarded TDS of the form in eq. (4.10), if the matrices A_0 and A_1 are considered to be uncertain, then their norm-bounded uncertainty representation is given by:

$$\begin{aligned} A_0 &= A_{0n} + \Delta A_0 \\ A_1 &= A_{1n} + \Delta A_1 \end{aligned} \tag{8.7}$$

where the uncertain parts ΔA_0 and ΔA_1 are described with:

$$\begin{pmatrix} \Delta A_0 & \Delta A_1 \end{pmatrix} = EF \begin{pmatrix} G_0 & G_1 \end{pmatrix} \tag{8.8}$$

A more general way to describe the norm-bounded uncertainty is using the Linear Fractional Transformation. It is more general because it allows to assume that the uncertainties are indepenedent. This more general representation is shown in eq. (8.9).

$$\begin{pmatrix} \Delta A_0 & \Delta A_1 \end{pmatrix} = E(I - FD)^{-1} F \begin{pmatrix} G_0 & G_1 \end{pmatrix} \tag{8.9}$$

Of course, since there is a matrix inversion involved in eq. (8.9), it should be ensured that this inversion is well-posed.

There are several Lemmas that are helpful for dealing with norm-bounded uncertainty, and they are discussed in section 6.2.3 of [75]. Moreover, an even more general category of norm-bounded uncertainty is discussed in section 6.2.4 of [75] which is block-diagonal uncertainty.

This page was intentionally left blank.

9

Tools for Robust Stability Analysis

The goal of this chapter is to present a number of concepts, principles, and theorems that have been found in the literature, which form a set of tools that are relevant for the robust stability analysis of uncertain TDSs. Several of those have been encountered in the case of the robust stability analysis of uncertain polynomials, and it will be explained here how they may be applied to the case of uncertain quasipolynomials.

The structure of the chapter is as follows. First, a number of preliminaries are presented in section 9.1. Thereafter, the approaches for robust stability of systems with uncertainty structures from different parts of the hierarchy are discussed in section 9.2.

9.1 Preliminaries

Because of their relevance to the methods that will be discussed in section 9.2, some preliminary concepts and principles will be explained in this section. Those are the concept of uncertain quasipolynomials, the concept of the value set, and the zero-exclusion principle.

9.1.1 Uncertain Quasipolynomial

Consider the quasipolynomial defined in eq. (9.1).

$$f(\lambda) = \sum_{j=0}^{n} \sum_{i=0}^{m} a_{ji} \lambda^{n-j} e^{-\tau_i \lambda} = \sum_{i=0}^{m} p_i(\lambda) e^{-\tau_i \lambda} \quad \text{where} \quad 0 = \tau_0 < \tau_1 < \ldots < \tau_m \tag{9.1}$$

There are two vectors defined in association with the equation of the quasipolynomial in eq. (9.1): the coefficient vector shown in eq. (9.2) and the exponent coefficient vector seen in eq. (9.3) [75].

$$\mathbf{a} = \left(a_{00}, \ldots, a_{0n}, a_{10}, \ldots, a_{1n}, \ldots, a_{mn}\right) \tag{9.2}$$

$$\mathbf{r} = \left(r_1, r_2, \ldots, r_m\right) \tag{9.3}$$

In the case of uncertainties, where the uncertain parameters belong to some uncertainty bounding set Q_F, the result is a family of uncertain quasipolynomials, denoted by F:

$$F = \left\{ f(s, \mathbf{a}, \mathbf{r}) | (\mathbf{a}, \mathbf{r}) \in Q \right\} \tag{9.4}$$

However, as previously mentioned, uncertainties in the time-delays will not be considered. Only the cases where there are uncertainties in the coefficient vector $\mathbf{a}$ will be of concern in this thesis. Thus, the elements of the coefficient vector may be in terms of a number of uncertain elements, where such uncertain elements, in alignment with the notation in section 8.1, shall be denoted by q_i.

9.1.2 Value Set

The value set is an important tool for the robust stability analysis of uncertain functions. However, before explaining why it is such an important concept, a definition of the value set, in the context of uncertain quasipolynomials, is presented in Definition 9.1. Informally stated, the value set is the range of an uncertain function at a particular imaginary frequency.

Definition 9.1 (Value Set [75]): *The value set of a family of quasipolynomials F is defined according to:*

$$V_F(\lambda_0) = \left\{ f(\lambda_0) \,|\, f \in F \right\} \tag{9.5}$$

where λ_0 is a complex number and specifically a pure imaginary complex number at which the value set is evaluated.

One particular reason why the value set is considered to be important is that it is needed to check for the zero-exclusion principle which is one of the more general principles that are applicable across the different uncertainty structures in the hierarchy, and which will be explained in the following subsection. Moreover, since the zero-exclusion principle has been instrumental to the derivation of several other theorems, the value set, by extension, can be needed to check the conditions of other theorems as well, as is the case, for example, for the Finite Inclusions Theorem. Another important, and often convenient, property of the value set is that it is always two-dimensional, irrespective of the nature of the uncertain function or of the type of uncertainty structure involved.

9.1.3 Zero-exclusion Principle

The zero-exclusion principle is an important principle in robust stability analysis because it provides a necessary and sufficient condition for the stability of uncertain polynomials and quasipolynomials. In the context of TDSs, i.e. in the context of uncertain quasipolynomials, the zero-exclusion principle is formulated as:

Theorem 9.1 (Zero-Exclusion Principle [75]): *Let the family of uncertain quasipolynomials, F, satisfy the following assumptions:*

1. *Every member of the uncertain quasipolynomial F has a non-zero principal term.*
2. *The exponent coefficient vector of every member of the uncertain quasipolynomial has only positive components, that is $r_i > 0, i = 1, 2, \ldots, m$ for every $f(\lambda) \in F$.*
3. *There exist $R > 0$ and $\epsilon > 0$ such that for every $f(\lambda)$ in the uncertain quasipolynomial the corresponding quasipolynomial $\psi_0(s)$ has no zeros of magnitude greater than R (if any) with real part greater than $-\epsilon$.*
4. *The uncertainty boundedness set of the uncertain quasipolynomial F, which is denoted by Q_F, is compact and path-wise connected.*

Then, all members of F are Hurwitz stable if and only if

1. *at least one member of F is Hurwitz stable*
2. *for every point $s = j\omega$ on the imaginary axis, the value set, $V_F(j\omega)$ computed at this point does not contain the origin of the complex plane.*

From the above, a number of concepts are mentioned that deserve attention. In the first point, it is mentioned that the uncertain quasipolynomial is required to have a non-zero principal term. In order to explain what a principal term is, consider again the description of the quasipolynomial appearing in eq. (9.1). Equation (9.1) is said to have a principal term if eq. (9.6) holds [75].

$$\deg(p_0) = n \geq \deg(p_i), \quad i = 1, 2, \ldots, m \tag{9.6}$$

The importance of the principal term is that its existence is a necessary condition for the stability of a quasipolynomial, which makes it a needed pre-requisite in the zero-exclusion principle. Indeed, in relation to the types of TDSs, retarded and neutral TDSs satisfy eq. (9.6) and have principal terms [84]. Moreover, as mentioned earlier in chapter 4, in physical applications, only delays of either retarded or neutral type will be encountered. Therefore, it may be safely assumed that this assumption holds for the cases studied in this thesis.

With regards to the third assumption, it is expressed by Gu et al. that this assumption is satisfied if a stricter version of the first assumption is satisfied [75]. Specifically, this condition is given by eq. (9.7):

$$\deg(p_0) = n > \deg(p_i), \quad i = 1, 2, \ldots, m \tag{9.7}$$

Thus, for example, eq. (9.8) has a principal term (since $\deg(\lambda^3 + 6\lambda^2 + 2) > \deg(4\lambda + 5)$) and so does eq. (9.9) since $\deg(\lambda^2 + 6\lambda^2 + 5) = \deg\left(7\lambda^2 + 5\right)$; whereas, eq. (9.10) does not have a principal term because $\deg(\lambda^2 + 5\lambda + 4) < \deg\left(\lambda^3 + 8\lambda + 9\right)$.

$$f(\lambda) = (\lambda^3 + 6\lambda^2 + 2) + e^{-\lambda\cdot\tau}\cdot\left(4\lambda + 5\right) \tag{9.8}$$

$$f(\lambda) = (\lambda^2 + 6\lambda^2 + 5) + e^{-\lambda\cdot\tau}\cdot\left(7\lambda^2 + 5\right) \tag{9.9}$$

$$f(\lambda) = (\lambda^2 + 5\lambda + 4) + e^{-\lambda\cdot\tau}\cdot\left(\lambda^3 + 8\lambda + 9\right) \tag{9.10}$$

As for the fourth assumption, it entails the path-wise connectedness of the uncertainty boundedness set Q_F. Formally stated, path-wise connectedness is defined as:

Definition 9.2 (Path-wise Connectedness [10]): *A set $X \subseteq \mathbf{R}^k$ is said to be path-wise connected if the following condition holds: Given any two points $x^0, x^1 \in X$ there is a continuous function $\Phi : [0,1] \to X$ such that $\Phi(0) = x^0$ and $\Phi(1) = x^1$.*

In words, this property means that for any two points in a set X, there is a continuous function defined over the interval $[0,1]$ and whose range is the considered set X, and for which those two points are the range of the function at the extremes of the domain, i.e. at 0 and at 1.

From the two main conditions for stability, it can be seen that the second condition can be considered the essence of the principle; it requires that the value sets of the system do not contain the origin which is also where the principle gets its name from.

As a final remark on the zero-exclusion principle, it should be mentioned that it is, in general, hard to verify this principle due to the fact that all the value sets associated with all possible values of ω must be checked that they do not contain the origin. As a result, alternatives to this principle are often resorted to such as the theorems that will be discussed in the following sections. This transition to other theorems is motivated by the concept of reduced test sets, which is explained next.

9.1.4 Test Set

In many of the theorems and tests that analyze for robust stability, it is required to check a certain condition for a typically large set of elements. As a result, reduced test sets have been sought. The result of such attempts has been the emergence of concepts and theorems such as the concept of convex directions, Kharitonov's theorem, and the edge theorem. Since reduced test sets are important for both uncertain polynomials and uncertain quasipolynomials (in the case of TDSs), the examples mentioned of the concept of convex directions, Kharitonov's theorem, and the edge theorem had been first encountered in the case of uncertain polynomials. Their variants have been later developed for the case of uncertain quasipolynomials.

9.2 Stability Results Based on the Hierarchy of Uncertainty Structure

In this section, the robust stability analysis based on the hierarchy of uncertainty structures will be discussed. A discussion on independent uncertainty structure is omitted as it is the lowest in the hierarchy. It will only be mentioned that Mori and Kokame have extended Kharitonov's theorem for the case of TDSs with an independent uncertainty structure [134].

9.2.1 Affine Uncertainty and the Edge Theorem

The edge theorem was originally developed for the stability of uncertain polynomials that have an affine uncertainty structure. This theorem was later extended to the case of retarded uncertain quasipolynomials by Fu et al. [135]. These results were further extended to the case of neutral TDS by the same researchers [136].

The theorem states that when the system can be described as a polytopic family of quasipolynomials, the stability of that family can be deduced from the stability of the edges of its polytope. Specifically, the family is stable if and only if all the edges of the family are stable.

Given the affine uncertainty structure, the quasipolynomial describing an edge can be determined from the linear combination of two vertex quasipolynomials pertaining to a particular edge, denoted by $f_0(s)$ and $f_1(s)$. This is shown in eq. (9.11).

$$f_\mu(\lambda) = (1-\mu)\, f_0(\lambda) + \mu f_1(\lambda), \text{ where } \mu \in [0,1] \tag{9.11}$$

Remark 9.1: *The explanation for why the vertex quasipolynomials are the generators for the polytope is presented in the following. Consider eq. (9.1) again. Since an affine uncertainty structure is considered, this means that each of the polynomials p_i in eq. (9.1) can be described as shown in eq. (9.12), where c_i are known coefficients that are not affected by uncertainty and q^k are generators of the uncertainty bounding set Q.*

$$p_i(\lambda) = \sum_{j=0}^{n} c_i q_i \lambda^i = \sum_{j=0}^{n} c_i \left(\sum_k \mu_k q^k \right) \lambda^i \tag{9.12}$$

This means that eq. (9.1) *can be written as follows:*

$$f(\lambda) = \sum_{i=0}^{m} p_i(\lambda) e^{-\tau_i \lambda} = \sum_{i=0}^{m} \sum_{j=0}^{n} c_i \left(\sum_k \mu_k q^k \right) \lambda^i e^{-\tau_i \lambda} \tag{9.13}$$

Some re-arrangements of eq. (9.13) *lead to eq.* (9.14).

$$f(\lambda) = \sum_{i=0}^{m} p_i(\lambda) e^{-\tau_i \lambda} = \sum_k \mu_k \left(\sum_{i=0}^{m} \sum_{j=0}^{n} c_i q^k \lambda^i e^{-\tau_i \lambda} \right) \tag{9.14}$$

The term in the parentheses is the evaluation of the uncertain quasipolynomial at q^k, which is a vertex of the uncertainty bounding set. Moreover, the structure shown in eq. (9.14) *is that of obtaining a convex combination. This means that every quasipolynomial can be described as the convex combination of quasipolynomials that are evaluated at the vertices of the uncertainty bounding set, Q*

In the literature, Tuzcu et al. have used the edge theorem to extend the stability analysis approach based on the direct method (explained in section 5.3.1.1) to the case of TDSs with polytopic uncertainty [137]. Along this line of research, it was interesting to attempt to extend the analytic curve frequency sweeping approach with the edge theorem. As the analytic curve frequency sweeping approach is more general than the direct method, this extension will lead to a robust stability analysis technique in the frequency domain that is applicable to a wider group of TDSs, consisting of TDSs with commensurate delays. To the knowledge of the author, this had not been previously presented in the literature. This extension has been made, and its results have been presented in the attached article.

There exist graphical methods for checking the stability of a TDS with affine uncertainty. One such test has been proposed by Fu et al., which allows to verify the results that are obtained based on a robust stability analysis method applied to a system with polytopic uncertainty. The theorem reads as follows:

Theorem 9.2 ([135]): *Consider a polytope of n-th order (real or complex) quasipolynomials P. $E_1, E_2, \ldots E_t$ are used to denote the edges of P and $p_{k0}(\lambda)$ and $p_{k1}(\lambda)$ to denote the vertix quasipolynomials of E_k. Then, P is stable if and only if the following two conditions apply for every E_k, $1 \leq k \leq t$:*

- *the frequency response plot of $p_{k0}(j\omega)/(j\omega+1)^n$ does not enclose the origin.*
- *the plot of $\frac{p_{k1}(j\omega)}{p_{k0}(j\omega)}$ does not cross $(-\infty, 0]$ (the non-positive part of the real axis).*

where n is is the order of the principal term.

An example of the plots obtained as part of these graphical tests are shown in fig. 9.1. These plots pertain to an example presented in the paper of Tuzcu et al. which studies the robust stability of eq. (9.15) [137],

$$f(\lambda, q_1, q_2) = \lambda^3 + (7+q_1)\cdot\lambda^2 + (22+q_2)\cdot\lambda + (25+q_1+2\cdot q_2) + \Big((3-q_1+q_2)\cdot\lambda^2 + (7+q_1-q_2)\cdot\lambda + (5-q_2) \Big) \cdot e^{-\tau\cdot\lambda} \tag{9.15}$$

where each of q_1 and q_2 belong to $[-1, 1]$. They have been generated for $\tau = 0.5$s, as was done in the paper itself. Indeed, these plots are in alignment with the robustly stable time-delay regions obtained in the paper, which have been determined to be [0,0.5832]s, [0.9738,1.8561]s, and [2.7331,3.1289]s. This can be seen from the fact that the curves appearing on the left side of fig. 9.1 do not encircle the origin, and the ones on the right side do not cross the negative real axis, which does indeed support that the system eq. (9.15) is robustly stable for $\tau = 0.5$s.

9.2.1.1 Convex Directions

Many of the concepts that had been developed and used in the stability analysis of uncertain polynomials have been revisited and extended to the case of uncertain quasipolynomials, and the concept of convex directions is no exception to this. It has been initially combined with the edge theorem to reduce the test set for the stability analysis of polytopic polynomials. It was later extended by Kharitonov and Zhabko to the case of uncertain quasipolynomials [113].

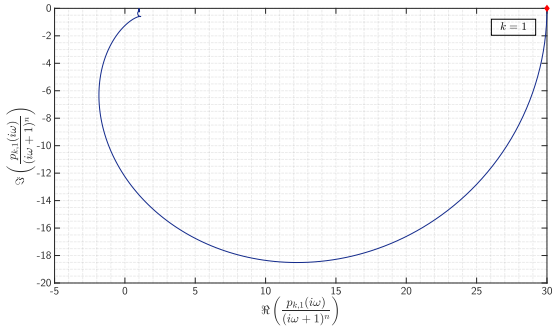

(a) The first test plot for the first edge of the polytope of quasipolynomials of eq. (9.15).

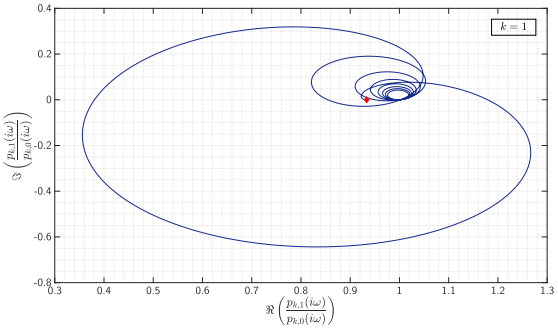

(b) The second test plot for the first edge of the polytope of quasipolynomials of eq. (9.15).

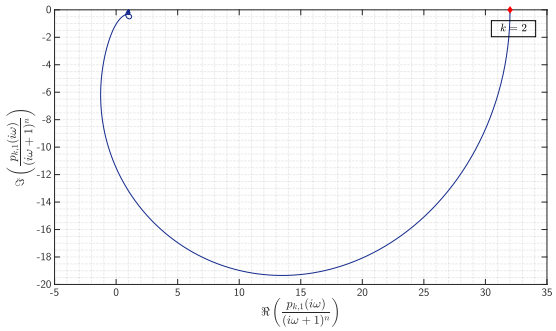

(c) The first test plot for the second edge of the polytope of quasipolynomials of eq. (9.15).

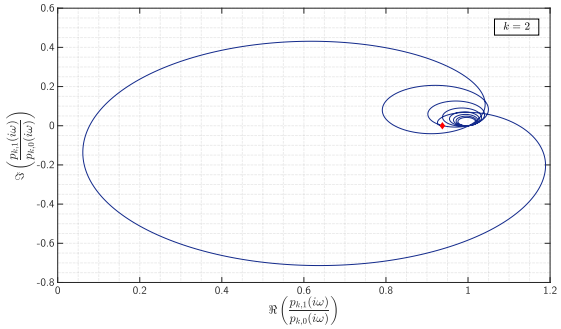

(d) The second test plot for the second edge of the polytope of quasipolynomials of eq. (9.15).

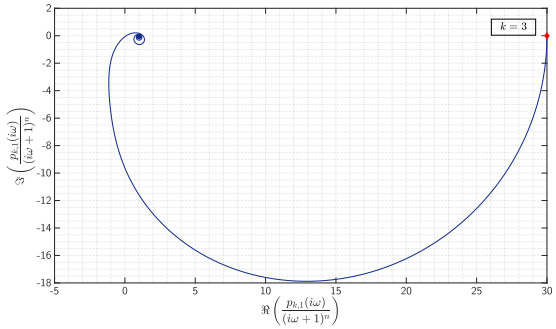

(e) The first test plot for the third edge of the polytope of quasipolynomials of eq. (9.15).

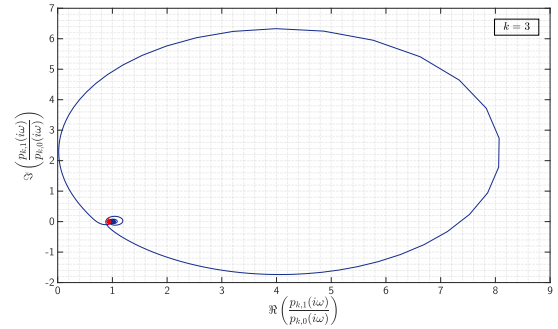

(f) The second test plot for the third edge of the polytope of quasipolynomials of eq. (9.15).

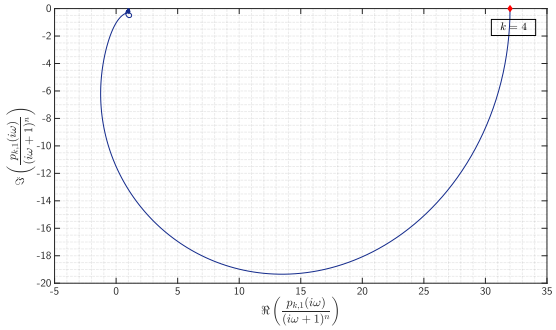

(g) The first test plot for the fourth edge of the polytope of quasipolynomials of eq. (9.15).

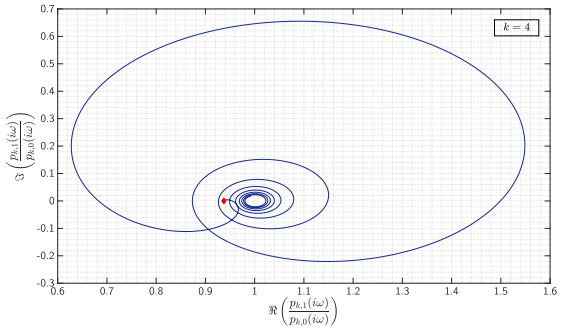

(h) The second test plot for the fourth edge of the polytope of quasipolynomials of eq. (9.15).

Figure 9.1: Plots showing the results of the tests for frequencies $\omega \in [0,100]$ rad/s (Note that the red diamond indicates the point corresponding to $\omega = 0$ rad/s).

Since the edge theorem is relied upon in the stability analysis of polytopic quasipolynomials, the test set is reduced to analyzing the stability of the edges of the polytope. A convex direction for such family of quasipolynomials is a quasipolynomial, usually denoted by $g(s)$, such that the stability of $f_0(s)$ and $f_0(s)+g(s)$ ensures the stability of $f_\mu(s)$ for all $\mu \in [0,1]$. That is why, it can be seen that finding a convex direction greatly reduces the test set of the family of polytopic quasipolynomials.

Theorem 9.3 (Necessary and Sufficient Conditions for a Convex Direction [75, 113]): *A quasipolynomial g(s) is a convex direction for the set of Hurwitz stable quasipolynomials of the form* $f(\lambda)=\sum_{i=0}^{m} p_i(\lambda)e^{-\tau_i\lambda}$ *if and only if for all* $\omega>0$ *where* $g(j\omega)\neq 0$ *the following inequality holds:*

$$\frac{\partial \arg(g(j\omega))}{\partial \omega} \leq -\frac{\tau_m}{2}+\left|\frac{\sin\left(2\arg(g(j\omega))+\tau_m\omega\right)}{2\omega}\right| \tag{9.16}$$

9.2.1.2 Finite Inclusions Theorem

The Finite Inclusions Theorem emerged as the byproduct of the Finite Nyquist Theorem as well as the Zero-Exclusion Principle. It was originally developed for the case of uncertain polynomials, and it has been extended to the case of uncertain quasipolynomials with independent and affine uncertainty structures, by Santos et al. [138–140]. In words, the theorem states that if it is possible to fit the value sets of the uncertain quasipolynomial inside sectors vertexed at the origin, then the system is stable.

9.2.2 Multilinear Uncertainty and the Mapping Theorem

While there have been discussions on the robust stability of interval and polytopic quasipolynomials, to the knowledge of the author, the discussion on the robust stability of multilinear and polynomic quasipolynomials has been mainly lacking. That is why, the literature on the robust stability of multilinear and polynomic polynomials is referred to as a starting point for the analysis of uncertain quasipolynomials with such uncertainty structures.

It is known that in the case of multilinear uncertainty structure that the vertex and edge results cannot be used for studying the robust stability of uncertain functions with multilinear uncertainty. For example, it may be the case that the system is stable for the parameters on the edges of the uncertainty bounding set. However, there may still be a point in the interior of the uncertainty bounding set such that the system is unstable.

This problem can be dealt with using the mapping theorem, which state states that for a set of uncertain parameters q_i (the set of which is denoted by Q) and a multilinear function f, such that $f(Q)=\{f(q): q\in Q\}$, the convex hull of $f(Q)$ is equal to the convex hull of the set $\{f(q_i)\}$ [10]. This is graphically explained with fig. 9.2 [10]. Formally, this is expressed as follows:

Theorem 9.4 (The Mapping Theorem [10]): *Suppose* $Q\subset \mathbf{R}^\ell$ *is a box with extreme points* $\left\{q^i\right\}$ *and* $f: Q\to \mathbf{R}^k$ *is multilinear. Let*

$$f(Q)=\{f(q): q\in Q\} \tag{9.17}$$

denote the range of f. Then it follows that

$$\operatorname{conv} f(Q)=\operatorname{conv}\left\{f\left(q^i\right)\right\} \tag{9.18}$$

Such overbounding of the value set with a convex polytope means that the edge theorem can now be applied to the overbounded value set. Consider, for example, the multilinear polynomial given by eq. (9.19),

$$\left(5+2q_1-q_2+3q_1q_2\right)+\left(7-6q_1-5q_2+10q_1q_2\right)\lambda \quad \text{where } q_1,q_2\in[0,1] \tag{9.19}$$

The value set for this function for some imaginary value, say $\lambda_0=1j$, is constructed. The result is shown as the blue scatter plot in fig. 9.3. Moreover, the convex hull of the evaluation at the extreme points of the bounding uncertainty set is shown in red. It is clear that the convex hull of the blue region in fig. 9.3 is indeed the red plot.

This is an example involving an uncertain polynomial. However, the mapping theorem was defined for generic functions, as can be seen in Theorem 9.4. Therefore, it is applicable to uncertain quasipolynomials as well. This will be demonstrated with an example that is similar to the one in eq. (9.19).

$$\left(5+2q_1-q_2+3q_1q_2\right)+\left(7-6q_1-5q_2+10q_1q_2\right)\lambda\cdot e^{-0.1\cdot\lambda} \quad \text{where } q_1,q_2\in[0,1] \tag{9.20}$$

The value set of this quasipolynomial for $\lambda=1j$ can be seen as the scatter plot shown in fig. 9.4. Moreover, the red contour is formed by the convex hull of the vertex quasipolynomials of this family of uncertain quasipolynomials. It is clear that indeed this convex hull is also the convex hull of the value set.

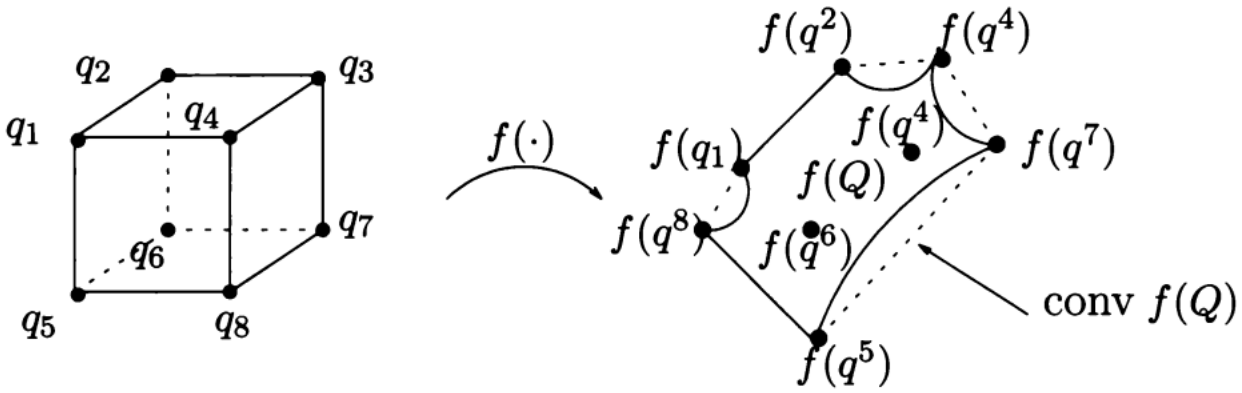

Figure 9.2: An illustration of the implication of the mapping theorem [10]

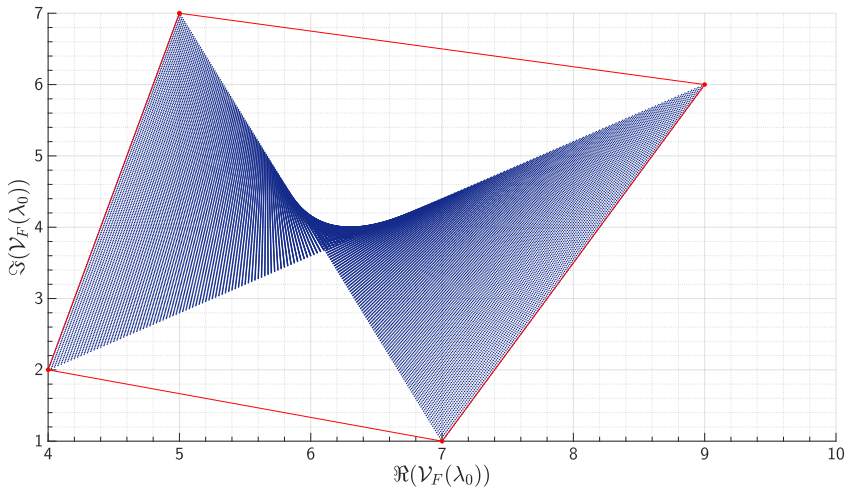

Figure 9.3: Value set of the function eq. (9.19) at $\lambda = 1\,j$

It should be noted that this solution comes at the cost of conservativeness. This means that the stability of the overbounded region is only sufficient for the stability of the actual range of the uncertain quasipolynomial. Hence, if the overbounded system is unstable, then a conclusion cannot be made about the stability of the system.

9.2.3 Polynomic Uncertainty

As in the case of dealing with a multilinear uncertainty structure, here too, the problem needs to be transformed into that of analyzing the stability of an uncertain system with an affine uncertainty structure, so that it is possible to apply the edge theorem.

It has already been established that a system with multilinear uncertainty can be overbounded with a system of an affine uncertainty structure. Thus, for the case of a system with polynomic uncertainty, only the means to transform a system with a polynomic uncertainty structure to that of a system with a multilinear uncertainty structure needs to be found. The solution to this problem, in the case of uncertain polynomials, is the following theorem which was proposed by Sideris and Sanchez Pena [141].

Theorem 9.5 ([141] as seen in [10]): *Consider the family of polynomials $\mathscr{P} = \{p(\cdot, q) : q \in Q\}$ with $p(s, q)$ having polynomic uncertainty structure and uncertainty bounding set Q which is a polytope. Then there exists a second family of polynomials $\tilde{\mathscr{P}} = \{\tilde{p}(\cdot, \tilde{q}) : \tilde{q} \in \tilde{Q}\}$ such that $\tilde{p}(s, \tilde{q})$ has multilinear uncertainty structure $\tilde{Q}$ is a polytope and*

$$\tilde{\mathscr{P}} = \mathscr{P} \tag{9.21}$$

Although this theorem has been developed for families of polynomials, this theorem may also be used to obtain an over-

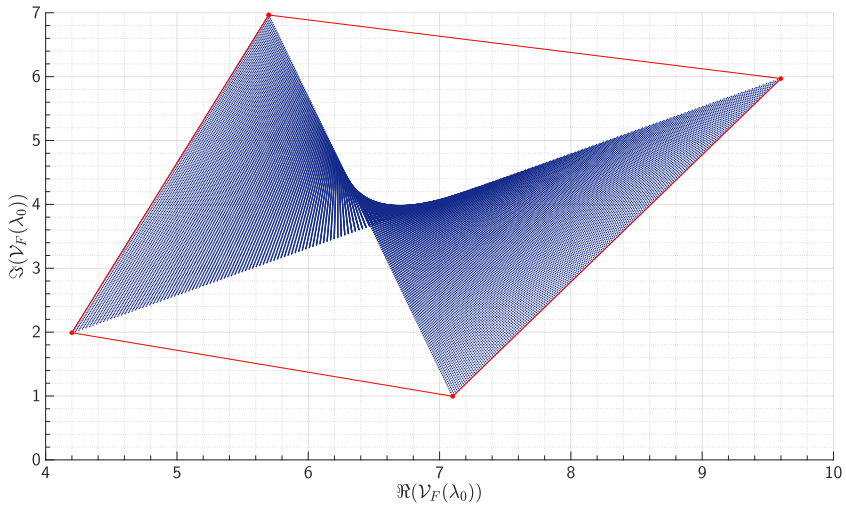

Figure 9.4: Value set of the function eq. (9.20) at $\lambda = 1\,j$

bounding set of the polynomic family of quasipolynomials. The reason for this is that a quasipolynomial is the sum of the product of polynomial and exponential terms. Thus, if the polynomic polynomials are transformed into equivalent polynomials with a multilinear structure, then a quasipolynomial with multilinear uncertainty is obtained.

In order to demonstrate how this can be done, consider the example uncertain quasipolynomial shown in eq. (9.22), which has a polynomic uncertainty structure due to the term q_2^2.

$$\left(5+2q_1-q_2^2+3q_1q_2\right)+\left(7-6q_1-5q_2+10q_1q_2\right)\lambda\cdot e^{-0.1\cdot\lambda} \quad \text{where } q_1,q_2\in[0,1] \tag{9.22}$$

The value set of eq. (9.22) is shown in fig. 9.5. Clearly, the convex hull of the vertex quasipolynomials (the red contour) does not contain all of the value set (the blue scatter plot). In other words, unlike in the cases of affine and multilinear uncertainty structures, the vertex quasipolynomials are not the generator quasipolynomials, where the generator quasipolynomials are quasipolynomials that can be used to construct the convex hull of the family of quasipolynomials.

In order to be able to apply the edge theorem, the generators of the convex hull of the value set need to be determined, and this is facilitated with Theorem 9.5. Based on the theorem, the following transformation is obtained:

$$q_2^2 \rightarrow \tilde{q}_2\cdot\tilde{q}_3 \tag{9.23}$$

This means that the quasipolynomial eq. (9.22) is equivalent to the uncertain quasipolynomial shown in eq. (9.24).

$$\left(5+2q_1-\tilde{q}_2\tilde{q}_3+3q_1\tilde{q}_2\right)+\left(7-6q_1-5\tilde{q}_2+10q_1\tilde{q}_2\right)\lambda\cdot e^{-0.1\cdot\lambda} \quad \text{where } q_1,\tilde{q}_2=\tilde{q}_3\in[0,1] \tag{9.24}$$

Based on this reformulation, the new obtained bounding contour contains the entire value set. This can be seen in fig. 9.6.

Remark 9.2 (Refinement for Tighter Bound on the Value Set): *Note that, in the construction of the convex hull, the relation $\tilde{q}_2=\tilde{q}_3$ is not accounted for. In order to heed this dependence, a concept from interval analysis which is refinement can be used. Refinement entails that breaking down the uncertainty bounding set into parts and performing the analysis on these parts will lead to less conservative results than performing the stability analysis for the original uncertainty bounding set.*
For example, consider eq. (9.24) again. Its bounding set is $Q: q_1, \tilde{q}_2=\tilde{q}_3\in[0,1]$. If this bounding set is split up into two bounding sets $Q_a: q_1\in[0,0.5], \tilde{q}_2=\tilde{q}_3\in[0,1]$ and $Q_b: q_1\in[0.5,1], \tilde{q}_2=\tilde{q}_3\in[0,1]$, then the obtained value sets for $\lambda=1\,j$ rad/s are shown in fig. 9.7a and fig. 9.7b. From these figures, it is seen that the union of the regions enclosed by the red contours in fig. 9.7a and fig. 9.7b is smaller than the region enclosed by the red contour in fig. 9.6. This means that the intersection of the obtained stability results from performing the analyses for Q_a and Q_b is expected to be less conservative than the result obtained from performing the stability analysis for Q.

Remark 9.3 (Gridding Approach): *Another approach which can be applied is to grid the uncertainty set and perform the stability analysis at each grid point in the stability set. This approach will be used to verify the results of the robust stability analysis. Albeit*

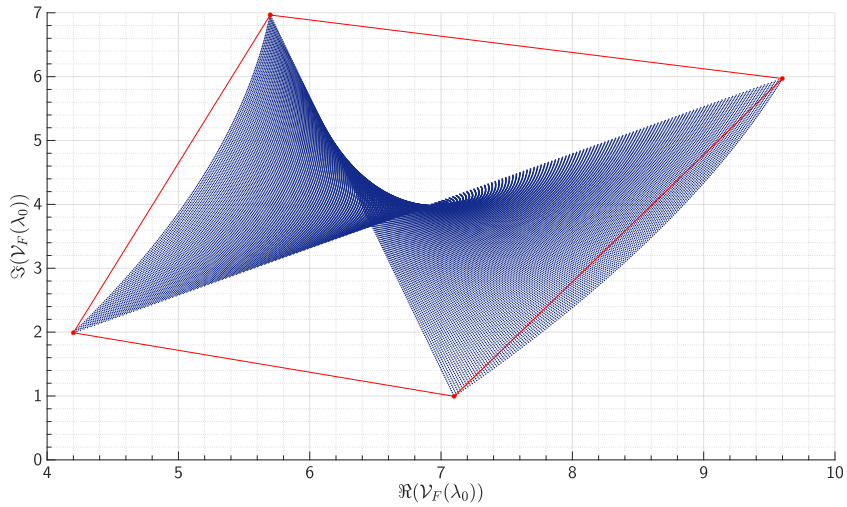

Figure 9.5: Value set of eq. (9.22) for $\lambda = 1\,j$ rad/s.

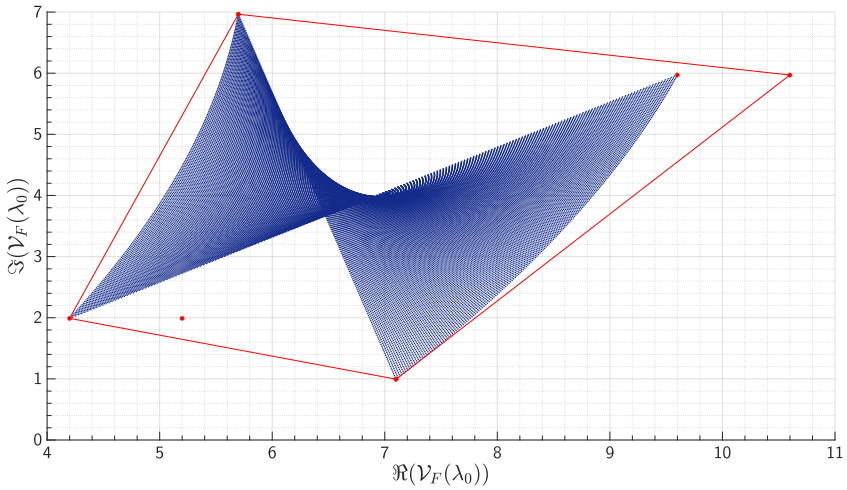

Figure 9.6: Value set of eq. (9.24) at for $\lambda = 1\,j$ rad/s.

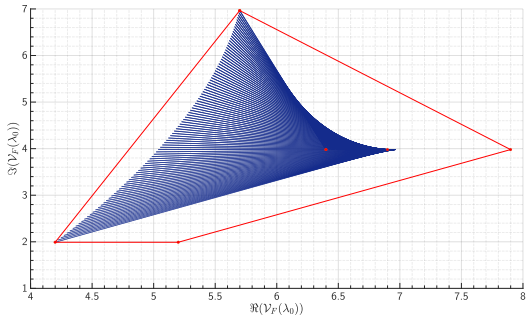

(a) Value set of eq. (9.24) at for $\lambda = 1\,j$ rad/s for $q_1 \in [0.5, 1]$ and $\tilde{q}_2, \tilde{q}_3 \in [0.5, 1]$.

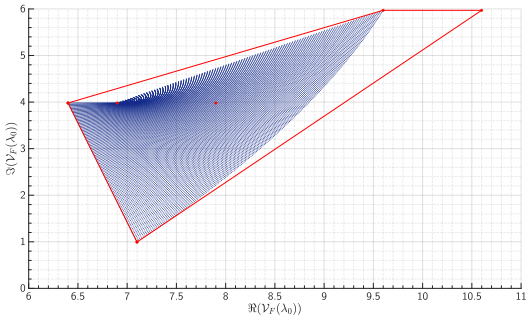

(b) Value set of eq. (9.24) at for $\lambda = 1\,j$ rad/s for $q_1 \in [0.5, 1]$ and $\tilde{q}_2, \tilde{q}_3 \in [0, 0.5]$.

computationally intensive, it is important to make in order to verify the correctness of the implemented robust stability analysis methods.

This page was intentionally left blank.

IV

Additional Results

This page was intentionally left blank.

10

Proposed Stability Results for Neutral Time-delay Systems

In this chapter, an extension of the previously presented stability results summarized in Theorem 6.7, whose derivation was reviewed in section 6.6, to the case of neutral TDSs is proposed. As a first step, consider a neutral TDS of the form shown in eq. (10.1).

$$\begin{aligned} &\dot{x}(t) - C\dot{x}(t-\tau) = A_0 x(t) + A_1 x(t-\tau) \\ &x(t) = \phi(t), \quad t \in [-\tau, 0] \end{aligned} \tag{10.1}$$

It should be noted that analyzing the stability of neutral TDSs requires taking into account two particular aspects. First, for the case of neutral TDSs, there is an additional necessary condition for stability which is that the strong stability of the delay-difference operator needs to be ensured. This can be checked using the Schur-Cohn stability criterion on the matrix C. This means that the delay-difference operator of the neutral TDS is strongly stable if the eigenvalues of the matrix C lie within a unit circle. This is expressed in eq. (10.2).

$$\|\lambda_i(C)\| < 1 \tag{10.2}$$

The second aspect that needs to be taken into account is that the complete Lyapunov-Krasovskii functional for the case of neutral TDSs is slightly different than that of a retarded TDS. Several complete Lyapunov functionals for neutral TDSs have been derived. For example, in [124] and [125], the functional shown in eq. (10.3) is used.

$$\begin{aligned} V(x_t) = &\left[x(t) - Cx(t-\tau)\right]^\top \cdot P \cdot \left[x(t) - Cx(t-\tau)\right] + 2 \cdot \left[x(t) - Cx(t-\tau)\right]^\top \int_{-\tau}^{0} Q(\theta) x_t(\theta) \mathrm{d}\theta \\ &+ \int_{-\tau}^{0} \int_{-\tau}^{0} x_t^\top(\theta_1)\, T(\theta_1, \theta_2)\, x_t(\theta_2)\, \mathrm{d}\theta_1 \mathrm{d}\theta_2 + \int_{-\tau}^{0} x_t^\top(\theta) S(\theta) x_t(\theta) \mathrm{d}\theta \end{aligned} \tag{10.3}$$

However, according to Xu-guang et al. [118], the functional is not general enough. Instead, they propose to use the functional shown in eq. (10.4) which includes an additional term shown at the end of the equation, which is $\int_{-\tau}^{0} \dot{x}_t^\top(\theta) R(\theta) \dot{x}_t(\theta) \mathrm{d}\theta$.

$$\begin{aligned} V(x_t) = &\left[x(t) - Cx(t-\tau)\right]^\top \cdot P \cdot \left[x(t) - Cx(t-\tau)\right] + 2 \cdot \left[x(t) - Cx(t-\tau)\right]^\top \int_{-\tau}^{0} Q(\theta) x_t(\theta) \mathrm{d}\theta \\ &+ \int_{-\tau}^{0} \int_{-\tau}^{0} x_t^\top(\theta_1)\, T(\theta_1, \theta_2)\, x_t(\theta_2)\, \mathrm{d}\theta_1 \mathrm{d}\theta_2 + \int_{-\tau}^{0} x_t^\top(\theta) S(\theta) x_t(\theta) \mathrm{d}\theta \\ &+ \int_{-\tau}^{0} \dot{x}_t^\top(\theta) X(\theta) \dot{x}_t(\theta) \mathrm{d}\theta \end{aligned} \tag{10.4}$$

The same discretizations for the matrices Q, T, and S, which were used in the case of retarded TDSs and as was done in [110], will be taken here as well.

$$\begin{aligned} Q(\theta) &= \sum_{i=0}^{N} Q_i L_i(\theta) \\ T(\theta,\lambda) &= \sum_{i=0}^{N}\sum_{j=0}^{N} L_i(\theta) L_j(\lambda) T_{ij} \\ S(\theta) &= S + (\tau+\theta)R \end{aligned} \tag{10.5}$$

Similar to the case of matrix S, a piece-wise linear discretization is applied to matrix $X(\theta)$, as shown in eq. (10.6):

$$X(\theta) = X + (\tau+\theta)Y \tag{10.6}$$

In the following, the expansion and the manipulation of the terms in eq. (10.4) to obtain their quadratic forms will be presented. An augmented state is proposed, denoted by ξ_N, and its definition is shown in eq. (10.7). It will become clear why such an augmentation is needed.

$$\xi_N(t) = \begin{bmatrix} x_t(0) \\ x_t(-\tau) \\ \frac{1}{\tau}\int_{-\tau}^{0} L_0(s)x_t(s)\mathrm{d}s \\ \vdots \\ \frac{1}{\tau}\int_{-\tau}^{0} L_N(s)x_t(s)\mathrm{d}s \end{bmatrix}^{\top}, \quad N \geq 0 \tag{10.7}$$

The derivation of the quadratic form for term 1 from eq. (10.4), in terms of the augmented state ξ_N, is shown in eq. (10.8).

$$\begin{aligned} &[x(t)-Cx(t-\tau)]^{\top} P [x(t)-Cx(t-\tau)] \\ &= \left[x^{\top}(t) - x^{\top}(t-\tau)C^{\top}\right] P [x(t)-Cx(t-\tau)] \\ &= x^{\top}(t)Px(t) - x^{\top}(t)PCx(t-\tau) - x^{\top}(t-\tau)C^{\top}Px(t) + x^{\top}(t-\tau)C^{\top}PCx(t-\tau) \\ &= \xi_N^{\top} \begin{bmatrix} P & 0 & \cdots & 0 \\ 0 & 0 & \cdots & 0 \\ 0 & 0 & \cdots & 0 \\ \vdots & \vdots & & \vdots \\ 0 & 0 & \cdots & 0 \end{bmatrix} \xi_N + \xi_N^{\top} \begin{bmatrix} 0 & -PC & 0 & \cdots & 0 \\ 0 & 0 & 0 & \cdots & 0 \\ 0 & 0 & 0 & \cdots & 0 \\ \vdots & \vdots & \vdots & & \vdots \\ 0 & 0 & 0 & \cdots & 0 \end{bmatrix} \xi_N + \xi_N^{\top} \begin{bmatrix} 0 & 0 & \cdots & 0 \\ -C^{\top}P & 0 & \cdots & 0 \\ 0 & 0 & \cdots & 0 \\ \vdots & \vdots & & \vdots \\ 0 & 0 & \cdots & 0 \end{bmatrix} \xi_N + \xi_N \begin{bmatrix} 0 & 0 & 0 & 0 & 0 \\ 0 & C^{\top}PC & 0 & \dots & 0 \\ 0 & 0 & 0 & \dots & 0 \\ \vdots & \vdots & \vdots & & \vdots \\ 0 & 0 & 0 & \cdots & 0 \end{bmatrix} \xi_N \\ &= \xi_N^{\top} \begin{bmatrix} P & -PC & 0 & \cdots & 0 \\ -C^{\top}P & C^{\top}PC & 0 & \cdots & 0 \\ 0 & 0 & 0 & \cdots & 0 \\ \vdots & \vdots & \vdots & & \vdots \\ 0 & 0 & 0 & \cdots & 0 \end{bmatrix} \xi_N \end{aligned} \tag{10.8}$$

As for term 2 of eq. (10.4), obtaining its quadratic form is shown in eq. (10.9).

$$
\begin{aligned}
&2\cdot\left[x(t)-Cx(t-\tau)\right]^{\top}\int_{-\tau}^{0}Q(\theta)x_t(\theta)\mathrm{d}\theta\\
&=2\cdot x^{\top}(t)\int_{-\tau}^{0}Q(\theta)x_t(\theta)\mathrm{d}\theta-2x^{\top}(t-\tau)C^{\top}\int_{-\tau}^{0}Q(\theta)x_t(\theta)\mathrm{d}\theta\\
&=2\cdot x^{\top}(t)\int_{-\tau}^{0}\left(\sum_{i=0}^{N}Q_iL_i(\theta)\right)x_t(\theta)\mathrm{d}\theta-2x^{\top}(t-\tau)C^{\top}\int_{-\tau}^{0}\left(\sum_{i=0}^{N}Q_iL_i(\theta)\right)x_t(\theta)\mathrm{d}\theta\\
&=2\xi_N^{\top}\begin{bmatrix}0&0&\tau\cdot Q_0&\tau\cdot Q_1&\dots&\tau\cdot Q_N\\0&0&0&0&\dots&0\\\vdots&\vdots&\vdots&\vdots&&\vdots\\0&0&0&0&\cdots&0\end{bmatrix}\xi_N-2\xi_N^{\top}\begin{bmatrix}0&0&0&0&\dots&0\\0&0&\tau\cdot C^{\top}Q_0&\tau\cdot C^{\top}Q_1&\dots&\tau\cdot C^{\top}Q_N\\0&0&0&0&\dots&0\\\vdots&\vdots&\vdots&\vdots&&0\\0&0&0&0&\dots&0\end{bmatrix}\xi_N\\
&=\xi_N^{\top}\begin{bmatrix}0&0&2\tau\cdot Q_0&2\tau\cdot Q_1&\dots&2\tau\cdot Q_N\\0&0&-2\tau\cdot C^{\top}Q_0&-2\tau\cdot C^{\top}Q_1&\dots&-2\tau\cdot C^{\top}Q_N\\\vdots&\vdots&\vdots&\vdots&&\vdots\\0&0&0&0&\cdots&0\end{bmatrix}\xi_N
\end{aligned}
\tag{10.9}
$$

Making this contribution symmetric, the expression in eq. (10.10) is obtained.

$$
\xi_N^{\top}\begin{bmatrix}0&0&\tau\cdot Q_0&\tau\cdot Q_1&\dots&\tau\cdot Q_N\\0&0&-\tau\cdot C^{\top}Q_0&-\tau\cdot C^{\top}Q_1&\dots&-\tau\cdot C^{\top}Q_N\\\tau\cdot Q_0^{\top}&-\tau\cdot Q_0^{\top}C&0&0&\dots&0\\\tau\cdot Q_1^{\top}&-\tau\cdot Q_1^{\top}C&0&0&\cdots&0\\\vdots&\vdots&\vdots&\vdots&&\vdots\\\tau\cdot Q_N^{\top}&-\tau\cdot Q_N^{\top}C&0&0&\cdots&0\end{bmatrix}\xi_N
\tag{10.10}
$$

As for term 3 in eq. (10.4), the contribution is the same as was in the case of the retarded TDS, and it is shown in eq. (10.11).

$$
\xi_N^{\top}G_N^{\top}\begin{bmatrix}0&0&\dots&0\\0&T_{00}&\dots&T_{0N}\\\vdots&\vdots&&\vdots\\0&T_{N0}&\dots&T_{NN}\end{bmatrix}G_N\xi_N
\tag{10.11}
$$

where

$$
G_N(\tau)=\begin{bmatrix}I&0_n&0_{n,n(N+1)}\\0_{n(N+1),n}&0_{n(N+1),n}&\tau I_{n(N+1)}\end{bmatrix}
\tag{10.12}
$$

At this point, it is possible to group the contributions of the first three terms of eq. (10.4). Thus, the expression for may be rewritten as shown in eq. (10.13).

$$
V_{N_2}=\xi_N^{\top}P_{N_2}\xi_N+\int_{-\tau}^{0}x^{\top}(\theta)(S+(\tau+\theta)R)x(\theta)\mathrm{d}\theta+\int_{-\tau}^{0}\dot{x}^{\top}(\theta)(X+(\tau+\theta)Y)\dot{x}(\theta)\mathrm{d}\theta
\tag{10.13}
$$

where

$$P_{N_2} = \begin{bmatrix} P & -PC & 0 & \cdots & 0 \\ -C^\top P & C^\top PC & 0 & \cdots & 0 \\ 0 & 0 & 0 & \cdots & 0 \\ \vdots & \vdots & \vdots & & \vdots \\ 0 & 0 & 0 & \cdots & 0 \end{bmatrix} + \begin{bmatrix} 0 & 0 & \tau\cdot Q_0 & \tau\cdot Q_1 & \dots & \tau\cdot Q_N \\ 0 & 0 & -\tau\cdot C^\top Q_0 & -\tau\cdot C^\top Q_1 & \dots & -\tau\cdot C^\top Q_N \\ \tau\cdot Q_0^\top & -\tau\cdot Q_0^\top C & 0 & 0 & \dots & 0 \\ \tau\cdot Q_1^\top & -\tau\cdot Q_1^\top C & 0 & 0 & \cdots & 0 \\ \vdots & \vdots & \vdots & \vdots & & \vdots \\ \tau\cdot Q_N^\top & -\tau\cdot Q_N^\top C & 0 & 0 & \cdots & 0 \end{bmatrix} \tag{10.14}$$
$$+ G_N^\top \begin{bmatrix} 0 & 0 & \dots & 0 \\ 0 & T_{00} & \dots & T_{0N} \\ \vdots & \vdots & & \vdots \\ 0 & T_{N0} & \dots & T_{NN} \end{bmatrix} G_N$$

For term 4 of eq. (10.4), the Bessel-Legendre inequality is applied (see Lemma 6.5). Moreover, some modifications to account for the fact that the expression needs to be in terms of $\xi_N(t)$, rather than $\tilde{x}_N(t)$, are made.

$$\begin{aligned} \int_{-\tau}^{0} x^\top(s) S x(s) \mathrm{d}s &\geq \frac{1}{\tau} \tilde{x}_N^\top(t)\, \mathrm{diag}(0, S, 3S, \dots, (2N+1)S)\, \tilde{x}_N^\top(t) \\ &= \frac{1}{\tau} \xi_N^\top(t) G_N^\top \mathrm{diag}(0, S, 3S, \dots, (2N+1)S) G_N \xi_N \end{aligned} \tag{10.15}$$

which is also equivalent to

$$\int_{-\tau}^{0} x^\top(s) S x(s) \mathrm{d}s \geq \frac{1}{\tau} \xi_N^\top(t)\, \mathrm{diag}(0, 0, S, 3S, \dots, (2N+1)S)\, \xi_N \tag{10.16}$$

As for term 5 in eq. (10.4), based on eq. (10.6)

$$\int_{-\tau}^{0} \dot{x}_t^\top(\theta) X(\theta) \dot{x}_t(\theta) d\theta = \int_{-\tau}^{0} \dot{x}_t^\top(\theta) [X + (\tau+\theta) Y] \dot{x}_t(\theta) d\theta = \int_{-\tau}^{0} \dot{x}_t^\top(\theta) X \dot{x}_t(\theta) d\theta + \int_{-\tau}^{0} \dot{x}_t^\top(\theta) [(\tau+\theta) Y] \dot{x}_t(\theta) d\theta \tag{10.17}$$

With regards to the first term in eq. (10.17)

$$\begin{aligned} \int_{-\tau}^{0} \dot{x}_t^\top(\theta) X \dot{x}_t(\theta) ds &\geqslant \frac{1}{\tau} \begin{bmatrix} \int_{-\tau}^{0} L_0(s)\dot{x}(s) ds \\ \vdots \\ \int_{0}^{0} L_N(s)\dot{x}(s) ds \end{bmatrix}^\top \mathrm{diag}(X, 3X, \dots, (2N+1)X) \begin{bmatrix} \int_{-\tau}^{0} L_0(s)\dot{x}(s) ds \\ \vdots \\ \int_{0}^{0} L_N(s)\dot{x}(s) ds \end{bmatrix} \\ &= \frac{1}{\tau} \dot{\tilde{x}}_N^\top \mathrm{diag}\left(0, X, 3X, \dots, (2N+1)X\right) \dot{\tilde{x}}_N \\ &= \frac{1}{\tau} \xi_N^\top H_N^\top \mathrm{diag}\left(0, X, 3X, \dots, (2N+1)X\right) H_N \xi_N \end{aligned} \tag{10.18}$$

The contributions from the terms can be combined, and the result is eq. (10.19).

$$V_{N_2}\left(x_t\right) \geq \xi_N^\top \Phi_{N_2}^{+}(\tau) \xi_N + \int_{-\tau}^{0} x_t^\top(\theta) [(\tau+\theta) R] x_t(\theta) d\theta + \int_{-\tau}^{0} \dot{x}_t^\top(\theta) [(\tau+\theta) Y] \dot{x}_t(\theta) d\theta \tag{10.19}$$

where

$$\Phi^{+}_{N_2}(\tau) = \begin{bmatrix} P & -PC & 0 & \cdots & 0 \\ -C^\top P & C^\top PC & 0 & \cdots & 0 \\ 0 & 0 & 0 & \cdots & 0 \\ \vdots & \vdots & \vdots & & \vdots \\ 0 & 0 & 0 & \cdots & 0 \end{bmatrix} + \begin{bmatrix} 0 & 0 & \tau\cdot Q_0 & \tau\cdot Q_1 & \dots & \tau\cdot Q_N \\ 0 & 0 & -\tau\cdot C^\top Q_0 & -\tau\cdot C^\top Q_1 & \dots & -\tau\cdot C^\top Q_N \\ \tau\cdot Q_0^\top & -\tau\cdot Q_0^\top C & 0 & 0 & \dots & 0 \\ \tau\cdot Q_1^\top & -\tau\cdot Q_1^\top C & 0 & 0 & \cdots & 0 \\ \vdots & \vdots & \vdots & \vdots & & \vdots \\ \tau\cdot Q_N^\top & -\tau\cdot Q_N^\top C & 0 & 0 & \cdots & 0 \end{bmatrix}$$
$$+ G_N^\top \begin{bmatrix} 0 & 0 & \dots & 0 \\ 0 & T_{00} & \dots & T_{0N} \\ \vdots & \vdots & & \vdots \\ 0 & T_{N0} & \dots & T_{NN} \end{bmatrix} G_N + \frac{1}{\tau} G_N^\top \operatorname{diag}(0, S, 3S, \dots, (2N+1)S) G_N$$
$$+ \frac{1}{\tau} H_N^\top \operatorname{diag}\left(0, X, 3X, \dots, (2N+1)X\right) H_N \tag{10.20}$$

The positive definiteness of the expression for the lower bound in eq. (10.19) needs to be ensured. Towards this goal, the following result is proposed:

Proposition 10.1 (Lyapunov Functional Condition): *The positive definiteness of the Lyapunov Functional Condition V is ensured when the following expressions hold:*

$$\begin{cases} \Phi^{+}_{N_2}(\tau) > 0 \\ R > 0 \\ Y > 0 \end{cases} \tag{10.21}$$

where $\Phi^{+}_{N_2}(\tau)$ is defined in eq. (10.20).

Taking the derivative of eq. (10.13), eq. (10.22) is obtained.

$$\begin{aligned} \dot{V}_{N_2}\left(x_t\right) = {} & 2\xi_N^\top P_{N_2} \dot{\xi}_N + x_t^\top(0)(S+\tau R)x_t(0) - x_t^\top(-\tau) S x_t(-\tau) - \int_{-\tau}^{0} x_t^\top(s) R x_t(s) \mathrm{d}s \\ & + \dot{x}_t^\top(0)(X+\tau Y)\dot{x}_t(0) - \dot{x}_t^\top(-\tau) X \dot{x}_t(-\tau) - \int_{-\tau}^{0} \dot{x}_t^\top(s) Y \dot{x}_t(s) \mathrm{d}s \end{aligned} \tag{10.22}$$

The expression for $\dot{\xi}_N(t)$ is based on taking the derivative of eq. (10.7) with respect to time. This leads to eq. (10.23).

$$\dot{\xi}_N(t) = \begin{bmatrix} \dot{x}_t(0) \\ \dot{x}_t(-\tau) \\ \frac{1}{\tau}\int_{-\tau}^{0} L_0(s)\dot{x}_t(s)ds \\ \vdots \\ \frac{1}{\tau}\int_{-\tau}^{0} L_N(s)\dot{x}_t(s)ds \end{bmatrix} \quad , \quad N \geq 0 \tag{10.23}$$

By applying integration by parts and making use of the properties of the Legendre polynomials, then $\int_{-\tau}^{0} L_k(s)\dot{x}_t(s)ds$ evaluates to the expression shown in eq. (10.24).

$$\begin{aligned} \int_{-\tau}^{0} L_k(s)\dot{x}_t(s)ds &= L_k(s)x_t(s)\Big|_{-\tau}^{0} - \int_{-\tau}^{0} L_k(s)x_t(s)ds \\ &= L_k(0)x_t(0) - L_k(-\tau)x_t(-\tau) - \int_{-\tau}^{0} L_k^{\cdot}(s)\cdot x_t(s)ds \\ &= x_t(0) + (-1)^{k+1}x_t(-\tau) - \sum_{i=0}^{k-1}\frac{(2i+1)}{\tau}\left(1-(-1)^{k+i}\right)\int_{-\tau}^{0} L_i(s)x_t(s)ds \\ &= \Gamma_N(k)\xi_N(t) \end{aligned} \tag{10.24}$$

Moreover, $\dot{x}_t(0)$ can be expressed according to eq. (10.25).

$$\dot{x}_t(0) = A_0 x_t(0) + A_1 x_t(-\tau) + C\cdot\dot{x}_t(-\tau) \tag{10.25}$$

Incorporating those results into the expression for $\dot{\xi}_N(t)$ from eq. (10.23), the following is obtained.

$$\dot{\xi}_N(t) = \begin{bmatrix} A_0 x_t(0) + A_1 x_t(-\tau) + C \cdot \dot{x}_t(-\tau) \\ \dot{x}_t(-\tau) \\ \frac{1}{\tau}\Gamma_N(0)\xi_N(t) \\ \vdots \\ \frac{1}{\tau}\Gamma_N(N)\xi_N(t) \end{bmatrix} \quad , \quad N \geq 0 \tag{10.26}$$

From eq. (10.26), it can be seen that another augmentation of the state vector is due. In particular, $\dot{x}_t(-\tau)$ has to be added to the vector $\xi_N(t)$ to form a new vector which shall be denoted as $\psi_N(t)$.

$$\psi_N(t) = \begin{bmatrix} x_t(0) \\ x_t(-\tau) \\ \dot{x}_t(-\tau) \\ \frac{1}{\tau}\int_{-\tau}^{0} L_0(s)x_t(s)\mathrm{d}s \\ \vdots \\ \frac{1}{\tau}\int_{-\tau}^{0} L_N(s)x_t(s)\mathrm{d}s \end{bmatrix}, \quad N \geq 0 \tag{10.27}$$

In order to rewrite the expression for $\dot{V}_{N_2}\left(x_t\right)$ in terms of $\psi_N(t)$, the transformation between $\psi_N(t)$ and $\xi_N(t)$ has to be established. This transformation, denoted by J_N, is shown in eq. (10.28).

$$\begin{aligned} \xi_N(t) &= J_N \psi_N(t) \\ J_N &= \begin{bmatrix} I_{2n,2n} & 0_{2n,n} & 0_{2n,n(N+1)} \\ 0_{n(N+1),2n} & 0_{n(N+1),n} & I_{n(N+1),n(N+1)} \end{bmatrix} \end{aligned} \tag{10.28}$$

Note, that the transformation, in contrast to G_N, does not depend on τ. Rewriting the expression for $\dot{\xi}_N(t)$ in terms of $\psi_N(t)$ leads to eq. (10.29).

$$\begin{aligned} \dot{\xi}_N(t) &= \begin{bmatrix} A_0 x_t(0) + A_1 x_t(-\tau) + C \cdot \dot{x}_t(-\tau) \\ \dot{x}_t(-\tau) \\ \frac{1}{\tau}\Gamma_N(0) J_N \psi_N(t) \\ \vdots \\ \frac{1}{\tau}\Gamma_N(N) J_N \psi_N(t) \end{bmatrix} \quad , \quad N \geq 0 \\ &= \begin{bmatrix} \begin{bmatrix} A_0 & A_1 & C & 0_{n,n(N+1)} \end{bmatrix} \psi_N(t) \\ \begin{bmatrix} 0_{n,2n} & I_{n,n} & 0_{n,n\cdot(N+1)} \end{bmatrix} \psi_N(t) \\ \frac{1}{\tau}\Gamma_N(0) J_N \psi_N(t) \\ \vdots \\ \frac{1}{\tau}\Gamma_N(N) J_N \psi_N(t) \end{bmatrix} \quad , \quad N \geq 0 \\ &= \begin{bmatrix} A_0 & A_1 & C & 0_{n,n(N+1)} \\ 0_{n,2n} & I_{n,n} & 0_{n,n\cdot(N+1)} \\ \frac{1}{\tau}\Gamma_N(0) J_N \\ \vdots \\ \frac{1}{\tau}\Gamma_N(N) J_N \end{bmatrix} \psi_N(t) \quad , \quad N \geq 0 \end{aligned} \tag{10.29}$$

Thus, the first term in the expression for $\dot{V}_{N_2}\left(x_t\right)$, shown in eq. (10.22), becomes:

$$
\begin{aligned}
2\xi_N^\top P_{N_2}\dot{\xi}_N &= 2(J_N\psi_N(t))^\top P_{N_2}\begin{bmatrix} A_0 & A_1 & C & 0_{n,n(N+1)} \\ 0_{n,2n} & I_{n,n} & 0_{n,n\cdot(N+1)} \\ & \frac{1}{\tau}\Gamma_N(0)J_N & \\ & \vdots & \\ & \frac{1}{\tau}\Gamma_N(N)J_N & \end{bmatrix}\psi_N(t) \\
&= 2\psi_N^\top(t)J_N^\top P_{N_2}\begin{bmatrix} A_0 & A_1 & C & 0_{n,n(N+1)} \\ 0_{n,2n} & I_{n,n} & 0_{n,n\cdot(N+1)} \\ & \frac{1}{\tau}\Gamma_N(0)J_N & \\ & \vdots & \\ & \frac{1}{\tau}\Gamma_N(N)J_N & \end{bmatrix}\psi_N(t) \\
&= 2\psi_N^\top(t)\frac{1}{2}\mathrm{He}\left(J_N^\top P_{N_2}\begin{bmatrix} A_0 & A_1 & C & 0_{n,n(N+1)} \\ 0_{n,2n} & I_{n,n} & 0_{n,n\cdot(N+1)} \\ & \frac{1}{\tau}\Gamma_N(0)J_N & \\ & \vdots & \\ & \frac{1}{\tau}\Gamma_N(N)J_N & \end{bmatrix}\right)\psi_N(t) \\
&= \psi_N^\top(t)\underbrace{\mathrm{He}\left(J_N^\top P_{N_2}\begin{bmatrix} A_0 & A_1 & C & 0_{n,n(N+1)} \\ 0_{n,2n} & I_{n,n} & 0_{n,n\cdot(N+1)} \\ & \frac{1}{\tau}\Gamma_N(0)J_N & \\ & \vdots & \\ & \frac{1}{\tau}\Gamma_N(N)J_N & \end{bmatrix}\right)}_{\text{Contribution 1}}\psi_N(t)
\end{aligned}
\tag{10.30}
$$

Re-writing the second term of eq. (10.22), in terms of the new vector $\psi_N(t)$, eq. (10.31) is obtained.

$$
x_t^\top(0)(S+\tau R)x_t(0) = \psi_N^\top(t)\underbrace{\begin{bmatrix} S+\tau R & 0 & \cdots & 0 \\ 0 & 0 & \cdots & 0 \\ \vdots & \vdots & & \vdots \\ 0 & 0 & \cdots & 0 \end{bmatrix}}_{\text{Contribution 2}}\psi_N(t) \tag{10.31}
$$

As for the third term of $\dot{V}_{N_2}\left(x_t\right)$ (eq. (10.22)):

$$
-x_t^\top(-\tau)Sx_t(-\tau) = -\psi_N^\top(t)\begin{bmatrix} 0 & 0 & 0 & \dots & 0 \\ 0 & S & 0 & \dots & 0 \\ 0 & 0 & 0 & \dots & 0 \\ \vdots & \vdots & \vdots & & \vdots \\ 0 & 0 & 0 & \dots & 0 \end{bmatrix}\psi_N(t) = \psi_N^\top(t)\underbrace{\begin{bmatrix} 0 & 0 & 0 & \dots & 0 \\ 0 & -S & 0 & \dots & 0 \\ 0 & 0 & 0 & \dots & 0 \\ \vdots & \vdots & \vdots & & \vdots \\ 0 & 0 & 0 & \dots & 0 \end{bmatrix}}_{\text{Contribution 3}}\psi_N(t) \tag{10.32}
$$

With regards to the integral terms $-\int_{-\tau}^0 x_t^\top(s)Rx_t(s)\mathrm{d}s$ and $-\int_{-\tau}^0 \dot{x}_t^\top(s)Y\dot{x}_t(s)\mathrm{d}s$, they are overapproximated with the Bessel-Legendre inequality (Lemma 6.5).

$$
\begin{aligned}
-\int_{-\tau}^0 x_t^\top(s)Rx_t(s)\mathrm{d}s &\leq -\frac{1}{\tau}\tilde{x}_N^\top(t)\,\mathrm{diag}\left(0,R_N\right)\tilde{x}_N(t) \\
&= \psi_N^\top(t)\underbrace{\left(-\frac{1}{\tau}\xi_N^\top(t)G_N^\top(t)\,\mathrm{diag}\left(0,R_N\right)G_N(t)\xi_N(t)\right)}_{\text{Contribution 4}}\psi_N(t)
\end{aligned}
\tag{10.33}
$$

As for the term $-\int_{-\tau}^0 \dot{x}_t^\top(s)Y\dot{x}_t(s)\mathrm{d}s$, the following inequality holds.

$$-\int_{-\tau}^{0}\dot{x}_t^{\top}(s)\,Y\,\dot{x}_t(s)\mathrm{d}s \leq \psi_N^{\top}\underbrace{\left(-\frac{1}{\tau}J_N^{\top}H_N^{\top}\operatorname{diag}\left(0,Y_N\right)H_N J_N\right)}_{\text{Contribution 7}}\psi_N \tag{10.34}$$

Note, that the contribution from the above equation has been denoted by Contribution 7 because it pertains to the last term, which is the seventh term in eq. (10.22).

As for the fifth term of $\dot{V}_{N_2}\left(x_t\right)$ (eq. (10.22)), the result in eq. (10.35) is obtained.

$$\begin{aligned}
\dot{x}_t^{\top}(0)(X+\tau Y)\dot{x}_t(0) &= \left[A_0x_t(0)+A_1x_t(-\tau)\right]^{\top}(X+\tau Y)\left[A_0x_t(0)+A_1x_t(-\tau)\right]\\
&= \left[x_t^{\top}(0)A_0^{\top}+x_t^{\top}(-\tau)A_1^{\top}\right](X+\tau Y)\left[A_0x_t(0)+A_1x_t(-\tau)\right]\\
&= x_t^{\top}(0)A_0^{\top}(X+\tau Y)A_0x_t(0)+x_t^{\top}(0)A_0^{\top}(X+\tau Y)A_1x_t(-\tau)\\
&+ x_t^{\top}(-\tau)A_1^{\top}(X+\tau Y)A_0x_t(0)+x_t^{\top}(-\tau)A_1^{\top}(X+\tau Y)A_1x_t(-\tau)\\
&= \psi_N^{\top}\underbrace{\begin{bmatrix}
A_0^{\top}(X+\tau Y)A_0 & A_0^{\top}(X+\tau Y)A_1 & 0 & \cdots & 0\\
A_1^{\top}(X+\tau Y)A_0 & A_1^{\top}(X+\tau Y)A_1 & 0 & \dots & 0\\
0 & 0 & 0 & \cdots & 0\\
\vdots & \vdots & \vdots & & \vdots\\
0 & 0 & 0 & \dots & 0
\end{bmatrix}}_{\text{Contribution 5}}\psi_N
\end{aligned} \tag{10.35}$$

As for the sixth term of $\dot{V}_{N_2}\left(x_t\right)$ (eq. (10.22)), the contribution in eq. (10.36) is obtained.

$$\begin{aligned}
-\dot{x}_t^{\top}(-\tau)X\dot{x}_t(-\tau) &= -\left[A_0x_t(-\tau)+A_1x_t(-2\tau)\right]^{\top}X\left[A_0x_t(-\tau)+A_1x_t(-2\tau)\right]\\
&= -\left[x_t^{\top}(-\tau)A_0^{\top}+x_t^{\top}(-2\tau)A_1^{\top}\right]X\left[A_0x_t(-\tau)+A_1x_t(-2\tau)\right]\\
&= -x_t^{\top}(-\tau)A_0^{\top}XA_0x_t(-\tau)-x_t^{\top}(-\tau)A_0^{\top}XA_1x_t(-2\tau)\\
&- x_t^{\top}(-2\tau)A_1^{\top}XA_0x_t(-\tau)-x_t^{\top}(-2\tau)A_1^{\top}XA_1x_t(-2\tau)\\
&= \psi_N^{\top}\underbrace{\begin{bmatrix}
0 & 0 & 0 & 0 & \cdots & 0\\
0 & -A_0^{\top}XA_0 & -A_0^{\top}XA_1 & 0 & \dots & 0\\
0 & -A_1^{\top}XA_0 & -A_1^{\top}XA_1 & 0 & \cdots & 0\\
\vdots & \vdots & \vdots & \vdots & & \vdots\\
0 & 0 & 0 & 0 & \dots & 0
\end{bmatrix}}_{\text{Contribution 6}}\psi_N
\end{aligned} \tag{10.36}$$

Assimilating these contributions, the following proposition that ensures the negative definiteness condition of the derivative of the Lyapunov functional is obtained:

Proposition 10.2 (Negative Definiteness Condition): *If eq.* (10.37) *holds, then the negative definiteness of the Lyapunov functional is ensured.*

$$\begin{aligned}
\dot{V}_{N_2}(t) \leq \psi_N^{\top}\big(&\textit{Contribution 1}+\textit{Contribution 2}+\textit{Contribution 3}+\textit{Contribution 4}+\\
&\textit{Contribution 5}+\textit{Contribution 6}+\textit{Contribution 7}\big)\psi_N<0
\end{aligned} \tag{10.37}$$

Those two propositions are then combined into a stability result for the neutral TDS which was defined in eq. (10.1).

Proposition 10.3 (New Stability Results for Neutral TDSs): *For a given N and a constant delay τ, if matrices P, S, $X \in S_n$, and R, $Y \in S_n^+$ and $T_{00}\dots T_{NN}$ such that $T_{ij}=T_{ji}$ and $Q_0\dots Q_N \in \mathbb{R}_n$ are determined such that eq.* (10.21) *and eq.* (10.37) *hold, then the system eq.* (10.1) *is asymptotically stable for this particular time-delay value.*

The correctness and effectiveness of the proposed stability results is verified through applying the obtained stability results to an example from the literature. Specifically, consider the following example shown in eq. (10.38), which was taken from the paper of Han et al. [124].

Table 10.1: Comparison of results from previous stability results in the literature for the stability of eq. (10.38) for different values of c.

c	**0**	**0.1**	**0.3**	**0.5**	**0.75**	**0.9**
[142]	4.47	3.49	2.06	1.14	0.54	0.13
[143]	4.35	4.33	4.10	3.62	2.73	0.99
[144]	4.47	4.35	4.13	3.67	2.87	1.41
[145]	4.47	4.42	4.17	3.69	2.87	1.41
[146] (N=2)	5.72	5.61	5.18	4.46	3.34	1.52
[146](N=3)	5.97	5.84	5.39	4.61	3.44	1.54
[146] (N=4)	6.06	5.93	5.46	4.67	3.47	1.54
[146] (N=5)	6.10	5.97	5.49	4.69	3.50	1.55
[124]	6.17	6.03	5.54	4.73	3.5	1.57
Proposition 3 (N = 2)	6.17	6.03	5.54	4.73	3.5	1.57

$$A_0 = \begin{bmatrix} -2 & 0 \\ 0 & -0.9 \end{bmatrix} \quad A_1 \begin{bmatrix} -1 & 0 \\ -1 & -1 \end{bmatrix} \quad C = \begin{bmatrix} c & 0 \\ 0 & c \end{bmatrix} |c| < 1 \tag{10.38}$$

Applying the stability results of Proposition 3 with an N that is as small as 2 leads to the results obtained by Han et al. A comparison of those results with previously published results are shown in table 10.1. Moreover, the evolution of the constraint residuals from the implementation of the proposition and its application to this example are shown in fig. 10.1, fig. 10.2, fig. 10.3, fig. 10.4, fig. 10.5, and fig. 10.6 for values c equal to 0, 0.1, 0.3, 0.5, 0.75, and 0.9, respectively.

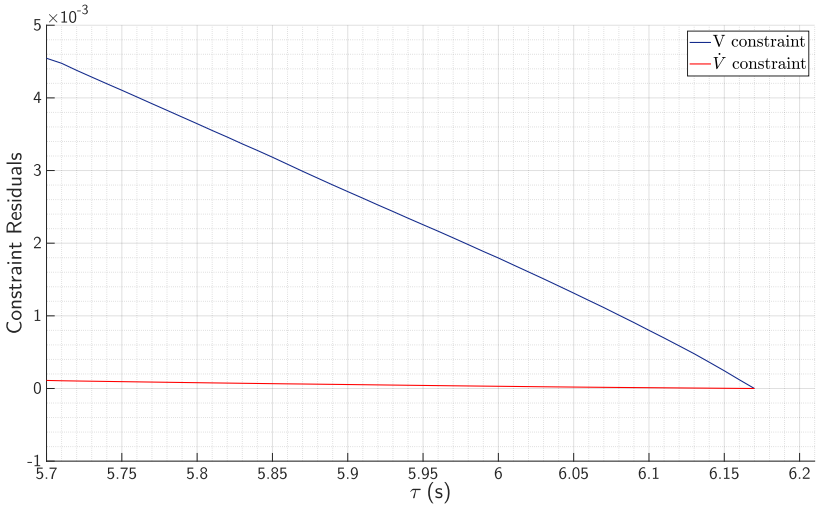

Figure 10.1: Plots of the evolution of the constaint residuals for case c = 0.

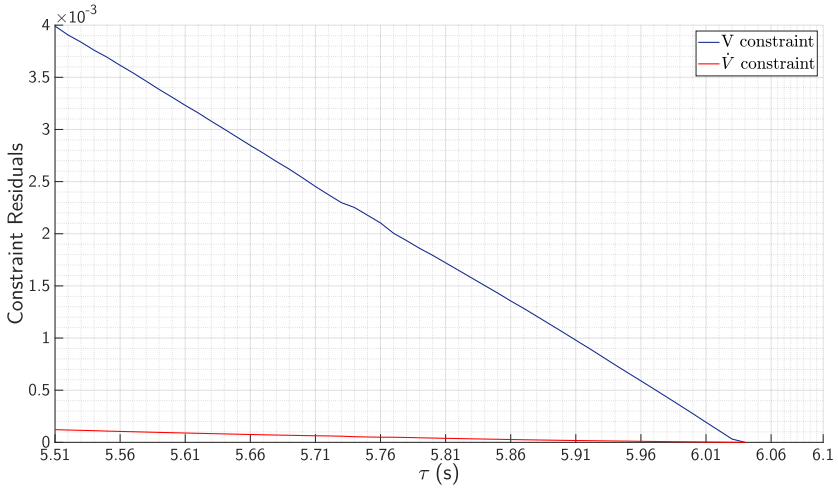

Figure 10.2: Plots of the evolution of the constaint residuals for case c = 0.1.

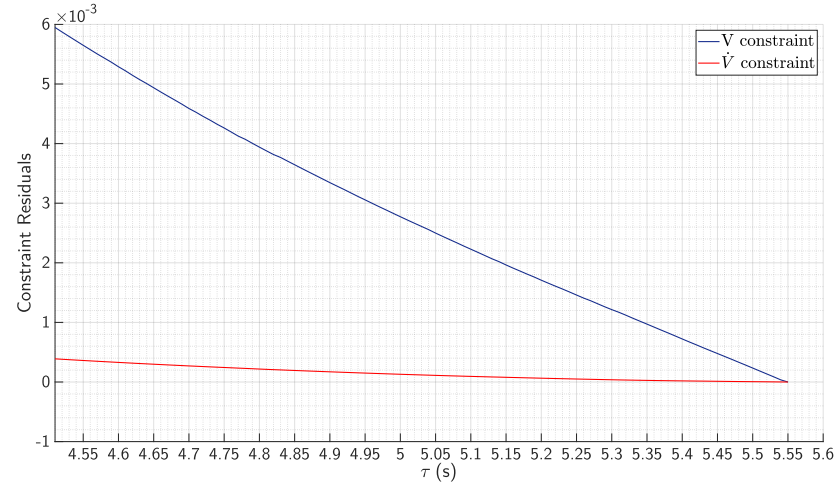

Figure 10.3: Plots of the evolution of the constaint residuals for case c = 0.3.

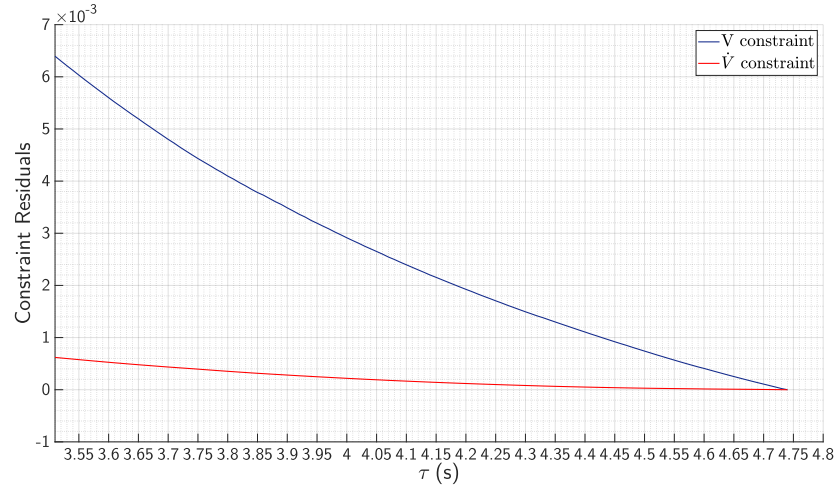

Figure 10.4: Plots of the evolution of the constaint residuals for case c = 0.5.

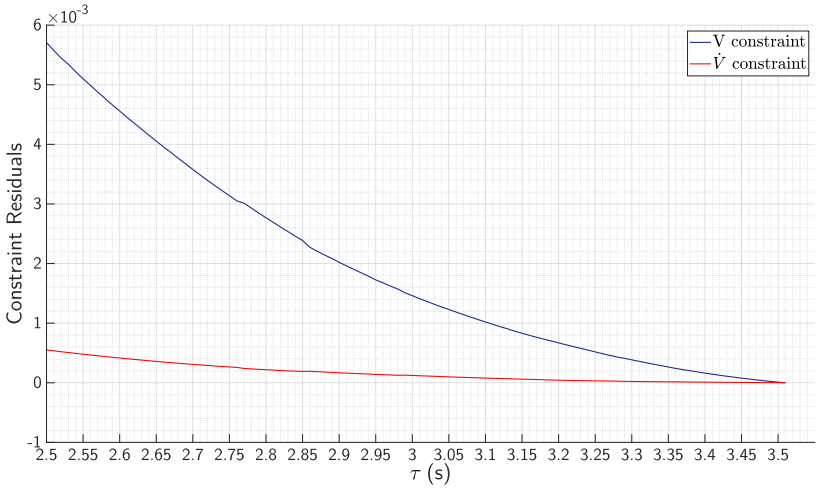

Figure 10.5: Plots of the evolution of the constaint residuals for case c = 0.75.

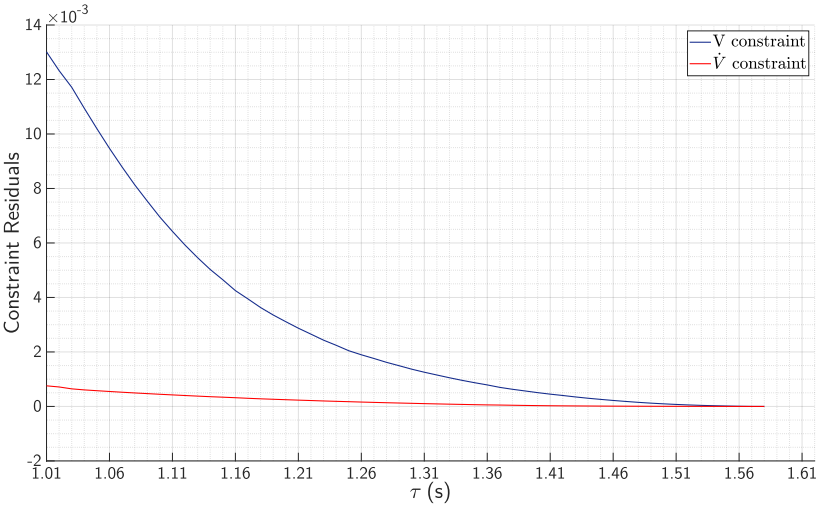

Figure 10.6: Plots of the evolution of the constaint residuals for case c = 0.9.

This page was intentionally left blank.

V

Conclusions and Recommendations

This page was intentionally left blank.

11

Conclusions and Recommended Future Research

In this chapter, the progress made with this thesis work is reflected upon. Specifically, the progress made in addressing the research (sub)questions is reported in section 11.1. Based off this reflection, a number of recommendations are made for future research in section 11.2.

11.1 Synopsis

The work that was presented in this thesis targeted the research aim which is to establish the means to determine the stable time-delay regions of an incremental control system, while considering actuator dynamics and uncertainties.

The report comprises of a large portion dedicated to a literature review which began in chapter 2. This chapter consisted of a review of the incremental control technique which is INDI, as well as its "prequel" NDI. In doing so, the steps of constructing an INDI controller were established, and ***Q1.1* (*What are the steps involved in constructing an INDI controller?*)** was addressed.

The goal of the chapter that followed, chapter 3, was to present a commonly-used model of a digital computer, and thereafter, to show different ways with which to model sampled-data systems. The models that were found were either entirely in continuous time or entirely in discrete time. Since it is intended to employ the time-delay framework, the model was required to be in continuous time. The discussion based on the work of Noijen et al. showed that the fidelity of two particular models that were modeled fully in continuous were higher than those of others. Based on those models, two generic block diagrams for an incremental control system were established. Therefore, the content of the chapter can be seen as an acceptable answer to ***Q1.2* (*What are the possibilities for modeling a sampled-data system as a fully continuous control system?*)**.

With the knowledge about INDI and about modeling sampled-data systems, it became evident how to construct the closed-loop formulation for the control system. Thus, chapter 2 and chapter 3 had successfully addressed the first main research question, ***Q1* (*What are the ways to represent the nonlinear system and the incremental controller, which is implemented on a digital computer, in order to obtain the closed-loop formulation in the form of a linear TDS?*)**.

In chapter 4, an introduction to TDSs was provided. Specifically, the chapter discussed ways to represent TDSs, a taxonomy for the classification of TDSs, and some important properties of TDSs. Thus, this chapter addressed the first sub-question of the second main research question, ***Q2.1* (*What are TDSs?*)**. The following chapter, chapter 5, focused on answering the sub-question that followed, ***Q2.2* (*What techniques can be used for the stability analysis of linear TDSs in the frequency domain?*)**, by giving an overview of different frequency domain techniques that can be used to analyze the stability of linear LTI TDS. Moreover, the chapter nominated the analytic curve frequency sweeping approach as the method of choice for the stability analysis in the frequency domain. In alignment with the sequence of sub-questions, the chapter after that, chapter 6, provided a review of stability results in the time domain which are based on the extension of Lyapunov's second method to TDSs. This chapter thereby gave an answer to ***Q2.3* (*What techniques can be used for the stability analysis of linear TDSs in the time domain?*)**, which is the final part of the second main research question,***Q2* (*What methods are suitable to analyze the stability of linear TDSs?*)**. Moreover, as in the case of chapter 5, a stability result was selected to be applied later on in the analyses, and the motivation for its selection was presented in the concluding remarks of the chapter. The chosen stability results are applicable to retarded TDSs and are based on the discretized Lyapunov functional method.

In chapter 7, the selected stability analysis methods were applied to a pendulum control system. The implementations of the selected stability results obtained from the answers of ***Q2.2*** and ***Q2.3***, provided answers that concurred. This was a nice verification test of the correct implementation of the stability results. Another form of verification of the implemented approaches was that the analytical results correctly predicted the stability (or lack thereof) of the Simulink® model for different time-delays. As for checking whether the control system has been modeled appropriately, this, unfortunately, could not be ad-

dressed. It is predicted that appropriate validation would be possible with real-world experiments or high fidelity simulations, which is beyond the scope of this research work.

Chapter 8 discussed two main possibilities to characterize uncertainties and, in doing so, addressed sub-question ***Q3.1 (What are suitable ways to characterize the uncertainties in the TDS system?)***. From this chapter, the hierarchy of uncertainty structures was the main framework that was employed for uncertainty characterization in the examples presented in the article.

The chapter that followed, chapter 9, presented a number of concepts, theorems, and principles that are relevant for the robust stability of TDSs. The review was not exhaustive, as time-limitations did not allow to investigate techniques such as $\mu-$analysis and multivariable approaches, for example. However, the chapter has indicated the zero-exclusion principle, the finite exclusion principle, the edge theorem as tools that have been previously used to analyze the robust stability of TDSs, which provided an answer to ***Q3.2 (Which existing robust stability analysis techniques for TDSs are applicable for the linear TDS obtained?)***. With regards to the last sub-question, ***Q3.3 (Can a new technique for the robust stability analysis of TDSs be developed?)***, a new technique that is based on the combination of the analytic curve frequency sweeping approach and the edge theorem, which has been referred to in the article as the "robust analytic curve frequency sweeping approach", has been proposed and applied. This amalgamation was inspired by the work of Tuzcu et al. who proposed to combine the direct method with the edge theorem as a novel robust stability approach [137]. Moreover, besides the novelty of this combination, the discussion in section 9.2 outlined how this new approach can be made applicable to systems with an uncertainty structure that is not necessarily polytopic. In particular, the multilinear theorem allows the robust analytic frequency sweeping approach to be applied to TDSs with a multilinear uncertainty structure because it indicates how to obtain a convex overbound of the mutlinear family of quasipolynomials. Moreover, Theorem 9.5 allows to further expand the reach of this new approach to polynomic families of quasipolynomials. Similar to the multilinear theorem, Theorem 9.5 presents the means to obtain the generator quasipolynomials of the convex hull enclosing the polynomic family of quasipolynomials. Thus, the main steps that are involved in the augmentation of the analytic curve frequency sweeping approach to make it a robust technique are to first obtain the convex hull of the quasipolynomial family that is being analysed, which may require the use of either the multilinear theorem and/or Theorem 9.5, depending on the uncertainty structure. Thereafter, based on the edge theorem, the robustly stable time-delay intervals of the obtained convex hull are determined by obtaining the time-delay intervals that the ensure the stability of all of its edges. These outlined steps address ***Q3.3.2 (What are the steps that can be taken in order to augment the delay-dependent stability analysis techniques implemented with those newly considered techniques, in order to make the resultant method applicable to the robust stability analysis of time-delay systems?)***. Furthermore, it should be noted that many of the tools mentioned in chapter 9 have been previously encountered in the stability of uncertain polynomials, the literature for which was mainly based on the book of Barmish [10]. The multilinear theorem and the theorem of Sideris and Sanchez Pena (Theorem 9.5) were encountered there. Thus, the group of techniques for the robust stability analysis of uncertain polynomials have inspired parts of the discussion on the approach to the robust stability analysis of uncertain quasipolynomials. Therefore, these techniques are the answer to the research subquestion, ***(Q3.3.1 - What are techniques, that have been used for the robust stability analysis of systems without time-delays, which can be used to inspire a new robust stability analysis technique for the linear time-delay systems considered?)***.

In relation to this sub-question ***(Q3.3.1)***, there was another source of inspiration for the possibility of a new robust stability analysis technique for TDSs, which was the subject of interval analysis. The reason for this interest is that interval analysis has been previously applied to analyze the robust stability of systems without time-delays. For example, Sinar has applied it in the robust stability analysis of re-entry vehicles, and she has shown a number of advantages of interval analysis in comparison to more traditional techniques, such as μ-analysis [147]. In relation to TDSs, some previous work has been uncovered that applies interval analysis to the robust stability analysis of TDSs. Specifically, di Loreto et al. have investigated the use of interval analysis for studying the delay-independent stability of TDSs. In particular, the Set Inversion Via Interval Analysis (SIVIA) algorithm was used in order to determine the presence of the characteristic roots of the TDS in a certain region in the right-half plane. When analyzing for robust stability, this procedure was performed for all the quasipolynomials in the quasipolynomial family. Ultimately, the system is said to be robustly stable if the family of quasipolynomials are Hurwitz stable [148]. Apart from the mentioned academic work, to the knowledge of the author, no further research has been done on making use of interval analysis to address the robust stability problem of TDSs. However, it seemed that, for the task of delay-dependent stability, that the use of interval analysis would a cumbersome approach.

Nonetheless, as mentioned in Remark 9.2, it seems promising to make use of the concept of refinement, a concept from the field of interval analysis, to reduces the conservatism of the robust analytic curve, for the cases of multilinear and polynomic uncertainty structures.

The final milestone of this thesis work was the application of the mentioned techniques to an aerospace plant. Namely, the analyses were applied to the short period dynamics of the Cessna Citation aircraft, and the results were presented in the attached article. Moreover, the outcomes from both the pendulum control system and the control system for the short period dynamics demonstrated the effectiveness of the methods in determining the robustly stable time-delay intervals of the

incremental control systems.

11.2 Recommendations for Future Research

Branching off the reflections made in the synopsis, a number of directions will be proposed for future research work. These recommendations can be grouped into categories: further analyses, and the development of new stability results.

In the category of further analyses, a number of suggestions are made. First, it is recommended to apply the methods proposed in this thesis to the stability analysis of IBS-controlled systems. IBS is a sibling and competing incremental control technique to INDI, and part of unraveling the theoretical gaps regarding incremental control is to compare those two methods. It is particularly interesting to show how the time-delay stability regions for these control techniques compare. Equally as important is to make a similar analysis to NDI-controlled systems. This would address the question of which of the two control techniques, NDI or INDI, is more robust to time-delays.

Another set of analyses based on the consideration of the ZOH are recommended in order to determine how changing the sampling period affects the resultant stability regions. This may be done by performing the stability analysis for different sampling periods through fixing the sampling period or through a more sophisticated analysis that accommodates for multiple time-delays. Furthermore, the results presented in the article show that even large sampling periods admit stable time-delay intervals, which is a slightly suspicious result. Therefore, it is recommended to re-assess the model used for the sampled-data system and to attempt to check how representative it is of the control system, in addition to checking whether it may be that the analytic curve frequency sweeping approach cannot be applied in this case, even when the sampling period is fixed. Rather, perhaps an approach that accommodates for multiple delays needs to be applied, instead. This realization makes leeway to the next recommendation.

In reality, incommensurate delays are often encountered. That is why, the stability results need to be extended to the case of multiple incommensurate delays. In the frequency domain, such an extension of the analytic curve frequency sweeping approach has already been proposed in the literature. It is called the "Iterative Frequency Sweeping Approach", and it has been presented in section 5.3.4. As for the time domain, the stability results for both the retarded and neutral cases need to be extended for the case of multiple delays. Moreover, it is recommended to revisit the results that were derived in chapter 10 and verify them further. Thereafter, once they are properly verified, they can be applied to the short period dynamics example that is presented in the paper. It should be checked whether the results corroborate those that were obtained from the analysis in the frequency domain.

It is also recommended to develop robust stability results in the time domain that are based on norm-bounded uncertainty. The reason for making this recommendation is that the analyses based on norm-bounded uncertainty can be more tractable (although more conservative) than the robust analyses that were presented in this thesis.

Furthermore, as mentioned in Remark 9.2, it is worth attempting to combine the "robust analytic curve frequency sweeping approach" with the concept of refinement to reduce the conservativeness in case of the analysis of systems with multilinear or polynomic uncertainty structures.

The focal point of this thesis has been on LTI systems. While the toolkit for the LTI analysis can be further developed, the branch of the robust stability analysis of time-varying or nonlinear TDS remains untouched. Therefore, it might be interesting to investigate the topic of the robust stability of the TDS under dynamic uncertainty as that might allow to consider the system as an Linear Parameter Varying (LPV) system.

As mentioned before, for some control applications, a more representative way to model the time-delays in the system is as distributed delays. That is why, another recommendation is to develop the time-domain stability results for the case of distributed delays. As mentioned earlier, in section 4.3.1, the results of the analyses are not equivalent, and this discrepancy manifests itself in the phenomenon of quenching.

Finally, in relation to tackling the theoretical gap that relates to sampling-time, the analysis of the sampled-data system may be based on consideration of the system as a hybrid system, as it truly is. However, this means that the TDS framework is shifted from, and approaches for the stability analysis of hybrid systems need to be studied and utilized instead.

This page was intentionally left blank.

Bibliography

[1] Y. Huang, D. M. Pool, O. Stroosma, and Q. Chu, "Long-stroke hydraulic robot motion control with incremental nonlinear dynamic inversion," *IEEE/ASME Transactions on Mechatronics*, 2019.

[2] X. Wang, E. Van Kampen, Q. P. Chu, and R. De Breuker, "Flexible Aircraft Gust Load Alleviation with Incremental Nonlinear Dynamic Inversion," *Journal of Guidance, Control, and Dynamics*, 2019.

[3] E. J. Smeur, G. C. De Croon, and Q. Chu, "Gust disturbance alleviation with incremental nonlinear dynamic inversion," in *IEEE International Conference on Intelligent Robots and Systems*, 2016.

[4] G. F. Franklin, J. D. Powell, M. L. Workman, *et al.*, *Digital control of dynamic systems*, vol. 3. Addison-wesley Menlo Park, CA, 1998.

[5] M. S. Fadali and A. Visioli, *Digital control engineering: analysis and design*. Academic Press, 2013.

[6] N. S. Nise, *Control Systems Engineering, (With CD)*. John Wiley & Sons, 2007.

[7] S. Noijen, H. Nijmeijer, and I. P. Lambrechts, "Modelling and analysis of digital control systems," *DCT rapporten*, vol. 2003, 2003.

[8] W. Michiels and S.-I. Niculescu, *Stability, control, and computation for time-delay systems: an eigenvalue-based approach*, vol. 27. Siam, 2014.

[9] X.-G. Li, S.-I. Niculescu, and A. Cela, *Analytic curve frequency-sweeping stability tests for systems with commensurate delays*. Springer, 2015.

[10] B. R. Barmish, *New tools for robustness of linear systems*. Macmilllan, 1994.

[11] X.-G. Li, S.-I. Niculescu, and A. Çela, "An iterative frequency-sweeping approach for stability analysis of linear systems with multiple delays," *IMA Journal of Mathematical Control and Information*, vol. 36, no. 02, pp. 379–398, 2017.

[12] X. Wang, E.-J. van Kampen, Q. Chu, and P. Lu, "Stability Analysis for Incremental Nonlinear Dynamic Inversion Control," *Journal of Guidance, Control, and Dynamics*, 2019.

[13] S. Kim, A. Tsourdos, and B. A. White, *Nonlinear Flight Control Systems*. American Cancer Society, 2010.

[14] J.-J. E. Slotine, W. Li, *et al.*, *Applied nonlinear control*, vol. 199. Prentice hall Englewood Cliffs, NJ, 1991.

[15] H. K. Khalil and J. W. Grizzle, *Nonlinear systems*, vol. 3. Prentice hall Upper Saddle River, NJ, 2002.

[16] X. Wang and E.-J. Van Kampen, "Incremental Backstepping Sliding Mode Fault-Tolerant Flight Control," in *AIAA Scitech 2019 Forum*, 2019.

[17] X. Wang, E.-J. van Kampen, Q. Chu, and P. Lu, "Incremental Sliding-Mode Fault-Tolerant Flight Control," *Journal of Guidance, Control, and Dynamics*, 2018.

[18] X. Wang, *Incremental Sliding Mode Flight Control*. PhD thesis, Delft University of Technology, jul 2019.

[19] R. van 't Veld, E.-J. Van Kampen, and Q. P. Chu, "Stability and Robustness Analysis and Improvements for Incremental Nonlinear Dynamic Inversion Control," 2018.

[20] O. S. Q. C. D. P. Y. Huang, Y. Zhang, "Robustness and time delay margin of incremental nonlinear dynamic inversion control with model uncertainties." 2019.

[21] C. Russell, *The Galileo Mission*. Springer Netherlands, 2012.

[22] E. Fridman, *Introduction to time-delay systems: Analysis and control*. Springer, 2014.

[23] G. Perdikaris, *Computer Controlled Systems: Theory and Applications*. Intelligent Systems, Control and Automation: Science and Engineering, Springer Netherlands, 2013.

[24] R. H. Middleton and D. E. Miller, "On the achievable delay margin using lti control for unstable plants," *IEEE Transactions on Automatic Control*, vol. 52, no. 7, pp. 1194–1207, 2007.

[25] S.-I. Niculescu, *Delay effects on stability: a robust control approach*, vol. 269. Springer Science & Business Media, 2001.

[26] B. L. Stevens, F. L. Lewis, and E. N. Johnson, *Aircraft control and simulation: dynamics, controls design, and autonomous systems*. John Wiley & Sons, 2015.

[27] S. Sieberling, Q. P. Chu, and J. A. Mulder, "Robust Flight Control Using Incremental Nonlinear Dynamic Inversion and Angular Acceleration Prediction," *Journal of Guidance, Control, and Dynamics*, 2010.

[28] R. van't Veld, "Incremental nonlinear dynamic inversion flight control: Stability and robustness analysis and improvements," Master's thesis, Delft University of Technology, sep 2016.

[29] D. T. McRuer and H. R. Jex, "A review of quasi-linear pilot models," *IEEE Transactions on Human Factors in Electronics*, no. 3, pp. 231–249, 1967.

[30] C. Fielding and P. K. Flux, "Non-linearities in flight control systems," *The Aeronautical Journal (1968)*, vol. 107, no. 1077, p. 673–686, 2003.

[31] J.-P. Richard, "Time-delay systems: an overview of some recent advances and open problems," *Automatica*, vol. 39, no. 10, pp. 1667–1694, 2003.

[32] R. van 't Veld, E.-J. Van Kampen, and Q. P. Chu, "Stability and Robustness Analysis and Improvements for Incremental Nonlinear Dynamic Inversion Control," 2018.

[33] A. Dorobantu, P. Seiler, and G. J. Balas, "Time-delay margin analysis for an adaptive controller," *Journal of Guidance, Control, and Dynamics*, vol. 35, no. 5, pp. 1418–1425, 2012.

[34] A. M. Pacheco, "Time delay margin analysis for model reference adaptive flight control laws," Master's thesis, Delft University of Technology, nov 2018.

[35] E. Smeur, *Incremental Control for Hybrid Micro Air Vehicles*. PhD thesis, Delft University of Technology, nov 2018.

[36] J. Koschorke, "Advanced flight control design and evaluation: An application of time delayed incremental backstepping," Master's thesis, Delft University of Technology, jun 2012.

[37] D. BUGAJSKI, D. ENNS, and M. ELGERSMA, "A dynamic inversion based control law with application to the high angle-of-attack research vehicle," in *Guidance, Navigation and Control Conference*, p. 3407, 1990.

[38] P. Smith, "A simplified approach to nonlinear dynamic inversion based flight control," in *23rd Atmospheric Flight Mechanics Conference*, p. 4461, 1998.

[39] B. J. Bacon, A. J. Ostroff, and S. M. Joshi, "Reconfigurable ndi controller using inertial sensor failure detection & isolation," *IEEE Transactions on Aerospace and Electronic Systems*, vol. 37, no. 4, pp. 1373–1383, 2001.

[40] W. Falkena, C. Borst, Q. Chu, and J. Mulder, "Investigation of Practical Flight Envelope Protection Systems for Small Aircraft," *Journal of Guidance, Control, and Dynamics*, 2012.

[41] P. Acquatella, W. Falkena, E.-J. van Kampen, and Q. P. Chu, "Robust Nonlinear Spacecraft Attitude Control using Incremental Nonlinear Dynamic Inversion.," 2012.

[42] H. Prathap, V. Brinda, and S. Ushakumari, "Robust flight control of a typical RLV during re-entry phase," in *Proceedings of the IEEE International Conference on Control Applications*, 2013.

[43] P. Simplício, M. D. Pavel, E. van Kampen, and Q. P. Chu, "An acceleration measurements-based approach for helicopter nonlinear flight control using incremental nonlinear dynamic inversion," *Control Engineering Practice*, 2013.

[44] G. Di Francesco, M. Mattei, and E. D'Amato, "Incremental Nonlinear Dynamic Inversion and Control Allocation for a Tilt Rotor UAV," 2014.

[45] Q. Lin, Z. Cai, and Y. Wang, "Design, model and attitude control of a model-scaled gyroplane," in *2014 IEEE Chinese Guidance, Navigation and Control Conference, CGNCC 2014*, 2015.

[46] M. Bronz, E. J. Smeur, H. Garcia de Marina, and G. Hattenberger, "Development of A Fixed-Wing mini UAV with Transitioning Flight Capability," 2017.

[47] Z. Liu, J. Guo, M. Li, S. Tang, and X. Wang, "VTOL UAV Transition Maneuver Using Incremental Nonlinear Dynamic Inversion," *International Journal of Aerospace Engineering*, 2018.

[48] F. Grondman, G. Looye, R. O. Kuchar, Q. P. Chu, and E.-J. Van Kampen, "Design and Flight Testing of Incremental Nonlinear Dynamic Inversion-based Control Laws for a Passenger Aircraft," 2018.

[49] Y. Huang, D. M. Pool, O. Stroosma, Q. P. Chu, and M. Mulder, "A Review of Control Schemes for Hydraulic Stewart Platform Flight Simulator Motion Systems," 2016.

[50] Y. Huang, D. Pool, O. Stroosma, and Q. Chu, "Incremental Nonlinear Dynamic Inversion Control for Hydraulic Hexapod Flight Simulator Motion Systems * *The first author is sponsored by Chinese Scholarship Council.," *IFAC-PapersOnLine*, 2017.

[51] Y. Huang, D. M. Pool, O. Stroosma, and Q. Chu, "Robust Incremental Nonlinear Dynamic Inversion Controller of Hexapod Flight Simulator Motion System," in *Advances in Aerospace Guidance, Navigation and Control*, 2017.

[52] Y. Huang, *Incremental nonlinear control of hydraulic parallel robots An application to the SIMONA research simulator*. PhD thesis, Delft University of Technology, mar 2019.

[53] M. Pavel, P. Shanthakumaran, O. Stroosma, Q. Chu, M. Wolfe, and H. Cazemier, "Development of advanced flight control laws for the ah-64 apache helicopter: Sketches from the work of tu delft-boeing project in simona simulator," in *72nd Annual Forum of the American Helicopter Society*, 2016.

[54] P. Lu and E. J. Van Kampen, "Active fault-tolerant control for quadrotors subjected to a complete rotor failure," in *IEEE International Conference on Intelligent Robots and Systems*, 2015.

[55] P. Lu, E. J. van Kampen, C. de Visser, and Q. Chu, "Aircraft fault-tolerant trajectory control using Incremental Nonlinear Dynamic Inversion," *Control Engineering Practice*, 2016.

[56] Y. Beyer, A. Kuzolap, M. Steen, J. H. Diekmann, and N. Fezans, "Adaptive Nonlinear Flight Control of STOL-Aircraft Based on Incremental Nonlinear Dynamic Inversion," 2018.

[57] E. J. Smeur, G. C. de Croon, and Q. Chu, "Cascaded incremental nonlinear dynamic inversion for MAV disturbance rejection," *Control Engineering Practice*, 2018.

[58] X. Wang, E.-J. Van Kampen, and Q. P. Chu, "Gust Load Alleviation and Ride Quality Improvement with Incremental Nonlinear Dynamic Inversion," 2017.

[59] T. Pollack, G. Looye, and F. Van der Linden, "Design and flight testing of flight control laws integrating incremental nonlinear dynamic inversion and servo current control," 2019.

[60] E. Tal and S. Karaman, "Accurate tracking of aggressive quadrotor trajectories using incremental nonlinear dynamic inversion and differential flatness," in *2018 IEEE Conference on Decision and Control (CDC)*, pp. 4282–4288, IEEE, 2018.

[61] H. Du, Z. Pu, J. Yi, and H. Qian, "Advanced quadrotor takeoff control based on incremental nonlinear dynamic inversion and integral extended state observer," in *CGNCC 2016 - 2016 IEEE Chinese Guidance, Navigation and Control Conference*, 2017.

[62] B. Bacon and A. Ostroff, "Reconfigurable flight control using nonlinear dynamic inversion with a special accelerometer implementation," in *AIAA Guidance, Navigation, and Control Conference and Exhibit*, p. 4565, 2000.

[63] E. J. J. Smeur, Q. Chu, and G. C. H. E. de Croon, "Adaptive Incremental Nonlinear Dynamic Inversion for Attitude Control of Micro Air Vehicles," *Journal of Guidance, Control, and Dynamics*, 2015.

[64] C. Cakiroglu, E.-J. Van Kampen, and Q. P. Chu, "Robust Incremental Nonlinear Dynamic Inversion Control Using Angular Accelerometer Feedback," 2018.

[65] Z. Su, H. Wang, and X. Shao, "Vehicle attitude control using finite time convergence incremental nonlinear dynamic inversion combined the command differential signals," in *2014 IEEE Chinese Guidance, Navigation and Control Conference, CGNCC 2014*, 2015.

[66] X. Li, Y. Jiang, J. Zhang, S. Shi, and L. Zhao, "A Method to Compensate Interaction between Actuator Dynamics and Control Allocator under Incremental Nonlinear Dynamic Inversion Controller," in *IOP Conference Series: Materials Science and Engineering*, 2018.

[67] S. Niculescu, C. Abdallah, W. Michiels, and K. Gu, "Dynamical systems with delays modeling, analysis, and design,"

[68] A. Bensoussan, G. Da Prato, M. C. Delfour, and S. K. Mitter, *Representation and control of infinite dimensional systems*. Springer Science & Business Media, 1993.

[69] L. Dugard and E. I. Verriest, *Stability and control of time-delay systems*, vol. 228. Springer, 1998.

[70] J. K. Hale and S. M. V. Lunel, *Introduction to functional differential equations*, vol. 99. Springer Science & Business Media, 2013.

[71] E. W. Kamen, "An operator theory of linear functional differential equations," *Journal of Differential Equations*, vol. 27, no. 2, pp. 274–297, 1978.

[72] A. Seuret, F. Gouaisbaut, and L. Baudouin, "D1. 1-overview of lyapunov methods for time-delay systems," 2016.

[73] A. Papachristodoulou, M. M. Peet, and S.-I. Niculescu, "Stability analysis of linear systems with time-varying delays: Delay uncertainty and quenching," in *2007 46th IEEE Conference on Decision and Control*, pp. 2117–2122, IEEE, 2007.

[74] R. Sipahi, *Mastering Frequency Domain Techniques for the Stability Analysis of LTI Time Delay Systems*, vol. 20. SIAM, 2019.

[75] K. Gu, J. Chen, and V. L. Kharitonov, *Stability of time-delay systems*. Springer Science & Business Media, 2003.

[76] R. Sipahi and S.-I. Niculescu, "Stability of car following with human memory effects and automatic headway compensation," *Philosophical Transactions of the Royal Society A: Mathematical, Physical and Engineering Sciences*, vol. 368, no. 1928, pp. 4563–4583, 2010.

[77] T. Van Vu and Y. Hasegawa, "Uncertainty relations for time-delayed langevin systems," *arXiv preprint arXiv:1902.06930*, 2019.

[78] K. Gu and S.-I. Niculescu, "Survey on recent results in the stability and control of time-delay systems," *Journal of Dynamic Systems, Measurement, and Control*, vol. 125, no. 2, pp. 158–165, 2003.

[79] A. Fioravanti, *H analysis and control of time-delay systems by methods in frequency domain*. PhD thesis, Paris 11, 2011.

[80] G. M. SCHOEN, *Stability and Stabilization of Time-Delay Systems*. PhD thesis, SWISS FEDERAL INSTITUTE OF TECHNOLOGY ZURICH, 1995.

[81] G. J. Silva, A. Datta, and S. P. Bhattacharyya, *PID controllers for time-delay systems*. Springer Science & Business Media, 2007.

[82] N. N. M. N. G. Chebotarev, "The routh-hurwitz problem for polynomials and entire functions," *Trudy Mat. Inst. Steklov.*, vol. 26, pp. 3–331, 1949.

[83] J. Neimark, "D-subdivisions and spaces of quasi-polynomials," *Prikl. Math. Mech. ,*, vol. 13, pp. 349–380, 1949.

[84] R. E. Bellman and K. L. Cooke, "Differential-difference equations," 1963.

[85] D. Breda, S. Maset, and R. Vermiglio, *Stability of linear delay differential equations: A numerical approach with MATLAB*. Springer, 2014.

[86] D. Breda, S. Maset, and R. Vermiglio, "Pseudospectral approximation of eigenvalues of derivative operators with nonlocal boundary conditions," *Applied numerical mathematics*, vol. 56, no. 3-4, pp. 318–331, 2006.

[87] K. Walton and J. Marshall, "Direct method for tds stability analysis," in *IEE Proceedings D-Control Theory and Applications*, vol. 134, pp. 101–107, IET, 1987.

[88] Z. Rekasius, "A stability test for systems with delays," in *Joint Automatic Control Conference*, no. 17, p. 39, 1980.

[89] N. MacDonald, "Comments on a simplified analytical stability test for systems with delay," in *IEE Proceedings D-Control Theory and Applications*, vol. 132, pp. 237–238, IET, 1985.

[90] A. Thowsen, "The routh-hurwitz method for stability determination of linear differential-difference systems," *International Journal of Control*, vol. 33, no. 5, pp. 991–995, 1981.

[91] N. Olgac and R. Sipahi, "An exact method for the stability analysis of time-delayed linear time-invariant (lti) systems," *IEEE Transactions on Automatic Control*, vol. 47, no. 5, pp. 793–797, 2002.

[92] J. Chen, "On computing the maximal delay intervals for stability of linear delay systems," *IEEE Transactions on Automatic Control*, vol. 40, no. 6, pp. 1087–1093, 1995.

[93] J. Chen, G. Gu, and C. N. Nett, "A new method for computing delay margins for stability of linear delay systems," *Systems & Control Letters*, vol. 26, no. 2, pp. 107–117, 1995.

[94] J. Chen and H. A. Latchman, "Frequency sweeping tests for stability independent of delay," *IEEE Transactions on automatic control*, vol. 40, no. 9, pp. 1640–1645, 1995.

[95] S. Barnett, *Polynomials and linear control systems*. Marcel Dekker, Inc., 1983.

[96] S.-I. Niculescu, P. Fu, and J. Chen, "Stability switches and reversals of linear systems with commensurate delays: A matrix pencil characterization," *IFAC Proceedings Volumes*, vol. 38, no. 1, pp. 406–411, 2005.

[97] P. Fu, S.-I. Niculescu, and J. Chen, "Stability of linear neutral time-delay systems: Exact conditions via matrix pencil solutions," *IEEE Transactions on Automatic Control*, vol. 51, no. 6, pp. 1063–1069, 2006.

[98] J. Chen, P. Fu, and S.-I. Niculescu, "When will zeros of time-delay systems cross imaginary axis?," in *2007 European Control Conference (ECC)*, pp. 5631–5638, IEEE, 2007.

[99] O. Toker and H. Özbay, "Complexity issues in robust stability of linear delay-differential systems," *Mathematics of control, signals and systems*, vol. 9, no. 4, pp. 386–400, 1996.

[100] R. H. Gielen, "Stability analysis and control of discrete-time systems with delay," *Doctorial Thesis. Technische Universiteit Eindhoven*, p. 169, 2013.

[101] M. Wu, Y. He, and J.-H. She, *Stability analysis and robust control of time-delay systems*, vol. 22. Springer, 2010.

[102] C. Briat, "Linear parameter-varying and time-delay systems," *Analysis, observation, filtering & control*, vol. 3, 2014.

[103] K. Gu and S.-I. Niculescu, "Additional dynamics in transformed time-delay systems," *IEEE Transactions on automatic control*, vol. 45, no. 3, pp. 572–575, 2000.

[104] E. Fridman, "New lyapunov–krasovskii functionals for stability of linear retarded and neutral type systems," *Systems & control letters*, vol. 43, no. 4, pp. 309–319, 2001.

[105] E. Fridman, "Descriptor discretized lyapunov functional method: Analysis and design," *IEEE Transactions on Automatic control*, vol. 51, no. 5, pp. 890–897, 2006.

[106] K. Gu, "An integral inequality in the stability problem of time-delay systems," in *Proceedings of the 39th IEEE Conference on Decision and Control (Cat. No. 00CH37187)*, vol. 3, pp. 2805–2810, IEEE, 2000.

[107] A. Seuret and F. Gouaisbaut, "Wirtinger-based integral inequality: Application to time-delay systems," *Automatica*, vol. 49, no. 9, pp. 2860–2866, 2013.

[108] J. Tian, Z. Ren, and S. Zhong, "A new integral inequality and application to stability of time-delay systems," *Applied Mathematics Letters*, vol. 101, p. 106058, 2020.

[109] M.-J. Park, O. Kwon, and J. Ryu, "Generalized integral inequality: Application to time-delay systems," *Applied Mathematics Letters*, vol. 77, pp. 6–12, 2018.

[110] A. Seuret and F. Gouaisbaut, "Complete quadratic lyapunov functionals using bessel-legendre inequality," in *2014 European Control Conference (ECC)*, pp. 448–453, IEEE, 2014.

[111] S. Xu and J. Lam, "A survey of linear matrix inequality techniques in stability analysis of delay systems," *International Journal of Systems Science*, vol. 39, no. 12, pp. 1095–1113, 2008.

[112] A. Seuret and F. Gouaisbaut, "Hierarchy of lmi conditions for the stability analysis of time-delay systems," *Systems & Control Letters*, vol. 81, pp. 1–7, 2015.

[113] V. L. Kharitonov and A. P. Zhabko, "Robust stability of time-delay systems," *IEEE Transactions on Automatic Control*, vol. 39, no. 12, pp. 2388–2397, 1994.

[114] V. L. Kharitonov and A. P. Zhabko, "Lyapunov–krasovskii approach to the robust stability analysis of time-delay systems," *Automatica*, vol. 39, no. 1, pp. 15–20, 2003.

[115] V. Kharitonov, *Time-delay systems: Lyapunov functionals and matrices*. Springer Science & Business Media, 2012.

[116] E. Fridman and S.-I. Niculescu, "On complete lyapunov–krasovskii functional techniques for uncertain systems with fast-varying delays," *International Journal of Robust and Nonlinear Control: IFAC-Affiliated Journal*, vol. 18, no. 3, pp. 364–374, 2008.

[117] A. V. Egorov, "A new necessary and sufficient stability condition for linear time-delay systems," *IFAC Proceedings Volumes*, vol. 47, no. 3, pp. 11018–11023, 2014.

[118] X.-g. Li, X.-j. Zhu, and G.-y. Cao, "Robust stability of neutral systems: A discretized lyapunov functional method," *Journal of Shanghai Jiaotong University (Science)*, vol. 14, no. 3, pp. 279–285, 2009.

[119] A. Papachristodoulou, "Analysis of nonlinear time-delay systems using the sum of squares decomposition," in *Proceedings of the 2004 American Control Conference*, vol. 5, pp. 4153–4158, IEEE, 2004.

[120] M. M. Peet, A. Papachristodoulou, and S. Lall, "Positive forms and stability of linear time-delay systems," *SIAM Journal on Control and Optimization*, vol. 47, no. 6, pp. 3237–3258, 2009.

[121] K. Gu, A. C. Luo, and S.-I. Niculescu, "Discretized lyapunov functional for systems with distributed delay," in *1999 European Control Conference (ECC)*, pp. 3649–3654, IEEE, 1999.

[122] K. Gu, "A further refinement of discretized lyapunov functional method for the stability of time-delay systems," *International Journal of Control*, vol. 74, no. 10, pp. 967–976, 2001.

[123] K. Gu, "Refined discretized lyapunov functional method for systems with multiple delays," *International Journal of Robust and Nonlinear Control: IFAC-Affiliated Journal*, vol. 13, no. 11, pp. 1017–1033, 2003.

[124] Q.-L. Han, X. Yu, and K. Gu, "On computing the maximum time-delay bound for stability of linear neutral systems," *IEEE Transactions on Automatic Control*, vol. 49, no. 12, pp. 2281–2285, 2004.

[125] Q.-L. Han, "On stability of linear neutral systems with mixed time delays: a discretized lyapunov functional approach," *Automatica*, vol. 41, no. 7, pp. 1209–1218, 2005.

[126] Q.-L. Han, "A discrete delay decomposition approach to stability of linear retarded and neutral systems," *Automatica*, vol. 45, no. 2, pp. 517–524, 2009.

[127] X.-G. Li, X.-J. Zhu, A. Cela, and A. Reama, "Stability analysis of neutral systems with mixed delays," *Automatica*, vol. 44, no. 11, pp. 2968–2972, 2008.

[128] J. G. VanAntwerp and R. D. Braatz, "A tutorial on linear and bilinear matrix inequalities," *Journal of process control*, vol. 10, no. 4, pp. 363–385, 2000.

[129] J. Löfberg, "Yalmip: A toolbox for modeling and optimization in matlab," in *Proceedings of the CACSD Conference*, vol. 3, Taipei, Taiwan, 2004.

[130] O. Toker and H. Ozbay, "On the np-hardness of solving bilinear matrix inequalities and simultaneous stabilization with static output feedback," in *Proceedings of 1995 American Control Conference-ACC'95*, vol. 4, pp. 2525–2526, IEEE, 1995.

[131] X.-G. Li, S.-I. Niculescu, A. Çela, H.-H. Wang, and T.-Y. Cai, "On τ-decomposition frequency-sweeping test for a class of time-delay systems. part i: Simple imaginary roots case," *IFAC Proceedings Volumes*, vol. 45, no. 14, pp. 132–137, 2012.

[132] X.-G. Li, S.-I. Niculescu, A. Çela, H.-H. Wang, and T.-Y. Cai, "On τ-decomposition frequency-sweeping test for a class of time-delay systems. part ii: Multiple roots case," *IFAC Proceedings Volumes*, vol. 45, no. 14, pp. 138–143, 2012.

[133] S. Skogestad and I. Postlethwaite, *Multivariable feedback control: analysis and design*, vol. 2. Wiley New York, 2007.

[134] T. Mori and H. Kokame, "An extension of kharitonov's theorem and its application," in *1987 American Control Conference*, pp. 892–896, IEEE, 1987.

[135] M. Fu, A. W. Olbrot, and M. P. Polis, "Robust stability for time-delay systems: the edge theorem and graphical tests," *IEEE Transactions on Automatic Control*, vol. 34, no. 8, pp. 813–820, 1989.

[136] M. Fu, A. W. Olbrot, and M. P. Polis, "The edge theorem and graphical tests for robust stability of neutral time-delay systems," *Automatica*, vol. 27, no. 4, pp. 739–741, 1991.

[137] İ. Tuzcu, "A computational approach to stability of polytopic families of quasi-polynomials with single delay," *International Journal of Robust and Nonlinear Control*, vol. 20, no. 17, pp. 1981–1992, 2010.

[138] J. Santos, S. Mondié, and V. Kharitonov, "The finite inclusions theorem/finite zero exclusion principle for complex quasipolynomials," *IFAC Proceedings Volumes*, vol. 36, no. 19, pp. 245–250, 2003.

[139] J. Santos, S. Mondié, and V. Kharitonov, "A semi analytic approach to the robust stability of quasipolynomials," *IFAC Proceedings Volumes*, vol. 38, no. 1, pp. 511–516, 2005.

[140] S. Mondie, J. Santos, and V. L. Kharitonov, "Robust stability of quasi-polynomials and the finite inclusions theorem," *IEEE Transactions on Automatic Control*, vol. 50, no. 11, pp. 1826–1831, 2005.

[141] R. S. Sanchez Pena, *Robust analysis of feedback systems with parametric and dynamic structured uncertainty*. PhD thesis, California Institute of Technology, 1989.

[142] E. Fridman and U. Shaked, "Delay-dependent stability and h control: constant and time-varying delays," *International Journal of Control*, vol. 76, no. 1, pp. 48–60, 2003.

[143] Q.-L. Han, "Robust stability of uncertain delay-differential systems of neutral type," *Automatica*, vol. 38, no. 4, pp. 719–723, 2002.

[144] Y. He, M. Wu, J.-H. She, and G.-P. Liu, "Delay-dependent robust stability criteria for uncertain neutral systems with mixed delays," *Systems & Control Letters*, vol. 51, no. 1, pp. 57–65, 2004.

[145] D. Yue and Q.-L. Han, "A delay-dependent stability criterion of neutral systems and its application to a partial element equivalent circuit model," in *Proceedings Of the 2004 American Control Conference*, vol. 6, pp. 5438–5442, IEEE, 2004.

[146] P. Balasubramaniam, R. Krishnasamy, and R. Rakkiyappan, "Delay-dependent stability of neutral systems with time-varying delays using delay-decomposition approach," *Applied Mathematical Modelling*, vol. 36, no. 5, pp. 2253–2261, 2012.

[147] S. Juliana, *Re-entry Flight Clearance*. Phd dissertation, Delft University of Technology, sep 2006.

[148] M. Di Loreto, M. Dao, L. Jaulin, J.-F. Lafay, and J. J. Loiseau, "Applied interval computation: A new approach for time-delays systems analysis," in *Applications of time delay systems*, pp. 175–197, Springer, 2007.